2011

High Resolution Antarctic Glaciochemical Climate Proxy Records and Their Global Implications

Daniel Arthur Dixon

HIGH RESOLUTION ANTARCTIC GLACIOCHEMICAL CLIMATE PROXY RECORDS AND THEIR GLOBAL IMPLICATIONS

By

Daniel Arthur Dixon

B.S. University of Southampton, U.K., 2000

M.S. University of Maine, U.S.A., 2004

A THESIS

Submitted in Partial Fulfillment of the

Requirements for the Degree of

Doctor of Philosophy

(in Earth Sciences)

The Graduate School

The University of Maine

May, 2011

Advisory Committee:

Paul A. Mayewski, Professor of Earth Sciences and Climate Studies, and Director of Climate Change Institute, Advisor

Karl Kreutz, Assistant Professor of Earth Sciences and Climate Studies

Gordon Hamilton, Assistant Professor of Earth Sciences and Climate Studies

Kirk Maasch, Associate Professor of Earth Sciences and Climate Studies

Andrew Carleton, Professor of Physical Geography, Pennsylvania State University

THESIS

ACCEPTANCE STATEMENT

On behalf of the Graduate Committee for Daniel Arthur Dixon, I affirm that this manuscript is the final and accepted thesis. Signatures of all committee members are on file with the Graduate School at the University of Maine, 42 Stodder Hall, Orono

12/24/10

Paul A. Mayewski, Professor of Earth Sciences and Climate Studies, and Director of Climate Change Institute

LIBRARY RIGHTS STATEMENT

In presenting this thesis in partial fulfillment of the requirements for an advanced degree at The University of Maine, I agree that the Library shall make it freely available for inspection. I further agree that permission for "fair use" copying of this thesis for scholarly purposes may be granted by the Librarian. It is understood that any copying or publication of this thesis for financial gain shall not be allowed without my written permission.

Signature:

Date:

HIGH RESOLUTION ANTARCTIC GLACIOCHEMICAL CLIMATE PROXY RECORDS AND THEIR GLOBAL IMPLICATIONS

By Daniel Arthur Dixon

Thesis Advisor: Dr. Paul A. Mayewski

An Abstract of the Thesis Presented
in Partial Fulfillment of the Requirements for the
Degree of Doctor of Philosophy
(in Earth Sciences)
May, 2011

The first section of this study presents major ion, trace element, heavy metal, rare earth element and oxygen isotope data from a series of surface snow samples and shallow firn sections collected along four US ITASE traverses across extensive regions of East and West Antarctica. In each sample the dissolved major ion, total trace element, and $\delta^{18}O$ concentrations are measured. This provides a baseline from which changes in the chemistry of the atmosphere over Antarctica can be monitored under expected warming scenarios and continued intensification of industrial activities in the Southern Hemisphere.

Satellite remote sensing measurements of microwave backscatter and grain size assist in the identification of glaze/dune areas across Antarctica and show how chemical

concentrations are higher in these areas, precluding them from containing useful high-resolution chemical climate records. The majority of the non-glaze/dune samples in this study exhibit similar, or lower, concentrations to those from previous studies. Consequently, the results presented here comprise a conservative baseline for Antarctic surface snow chemical concentrations.

The second section of this study presents a 200-year proxy for Northerly Air Mass Incursions (NAMI) into central and western West Antarctica. The NAMI proxy is developed from the examination of 19 shallow (21m – 150m deep) Antarctic ice core non-sea-salt (nss) Ca^{2+} concentration records and it exhibits a significant rise in recent decades. This rise is unprecedented for at least the last 200 years and is coincident with anthropogenically-driven changes in other large-scale Southern Hemisphere (SH) environmental phenomena such as greenhouse gas induced warming, ozone depletion and the associated intensification of the SH westerlies. Statistical analysis suggests that atmospheric circulation is the dominant factor affecting $nssCa^{2+}$ concentrations throughout central and western West Antarctica.

ACKNOWLEDGEMENTS

First and foremost, I wish to express gratitude to my advisor, Paul, for believing in me (or pretending not to) and giving me the time I needed to complete this research. I hope that our paths will continue to cross far into the future.

I am grateful to my committee members, Kirk, Gordon, Karl, and Andrew, for their encouragement and support and to everyone in the Climate Change Institute who has helped me over the years; I could not have done it without you.

Warm thanks to all the fellow graduate students who have blessed me with their company during these past years; the days (and nights) would not have been anywhere near as exciting, fun, and colorful without you. To my good Neighbor, and Delnami, thanks for always lending me a willing ear for my spontaneous science lessons, I thoroughly enjoy our 20-volume word searches and impromptu poetry readings. To Bronco, thanks for many a peaceful evening at the cottage and for turning the tables and giving me the science lessons!

Last, but unquestionably not least, thanks a googol to my wonderful family, on both sides of the pond. My gorgeous wife, Erika, in particular, deserves a lot more than a medal for her near-superhuman efforts to keep some semblance of sesquinormality in the house, despite my seemingly random all-nighters. You are the best.

Acknowledgements for each chapter are detailed below.

Chapter 1: A spatial framework for assessing current conditions and monitoring future change in the chemistry of the Antarctic atmosphere

The International Trans Antarctic Scientific Expedition (ITASE) is funded by NSF OPP (0096299, 0439589, 063740, 063650 and 0837883). I greatly acknowledge the support of the Office of Polar Programs, the 109th Air National Guard (Scotia, New York), M. Wumkes, M. Waszkiewicz of Ice Core Drilling Services (University of Wisconsin), Raytheon Polar Services, and all U.S. ITASE field team personnel. I thank Elena Korotkikh, Sharon B. Sneed, Michael J. Handley, Douglas S. Introne and Ted A. Scambos for their helpful comments and contributions.

Chapter 2: An Ice Core Proxy for Northerly Air Mass Incursions (NAMI) into West Antarctica

This research was supported by the U.S. National Science Foundation Office of Polar Programs grants (0096305, 0096299, 0439589, 063740, 063650 and 0837883) and the W.M. Keck Foundation to P.M. I thank the U.S. Antarctic Program, the 109th N.Y. Air National Guard, Ice Core Drilling Services, Raytheon Polar Services Company and all my U.S. ITASE field colleagues for their support. I would also like to thank Ian D. Goodwin, Gareth J. Marshall, Rhaelene Freeman, Kirk A. Maasch and Sharon B. Sneed for all their helpful comments and advice during the write-up of these results.

TABLE OF CONTENTS

LIST OF TABLES

LIST OF FIGURES

Chapter 1

INTRODUCTION

1.1 Antarctica in the Climate System

Recent discoveries have shown that major changes in Earth's climate system, such as temperature and atmospheric circulation, can occur in a matter of years to decades [*Dansgaard et al.*, 1993; *Mayewski et al.*, 1993a]. As a result the scientific community is striving to understand these changes and hopes to be able to predict rapid climate change events in order to lessen their harmful impact on life.

The earth's climate is essentially a dynamic, heat-driven, multi-component, coupled system. The heat energy driving the climate system comes almost entirely from the Sun. Antarctica plays a very important role in global climate variability and change, especially in the Southern Hemisphere. The higher latitudes of the Southern Hemisphere, including the ice sheet and the surrounding sea-ice zone, constitute one of the two primary areas on Earth where there is net loss of energy from the atmosphere to space, the other being the North Polar regions. Studies with global climate models (GCM) have suggested that both Southern Hemisphere and global atmospheric circulations are sensitive to modest changes in the temperature of the Antarctic atmosphere [*Parish and Bromwich*, 1997]. The isolated Antarctic continent is an ideal place to study natural atmospheric variability thanks to its remoteness from major anthropogenic pollution sources that can confound the investigation of natural variability compared to more populated regions [*Legrand and Mayewski*, 1997; *Shaw*, 1982].

For GCMs of global climate to be accurate they must be calibrated with instrumental climate records and in order to understand the dynamic range of climate,

proxy records ranging from multi-annual to multi-millennial scales are necessary. In the Northern Hemisphere, high quality instrumental records exist for the last ~100 years. However, in the Southern Hemisphere records only cover the last ~50-100 years and apart from very few isolated sites, direct observational and instrumental records of Antarctic climate cover only the last 30-40 years. A longer perspective on Southern Hemisphere climate variability can be obtained by studying natural archives that provide proxies for past climate, such as tree rings, sediment cores, and ice cores.

Antarctic ice cores are a valuable resource for reconstructing the climate of the past because they can provide sub-annually resolved, continuous proxy records of atmospheric temperature, atmospheric circulation, precipitation, the El Niño-Southern Oscillation, and sea ice extent among others [*Mayewski and Bender*, 1995; *Mayewski et al.*, 2004]. Furthermore strong teleconnections link the Antarctic to the mid- and low-latitudes [*Carleton*, 2003] ensuring that records of Southern Hemisphere climate are captured in Antarctic snow and ice layers.

The Antarctic atmosphere is inherently complex; it exhibits a high degree of variability on both spatial and temporal scales. To clearly understand the spatial and temporal variability of the Antarctic atmosphere a suite of high-resolution ice core records are needed that are well distributed enough to allow for objective analysis of spatial variability and deep enough for analysis of decadal-scale variability. The research presented in this dissertation is primarily based on results stemming from the International Trans Antarctic Scientific Expedition (ITASE). ITASE is designed to address several key scientific objectives [*Mayewski et al.*, 2005b] including:

1) What is the spatial and temporal variability of Antarctic climate (e.g. extreme events, regional to global atmospheric phenomena, and snow accumulation variations) over the last 200-1000 years?

2) What are the environmental changes (e.g. sea-ice variation, ocean productivity, anthropogenic activity, volcanic activity) impacting Antarctica over the last 200-1000 years?

1.2 ITASE and U.S. ITASE

ITASE is a multi-national (currently 21 nations), multi-disciplinary polar field research program with the broad aim of understanding the recent environmental history of Antarctica [*Mayewski and Goodwin*, 1997; *Mayewski et al.*, 2005b]. By operating primarily in oversnow traverse mode, ITASE allows scientists to experience the Antarctic environment first hand while providing the interactive capabilities of oceanographic research vessels and large polar field camps. Most importantly, ITASE provides a rare, multidimensional examination of the ice sheet and its history. Thus far, ITASE has collected >20,000 km of ground penetrating radar, more than 7000 m of firn/ice core (>240 cores), images of the Antarctic bedrock to >4000 m beneath the ice sheet surface, and continuous measurements of the atmosphere to heights of >20 km (Figure 1.1). Furthermore, ITASE traverses have provided opportunities for the installation of automatic weather stations, and the measurement of, for example, atmospheric chemistry, ice dielectric and ice-core microparticles plus the deployment of experiments valuable for ground truth in remote-sensing missions and geophysical measurements for crustal investigation. Overall, ITASE is a highly multi- and interdisciplinary activity.

Figure 1.1. ITASE core sites and GPR surveys as of 2008. Core sites are represented by black circles and GPR surveys are marked by orange lines. Core and GPR data are overlain on a shaded relief map of the RAMP DEM [*Liu et al.*, 2001].

ITASE is focused on the last ~200 years of the firn/ice core record because this period covers the onset of the industrial age and ~100 years of non-anthropogenic climate variability. This period also overlaps global instrumental climate records.

From 1999-2008, the United States' component of the International Trans Antarctic Scientific Expedition (US ITASE) completed seven highly successful field seasons of oversnow traversing in Antarctica, ultimately ending up at South Pole Station

in East Antarctica twice, each time approaching from a different direction and in the process traversing major portions of East and West Antarctica (Figure 1.2).

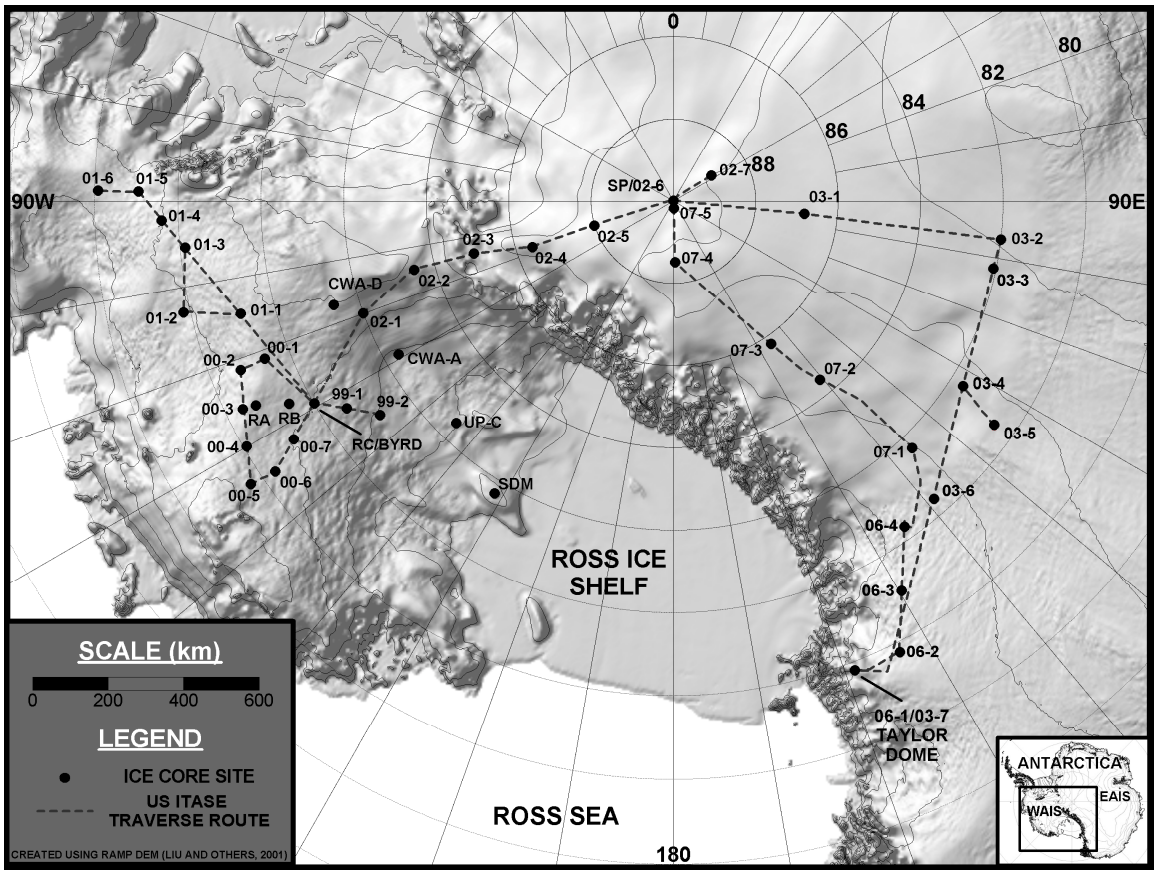

Figure 1.2. U.S. ITASE traverse map. A shaded digital elevation map of Antarctica showing the core sites and traverse routes for U.S. ITASE.

The US ITASE team traveled more than 10,000 km over the Antarctic ice sheet, drilling firn/ice cores every ~250 km, digging 2 m-deep snowpits at each core site, and collecting surface snow samples every ~30 km along the way. Of the more than 40 15-115 m-deep (typically 60-70 m deep) cores collected thus far by the US ITASE team, almost all have been sampled at high resolution (up to 50 samples per meter), for their entire length, to develop sub-annually resolved time series [*Dixon et al.*, 2004; *Steig et*

al., 2005]. It is these surface snow samples, snowpits, and ice core glaciochemical records that form the basis of this dissertation. By utilizing the spatially distributed, multi-parameter, sub-annually resolved ice core measurements from this collection of U.S. ITASE cores this study provides a high resolution representation of past Antarctic, and ultimately Southern Hemisphere, climate.

1.3 Thesis Outline

The body of this dissertation consists of 4 chapters: Chapter 1 is this Introduction and Chapter 4 is the Conclusion. Chapters 2 and 3 are written as individual papers, one of which (Chapter 3) has already been accepted for publication in a peer-reviewed journal, *The International Journal of Climatology* [*Dixon et al.*, in press]. These chapters each contain their own Summary, Introduction, Methods, Results, and Conclusion sections. There is one reference list, encompassing both chapters, following Chapter 4. Following the reference list, there is an appendix containing a selection of published papers which I have co-authored during my PhD research, each relevant to the research contained in this thesis [*Bertler et al.*, 2005; *Eisen et al.*, 2008; *Mayewski et al.*, 2005a; *Monaghan et al.*, 2006; *Schneider et al.*, 2006; *Steig et al.*, 2005].

The Steig et al. [2005] paper examines the development and validation of US ITASE ice core chronologies and provides a determination of their precision and accuracy. The Bertler et al. [2005] paper presents an updated compilation of published and new major ion data in snow from 520 Antarctic sites provided by the national ITASE programs. The study by Eisen et al. [2008] incorporates accumulation data from several ITASE nations in a thorough assessment of East Antarctic spatial and temporal snow

accumulation variability. Monaghan et al. [2006] investigate how snowfall has affected the thickness of the Antarctic ice sheets and provide a 50-year perspective by combining model simulations and observations primarily from ice cores. They show that there has been no statistically significant change in Antarctic snowfall since the 1950s. Schneider et al. [2006] present a 200-year reconstruction of Antarctic mean surface temperatures based upon stable isotopes from a suite of high-resolution, precisely dated ice cores. Their reconstruction reveals that Antarctic temperatures have increased by about 0.2 ºC since the late nineteenth century and that the long-term trends are strongly modulated by the Southern Annular Mode. Mayewski et al. [2005a] present highly resolved, annually dated, calibrated proxies for atmospheric circulation based upon a suite of Antarctic ice cores. They show, based upon a South Pole ice-core ^{10}Be proxy for solar variability, that increased (decreased) solar irradiance is associated with increased (decreased) zonal wind strength near the edge of the Antarctic polar vortex.

Chapter 2 addresses the second of the ITASE primary scientific objectives - how major and trace chemical species vary, spatially and temporally, over the Antarctic, and their natural background concentrations. This is the first study to measure more than 25 chemical constituents in the surface snow over extensive regions of Antarctica and it provides a baseline from which future changes in the chemistry of the atmosphere over Antarctica can be monitored. The results show that the majority of chemical concentrations in Antarctic snow are still within their natural range of variability. However, despite potential contributions from local and global volcanic sources, several elements (lead, cadmium, and arsenic) exhibit exceptionally high concentrations across Antarctica. Previous studies [*Wolff and Suttie*, 1994] have revealed anthropogenic

activity as the primary source of excess Antarctic lead levels. However, the source of excess cadmium in Antarctic precipitation is less certain and is likely also related to anthropogenic activities in the Southern Hemisphere. Excess Antarctic arsenic concentrations exhibit a pronounced annual signal, particularly in West Antarctica, and are most likely associated with photochemical and/or biogenic activity.

Chapter 3 addresses the first of the ITASE primary scientific objectives. A suite of 21 shallow firn/ice cores are used to develop a proxy record of northerly air mass incursions (NAMI) into central and western West Antarctica. The NAMI proxy record reveals that the recent increase in the strength of southern hemisphere westerly winds [*Marshall*, 2003; *Thompson and Solomon*, 2002; *Thompson et al.*, 2000] is unprecedented for at least the last 200 years [*Dixon et al.*, in press] The change in the westerlies is coincident with anthropogenically-driven changes in other large-scale Southern Hemisphere environmental phenomena such as greenhouse gas induced warming and ozone depletion. As ozone levels are believed to be the dominant factor behind the recent strengthening of the Southern Hemisphere westerlies, their predicted recovery is expected to rob Antarctica of one of its best defenses against greenhouse gas warming.

Chapter 2

A SPATIAL FRAMEWORK FOR ASSESSING CURRENT CONDITIONS AND MONITORING FUTURE CHANGE IN THE CHEMISTRY OF THE ANTARCTIC ATMOSPHERE

2.1 Chapter Summary

This is the first study to measure more than 25 chemical constituents in the surface snow and firn across extensive regions of Antarctica. It is also the first to report total-Cs concentrations. We present major ion, trace element, heavy metal, rare earth element and oxygen isotope data from a series of surface snow samples and shallow firn sections collected along four US ITASE traverses across East and West Antarctica. In each sample we measure dissolved concentrations of Na^+, K^+, Mg^{2+}, Ca^{2+}, Cl^-, NO_3^-, SO_4^{2-}, and MS^- using ion chromatography and total concentrations of Sr, Cd, Cs, Ba, La, Ce, Pr, Pb, Bi, U, As, Al, S, Ca, Ti, V, Cr, Mn, Fe, Co, Na, Mg, Li, and K using inductively coupled plasma sector field mass spectrometry. We also measure $\delta^{18}O$ by isotope ratio mass spectrometry.

The 2002/2003 traverse began at Byrd Surface Camp, West Antarctica, and ended close to South Pole, East Antarctica. The 2003/2004 traverse began at South Pole, passed through AGO4 in central East Antarctica before turning north and finishing at Taylor Dome. The combined 2006/2007 and 2007/2008 traverses started out at Taylor Dome and headed south, passing through the Byrd Glacier drainage basin and ending at South Pole.

In this study, we utilize satellite remote sensing measurements of microwave backscatter and grain size to assist in the identification of glaze/dune areas across

Antarctica and show how chemical concentrations are higher in these areas, precluding them from containing useful high-resolution chemical climate records.

The majority of the non-glaze/dune samples in this study exhibit similar, or lower, concentrations to those from previous studies. Consequently, the results presented here comprise a conservative baseline for Antarctic surface snow chemical concentrations.

The elements Cd, Pb, Bi, As, and Li are enriched across Antarctica relative to both ocean and upper crust elemental ratios. Global volcanic outgassing accounts for the majority of the Bi measured in East and West Antarctica and for a significant fraction of the Cd in East Antarctica. Nonetheless, global volcanic outgassing cannot account for the enriched values of Pb or As. Local volcanic outgassing from Mount Erebus may account for a significant fraction of the As and Cd in West Antarctica and for a significant fraction in East Antarctic glaze/dune areas. However, despite potential contributions from local and global volcanic sources, significant concentrations of Pb, Cd, and As remain across much of Antarctica.

Most importantly, this study provides a baseline from which changes in the chemistry of the atmosphere over Antarctica can be monitored under expected warming scenarios and continued intensification of industrial activities in the Southern Hemisphere.

2.2 Introduction

Deep ice cores from the high latitudes of both hemispheres provide us with valuable archives of past climate [*Jouzel et al.*, 1989; *Mayewski et al.*, 1993b], but the chemical proxies that they contain must be interpreted in the context of their geographic

location. For example, in Antarctica, the individual climate records contained in the Byrd and Taylor Dome deep ice cores do not necessarily reflect past conditions over the entire continent [*Masson et al.*, 2000]. There is considerable spatial variability between these deep-ice-core sites. Over-snow traverses, such as those conducted by the International Trans-Antarctic Scientific Expedition [*Mayewski et al.*, 2005b], provide us with the opportunity to collect a large number of shallow cores from broad geographic areas. These arrays provide the data needed, at a high enough spatial and temporal resolution, to form a more accurate assessment of the regional chemical and climate differences between deep core sites [*Bertler et al.*, 2005; *Dixon et al.*, in press; *Kaspari et al.*, 2004]. This paper presents chemistry data from shallow firn cores/snow pits (hereafter referred to as firn sections), and surface snow samples collected along the US ITASE-2002/2003 Byrd to South Pole traverse (ITASE-02), the US ITASE-2003/2004 South Pole to Taylor Dome traverse (ITASE-03), and the US ITASE-2006/2007 and 2007/2008 Taylor Dome to South Pole traverses (ITASE-06/07). We use these data to determine the spatial variability of chemical deposition over extensive and highly inaccessible areas of the Antarctic continent (Figure 2.1).

The ITASE-02 traverse started from Byrd Surface Camp, West Antarctica (80°S 120°W), and progressed southward (Figure 2.1), through the Transantarctic Mountains at the location known as "The Bottleneck", passing South Pole Station, ultimately ending up at a location ~100km beyond the South Pole in the direction of the Pole of Inaccessibility on the East Antarctic Plateau (89°S 60°E). The ITASE-03 traverse began at the South Pole and proceeded toward the interior of East Antarctica to the Automated Geophysical Observatory number 4 (03-2/AGO4, 82°S 96.76°E) passing through a glaze/dune area for

the last ~400km of the leg. From 03-2/AGO4 the traverse traveled northward through an extensive glaze/dune area, along the Transantarctic Mountain SEISmic (TAMSEIS) sensor line, passing directly through the Megadunes Camp (80.78°S 124.49°E), and finishing up at Taylor Dome (77.78°S 158.73°E). The ITASE-06/07 traverse started out from Taylor Dome and progressed southward parallel to, and approximately 300km to the west of, the Transantarctic Mountains ultimately ending up at the South Pole. From 06-4 to 07-3, the 06/07 traverse traveled through the eastern edge of the largest glaze/dune area in East Antarctica.

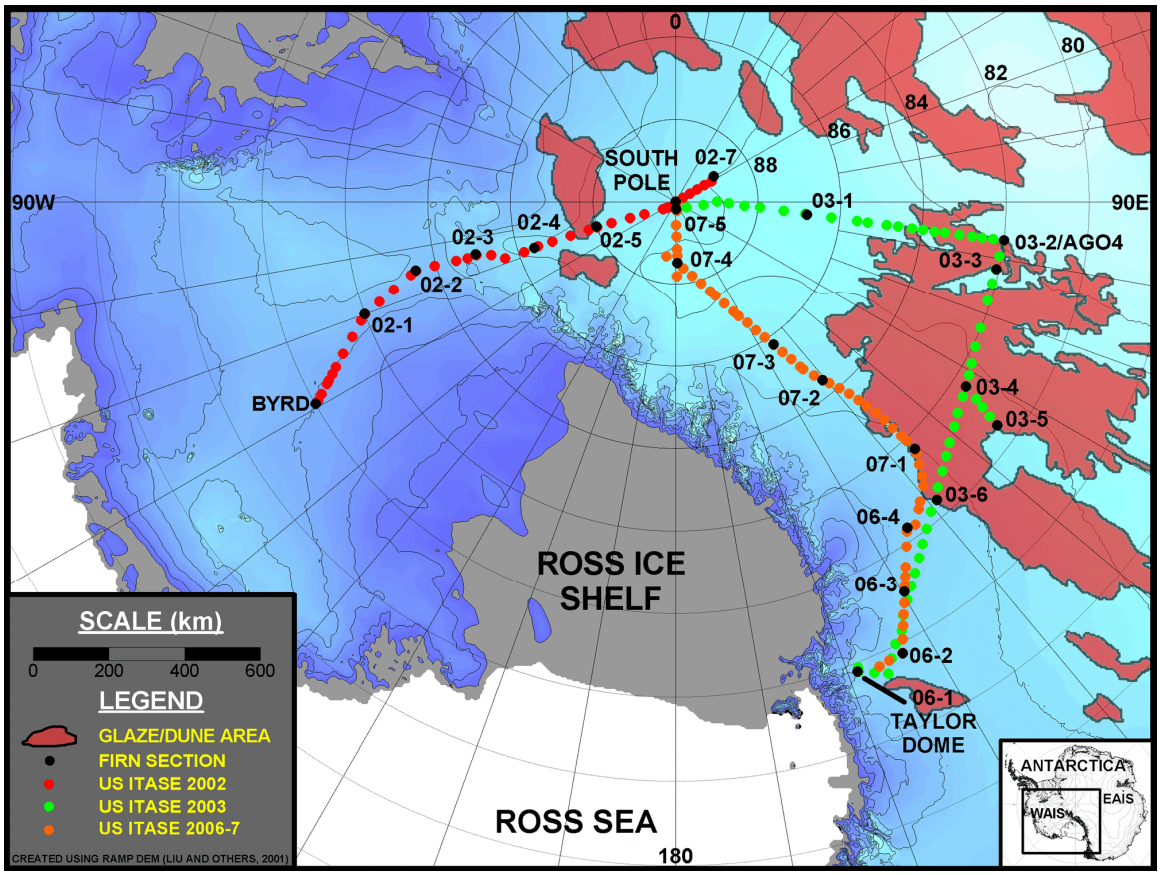

Figure 2.1. Polar stereographic map of Antarctica showing the location of surface snow samples and firn sections used in this study. Map also shows the location of known glaze/dune regions. WAIS = West Antarctic Ice Sheet; EAIS = East Antarctic Ice Sheet. Map created using the RAMP DEM [*Liu et al.*, 2001].

Since the very earliest trans-Antarctic expeditions, glaze/dune areas have been reported on the East-Antarctic Plateau [*Black and Budd*, 1964; *Lister and Pratt*, 1959], and characterized by extremely low accumulation [*Picciotto et al.*, 1970] and extensively recrystallized snow [*Giovinetto*, 1963]. However, it was not until the modern satellite remote sensing era that the full extent of these features became apparent. Swithinbank [1988] coined the term "megadunes" for large fields of dune-like features typical of the East Antarctic plateau. These fields cover more than 500,000 km^2 of the Antarctic ice sheet surface [*Fahnestock et al.*, 2000]. Megadunes typically have amplitudes of only a few meters, wavelengths of a few kilometers, and parallel crests (which can extend more than one hundred kilometers) oriented perpendicular to the regional katabatic wind direction [*Frezzotti et al.*, 2002a]. The leeward slope of each megadune consists of a glazed surface representing a long-term accumulation hiatus, while the windward slope is covered with accumulation-redistribution features in the form of severe sastrugi up to 1.5m high [*Frezzotti et al.*, 2002a]. Other glazed (non-megadune) surfaces, representing areas of nil or slightly negative snow accumulation, are also observed across extensive regions of the plateau [*Frezzotti et al.*, 2002b; *Goodwin*, 1990; *Watanabe*, 1978]. In this study we use an outline map from Bohlander and Scambos [2005] as a first step to determine which of our samples come from known Antarctic megadune regions (Figure 2.1). We then use statistical analysis of our chemical profiles to further infer surface conditions along our traverse routes.

Eight firn sections were either drilled or excavated along ITASE-02, six along ITASE-03, and nine along ITASE-06/07 (Table 2.1). The upper ~1-2.6m was sampled at each site (because this fragile upper section of the firn is often destroyed during transport)

and surface snow samples (upper 2cm) were collected every ~30-50 km along each traverse route (Figure 2.1). All samples are analyzed using an ion chromatograph (IC) for their soluble major ion content (Na^+, K^+, Mg^{2+}, Ca^{2+}, Cl^-, NO_3^-, SO_4^{2-}, $CH_3SO_3^-$ (Methylsulfonate: MS^-)). The surface snow samples are additionally analyzed for their stable oxygen isotopes ($\delta^{18}O$) by isotope ratio mass spectrometry (IRMS). All surface snow samples and several shallow firn sections (02-1, 02-5, South Pole, 03-1, 03-3, 06-2, 07-4, and 07-5; Table 2.1) are also analyzed for a suite of trace elements (Sr, Cd, Cs, Ba, La, Ce, Pr, Pb, Bi, U, As, Al, Ti, V, Cr, Mn, Fe, Co, and Li) by inductively coupled plasma sector field mass spectrometry (ICP-SFMS). The ICP-SFMS also measures the total Na, K, Mg, Ca, and S concentrations in each sample. The accuracy and precision of our IC, IRMS, and ICP-SFMS systems are mentioned later in this paper and discussed in more detail by Osterberg et al. [2006].

Lack of accumulation and extensive firn diagenesis at any site exhibiting glazed characteristics likely precludes that site from containing an easily interpreted, annually-resolved climate record [*Albert et al.*, 2004; *Fahnestock et al.*, 2000]. In addition, the unknown length of hiatus, possibly ranging from decades to centuries [*Scambos and Bauer*, 2006], represented by each glazed surface, presents a problem for a temporally-consistent surface snow sampling scheme across the continent. The majority of our surface snow samples and firn sections are collected in positive accumulation areas and therefore represent chemical concentrations typical of summer seasonal precipitation and multi-year averages, respectively (as discussed later). To minimize the possible concentration effects caused by glaze/dune hiatus surfaces, we only collected our surface samples from loosely-consolidated, accumulating snow drifts at all collection sites.

Location	Latitude (°N)	Longitude (°E)	Elevation (m)	Depth[a] (m)	Accumulation[b] (g cm^{-2} yr^{-1})	Age of Section[a] (Years AD)	Time Period Used[a] (Years AD)	Resolution[a] (cm)
ITASE-02								
02-Byrd	-80.009300	-119.424900	1530	0-1	(11)	2003-1998	2003-2000	2.3
02-1[c]	-82.000990	-110.008160	1746	0-1.8 (0.8-12.4)	19	2003-1998 (2001-1966)	2003-2000 (1975-1966)	4 (2.0-4.0)
02-2	-83.500781	-104.986806	1957	0-1.5	(19)	2003-1999	2003-2000	4
02-3	-85.000451	-104.995312	2396	0-1.7	(15)	2003-1999	2003-2000	4
02-4	-86.502500	-107.990313	2586	0-1.8	11	2003-1998	2003-2000	4.1
02-5[d]	-88.002153	-107.983333	2747	0-1.9 (1.1-9.1)	(11)	2003-1996 (1998-1967)	2003-2000 (1975-1967)	4.2 (1.7-2.3)
02-6/South Pole	-89.933250	144.393833	2808	0-2 (0.9-17.7)	(8)	2003-1991 (1997-1911)	2003-2000 (1975-1955)	2 (1.4-1.8)
02-7	-88.998900	59.974400	3000	0-1.7	8	2003-1993	2003-2000	2
ITASE-03								
03-1[d]	-86.840000	95.310000	3124	0-2.5 (2.5-21.2)	5	2004-1983 (1983-1768)	2004-2000 (1975-1955)	2 (1.4-2.9)
03-2/AGO 4	-82.010000	96.760000	3569	0-1.9	(3)	2004-1981	2004-2000	1.3
03-3[e]	-82.080000	101.960000	3444	2.1-15 (2.1-15)	3	1966-1737 (1966-1737)	1966-1955 (1966-1955)	1.5-2.5 (1.5-2.5)
03-4	-81.650000	122.600000	2966	0-1.9	(3)	2004-1981	2004-2000	1.2
03-5[f]	-80.780000	124.490000	2923	0-2.1	(3)	2004-1979	2004-2000	2.0
03-6	-80.390000	138.920000	2393	0-1	(3)	2004-1992	2004-2000	1.6
ITASE-06								
06-1/Taylor Dome	-77.880222	158.458222	2365	0-1.1	(11)	2007-2002	2006-2002	1.6
06-2	-77.781070	152.370500	2277	0-1.2 (0-1.2)	(11)	2007-2002 (2007-2002)	2006-2002 (2006-2002)	1 (1)
06-3	-79.036200	149.680300	2241	0-2.1	(11)	2007-2000	2006-2000	1.2 - 1.3
06-4	-80.308770	144.691980	2199	0-1.6	(8)	2007-1998	2006-2000	1.4
ITASE-07								
07-1	-81.658000	136.084000	2450	0-1.7	(8)	2008-1998	2006-2000	2
07-2	-84.395070	140.630800	2645	0-1.7	(8)	2008-1998	2006-2000	1.5
07-3	-85.781889	145.719484	2817	0-2.1	(8)	2008-1995	2006-2000	1.8 - 2.3
07-4	-88.509530	178.530790	3090	0-2.6 (0-1.4)	(8)	2008-1992 (2008-2000)	2006-2000 (2006-2000)	1.2 - 1.5 (1.2)
07-5	-89.782080	171.431810	2808	0-2.2 (0-1.7)	(8)	2008-1994 (2008-1998)	2006-2000 (2006-2000)	1.2 - 1.7 (1.2)

Table 2.1. Information for each ice core used in this study. Accumulation = mean annual accumulation; Resolution = sampling resolution; [a]values in brackets correspond to the firn sections used for ICP-SFMS analysis; [b]values in brackets are estimates; [c]no ICP-SFMS K analyses; [d]no ICP-SFMS K or Li analyses; [e]the top 2.1m of this core were not collected, no IC cation analyses; [f]no K values are reported for the upper portion of this firn section, the 1995-1985 period was used to calculate the K mean value and standard deviation.

2.3 Methodology

All sample-processing personnel wore non-particulating Tyvek suits, clean plastic gloves, and dust masks. The surface snow samples were collected wearing the same protective gear and always >100 m upwind of the traverse vehicles. Samples were only collected if the traverse vehicles could be determined not to have introduced any local contamination. All the ITASE-02 and ITASE-03 surface snow samples for major ion, stable isotope and trace element analysis were collected from the top 2 cm of a loosely consolidated, fresh snowdrift and transferred into two new Whirl-Pak bags using a de-ionized-ultra-pure-water (DI)-cleaned plastic scoop. The bags were immediately sealed and stored at –20°C. The ITASE-06/07 surface snow samples for major ion and stable isotope analysis were also collected using this method. However, the ITASE-06/07 surface snow samples for trace element analysis were collected directly into acid-cleaned 60 mL polypropylene Nalgene wide mouth jars and stored at -20ºC. No apparent difference in results was detected between the two analytical sampling plans.

The DI-cleaning process for vials and jars consists of a triple rinse in DI, immediately followed by an overnight soak in DI, and finally another triple rinse in DI before drying under a class-100 HEPA clean bench and capping. The DI-cleaning process for sampling equipment is identical to the aforementioned DI-cleaning process for vials with the addition of a thorough scrub with a 2% Citranox detergent solution beforehand (Citranox was not used on the sample containers or vials). The aci cleaning process consists of soaking in 10% trace metal grade HNO_3 for one week, triple-rinsed in DI, then DI-soaked for one week, triple-rinsed in DI, and finally dried under a class-100 HEPA clean bench and capped.

The bags containing surface snow samples were kept at –20°C. Each one was opened under a class-100 HEPA clean bench located in our main freezer and the snow was mounted on a plastic lathe (at this point the snow had sintered into a fairly solid block). The outermost 2-3 cm of each snow block was removed using a DI-cleaned ceramic blade. The sample was then handled using DI-cleaned plastic tongs and a further 2-3 cm was removed from each end. Each clean sample was split between two pre-cleaned 60 mL polypropylene Nalgene wide mouth jars. The first 60 mL jar, for major ion and stable isotope analysis, was DI-cleaned. The second 60 mL jar, for trace element analysis, was acid cleaned. The two sets of jars were then transferred to our clean room and allowed to melt overnight at room temperature. The major ion and stable isotope samples were poured into their respective vials for analysis. The trace element samples were each acidified to 1% with Optima double-distilled HNO_3 under a class-100 HEPA clean bench, capped, shaken, left to digest for one week, and then poured into a set of acid-cleaned polypropylene vials ready for analysis. Major ion, trace element, and stable isotope lab procedures follow those in [*Osterberg et al.*, 2006].

The majority of the firn sections were manually or electromechanically drilled, the cores subsequently being subsampled for major ion analysis on a DI-cleaned plastic core tray using a DI-cleaned plastic knife to cut the core into slices (several test cores were drilled beforehand in order to clean the drill barrel). Each subsample of core was placed inside a new Whirl-Pak plastic bag, sealed, and stored at -20ºC. Prior to analysis, the Whirl-Pak bags from each firn section were left to melt (upright in a clean lab) overnight. The following morning, under a class-100 HEPA clean bench, they were poured into DI-cleaned vials ready for major ion analysis. Firn section cores for trace

element analysis were melted using the University of Maine continuous melter system [*Osterberg et al.*, 2006].

Firn sections that were not drilled were collected from snow pits excavated using DI-cleaned plastic shovels and sampled using a DI-cleaned ultra-pure-nickel (Ni 270) blade. Each firn section snow pit sample for trace element analysis was collected directly into an acid-cleaned 60 mL polypropylene Nalgene wide mouth jar and treated in the same manner as the ITASE-06/07 surface snow trace element samples (above). Each firn section snow pit sample for major ion analysis was placed inside a new Whirl-Pak plastic bag, sealed and treated as the firn section core samples (above).

2.3.1 Chemistry Quality Control

We ran a series of method blanks, these are a series of vials prepared and treated in precisely the same way as the sample vials, the only difference being that they contain DI water instead of a snow sample. The results from the method blanks define our method detection limits, whereby the Method Detection Limit (MDL) for each element is equal to three times the standard deviation of that element in a series of method blanks. We used seven method blanks to calculate the MDL for our IC samples and eight for our ICP-SFMS MDL (Table 2.2).

The mean surface snow concentrations for each traverse year are above the mean blank concentrations and MDL for each IC ion and ICP-SFMS element (Table 2.2). Additionally, the MDL and mean blank concentrations for each ICP-SFMS element are similar to, and in most cases lower than, published values using similar methods and

identical/comparable instruments [*Barbante et al.*, 1999; *Knusel et al.*, 2003; *Krachler et al.*, 2005; *Osterberg et al.*, 2006]

The MDL, when expressed as a percentage of the mean surface snow sample concentration for each traverse year, is below 10% for the majority of the ions/elements (Table 2.2). For the ITASE-02 ions the MDL is 63%, 38%, and 20% of the mean concentrations for Mg, Ca, and Na, respectively. For the ITASE-03 ions, the MDL is 33% and 17% of Ca and Mg and for ITASE-06/07 the MDL is 35%, 32%, and 25% of Ca, K, and Mg ions, respectively (Table 2.2).

For the ITASE-02 elements the MDL is 61% and 59% of the Al and Fe; 47%, 34%, 33%, and 33% of the Co, Li, Cr, and As; and 18%, 18%, 16%, and 13% of the Ti, U, V, and Cd, respectively. For the ITASE-03 elements the MDL is 44%, 43%, 40%, and 28% of the Co, Cr, Li, and Al; 23%, 15%, 13%, 12%, and 10% of the Fe, Ti, Cd, V, and Ba, respectively. For ITASE-06/07 elements the MDL is 36% and 26% of the Li and Co; 13%, 11%, and 10% of the V, Al, and Fe, respectively. The MDL for the remaining elements is <10% of the mean surface snow concentration (Table 2.2).

2.3.2 Flux vs. Concentration

Ideally, we would view these data as chemical flux. However, it would not be accurate to correct these surface snow chemical concentration data for flux because we do not know when the precipitation occurred, or its volume. As a flux correction experiment we calculate accumulation rates along the traverse routes using a compilation of net surface mass balance data from [*Vaughan et al.*, 1999].

Ion/Element	Blank	MDL	ITASE-02 min-max (mean)	ITASE-02 MDLC (%)	ITASE-03 min-max (mean)	ITASE-03 MDLC (%)	ITASE-06/07 min-max (mean)	ITASE-06/07 MDLC (%)
IC								
Na (µg/L)	0.44	1.29	2.89 - 17.9 (6.38)	20	3.74 - 144 (25.7)	5	1.85 - 79.9 (13.6)	9
K (µg/L)	<0.33	0.33	3.00 - 3.95 (3.47)	9	3.17 - 6.77 (3.77)	9	0.84 - 1.95 (1.02)	32
Mg (µg/L)	0.4	0.51	0.49 - 2.42 (0.80)	63	0.56 - 21.0 (3.03)	17	0.68 - 8.04 (2.02)	25
Ca (µg/L)	0.79	0.63	0.71 - 4.60 (1.69)	38	0.58 - 6.25 (1.92)	33	0.76 - 7.97 (1.81)	35
MS (µg/L)	<0.43	0.43	3.02 - 24.3 (10.3)	4	6.73 - 50.5 (17.4)	2	1.13 - 52.9 (12.4)	4
Cl (µg/L)	2.68	1.78	8.25 - 40.4 (21.9)	8	27.5 - 381 (128)	1	11.1 - 185 (72.8)	2
NO3 (µg/L)	<0.35	0.35	27.6 - 554 (185)	<1	140 - 1869 (628)	<1	68.4 - 896 (388)	<1
SO4 (µg/L)	<0.76	0.76	24.3 - 95.8 (54.7)	1	57.6 - 478 (143)	1	14.7 - 140 (68.7)	1
ICP-SFMS								
Sr (ng/L)	0.23	0.23	0.67 - 33.0 (4.51)	5	1.55 - 98.1 (18.4)	1	2.21 - 115 (21.2)	1
Cd (ng/L)	0.12	0.040	0 - 2.90 (0.32)	13	0.017 - 1.13 (0.31)	13	0.11 - 6.76 (0.88)	5
Cs (ng/L)	0.0059	0.0029	0 - 0.14 (0.043)	7	0.047 - 0.51 (0.17)	2	0.053 - 0.45 (0.21)	1
Ba (ng/L)	0.35	0.63	0 - 76.6 (10.1)	6	0.78 - 30.3 (6.12)	10	1.19 - 94.0 (14.9)	4
La (ng/L)	0.0055	0.0074	0.024 - 0.66 (0.18)	4	0.13 - 1.64 (0.53)	1	0.031 - 1.00 (0.38)	2
Ce (ng/L)	0.18	0.0095	0.030 - 1.41 (0.35)	3	0.23 - 4.19 (1.11)	1	0.21 - 9.58 (1.24)	1
Pr (ng/L)	0.0074	0.0036	0.0042 - 0.17 (0.045)	8	0.017 - 0.38 (0.13)	3	0.022 - 0.28 (0.12)	3
Pb (ng/L)	0.36	0.076	0.39 - 8.60 (3.05)	3	0.69 - 24.3 (5.66)	1	0.60 - 35.8 (7.00)	1
Bi (ng/L)	0.013	0.0060	0 - 1.14 (0.17)	3	0.0021 - 0.86 (0.21)	3	0.0082 - 1.55 (0.15)	4
U (pg/L)	11.3	5.52	0 - 65.5 (30.2)	18	16.9 - 245 (81.4)	7	48.7 - 700 (117)	5
As (ng/L)	0.35	0.18	0.092 - 2.08 (0.54)	33	0.39 - 8.15 (2.17)	8	0.71 - 6.69 (2.98)	6
Li (ng/L)	3.14	1.88	4.40 - 9.75 (5.48)	34	2.26 - 6.93 (4.68)	40	0.68 - 10.3 (5.24)	36
Al (µg/L)	0.21	0.14	0.079 - 0.82 (0.23)	61	0.10 - 3.14 (0.51)	28	0.35 - 3.34 (1.28)	11
S (µg/L)	1.13	0.27	3.37 - 20.0 (8.20)	3	5.71 - 106 (26.4)	1	2.78 - 31.1 (14.0)	2
Ca (µg/L)	0.095	0.034	0.018 - 4.81 (0.47)	7	0 - 5.95 (1.21)	3	0.055 - 48.6 (3.62)	1
Ti (ng/L)	3.81	2.65	1.11 - 87.0 (14.8)	18	3.68 - 47.7 (17.8)	15	8.38 - 104 (32.8)	8
V (ng/L)	0.49	0.21	0.41 - 3.37 (1.29)	16	0.63 - 4.85 (1.72)	12	0.16 - 3.40 (1.54)	13
Cr (ng/L)	0.72	0.90	0.028 - 11.5 (2.75)	33	0.033 - 6.68 (2.11)	43	1.13 - 298 (15.3)	6
Mn (ng/L)	0.45	1.25	2.15 - 20.7 (6.21)	20	2.67 - 42.9 (15.8)	8	0.32 - 97.3 (16.4)	8
Fe (µg/L)	0.12	0.077	0 - 0.65 (0.13)	59	0.055 - 0.98 (0.33)	23	0.12 - 8.01 (0.78)	10
Co (ng/L)	0.17	0.19	0 - 3.03 (0.41)	47	0.0055 - 2.06 (0.44)	44	0.051 - 11.5 (0.74)	26
Na (µg/L)	0.38	0.30	2.52 - 43.4 (7.74)	4	0.97 - 108 (20.7)	1	3.21 - 94.3 (17.0)	2
Mg (µg/L)	0.42	0.24	8.31 - 28.7 (17.3)	1	3.27 - 32.4 (13.1)	2	1.01 - 7.21 (2.70)	9
K (µg/L)	0.26	0.038	0.82 - 7.61 (1.44)	3	0.33 - 5.15 (1.82)	2	0.39 - 3.92 (1.39)	3

Table 2.2. Method blanks and detection limits. Average method blank concentration (blank), method detection limit (MDL), minimum, maximum and mean sample concentration for each traverse year, and a MDL-mean concentration comparison (MDLC) for each surface snow IC ion and ICP-SFMS element measured in this study. MDLC = method detection limit as an approximate percentage of the mean ion or element concentration.

We use these accumulation values to apply a flux correction to the surface snow major ion concentration data (Figure 2.2). Of all the major ion curves, the flux correction only significantly affects the spatial trend of K in all traverse years, the reason being that spatially, this ion has extremely low concentration variability. After the flux correction, the resulting K curve looks almost identical to the accumulation curve (Figure 2.2). The only other change of note occurs in the ITASE-02 SO_4 and Cl curves, with the rise from 02-3 to 02-7 being subdued.

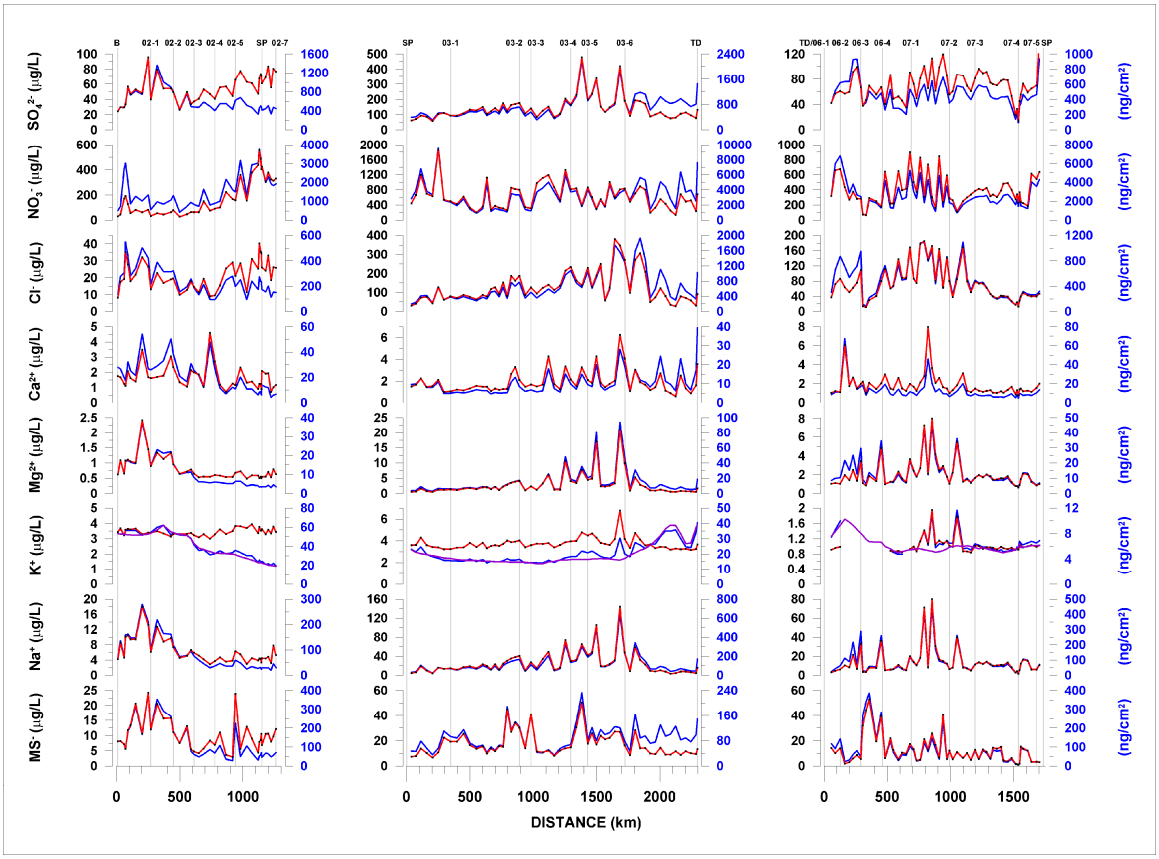

Figure 2.2. Surface snow major ion concentration (red) and flux (blue) versus distance for the ITASE-02 (left), ITASE-03 (middle) and ITASE-06/07 (right) traverses. Mean annual accumulation (purple) is shown on the K+ plot for comparison. Vertical lines indicate the locations of firn section collection sites along each traverse; B = Byrd; SP = South Pole; TD = Taylor Dome. Large vertical shaded areas behind plots highlight glaze/dune regions. Note that scales may vary between traverse years.

The spatial trends of the remaining ions do not change significantly enough to warrant using the flux correction, i.e. concentrations of sea-salt ions are already higher near the coast in West Antarctica and concentrations of all ions still remain high in the glaze/dune areas after the correction. So, for the remainder of this paper we will present and discuss chemical concentrations without a flux correction.

2.3.3 Sample Time Periods

The ITASE-02 traverse departed Byrd Surface Camp on December 7, 2002 and arrived at the South Pole on January 1, 2003. The first core of the ITASE-02 season was drilled at Byrd Surface Camp on December 1, 2002 and the last core of the season on January 4, 2003. The ITASE-03 traverse departed the South Pole on November 30, 2003, passed AGO4 on December 13th and arrived at Taylor Dome on January 20, 2004. The first core of the ITASE-03 season was drilled on December 6, 2003 and the last core of the season on January 21, 2004. The first leg of the ITASE-06/07 traverse left Taylor Dome on December 13, 2006 and finished in the Byrd Glacier Drainage on January 7, 2007. The first core of this season was drilled on November 23, 2006 and the last core of the season on January 8, 2007. The second leg of the ITASE-06/07 traverse departed the Byrd Glacier Drainage on November 17, 2007 and arrived at the South Pole on December 24, 2007. The first core of the season was drilled on November 21, 2007 and the last core was drilled on December 24, 2007.

Several of the firn cores are sub-annually dated based upon seasonal layers in the major ion time series. We approximately date the remaining firn sections using a firn-densification depth-age model. We estimate accumulation rates for the model based upon

nearby sub-annually dated cores combined with a net surface mass balance model [*Vaughan et al.*, 1999]. We use three different time periods from which to calculate the mean, and mean +/- 1 standard deviation concentrations in the firn sections: 2000-2006 for all the major ion data, 2000-2006 for the ITASE-06/07 ICPMS data, and 1955-1975 for the ITASE-02 and ITASE-03 ICPMS data. These time periods are chosen to best cover the existing overlap of firn chemistry data from each respective traverse. Not all firn sections wholly cover the chosen time periods, but all sections cover a minimum of at least three full years of data (see Table 2.1 for detailed info).

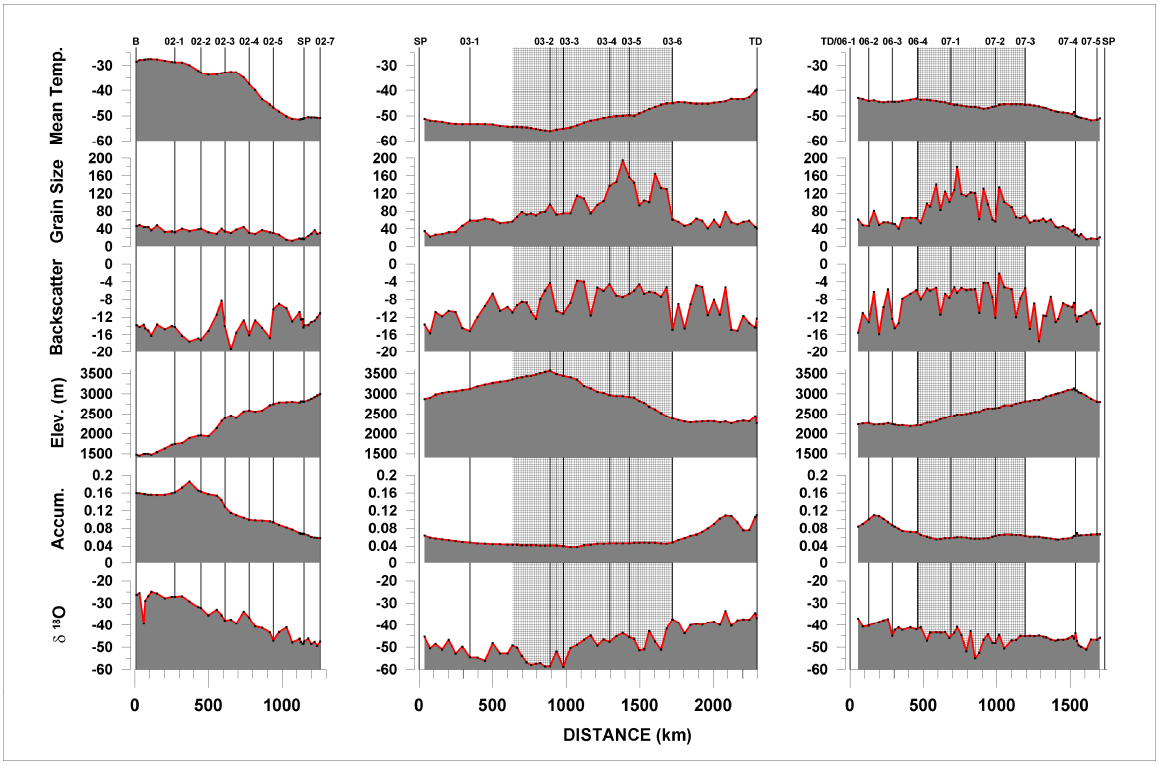

Figure 2.3. Surface snow $\delta^{18}O$, mean annual accumulation, surface elevation, RAMP microwave backscatter, MOA grain size and mean annual temperature (ºC). Physical parameters versus distance for the ITASE-02 (left), ITASE-03 (middle) and ITASE-06/07 (right) traverses. Vertical lines indicate the locations of firn section collection sites along each traverse; B = Byrd; SP = South Pole; TD = Taylor Dome. Large vertical shaded areas behind plots highlight glaze/dune regions.

To characterize environmental conditions we measure a set of physical parameters in addition to the chemistry at each sampling site (Figure 2.3). The physical measurements are: mean annual accumulation, calculated from the Vaughan et al. [1999] compilation of net surface mass balance; surface elevation, measured in the field by our on-board GPS system [*Hamilton and Spikes*, 2004]; mean annual temperature, calculated from an Antarctic compilation map created using a combination of instrumental mean annual temperatures and 10m downhole temperatures [*Dixon*, 2008]; RADARSAT-I Antarctic Mapping Project (RAMP) microwave backscatter [*Jezek et al.*, 2002; *Jezek*, 1999] and Moderate-resolution Imaging Spectroradiometer [*Justice et al.*, 2002; *Kaufman et al.*, 1998] Mosaic of Antarctica (MOA) grain size measurements [*Haran et al.*, 2005; *Scambos et al.*, 2007]. The RAMP measurements are extracted from the Antarctic Imaging Campaign-I (AIC-I) dataset. RAMP backscatter values, in decibels, represent the 1997 October mean normalized to an incidence angle of 27º (the center of the beam used most often in the RAMP 1997 AIC-I). The MOA snow grain size data are the mean optical grain size measurements, in microns, from November 5th to December 15, 2003.

2.4 Results and Discussion

2.4.1 Physical Parameters

Traditional pair-wise correlation between time series becomes difficult if three or more series are compared. Geophysical data sets are typically multidimensional (i.e. contain three or more related variables). A principal component analysis method called Empirical Orthogonal Function Analysis (EOF) compares multiple variates simultaneously and provides an organized description of the similarities and differences

among them. EOF analysis is a mathematical decomposition of a data set in terms of orthogonal basis functions (EOF modes) which are determined from the data. EOFs are designed to capture temporal variance using as few modes as possible. We order the EOFs such that the first mode (EOF 1) has the largest eigenvalue (percentage of the variance explained), the second mode (EOF 2) has the next largest eigenvalue, and so on.

a)

ITASE-02	EOF 1	EOF 2	EOF 3	EOF 4	EOF 5	EOF 6
	77.2	13	6.5	1.4	1.3	0.7
$\delta^{18}O$	91.3	0.8	-2.2	4.7	-0.9	-0.2
Accumulation	91.6	0.4	-3.5	-0.4	2.9	-1.1
Elevation	-91.1	-0.9	2.3	3	2.7	0
Backscatter	-27.5	71.7	-0.7	0	0	0
Grain Size	65.6	4.2	30.1	0	0	-0.1
Temperature	96	0.2	-0.1	0.1	0.9	2.7

b)

ITASE-03	EOF 1	EOF 2	EOF 3	EOF 4	EOF 5	EOF 6
	60.4	26.8	6.4	3.7	2.3	0.4
$\delta^{18}O$	83.3	5.9	0	-1.4	9.4	0
Accumulation	79.8	-1.8	4.1	14.3	0	0
Elevation	-89.2	-4.3	0.3	2.4	2.6	1.1
Backscatter	-11.7	67.8	20.2	-0.2	-0.1	0
Grain Size	-8.7	74.8	-12.9	3.5	0	0
Temperature	89.5	6.3	-0.8	-0.2	-1.9	1.4

c)

ITASE-06/07	EOF 1	EOF 2	EOF 3	EOF 4	EOF 5	EOF 6
	47.9	32.6	7.6	6.1	3.5	2.3
$\delta^{18}O$	-56.7	-15.9	7.3	19.8	-0.1	-0.2
Accumulation	-36.6	-43	6	-9.5	3.7	1.2
Elevation	85.5	0	3.6	3.5	0.2	7.3
Backscatter	-7	68.4	19.7	-2.3	-2.7	0
Grain Size	-20.2	66.6	-0.6	1.5	11.1	0.1
Temperature	-81.8	1.5	-8.2	0	-3.2	5.3

Table 2.3. EOF tables of physical traverse data. EOF tables of physical traverse data and δ18O as measured in the surface snow samples for a) ITASE-02, b) ITASE-03, and c) ITASE-06/07. Accumulation = mean annual accumulation; Elevation = surface elevation; Backscatter = RAMP microwave backscatter; Grain Size = MOA grain size; Temperature = mean annual temperature.

Typically, the first few EOF modes capture the majority of the overall variability in the data set and this is what makes EOF analysis such a useful tool for analyzing large, multidimensional, statistically- related data sets.

We examined each set (ITASE-02, -03, and -06/07) of physical traverse data (as described above) using EOF analysis (physical EOF). In each physical EOF we also included the $\delta^{18}O$ as measured in the surface snow samples (Table 2.3a, b, c; Figure 2.4). The first EOF in each case exhibits a strong association between $\delta^{18}O$, elevation and mean annual temperature. In addition, physical EOF 1 of ITASE-02 reveals a strong association between all parameters except backscatter (Table 2.3a). The association is in the same direction for all parameters except elevation. The backscatter is loaded primarily on physical EOF 2, the curve of which exhibits significant variability but no strong trend (Figure 2.4). The physical EOF of ITASE-03 looks very similar to the ITASE-02 physical EOF except that backscatter and grain size are both positively loaded on physical EOF 2 (Table 2.3b). The curve of ITASE-03 physical EOF 2 shows quite clearly how the backscatter and grain size increase towards the interior of East Antarctica and are highest in the glaze/dune area between 03-2 and 03-6 (Figure 2.4).

The ITASE-06/07 physical EOF is very similar to the ITASE-03 physical EOF except that 43% of the accumulation is inversely loaded onto physical EOF 2 along with the majority of both backscatter and grain size (Table 2.3c). The curve of the ITASE-06/07 physical EOF 2 (Figure 2.4) also indicates quite clearly how the backscatter and grain size are highest between 06-4 and 07-3, which is the part of the traverse that skirts/overlaps a large glaze/dune area. Although the ITASE-06/07 traverse is only shown to pass through known glaze/dune areas between 06-4 and 07-2 (Figure 2.1), we think the traverse route passes through several other glazed, non-dune areas based upon our field observations.

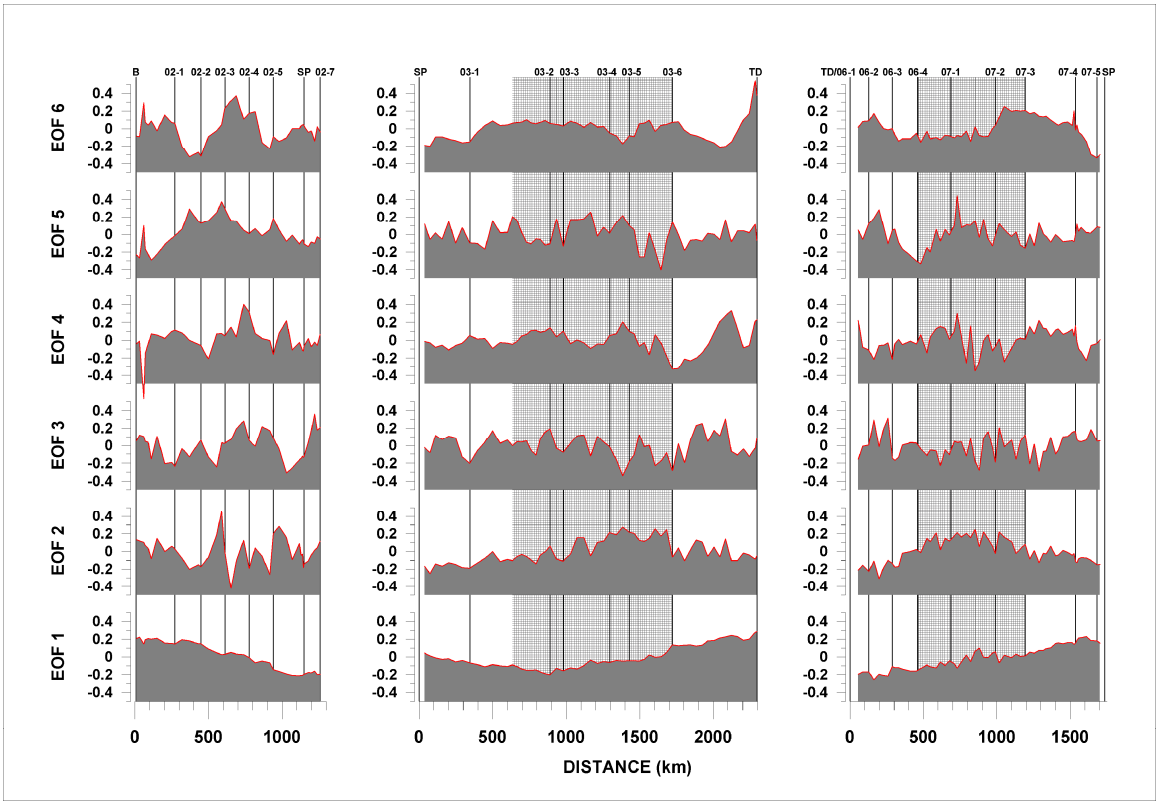

Figure 2.4. Physical EOF loading patterns versus distance for the ITASE-02 (left), ITASE-03 (middle) and ITASE-06/07 (right) traverses. Vertical lines indicate the locations of firn section collection sites along each traverse; B = Byrd; SP = South Pole; TD = Taylor Dome. Large vertical shaded areas behind plots highlight glaze/dune regions.

2.4.2 Seasonality of the Samples

High seasonal Na^+ concentrations in Antarctic ice cores are considered to be a deposition timing indicator of the turbulent winter-spring Antarctic atmosphere [*Legrand and Mayewski*, 1997]. Relative to the seasonal variability of Na^+, which is represented in Figure 5 by the mean +/- 1 standard deviation concentrations in the firn sections collected along the traverse routes, the surface snow Na^+ concentrations are low from Byrd to 03-1. Between 03-2 and 03-6 the surface snow Na^+ concentrations range between mean and high, relative to the seasonal variability. This is likely a consequence of sampling in

glazed/dune areas. Beyond 03-6, The Na concentrations vary between mean and low values up to Taylor Dome.

Surface snow Na^+ concentrations along the ITASE-06/07 traverse remain low relative to the seasonal variability from Taylor Dome to South Pole apart from three of peaks (06-3, 06-4, and one between 07-2 and 07-3) exhibiting mean values and a short section between 07-1 and 07-2 where concentrations are high (figure 2.5). However, all of these higher Na^+ concentrations occur in glazed or glaze/dune areas and are not representative of mean summer concentrations.

Peaks in SO_4^{2-} are observed to occur in the sunlit summer months as photosynthetic organisms prosper in the surface ocean surrounding Antarctica [*Legrand and Mayewski*, 1997]. Relative to the seasonal variability of SO_4^{2-} concentrations in the upper meters of firn, the surface snow SO_4^{2-} concentrations start out slightly below mean at Byrd, quickly increasing to high values, and then fluctuating between mean and high values from 02-1 to South Pole to Taylor Dome (Figure 2.5). Several exceptionally high values occur between 03-2 and 03-6, a huge East Antarctic glaze/dune area (Figure 2.1). The high concentrations observed in the glaze/dune areas are most likely a result of extremely low or slightly negative accumulation in combination with summer influx of fresh SO_4^{2-} to the hiatus surface. Therefore, the surface samples from glaze/dune areas likely represent concentrated values.

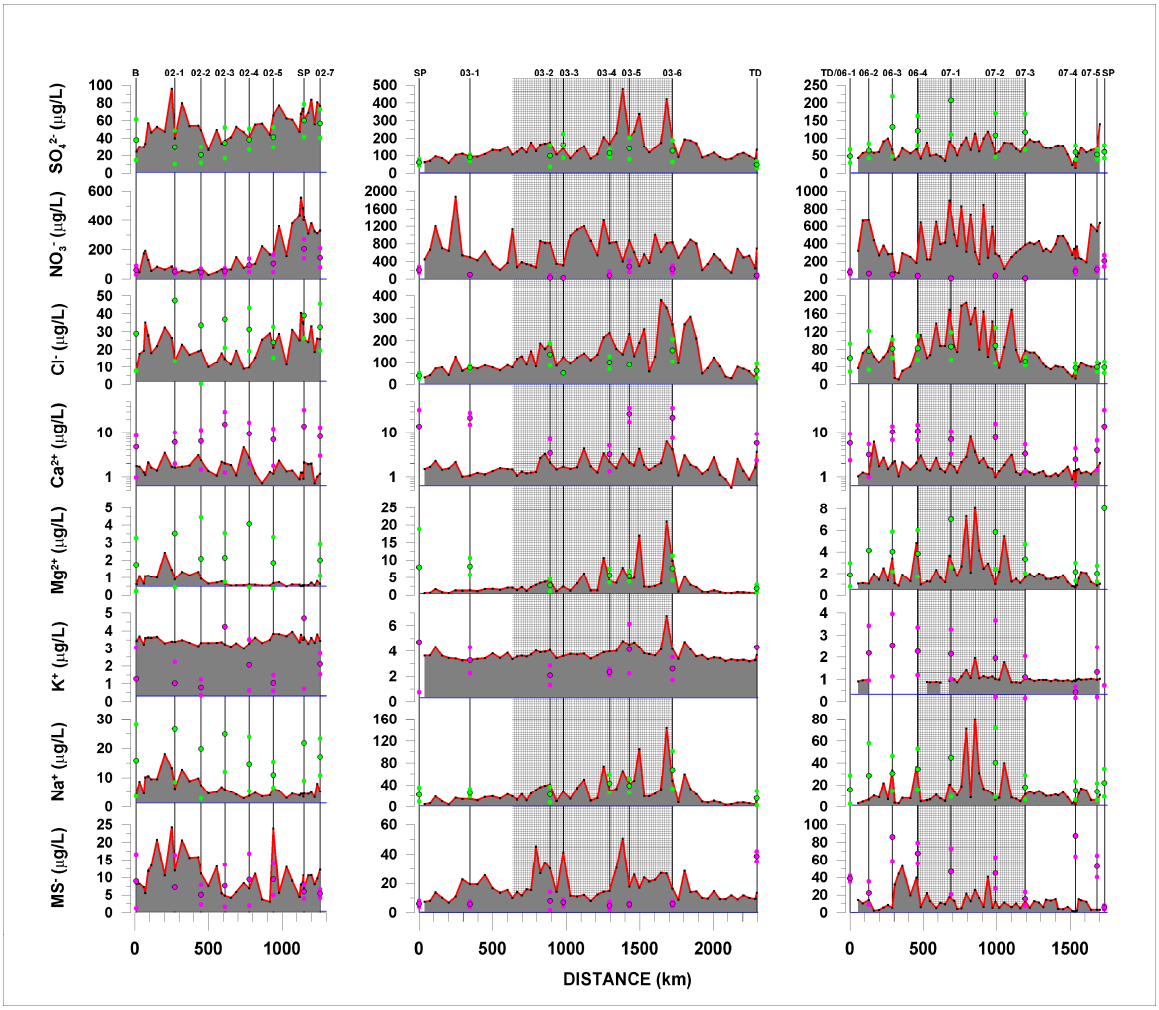

Figure 2.5. Surface snow major ion concentration versus distance for the ITASE-02 (left), ITASE-03 (middle) and ITASE-06/07 (right) traverses. Vertical lines indicate the locations of firn section collection sites along each traverse; B = Byrd; SP = South Pole; TD = Taylor Dome. The three (pink or green) dots in line with each firn collection site indicate the mean (black outline) and +/- 1 standard deviation concentrations in that firn section (if the lower dot is not visible its value is below zero). Large vertical shaded areas behind plots highlight glaze/dune regions. Horizontal (blue) lines signify detection limits. Note that scales may vary between traverse years.

Along the ITASE-06/07 traverse, surface snow concentrations of SO_4^{2-} are around the mean firn level between Taylor Dome and 06-3. In the glaze/dune areas between 06-3 and 07-3, surface snow concentrations of SO_4^{2-} are low compared to mean firn values. This is in contrast to the ITASE-03 glaze/dune samples which exhibit unusually high

values. ITASE-06/07 surface snow SO_4^{2-} concentrations return to mean/high values between 07-4 and South Pole. The surface snow concentration differences between the ITASE-03 and ITASE-06/07 glaze/dune areas may simply be a result of precipitation differences between the traverse years and/or the fact that during the ITASE-03 traverse we pass directly through the center of an extremely well-developed glaze/dune field and during ITASE-06/07 we skirt the periphery of the aforementioned field.

2.4.3 Major Ions

All the major ions, with the exception of K^+ and Ca^{2+}, exhibit lower summer surface snow concentrations in West Antarctica compared to East Antarctic non-glaze/dune areas (Table 2.4). Non-glaze/dune surface snow Ca^{2+} concentrations exhibit similar concentrations across Antarctica. All major ion surface snow concentrations from glaze/dune areas are above those from non-glaze/dune areas (Table 2.4). The sensitive nature of the IC instrument calibration for K^+, which must be performed for each sample run, results in background concentrations that can vary by as much as +/- 1 ppb between runs. This variability, although considered negligible when analyzing relatively high concentrations, becomes significant as the sample concentration approaches the detection limit (as is such with K^+ collected on the Antarctic plateau). However, K^+ analyses from a single instrument run, such as ITASE-02 and ITASE-03, can be compared to each other with relatively high confidence. The ITASE-06/07 K^+ samples were run separately and therefore must be interpreted separately. Despite this limitation, it is still clear that K^+ concentrations in ITASE-06/07 glaze/dune areas are elevated relative to ITASE-06/07 non-glaze/dune regions.

Surface Snow min-max (mean)	Na (ug/L)	K (ug/L)	Mg (ug/L)	Ca (ug/L)	MS (ug/L)	Cl (ug/L)	NO3 (ug/L)	SO4 (ug/L)
ITASE-02	2.89 - 17.9 (6.38)	3.00 - 3.95 (3.47)	0.49 - 2.42 (0.80)	0.71 - 4.60 (1.69)	3.02 - 24.3 (10.3)	8.25 - 40.4 (21.9)	27.6 - 554 (185)	24.3 - 95.8 (54.7)
ITASE-03 (non-glaze/dune)	3.64 - 59.2 (13.6)	3.17 - 4.72 (3.54)	0.56 - 5.35 (1.36)	0.58 - 3.58 (1.60)	6.73 - 28.2 (13.3)	27.5 - 307 (90.7)	140 - 1869 (569)	57.6 - 194 (107)
ITASE-03 (glaze/dune)	10.1 - 144 (37.3)	3.34 - 6.77 (3.98)	1.06 - 21.0 (4.64)	1.07 - 6.25 (2.24)	8.04 - 50.5 (21.4)	59.4 - 381 (164)	262 - 1330 (685)	81.3 - 478 (177)
ITASE-06/07 (non-glaze/dune)	1.85 - 36.3 (10.6)	0.91 - 1.03 (0.97)	0.68 - 4.82 (1.60)	0.76 - 6.09 (1.56)	1.13 - 52.9 (12.3)	11.1 - 110 (47.2)	68.4 - 673 (358)	14.7 - 140 (65.8)
ITASE-06/07 (glaze/dune)	5.06 - 79.9 (17.7)	0.84 - 1.95 (1.07)	0.98 - 8.04 (2.59)	0.98 - 7.97 (2.16)	4.43 - 40.6 (12.5)	37.8 - 185 (108)	116 - 896 (428)	34.6 - 119 (72.8)

Firn Sections (mean)	Na (ug/L)	K (ug/L)	Mg (ug/L)	Ca (ug/L)	MS (ug/L)	Cl (ug/L)	NO3 (ug/L)	SO4 (ug/L)
Byrd (2000-2003)	15.81	1.27	1.73	4.73	8.88	28.97	60.60	37.89
02-1 (2000-2003)	26.62	1.03	3.51	6.03	7.22	47.40	50.39	29.54
02-2 (2000-2003)	19.81	0.80	2.09	6.36	5.10	33.61	45.58	20.64
02-3 (2000-2003)	24.92	4.24	2.14	15.34	7.66	36.95	51.97	34.49
02-4 (2000-2003)	14.62	2.07	4.07	9.42	9.42	31.25	94.11	38.65
02-5 (2000-2003)	10.85	1.06	1.84	6.89	9.51	24.09	105.32	41.13
02-6/SP (2000-2003)	21.78	4.72	8.05	13.84	5.94	39.13	205.04	60.06
02-7 (2000-2003)	17.07	2.12	2.01	8.02	5.37	32.60	144.00	56.83
03-1 (2000-2004)	25.01	3.27	8.26		5.77	74.61	93.08	86.98
03-2/AGO4 (2000-2004)	22.37	2.08	2.79	3.44	7.99	137.08	30.28	97.37
03-3 (1955-1966)					6.88	52.23	19.37	160.97
03-4 (2000-2004)	42.44	2.32	5.59	3.20	4.69	100.03	76.19	112.78
03-5 (2000-2004)	38.59	4.17	5.46		5.64	89.41	286.70	140.26
03-6 (2000-2004)	67.05	2.59	7.71		5.92	156.52	219.63	125.71
06-1/TD (2002-2006)	15.55	4.29	1.88	5.80	38.54	61.17	76.88	47.56
06-2 (2001-2006)	28.41	2.19	4.13	3.18	22.32	77.20	61.10	62.89
06-3 (2000-2006)	30.36	2.55	4.02	10.26	85.96	82.37	49.72	132.43
06-4 (2000-2006)	34.24	2.27	3.85	10.80	67.70	83.07	35.90	121.51
07-1 (2000-2006)	44.73	2.14	7.01	6.93	46.69	87.28	7.95	207.14
07-2 (2000-2006)	40.34	1.95	5.83	7.72	44.91	88.60	36.23	108.14
07-3 (2000-2006)	17.74	1.10	3.36	3.32	15.72	53.16	7.86	117.28
07-4 (2000-2006)	14.69	0.42	2.16	2.50	87.33	37.79	87.05	58.64
07-5 (2000-2006)	13.74	1.34	1.99	3.93	52.54	39.64	108.69	52.20

Table 2.4. Major ion concentrations for surface snow samples and firn sections.

a)

ITASE-02	EOF 1	EOF 2	EOF 3	EOF 4	EOF 5	EOF 6	EOF 7	EOF 8
	49.7	18.5	8.5	7.5	5.7	3.2	2.7	1.7
$\delta^{18}O$	90.8	0.6	-1.1	0.0	0.2	-0.6	0.3	0.9
Accumulation	89.9	0.2	-2.5	-0.2	0.0	-0.3	-0.5	2.2
Elevation	-83.3	-1.7	5.6	3.8	-0.1	0.0	0.0	-3.3
Backscatter	-25.1	1.4	-8.8	12.7	44.6	2.2	-4.6	0.5
Grain Size	61.2	-1.7	-1.7	-0.1	1.4	24.5	7.0	-1.8
Temperature	94.4	-0.3	-0.9	-0.5	0.0	0.1	0.0	0.5
Na (ug/L)	41.6	48.9	2.2	-1.2	0.5	0.0	-1.6	-2.7
K (ug/L)	-17.1	29.7	-27.4	-0.6	4.1	-8.5	11.1	-1.4
Mg (ug/L)	43.6	38.5	7.0	-1.1	1.8	-0.3	-3.9	-2.2
Ca (ug/L)	16.5	-0.2	53.8	5.5	13.7	-1.9	7.2	1.0
Cl (ug/L)	-20.8	42.9	1.4	-28.0	0.3	2.3	0.1	1.6
NO3 (ug/L)	-78.3	4.8	0.8	-7.5	0.2	0.7	0.1	4.2
SO4 (ug/L)	-25.3	46.2	3.4	9.2	-5.7	3.2	0.6	0.0
MS (ug/L)	8.4	41.5	-2.8	33.9	-7.7	0.0	0.1	1.4

b)

ITASE-03	EOF 1	EOF 2	EOF 3	EOF 4	EOF 5	EOF 6	EOF 7	EOF 8
	42.59	25.70	9.06	7.62	4.64	3.23	2.15	1.56
$\delta^{18}O$	-5.13	82.44	0.01	2.79	-0.24	-1.21	-2.47	0.40
Accumulation	-27.99	54.78	-1.19	-0.20	-0.06	-2.86	6.42	0.00
Elevation	2.92	-89.94	0.20	-0.43	-1.69	-0.94	0.01	-0.07
Backscatter	30.77	-0.91	-0.05	50.05	-9.24	0.21	7.49	0.59
Grain Size	48.76	-0.06	-10.54	27.16	1.18	-2.63	-4.85	-1.23
Temperature	-2.25	91.89	-1.02	0.64	1.45	0.20	0.01	-0.20
Na (ug/L)	87.74	3.05	0.26	-3.18	-2.76	-0.01	-0.01	-0.04
K (ug/L)	75.55	4.11	-0.11	-2.84	-0.02	0.43	-0.38	15.09
Mg (ug/L)	76.64	6.61	0.76	-4.51	-6.82	0.01	-0.25	-1.34
Ca (ug/L)	58.32	12.08	9.08	-6.59	-1.03	-2.37	2.70	-1.46
Cl (ug/L)	56.97	3.38	2.54	0.80	11.49	22.03	0.48	-0.89
NO3 (ug/L)	9.03	-0.33	66.86	4.44	10.97	-7.15	-0.02	0.26
SO4 (ug/L)	79.52	3.69	-5.96	-0.45	-0.07	-1.25	-0.93	-0.22
MS (ug/L)	34.67	-6.46	-28.29	-2.56	17.90	-3.88	4.02	0.10

c)

ITASE-06/07	EOF 1	EOF 2	EOF 3	EOF 4	EOF 5	EOF 6	EOF 7	EOF 8
	30.3	24.9	13.1	8.7	5.7	4.9	3.9	2.4
$\delta^{18}O$	-30.2	-52.0	4.2	0.2	1.1	0.0	1.6	1.0
Accumulation	-17.5	-33.5	-2.0	29.4	-3.0	-0.8	6.2	0.1
Elevation	-0.4	87.2	1.3	-0.4	-0.7	0.9	1.5	0.1
Backscatter	34.0	-8.2	4.2	-24.7	-0.7	5.0	14.1	-4.4
Grain Size	40.5	-19.2	6.5	-19.8	0.0	-1.6	0.5	4.4
Temperature	0.6	-77.6	-1.1	-2.0	1.5	-6.6	-0.2	1.4
Na (ug/L)	66.3	0.0	-17.5	6.5	-2.4	-2.7	0.0	-1.2
K (ug/L)	39.7	35.9	0.5	0.0	0.1	-2.5	0.0	13.4
Mg (ug/L)	73.6	-0.4	-15.2	2.5	-1.9	-1.5	0.0	-0.4
Ca (ug/L)	17.0	-16.0	7.1	6.2	-24.4	23.5	-1.4	2.9
Cl (ug/L)	63.5	-7.6	10.3	1.7	0.3	-2.3	-2.9	-2.7
NO3 (ug/L)	5.0	-0.3	66.1	7.7	7.3	0.2	-5.7	-0.9
SO4 (ug/L)	33.6	0.5	-0.3	17.3	27.5	5.4	11.7	0.5
MS (ug/L)	2.0	-10.6	-47.5	-3.7	8.8	15.9	-8.1	0.1

Table 2.5. EOF tables of physical traverse data, $\delta^{18}O$ and major ions. Measured in the surface snow samples for a) ITASE-02, b) ITASE-03, and c) ITASE-06/07. Accumulation = mean annual accumulation; Elevation = surface elevation; Backscatter = RAMP microwave backscatter; Grain Size = MOA grain size; Temperature = mean annual temperature.

2.4.3.1 Major Ion EOF

To assess spatial associations between the major ions and the physical environment for each traverse we ran an EOF (ion EOF) with the following parameters for each traverse: $\delta^{18}O$, accumulation, elevation, backscatter, grain size, mean annual temperature, Na^+, K^+, Mg^{2+}, Ca^{2+}, Cl^-, NO_3^-, SO_4^{2-}, and MS^-.

The chemistry in Antarctic snow arrives in a variety of forms (e.g. aerosols, particles, and gases) and each of these arrives via an atmospheric transport pathway. For example, NO_3^- and Cl^- both have stratospheric sources and therefore travel though the stratosphere. But Cl^- also has an oceanic source and therefore also travels through the planetary boundary layer and free troposphere. For ease of discussion, from this point onward we will refer to the stratospheric pathway as upper-atmosphere and the planetary boundary layer and free tropospheric pathways as lower-atmosphere.

The first ion EOF for ITASE-02 (Table 2.5a) essentially captures the first ITASE-02 physical EOF (Table 2.3a) along with ~40% each of Na^+ and Mg^{2+} and more than 78% of NO_3^-. The ITASE-02 physical EOF 1 data show that as elevation increases, so does NO_3^-, and at the same time the sea salt ions (Na^+ and Mg^{2+}) decrease (Figure 2.6). The decrease of the sea salt ions is to be expected because distance from the coast is also increasing and the increase in the NO_3^- is expected because it has an upper-atmospheric source. Previous studies by Kreutz and Mayewski [1999] and Bertler et al. [2005] show a similar relationship between elevation, accumulation, NO_3^-, Na^+, and Mg^{2+}.

The ITASE-02 ion EOF 2 captures the second mode of behavior in the sea salt ions (Na^+ = 49%, K^+ = 30%, Mg^{2+} = 39%, Cl^- = 43%, SO_4^{2-} = 46% and MS = 42%; Table 2.5a). The structure of the second mode shows values higher between Byrd and 02-2,

dipping between 02-2 and 02-5, then rising again and remaining high from 02-5 to 02-7 (Figure 2.6). However, the individual ion concentrations do not all exhibit such a pronounced double-peak structure (Figure 2.5). SO_4^{2-} and Cl^- display the double-peak the strongest, confirming that their dominant sources are different in East and West Antarctica, upper-atmospheric and lower-tropospheric marine, respectively [*Legrand and Mayewski*, 1997]. K^+ exhibits a slightly pronounced, although weak, second peak (slightly stronger upper atmospheric source) and Na^+, Mg^{2+} and MS all have a much stronger first peak (stronger marine source). Major ion spatial variability maps in Bertler et al. [2005] exhibit a similar spatial pattern, with the multiple-source signature being more pronounced in the SO_4^{2-} and Cl^- pattern than in Na^+ and Mg^{2+}.

The third ITASE-02 ion EOF (Table 2.5a) captures 54% of the Ca^{2+} behavior, revealing that the greatest variability and the largest peaks occur in West Antarctica (Figure 2.6). This highlights the slightly variable nature of Ca^{2+} deposition and input timing and emphasizes its dominant lower-tropospheric transport pathway [*Dixon et al.*, in press].

The first EOF for ITASE-03 major ions captures the majority of the chemistry signal (Table 2.5b), including a significant percentage of all the ions except NO_3^-. A significant percentage of accumulation (28%), grain size (49%) and backscatter (31%) are also included in this first ITASE-03 ion EOF. The weak accumulation association in this EOF serves as additional proof that a chemistry-flux correction in this area is not justified. The EOF structure exhibits a steady rise from South Pole to 03-2, the rate of rise then increases along with the magnitude of the variability from 03-2 to 03-6. A sudden drop around 03-6 leads into a steady decline all the way to Taylor Dome (Figure 2.6).

This pattern suggests a strong positive association between concentration and grain size for all ions except NO_3^- in this area of East Antarctica and also highlights the effect of glaze/dune areas on chemistry.

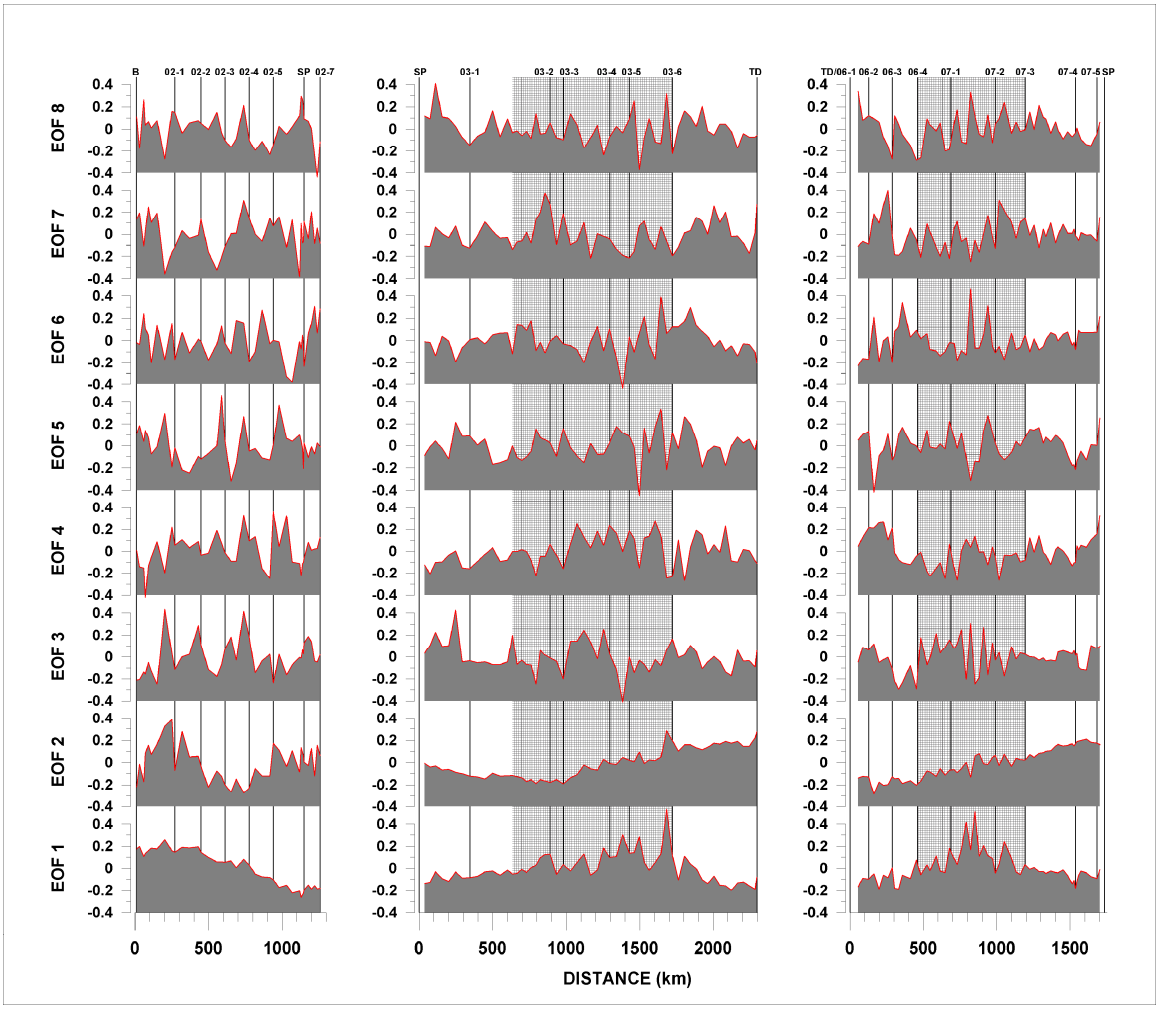

Figure 2.6. Ion EOF loading patterns versus distance for the ITASE-02 (left), ITASE-03 (middle) and ITASE-06/07 (right) traverses. Vertical lines indicate the locations of firn section collection sites along each traverse; B = Byrd; SP = South Pole; TD = Taylor Dome. Large vertical shaded areas behind plots highlight glaze/dune regions.

The second ITASE-03 ion EOF (Table 2.5b) is essentially the same as the first ITASE-03 physical EOF (Table 2.3b). The third ITASE-03 ion EOF (Table 2.5b) captures the majority (67%) of the NO_3^-, the structure of which exhibits two large peaks

close to South Pole followed by increased variability in the glaze/dune areas without a strong concentration trend (Figure 2.6). This EOF again highlights the strong upper-atmospheric NO_3^- source resulting in high concentrations all over East Antarctica. It also draws attention to the increased concentrations near the South Pole which may be a result of station-associated anthropogenic activity.

The fourth ITASE-03 ion EOF (Table 2.5b) captures the remainder of the backscatter and grain size operating together. The pattern of this ion EOF shows both parameters increasing in the East Antarctic glaze/dune areas (Figure 2.6), meaning that some fraction of the physical variability (mainly backscatter) in the glaze/dune areas is not reflected at all in the chemical concentrations.

Overall, the ITASE-06/07 ion EOF is similar to the ITASE-03 ion EOF, but with a few subtle differences. The First ITASE-06/07 ion EOF (Table 2.5c) captures a strong sea salt ion signal (Na^+ = 66%, K^+ = 40%, Mg^{2+} = 74%, Cl^- = 64% and SO_4^{2-} = 34%) in combination with 41% of grain size, 34% of backscatter, and 30% of the $\delta^{18}O$ which is the only negatively associated variate in this EOF. The ITASE-06/07 ion EOF 1 (Figure 2.6) structure shows a steady rise from Taylor Dome, peaking between 07-1 and 07-2, followed by a steady decline all the way to South Pole. The peak between 07-1 and 07-2 coincides with the glaze/dune overlap area, so we can again conclude that the widespread hiatus surfaces in this area of East Antarctica act to increase concentrations in the majority of the major ions and at the same time slightly increase $\delta^{18}O$ fractionation.

The second ITASE-06/07 ion EOF (Table 2.5c) is essentially the same as the first ITASE-06/07 physical EOF (Table 2.3c) but it also includes 36% of the K^+, suggesting that as elevation increases, so does K^+ (Figure 2.6). This association with K^+ may be a

by-product of the missing K^+ data (Figure 2.5). However, as the ITASE-02 ion EOF 2 (Table 2.5a) suggests, in the absence of a marine source (as is common during summer months on the plateau) K^+ seems to have a preferential source/transport pathway through the upper-atmosphere, most likely as long-traveled fine-grained terrestrial dust particles.

The third ITASE-06/07 ion EOF (Table 2.5c) captures the majority (66%) of the NO_3^- operating inversely with the majority (48%) of the MS, the structure of which exhibits significant variability between 06-4 and 07-3 (Figure 2.6), most likely related to the glaze/dune area. The inverse association between these two ions reflects the separate source for each, NO_3^- has an upper-atmospheric source and MS has a mid- to lower-tropospheric marine source.

2.4.4 Trace Elements

The majority of the mean surface snow trace element concentration data are at, or below, the multi-year mean values calculated from the firn sections (Figure 2.7, 2.8, & 2.9). This suggests that the surface snow concentrations presented here are a conservative estimate of Antarctic values for the majority of the trace elements. Four of the elements (Cs, S, Mg, and K) have no previously published data to compare with (Table 2.6), this is because S, Mg, and K are typically measured in their soluble forms by IC and are not often measured in their total form by ICP-SFMS analysis. Previous studies of Cs measure only one isotope, ^{137}Cs [*Pourchet et al.*, 1997; *Sbrignadello et al.*, 1994], not total Cs. The measurements of total Cs in this study may be the first analyses of this element conducted over extensive regions of Antarctica.

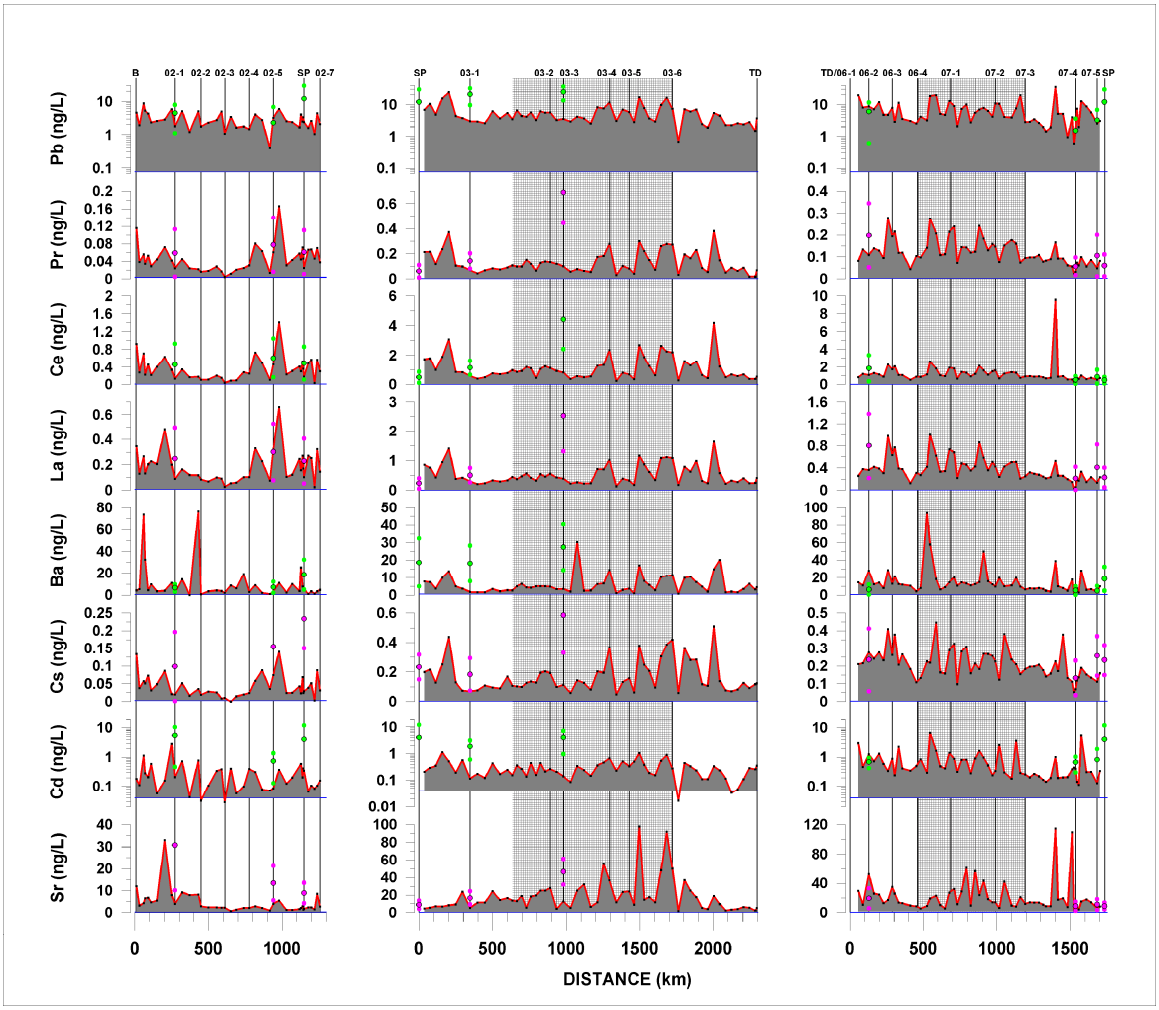

Figure 2.7. Surface snow trace element concentration versus distance for the ITASE-02 (left), ITASE-03 (middle) and ITASE-06/07 (right) traverses. Vertical lines indicate the locations of firn section collection sites along each traverse; B = Byrd; SP = South Pole; TD = Taylor Dome. The three (pink or green) dots in line with each firn collection site indicate the mean (black outline) and +/- 1 standard deviation concentrations in that firn section (if the lower dot is not visible its value is below zero). Large vertical shaded areas behind plots highlight glaze/dune regions. Horizontal (blue) lines signify detection limits. Note that scales may vary between traverse years.

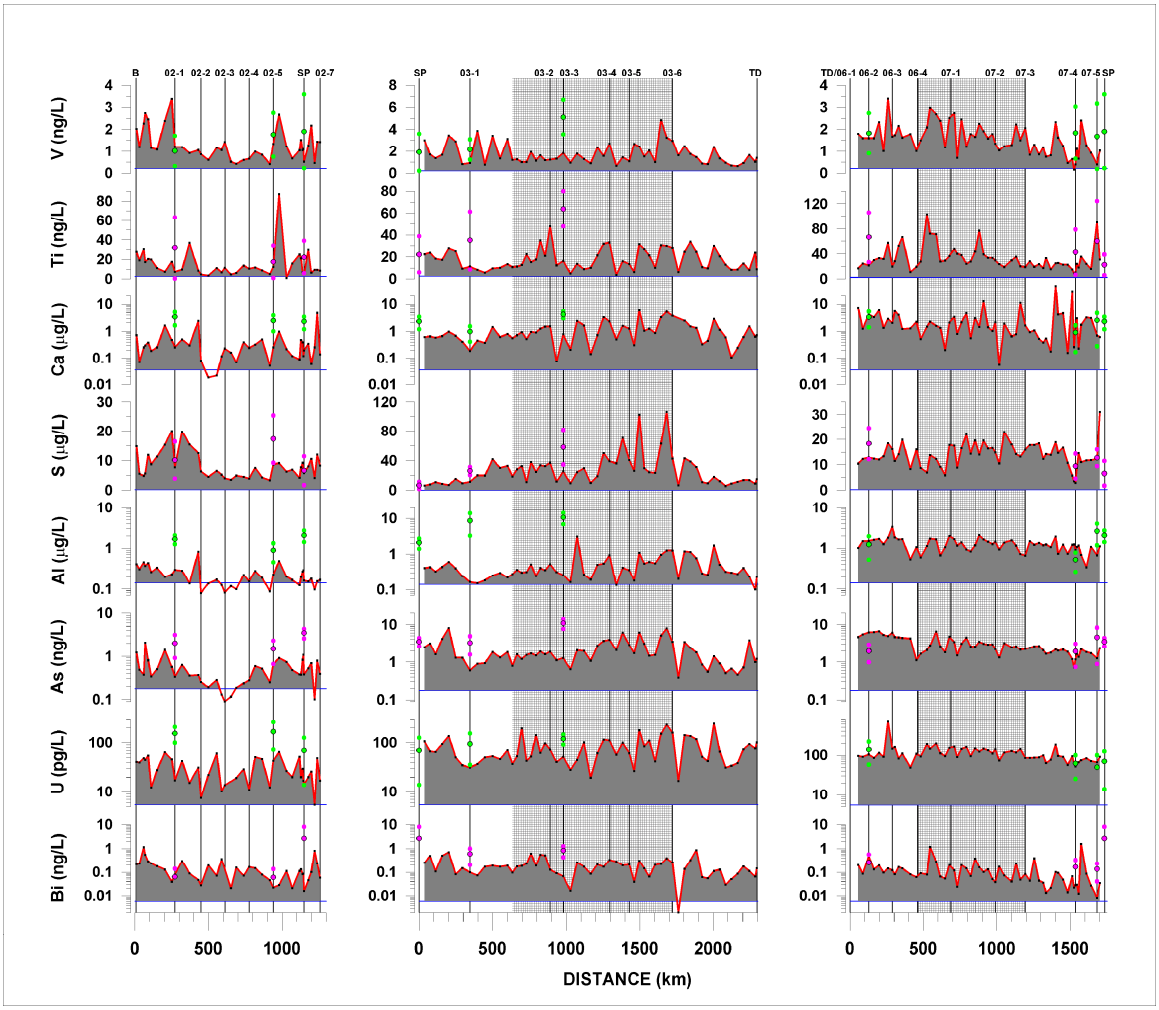

Figure 2.8. Surface snow trace element concentration versus distance for the ITASE-02 (left), ITASE-03 (middle) and ITASE-06/07 (right) traverses. Vertical lines indicate the locations of firn section collection sites along each traverse; B = Byrd; SP = South Pole; TD = Taylor Dome. The three (pink or green) dots in line with each firn collection site indicate the mean (black outline) and +/- 1 standard deviation concentrations in that firn section (if the lower dot is not visible its value is below zero). Large vertical shaded areas behind plots highlight glaze/dune regions. Horizontal (blue) lines signify detection limits. Note that scales may vary between traverse years.

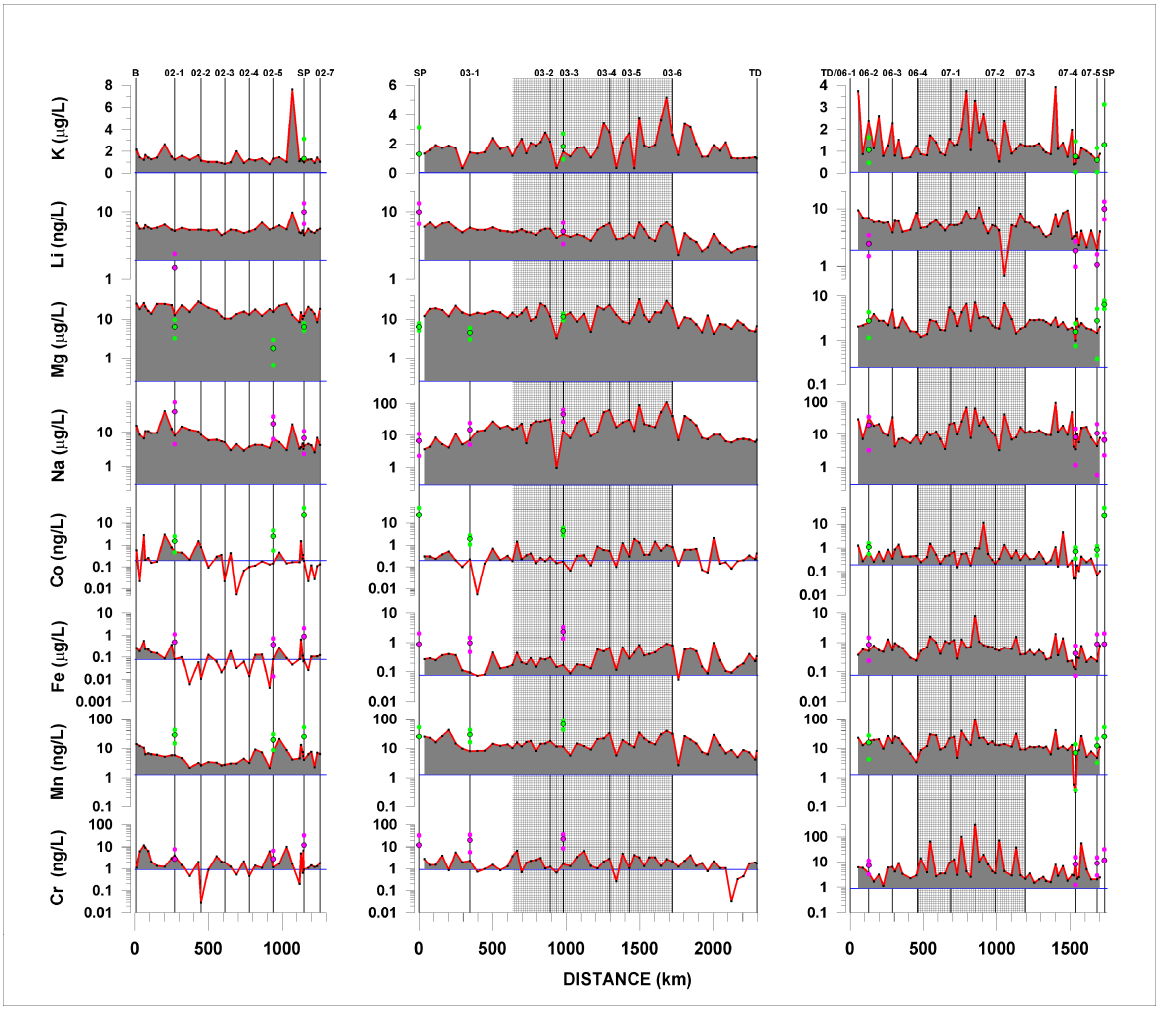

Figure 2.9. Surface snow trace element concentration versus distance for the ITASE-02 (left), ITASE-03 (middle) and ITASE-06/07 (right) traverses. Vertical lines indicate the locations of firn section collection sites along each traverse; B = Byrd; SP = South Pole; TD = Taylor Dome. The three (pink or green) dots in line with each firn collection site indicate the mean (black outline) and +/- 1 standard deviation concentrations in that firn section (if the lower dot is not visible its value is below zero). Large vertical shaded areas behind plots highlight glaze/dune regions. Horizontal (blue) lines signify detection limits. Note that scales may vary between traverse years.

The mean non-glaze/dune surface snow concentrations for each element for each traverse year reveals that the majority (Sr, Ba, La, Ce, Pr, Pb, As, Li, Al, Ca, Ti, Mn, Fe, Co, and Na) are in the region of, or below, concentrations measured in previous studies (Table 2.6). Cd, Bi, U, V and Cr exhibit non-glaze/dune concentrations between two and

five times higher than previous studies in one or more traverse years (Table 2.6). The elevated ITASE-06/07 values are likely a consequence of the traverse's proximity to the Transantarctic Mountains (Figure 2.1). The ITASE-06/07 samples likely contain a greater proportion of dust than the ITASE-02 and ITASE-03 samples as evidenced by higher concentrations of the dust 'signature' elements Cs, U, Al, Ca, Ti, and Fe (Table 2.6). There are likely two factors responsible for the elevated ITASE-03 values, first is the extensive glazed (low-accumulation/hiatus) non-dune areas occurring throughout the East Antarctic Plateau and second is the large station-associated concentration peak between South Pole and 03-1 that drives up the non-glaze/dune values considerably (Figure 2.7, 2.8, & 2.9). Bi is unusual because it is the only element in our surface snow samples to exhibit elevated values, relative to previous studies, in all traverse years (Table 2.6). The most likely reason for this is that all of our surface snow samples were collected on the East and West Antarctic Plateaus. The previous studies, to which we are comparing our samples, are all coastally-located sites. In Antarctica, the primary source of Bi during interglacial periods is volcanic emissions [*Gabrielli et al.*, 2005; *Hinkley et al.*, 1999; *Marteel et al.*, 2008; *Vallelonga et al.*, 2003; *Zreda-Gostynska et al.*, 1997] which are transported primarily through the upper-atmosphere. Chemical species transported via the upper atmosphere, such as Bi, should exhibit higher concentrations at high-elevation inland locations, such as the Antarctic Plateau.

The majority of the firn section trace element concentrations (Sr, Ba, La, Ce, Pr, Pb, As, Li, Al, Ca, Ti, Fe, and Na) are comparable to, or below, values from previous studies (Table 2.6). The 03-3 firn section repeatedly exhibits high trace element concentrations, relative to other firn sections and values from previous studies. This is

expected because it is located in a large glaze/dune area on the East Antarctic plateau (Figure 2.1). The remaining firn sections exhibit raised concentrations, relative to previous studies, for several elements (Cd, Bi, U, V, Cr, Mn, and Co). This is likely due to the same reasons, explained above, as the surface snow samples: proximity to the Transantarctic Mountains, location in glazed non-dune areas, station-associated anthropogenic impacts, and/or their interior-plateau positions relative to the coastal locations of most previous studies.

2.4.4.1 East vs. West Antarctic Trace Element Concentrations

To compare East- versus West-Antarctic trace element input timing differences we use the mean ITASE-03 non-glaze/dune and ITASE-02 surface snow samples to represent average summer concentrations. We also use the 03-1 (1955-1975) and 02-1 (1966-1975) firn sections to represent the non-glaze/dune multi-year concentrations. Section 02-5 is located on the East Antarctic side of the Transantarctic Mountains (and hence is not representative of West Antarctica). The South Pole firn section is located in close vicinity to a large active station (Amundsen-Scott South Pole Station) with aircraft passing through on a regular basis. Firn section 03-3 represents a well developed glaze/dune area on the East Antarctic Plateau and sections 06-2, 07-4, and 07-5 cover a more recent time period (~2001-2006) than the ITASE-02 and ITASE-03 firn sections.

Sr and Na, both elements that we know to be primarily marine-source, exhibit higher firn section (multi-year) concentrations in West Antarctica (lower-atmospheric) than East Antarctica (Table 2.6).

Surface Snow min-max (mean)	Sr (ng/L)	Cd (ng/L)	Cs (ng/L)	Ba (ng/L)	La (ng/L)	Ce (ng/L)	Pr (ng/L)	Pb (ng/L)	Bi (ng/L)	U (pg/L)	As (ng/L)	Li (ng/L)
ITASE-02	0.67 - 33.0 (4.51)	0 - 2.90 (0.32)	0 - 0.14 (0.043)	0 - 76.6 (10.1)	0.024 - 0.66 (0.18)	0.030 - 1.41 (0.35)	0.0042 - 0.17 (0.045)	0.39 - 8.60 (3.05)	0 - 1.14 (0.17)	0 - 65.5 (30.2)	0.092 - 2.08 (0.54)	4.40 - 9.75 (5.48)
ITASE-03 (non-glaze/dune)	1.55 - 37.0 (10.6)	0.017 - 1.13 (0.27)	0.058 - 0.51 (0.16)	0.78 - 20.2 (5.67)	0.18 - 1.64 (0.51)	0.27 - 4.19 (1.07)	0.017 - 0.38 (0.12)	0.69 - 24.3 (5.24)	0.0021 - 0.86 (0.20)	16.9 - 244.8 (75.4)	0.39 - 8.15 (1.78)	2.26 - 6.93 (4.38)
ITASE-03 (glaze/dune)	4.22 - 98.1 (26.0)	0.086 - 1.05 (0.35)	0.047 - 0.42 (0.18)	1.00 - 30.3 (6.56)	0.13 - 1.16 (0.54)	0.23 - 2.69 (1.15)	0.028 - 0.30 (0.14)	2.54 - 17.0 (6.07)	0.016 - 0.61 (0.22)	19.5 – 233 (87.2)	0.64 - 8.03 (2.55)	3.61 - 6.90 (4.96)
ITASE-06/07 (non-glaze/dune)	2.21 – 115 (21.0)	0.11 - 5.52 (0.71)	0.053 - 0.41 (0.20)	1.19 - 39.2 (11.4)	0.031 - 0.98 (0.31)	0.21 - 9.58 (1.18)	0.021 - 0.28 (0.10)	0.60 - 35.8 (6.24)	0.0082 - 1.55 (0.14)	48.7 – 701 (109)	0.71 - 6.69 (3.08)	1.89 - 9.37 (5.05)
ITASE-06/07 (glaze/dune)	5.44 - 60.9 (21.4)	0.19 - 6.76 (1.12)	0.098 - 0.45 (0.23)	6.45 - 94.0 (19.6)	0.21 - 1.00 (0.47)	0.64 - 2.60 (1.33)	0.072 - 0.28 (0.15)	2.09 - 19.8 (7.94)	0.024 - 1.17 (0.17)	73.8 – 197 (129)	1.33 - 6.54 (2.85)	0.68 - 10.3 (5.50)

Firn Sections (mean)	Sr (ng/L)	Cd (ng/L)	Cs (ng/L)	Ba (ng/L)	La (ng/L)	Ce (ng/L)	Pr (ng/L)	Pb (ng/L)	Bi (ng/L)	U (pg/L)	As (ng/L)	Li (ng/L)
02-1 (1966-1975)	30.78	5.50	0.10	6.52	0.25	0.46	0.06	4.50	0.06	153.17	2.01	1.47
02-5 (1967-1975)	13.46	0.75	0.16	7.25	0.30	0.60	0.08	2.27	0.06	168.01	1.49	
02-6/SP (1955-1975)	8.88	4.07	0.23	18.76	0.23	0.49	0.06	12.07	2.71	69.48	3.48	9.86
03-1 (1955-1975)	16.73	1.88	0.18	18.19	0.51	1.15	0.14	20.93	0.59	94.26	3.25	
03-3 (1955-1966) (glaze/dune)	46.61	4.03	0.59	27.44	2.53	4.43	0.69	24.99	0.85	119.01	10.83	5.02
06-2 (2002-2006)	19.59	0.69	0.24	6.36	0.80	1.85	0.20	6.06	0.26	136.75	1.97	2.44
07-4 (2000-2006)	8.46	0.67	0.13	5.34	0.22	0.51	0.06	1.51	0.16	62.40	1.92	1.82
07-5 (2000-2006)	10.93	0.83	0.26	5.12	0.41	0.88	0.11	3.28	0.14	49.64	4.61	1.05

Previous Studies (mean)	Sr (ng/L)	Cd (ng/L)	Cs (ng/L)	Ba (ng/L)	La (ng/L)	Ce (ng/L)	Pr (ng/L)	Pb (ng/L)	Bi (ng/L)	U (pg/L)	As (ng/L)	Li (ng/L)
Lambert Basin 1998-2002 [*Hur et al.*, 2007]		0.21		2.40				4.00	0.03	29.00	10.00	
Law Dome 1956-77 [*Vallelonga et al.*, 2004]	82.68	0.28		2.64				1.84	0.05	26.83		
Coats Land 1958-1975 [*Planchon et al.*, 2002]		0.20		3.13				3.73	0.06	37.14		
Collins Ice Cap, King George Island Jul-Dec 2000 [*Hong et al.*, 2002]		0.10						3.48				
Dolleman Island 1984-5 [*Suttie and Wolff*, 1992]		0.08						4.00				
D55 Adelie Land 1940-80 [*Gorlach and Boutron*, 1992]		0.30						4.80				
Coats Land 1923-86 [*Wolff et al.*, 1999]		0.10										
S. Palmer Land Feb 1980 Surface Snow [*Wolff and Peel*, 1985]		0.26						6.30				
Hercules Neve, Victoria Land 1986-1994 [*Van de Velde et al.*, 2005]				10.87				6.96				
Styx Glacier, Victoria Land 1954-1975 [*Van de Velde et al.*, 2005]				23.27				4.66				
Coats Land 1923-1986 [*Wolff and Suttie*, 1994]								4.00				
Styx Glacier, Victoria Land 1965-1975 [*Barbante et al.*, 1997]								4.10				
Adelie Land Jan 1983 Surface Snow [*Boutron and Patterson*, 1987]								5.43				
South Pole Jan 1984 Surface Snow [*Boutron and Patterson*, 1987]								6.30				
25cm-depth snow pits across Antarctica 1990 [*Xiao et al.*, 2000]								13.68				
Dome-C Holocene Average [*Siggaard-Andersen et al.*, 2007]												7.00
Dome-C Holocene Average [*Gabrielli et al.*, 2010]					0.39	0.91	0.09					

Table 2.6. Trace element concentrations for surface snow samples, firn sections and previous studies.

Surface Snow min-max (mean)	Al (µg/L)	S (µg/L)	Ca (µg/L)	Ti (ng/L)	V (ng/L)	Cr (ng/L)	Mn (ng/L)	Fe (µg/L)	Co (ng/L)	Na (µg/L)	Mg (µg/L)	K (µg/L)
ITASE-02	0.079 - 0.82 (0.23)	3.37 - 20.0 (8.20)	0.018 - 4.81 (0.47)	1.11 - 87.0 (14.8)	0.41 - 3.37 (1.29)	0.028 - 11.5 (2.75)	2.15 - 20.7 (6.21)	0 - 0.65 (0.13)	0 - 3.03 (0.41)	2.52 - 43.4 (7.74)	8.31 - 28.7 (17.3)	0.82 - 7.61 (1.44)
ITASE-03 (non-glaze/dune)	0.10 - 1.73 (0.43)	5.71 - 42.8 (16.7)	0 - 2.85 (0.82)	5.75 - 33.8 (16.0)	0.63 - 3.85 (1.72)	0.033 - 5.55 (1.72)	2.67 - 42.9 (13.9)	0.055 - 0.98 (0.28)	0.0055 - 2.06 (0.34)	3.55 - 40.6 (11.5)	4.19 - 22.5 (11.1)	0.33 - 3.40 (1.58)
ITASE-03 (glaze/dune)	0.14 - 3.14 (0.58)	9.54 – 106 (35.8)	0.075 - 5.95 (1.58)	3.68 - 47.7 (19.5)	0.66 - 4.85 (1.72)	0.27 - 6.68 (2.48)	5.70 - 40.0 (17.5)	0.089 - 0.93 (0.38)	0.066 - 1.87 (0.54)	0.97 – 108 (29.5)	3.27 - 32.4 (15.1)	0.34 - 5.15 (2.05)
ITASE-06/07 (non-glaze/dune)	0.35 - 3.34 (1.29)	2.78 - 31.1 (13.5)	0.16 - 48.6 (4.46)	8.38 - 90.3 (27.9)	0.16 - 3.40 (1.32)	1.13 - 55.8 (5.36)	0.32 - 41.3 (13.3)	0.12 - 1.94 (0.54)	0.051 - 4.51 (0.55)	3.42 - 94.3 (15.9)	1.01 - 4.92 (2.40)	0.39 - 3.92 (1.28)
ITASE-06/07 (glaze/dune)	0.60 - 2.13 (1.27)	5.86 - 23.0 (14.6)	0.055 - 13.0 (2.47)	18.7 – 104 (39.6)	0.69 - 2.98 (1.83)	2.13 – 298 (28.9)	4.75 - 97.3 (20.8)	0.28 - 8.01 (1.11)	0.15 - 11.5 (1.01)	3.21 - 69.8 (18.6)	1.22 - 7.21 (3.10)	0.52 - 3.73 (1.55)

Firn Sections (mean)	Al (µg/L)	S (µg/L)	Ca (µg/L)	Ti (ng/L)	V (ng/L)	Cr (ng/L)	Mn (ng/L)	Fe (µg/L)	Co (ng/L)	Na (µg/L)	Mg (µg/L)	K (µg/L)
02-1 (1966-1975)	1.68	10.17	3.43	31.85	1.01	2.80	28.86	0.49	1.48	41.60	6.42	
02-5 (1967-1975)	0.90	17.32	2.46	17.55	1.75	2.81	19.52	0.37	2.48	18.01	1.80	
02-6/SP (1955-1975)	2.07	6.60	2.29	22.33	1.90	11.87	25.33	0.90	22.55	6.60	6.48	1.29
03-1 (1955-1975)	8.62	25.93	0.95	35.10	2.15	20.16	29.60	0.99	1.89	14.63	4.49	
03-3 (1955-1966) (glaze/dune)	10.52	58.23	4.23	63.94	5.11	22.41	67.26	2.34	4.29	45.43	11.65	1.82
06-2 (2002-2006)	1.25	18.38	3.38	66.31	1.82	7.37	15.95	0.86	1.07	19.03	2.76	1.05
07-4 (2000-2006)	0.53	9.48	0.90	42.83	1.84	8.44	7.09	0.42	0.71	8.05	1.58	0.76
07-5 (2000-2006)	2.61	12.71	2.53	59.73	1.67	9.17	12.41	0.89	0.84	10.72	2.77	0.59

Previous Studies (mean)	Al (µg/L)	S (µg/L)	Ca (µg/L)	Ti (ng/L)	V (ng/L)	Cr (ng/L)	Mn (ng/L)	Fe (µg/L)	Co (ng/L)	Na (µg/L)	Mg (µg/L)	K (µg/L)
Lambert Basin 1998-2002 [*Hur et al.*, 2007]	0.17				0.46		3.70	0.05				
Law Dome 1956-77 [*Vallelonga et al.*, 2004]			2.33		0.65		4.97		0.73	57.33		
Coats Land 1958-1975 [*Planchon et al.*, 2002]	0.52				0.63	1.91	10.37		0.41			
Collins Ice Cap, King George Island Jul-Dec 2000 [*Hong et al.*, 2002]	4.67											
Dolleman Island 1984-5 [*Suttie and Wolff*, 1992]	1.00											
D55 Adelie Land 1940-80 [*Gorlach and Boutron*, 1992]												
Coats Land 1923-86 [*Wolff et al.*, 1999]	1.70									60.00		
S. Palmer Land Feb 1980 Surface Snow [*Wolff and Peel*, 1985]	0.70											
Dome-C Holocene Average [*Marino et al.*, 2004]				120.00				0.75				
WAIS Divide Snow pit 1999-2005 [*Koffman et al.*, 2008]								1.84				

Table 2.6 Continued. Trace element concentrations for surface snow samples, firn sections and from previous studies.

The surface snow (summer) concentrations for these two elements are lower overall and exhibit the opposite pattern with higher values in East Antarctica (upper-atmospheric). Therefore, we can conclude that Na and Sr have a dominant lower-atmospheric transport pathway and are primarily deposited outside of the summer season. If we apply a similar rationale to the remaining elements we see that Cd, U, Ca, and Mg exhibit a similar pattern to Sr and Na (Table 2.6). This is hardly surprising for Ca and Mg, both which have a strong marine source, but is perhaps a little surprising for Cd, and U, both of which have relatively low concentrations in ocean water (Table 2.7). Despite having slightly higher multi-year East Antarctic concentrations, Cs and Mn are similar to Sr and Na in that the most significant concentration increases occur in West Antarctica outside of the summer season (Table 2.6).

Element	Symbol	Ocean Water (ppb)	Upper Crust (ppb)
Strontium	Sr	7900	316000
Cadmium	Cd	0.11	102
Caesium	Cs	0.3	5800
Barium	Ba	13	668000
Lanthanum	La	0.0034	32300
Cerium	Ce	0.0012	65700
Praseodymium	Pr	0.00064	6300
Lead	Pb	0.03	17000
Bismuth	Bi	0.02	123
Uranium	U	3.2	2500
Arsenic	As	3.7	2000
Aluminium	Al	2	77440000
Sulphur	S	905000	953000
Calcium	Ca	412000	29450000
Titanium	Ti	1	3117000
Vanadium	V	2.5	53000
Chromium	Cr	0.3	35000
Manganese	Mn	0.2	527000
Iron	Fe	2	30890000
Cobalt	Co	0.02	11600
Lithium	Li	180	22000
Sodium	Na	10800000	25670000
Magnesium	Mg	1290000	13510000
Potassium	K	399000	28650000

Table 2.7. Average elemental abundances in the global ocean (Lide, 2005) and Earth's upper crust (Wedepohl, 1995).

The rare-earth elements La, Ce, and Pr exhibit higher East Antarctic concentrations in both their summer and multi-year samples. These three elements do not show any significant seasonal change in concentration (Table 2.6). This suggests an upper-atmospheric transport pathway but does not give us any clue as to their input timing. Despite the lack of multi-year data, mean K concentrations are remarkably consistent across East and West Antarctica (including glaze/dune areas) and do not show any significant seasonal change in concentration (Table 2.6).

Pb, Al, S, and Fe are similar to the rare-earths in that they exhibit higher East Antarctic concentrations in both the summer and multi-year samples. However, they are different in that they have a strong seasonal input via the upper-atmosphere outside of the summer season. Cr is also similar to this group of elements, except that it has slightly higher West Antarctic concentrations in summer (Table 2.6).

As and Ti also exhibit higher East Antarctic concentrations in both the summer and multi-year samples and exhibit a strong seasonal input outside of the summer season. However, the seasonal input does not have a preferred atmospheric transport pathway, displaying increases of a similar magnitude in both East and West Antarctica. Co also behaves as As and Ti, but it displays slightly higher West Antarctic concentrations in summer (Table 2.6).

The final group of elements (Ba, Bi and V) exhibit a summer input via the lower atmosphere and a winter input via the upper atmosphere, with the latter input being by far the stronger of the two. We know this because the relative summer to multi-year increase is much greater for the East Antarctic sites.

a)

ITASE-02	EOF 1	EOF 2	EOF 3	EOF 4	EOF 5	EOF 6	EOF 7	EOF 8
	30.5	19.4	10.8	6.8	5.6	4.5	4.2	3.1
$\delta^{18}O$	15.5	62.3	4.5	-9.8	1.0	1.1	0.0	0.4
Accumulation	16.2	68.8	1.3	-4.4	0.9	0.5	-0.2	0.0
Elevation	-28.4	-59.5	-0.4	3.4	-2.7	0.0	-0.5	0.0
Backscatter	1.3	-40.3	-3.8	-0.8	0.0	0.0	7.6	0.0
Grain Size	10.6	40.8	0.0	-19.8	0.9	-6.9	-1.1	-0.7
Temperature	13.6	72.6	0.6	-6.2	0.7	0.0	0.0	-0.8
Sr	43.4	4.0	27.9	2.8	-9.8	-2.7	3.6	-2.5
Cd	14.4	6.5	-11.8	6.5	-8.3	39.1	-0.2	0.0
Cs	54.1	-21.3	4.8	-5.7	0.2	-4.2	-0.4	0.1
Ba	18.4	6.7	-31.3	15.3	-0.1	-4.8	-15.9	0.3
La	54.2	-30.4	3.8	-2.2	-1.0	0.0	-0.1	-1.8
Ce	54.1	-34.9	0.1	-3.7	0.3	0.0	-1.0	-0.9
Pr	43.2	-44.7	1.2	-4.5	0.3	0.0	-0.7	-0.7
Pb	57.1	0.0	-20.4	2.6	-0.7	0.4	-0.9	0.1
Bi	7.8	5.3	-27.1	0.5	1.8	-16.8	3.0	-11.8
U	56.9	-5.2	0.6	-0.8	-0.3	-0.8	1.9	0.6
As	40.0	-3.2	3.7	0.8	0.6	-3.6	16.6	15.9
Al	46.1	1.4	-6.2	0.1	0.3	-2.4	-18.1	13.2
S	35.9	2.2	14.3	0.3	-13.3	12.0	-0.6	2.8
Ca	12.0	-3.0	3.5	4.3	-26.5	-13.0	-8.5	1.8
Ti	28.9	-13.8	-1.2	-10.7	5.1	4.5	-5.3	-4.6
V	63.9	-0.2	-1.4	0.0	-1.2	6.6	11.0	1.2
Cr	6.9	2.8	-38.3	3.7	6.5	-2.3	18.5	7.5
Mn	41.5	-25.5	-6.1	-6.3	3.7	1.0	0.0	0.0
Fe	32.0	-0.1	-32.9	1.3	0.1	6.6	0.8	-4.5
Co	37.6	3.8	-2.4	21.7	-5.5	-2.0	0.4	-14.5
Li	12.3	-1.6	17.3	15.9	44.2	0.3	-1.5	0.1
Na	32.3	8.4	38.8	10.9	-0.2	-0.2	3.7	-2.9
Mg	35.1	10.0	-0.3	0.0	0.5	0.0	-0.7	3.6
K	2.3	-1.1	17.2	38.4	30.2	1.8	-1.9	-0.2

b)

ITASE-03	EOF 1	EOF 2	EOF 3	EOF 4	EOF 5	EOF 6	EOF 7	EOF 8
	45.8	15.1	9.7	4.9	4.2	3.4	3.1	2.5
$\delta^{18}O$	-0.5	-80.1	5.2	0.0	-1.3	0.6	1.7	0.1
Accumulation	-7.0	-71.9	-0.5	-1.8	-0.1	0.0	1.0	-2.2
Elevation	-0.4	86.4	-2.8	2.2	0.9	-0.1	-0.2	0.0
Backscatter	12.6	6.3	25.4	9.3	5.6	15.1	-2.0	-0.6
Grain Size	7.0	5.8	50.4	5.7	-0.1	13.8	-2.0	2.6
Temperature	0.0	-85.4	6.7	-2.8	-0.8	0.2	0.2	0.0
Sr	67.0	1.5	15.2	-7.9	1.0	-1.7	0.2	-0.1
Cd	57.7	1.4	0.0	-0.1	-8.1	0.4	13.8	0.0
Cs	78.3	-7.5	-6.0	0.3	0.5	0.0	-1.8	-0.2
Ba	39.9	-4.4	-1.6	8.4	23.0	-1.0	14.1	1.5
La	72.2	-6.5	-14.3	0.7	0.0	0.3	-3.0	-0.2
Ce	70.3	-5.0	-14.0	1.5	0.0	0.0	-4.4	0.0
Pr	74.0	-3.1	-15.9	0.7	0.0	0.5	-2.1	-0.1
Pb	67.6	0.6	-10.8	-0.7	-3.8	5.8	4.9	0.5
Bi	25.4	2.1	-12.6	0.0	0.1	25.3	6.2	-5.5
U	61.8	-7.4	0.0	-0.5	0.2	-0.6	-2.8	-1.1
As	68.3	0.1	0.0	-1.2	-5.9	5.9	4.2	4.1
Al	35.7	-4.5	0.9	14.7	27.9	-2.5	5.2	1.8
S	54.8	3.4	28.3	-5.5	0.0	0.1	0.0	0.0
Ca	76.8	-0.9	10.3	-2.4	2.2	-2.4	0.2	0.0
Ti	52.8	-0.2	-3.7	-0.1	4.5	-0.2	-4.8	-9.5
V	37.6	0.1	-1.8	0.0	-2.8	-5.1	-1.5	30.4
Cr	7.0	4.3	7.0	24.2	-12.6	-13.9	9.0	-10.1
Mn	88.1	0.0	-5.7	0.2	-0.8	0.1	0.0	0.7
Fe	73.7	-6.8	3.2	2.9	-4.2	-0.6	-2.1	-0.2
Co	29.6	-2.4	7.9	26.6	-15.3	-0.5	-3.6	-0.2
Li	48.4	27.2	-12.3	-1.0	-0.7	-1.7	0.0	0.4
Na	61.7	2.1	22.1	-9.0	1.1	-0.3	0.0	-0.1
Mg	32.4	24.2	0.0	-8.9	-1.4	-2.4	0.5	-3.4
K	66.2	0.2	6.0	-7.8	1.9	-0.3	-0.3	-0.9

Table 2.8. EOF tables of physical traverse data, δ18O and trace elements. As measured in the surface snow samples for a) ITASE-02 and b) ITASE-03. Accumulation = mean annual accumulation; Elevation = surface elevation; Backscatter = RAMP microwave backscatter; Grain Size = MOA grain size; Temperature = mean annual temperature.

c)

ITASE-06/07	EOF 1	EOF 2	EOF 3	EOF 4	EOF 5	EOF 6	EOF 7	EOF 8
	29.4	14.8	10.1	7.9	6.7	5.7	3.9	3.2
$\delta^{18}O$	0.0	50.0	17.1	0.1	5.0	8.0	-0.9	-0.8
Accumulation	2.1	28.9	20.4	-2.0	20.5	-3.1	-0.3	-9.4
Elevation	-25.9	-46.1	0.0	1.5	-6.7	-5.3	0.3	0.4
Backscatter	4.7	0.6	-29.7	-3.1	-7.0	27.0	0.8	-0.2
Grain Size	18.1	1.3	-21.8	-5.3	-1.1	33.2	2.7	0.3
Temperature	22.1	37.5	0.1	-2.7	4.9	14.6	0.0	0.8
Sr	31.5	-33.3	16.8	-0.3	0.0	2.2	0.0	-4.6
Cd	16.4	0.5	-3.5	50.0	8.6	-1.1	11.4	0.3
Cs	51.1	7.0	0.1	-8.4	-3.2	-3.5	1.9	0.0
Ba	29.9	0.7	-1.0	21.5	-8.7	3.4	0.0	-15.1
La	68.7	8.8	-1.4	0.4	-6.8	-4.4	-0.1	1.3
Ce	40.3	-9.3	15.5	4.1	-6.8	0.0	-4.7	2.4
Pr	67.1	9.0	-1.2	0.0	-10.2	-3.8	0.0	1.4
Pb	36.3	-4.5	14.2	17.4	0.5	1.5	0.6	5.1
Bi	13.6	0.0	-7.0	39.5	9.8	-5.3	10.1	-0.1
U	30.4	7.0	0.0	-0.5	-11.0	-1.0	-16.5	-0.2
As	33.7	25.9	9.3	-6.0	8.5	-2.4	2.0	-0.5
Al	36.8	3.7	5.4	-3.9	-2.2	-10.1	0.1	-1.7
S	17.8	-3.1	-0.5	-18.1	-4.1	-14.1	3.9	5.2
Ca	13.0	-30.1	36.2	3.9	-2.5	5.6	-2.5	-1.4
Ti	15.6	7.6	-12.9	8.5	-7.5	-1.0	-6.0	-2.4
V	59.2	9.5	-0.6	7.7	-0.5	-0.2	-0.3	1.8
Cr	14.1	-15.7	-35.9	0.0	22.8	0.0	-5.3	-1.0
Mn	55.3	-11.6	-9.6	-0.1	11.8	-0.6	-5.8	-0.1
Fe	29.7	-15.5	-21.1	-1.8	11.9	-0.2	-12.2	-0.1
Co	9.9	-1.7	-0.1	-0.1	-8.7	3.4	19.3	-9.0
Li	18.7	0.2	4.0	0.0	2.9	8.6	-0.1	30.3
Na	35.6	-44.8	7.8	-2.8	0.7	1.6	0.1	-0.9
Mg	33.7	-10.3	-3.9	-26.8	1.4	-3.1	6.7	-0.3
K	49.1	-18.4	7.4	-1.8	3.8	1.7	3.7	0.0

Table 2.8 Continued. EOF tables of physical traverse data, δ18O and trace elements as measured in the surface snow samples for c) ITASE-06/07. Accumulation = mean annual accumulation; Elevation = surface elevation; Backscatter = RAMP microwave backscatter; Grain Size = MOA grain size; Temperature = mean annual temperature.

Li also follows this pattern, at least for the lower-atmospheric site. Unfortunately, Li was not included in the 03-1 analyses, so lack of East Antarctic Li data precludes observation of the multi-year upper-atmospheric transport pathway (Table 2.6).

2.4.4.2 Trace Element EOF

To assess the spatial associations between the ICP-SFMS trace elements and the physical environment for each traverse we ran trace EOFs with the following parameters: $\delta^{18}O$, accumulation, elevation, backscatter, grain size, mean annual temperature, Sr, Cd, Cs, Ba, La, Ce, Pr, Pb, Bi, U, As, Al, S, Ca, Ti, V, Cr, Mn, Fe, Co, Li, Na, Mg, and K.

The first trace EOF for ITASE-02 captures a large proportion of the chemistry signal (Table 2.8a), with the majority of the "dust" elements being strongly represented along with a weak negative association with elevation. The spatial pattern of the ITASE-02 trace EOF 1 (Figure 2.10) is similar to that of the ITASE-02 ion EOF 2 (Figure 2.6), having a double-peak structure with values higher in West Antarctica (Byrd to 02-2).

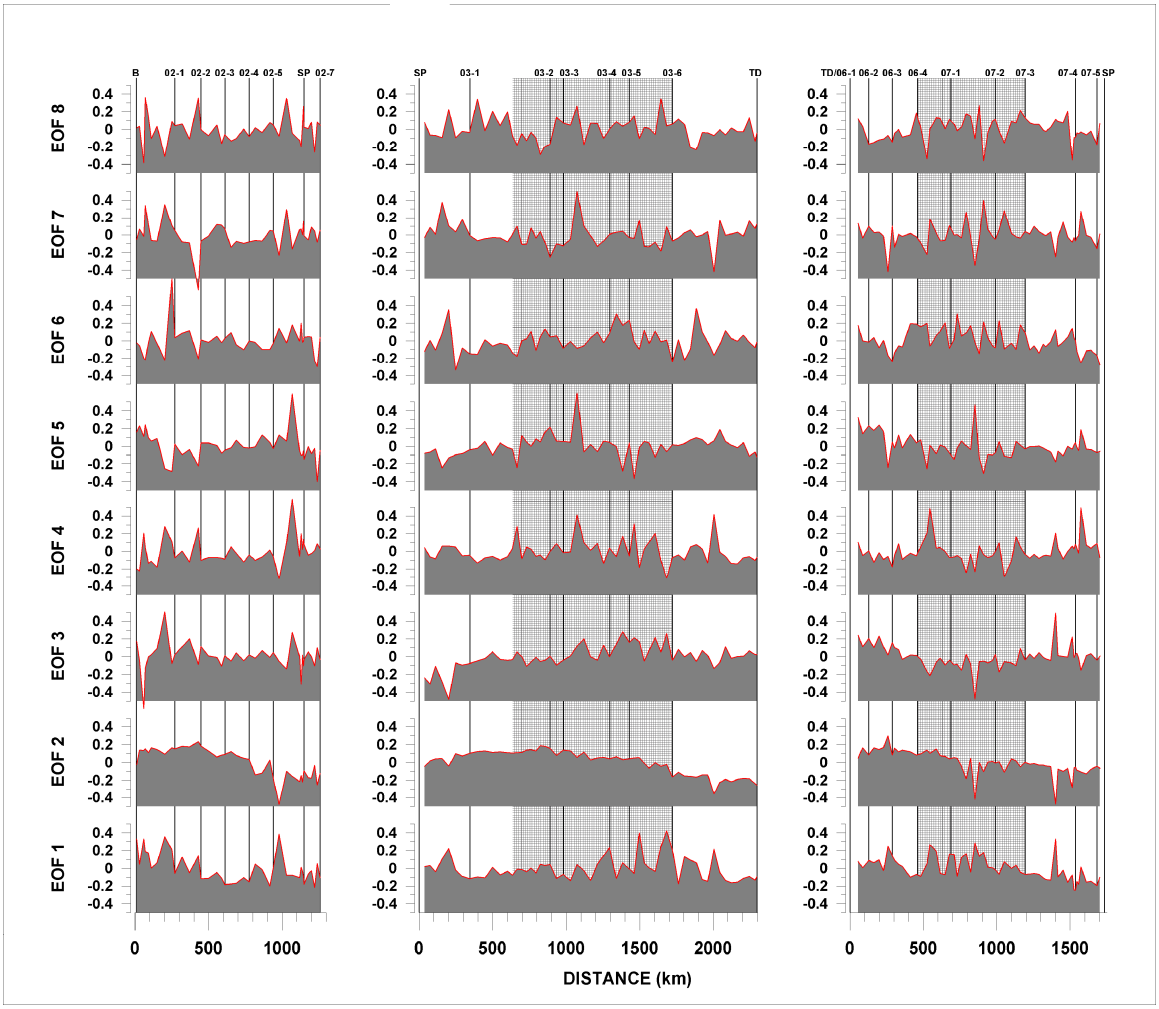

Figure 2.10. Trace EOF loading patterns versus distance for the ITASE-02 (left), ITASE-03 (middle) and ITASE-06/07 (right) traverses. Vertical lines indicate the locations of firn section collection sites along each traverse; B = Byrd; SP = South Pole; TD = Taylor Dome. Large vertical shaded areas behind plots highlight glaze/dune regions.

Values then dip between 02-2 and 02-4, peak again around 02-4 and 02-5, then level off past South Pole and out to 02-7. This trace EOF shows that most of the elements exhibit a summer minimum in concentration between 02-2 and 02-4 and suggests that multiple transport pathways and/or sources exist for these elements.

The second ITASE-02 trace EOF (Table 2.8a) contains the majority of all the physical parameters operating inversely with several of the dust elements (Cs, La, Ce, Pr, Mn). The trace EOF 2 Structure is such that as the $\delta^{18}O$, accumulation, grain size and mean annual temperature go down towards East Antarctica, the elevation, backscatter, Cs, La, Ce, Pr, and Mn all go up (Figure 2.10). The majority of this trace EOF signal is dominated by the physical parameters. However, the EOF signal is punctuated a large chemistry peak in the vicinity of 02-5 (Figure 2.7 & 2.9) that is likely caused by the glaze/dune field in this area (Figure 2.1). The hiatus surfaces of the glaze/dune areas saturate the chemistry at the surface causing higher concentrations in affected samples.

The third ITASE-02 trace EOF (Table 2.8a) contains several of the marine elements (Sr, S, Li, Na, & K) behaving inversely to several of the heavy metals (Cd, Ba, Pb, Bi, Cr, & Fe). The structure of EOF 3 shows the sea salt elements peaking in West Antarctica in the vicinity of 02-1 (Figure 2.10) and declining slightly towards East Antarctica highlighting the fact that these groups of elements have different spatial distribution patterns, related to distance inland and elevation across this region of Antarctica during the summer.

The ITASE-02 trace EOF 6 (Table 2.8a) captures 39% of the Cd. The spatial pattern is dominated by a large peak in the vicinity of 02-1 and significant variability without trend elsewhere (Figure 2.10). This trace EOF suggests that the majority of the

Cd reaching this area of Antarctica is from a unique source, the origin of which will be investigated later in this paper.

The first trace EOF for ITASE-03 captures the greater part of the signal for the majority of the ICP-SFMS elements (Table 2.8b) and shows a distinct peak between South Pole and 03-1 and increased variability in the Megadunes area (Figure 2.10). This trace EOF emphasizes the considerable effect that the glaze/dune areas have on the chemical concentrations in East Antarctica and at the same time draws attention to the magnitude of the concentration increase between South Pole and 03-1 that cannot be attributed to glaze/dune fields and is likely a result of station-associated anthropogenic activity.

The second and third trace EOFs for ITASE-03 (Table 2.8b) capture patterns very similar to the first and second physical EOFs of ITASE-03 (Table 2.3b). The ITASE-03 trace EOF 2 contains 27% of Li and 24% of Mg associated positively with 86% of the elevation, highlighting only a weak association (Table 2.8b). ITASE-03 trace EOF 3 (Table 2.8b) contains 28% of S, 22% of Na, and a significantly weaker backscatter signal relative to physical EOF 2 of ITASE-03 (25% versus 68%). Despite these differences, the spatial EOF patterns are still similar (Figure 2.10 & 2.4). This shows that East Antarctic glaze/dune areas significantly affect S and Na concentrations, increasing them considerably between 03-3 and 03-6.

The remaining ITASE-03 trace EOFs (4, 5, 6, 7 and 8) primarily capture only one or two elements (Table 2.8b) and in each case the structure shows increased variability and/or large peaks in the glaze/dune areas without significant trend elsewhere (Figure

2.10). This again highlights the significant effect that the glaze/dune areas have on the chemical concentrations in East Antarctica.

Much like the ITASE-03 trace EOF 1, the first trace EOF for ITASE-06/07 captures a significant percentage of the signal for the majority of the ICP-SFMS elements (Table 2.8c) associated inversely with 26% of the elevation suggesting that as elevation increases, towards the South Pole away from the glaze/dune areas and mountains, the concentration of several elements decreases slightly. The trace EOF structure also indicates a higher degree of variability in the glaze/dune area between 06-4 and 07-2 and exhibits distinct peaks around 06-3 and between 07-3 and 07-4 (Figure 2.10). This EOF underscores the considerable chemical variability present in this area of Antarctica. Chemical concentrations are complicated by multiple influencing factors such as proximity to the Transantarctic Mountains, glaze/dune areas, glazed non-dune areas, and anthropogenic activity in the vicinity of South Pole.

The second trace EOF for ITASE-06/07 (Table 2.8c) shows the elevation (46%), Sr (33%), Ca (30%), and Na (45%) associated inversely to the $\delta^{18}O$ (50%), accumulation (29%), mean annual temperature (38%), and As (26%). The structure of ITASE-06/07 trace EOF 2 confirms that while $\delta^{18}O$, accumulation, mean annual temperature, and As decrease with increasing elevation, Sr, Ca, and Na increase slightly (Figure 2.10). This trace EOF signal is dominated by the physical parameters. However, the signal is also influenced by the marine species Sr, Ca and Na which exhibit considerable variability in the glaze/dune areas and higher values near South Pole compared to Taylor Dome (Figure 2.7, 2.8, & 2.9). The distribution of As is captured in this trace EOF as a decreasing trend from Taylor Dome to South Pole (Figure 2.8). It is worth noting that the

decreasing As trend seen in the surface snow concentrations is in contrast to the trend exhibited by the multi-annual firn sections (Figure 2.8). This means that As is likely dominated by different sources in summer compared to other times of year.

The remaining ITASE-06/07 trace EOFs (Table 2.8c) highlight the glaze/dune areas and exhibit higher values and/or increased variability in their vicinity (Figure 2.10). This again underscores the fact that glaze/dune areas exercise the dominant control on chemistry in these areas of East Antarctica.

The results of the EOF analyses clearly emphasize the highly-variable nature of the glaze/dune areas, not just with respect to the major ion and trace element concentrations, but also with respect to the physical parameters, backscatter and grain size. Examination of the traverse map (Figure 2.1) in conjunction with the physical parameter profiles, chemical concentration profiles, and EOF analyses, leads us to classify extensive areas of East Antarctica as 'glaze/dune'. All samples starting from midway between 03-1 and 03-2 to 03-6 and all samples between 06-4 and 07-3 (shaded areas on concentration plots) are classified as glaze/dune. The chemistry samples in these glaze/dune areas do not represent typical summer surface snow concentrations, but most likely represent a mean, multi-annual value. Glazed, non-dune areas likely exist in the vicinity of 02-5 and 06-3. These areas affect the concentrations of several of our chemical species, but not all. Therefore, we do not definitively classify them as glaze/dune and we do not shade these areas on our spatial plots. The glazed, non-dune data are included in the calculation of our mean 'non-glaze/dune' concentrations.

2.4.4.3 Trace Element Enrichment Factors

To elucidate potential sources for the trace elements in these surface snow samples we ran enrichment factor (EF) calculations on each set of samples. We calculated the average crustal enrichment factors (EF_c) and average oceanic enrichment factors (EF_o) for each element using mean upper crust elemental abundances (Table 2.7) from [*Wedepohl*, 1995] and mean ocean water elemental abundances from [*Lide*, 2005].

Values were calculated according to the following: Crustal EF for element x [$EF_c(x) = \text{mean}([x/r]_{sample}/[x/r]_{upper\ crust})$], where r = Cs, La, Ce, Pr, V, and Mn to reduce the potential bias from using only a single conservative crustal element; Oceanic EF for element x [$EF_o(x) = \text{mean}([x/r]_{sample}/[x/r]_{ocean\ water})$], where r = Sr and Na.

The following elements are enriched in the summer surface snow with respect to Earth's upper crust: Cd, Pb, Bi, As, Li, S, Cr, Na, Mg, and K (Table 2.9), and the following are enriched relative to ocean water: Cd, Cs, Ba, La, Ce, Pr, Pb, Bi, U, As, Li, Al, S, Ti, V, Cr, Mn, Fe, Co, and Mg. To separate these two potential sources we calculated the ocean water fraction of each element according to the following formula: Oceanic Fraction for element x ($x_o = \text{mean}(r_{sample} * [x_{ocean\ water}/r_{ocean\ water}])$, where r = Sr and Na). We then subtracted the oceanic fraction from each element in each sample and recalculated the EF_c (Table 2.9) to give $nssEF_c$ values. We consider an element highly enriched if it exhibits an $nssEF_c$ value of 10 or more for each traverse year. We choose a value of 10 following Duce et al. [1975].

Surface Snow												
EF_c (mean)	Sr	Cd	Cs	Ba	La	Ce	Pr	Pb	Bi	U	As	Li
ITASE-02	2.19	541.64	0.98	2.54	0.76	0.68	1.09	30.82	355.77	1.83	39.17	51.38
ITASE-03 (non-glaze/dune)	1.86	147.75	1.45	0.43	0.79	0.77	0.92	14.80	76.11	1.69	47.68	12.50
ITASE-03 (glaze/dune)	3.58	169.89	1.34	0.46	0.73	0.74	0.94	16.36	95.10	1.69	60.80	12.23
ITASE-06/07 (non-glaze/dune)	4.25	495.88	2.31	1.00	0.56	1.01	1.03	22.10	67.73	3.01	101.78	18.34
ITASE-06/07 (glaze/dune)	2.85	433.46	1.71	1.24	0.59	0.85	0.99	20.60	50.71	2.30	61.05	11.68

Surface Snow												
nss-EF_c (mean)	Sr	Cd	Cs	Ba	La	Ce	Pr	Pb	Bi	U	As	Li
ITASE-02	<0	542.66	0.98	2.54	0.77	0.68	1.09	30.87	356.97	1.70	39.02	50.60
ITASE-03 (non-glaze/dune)	0.10	147.78	1.45	0.42	0.79	0.77	0.92	14.81	76.15	1.60	47.57	11.93
ITASE-03 (glaze/dune)	0.24	169.96	1.34	0.45	0.73	0.75	0.94	16.38	95.19	1.52	60.63	11.15
ITASE-06/07 (non-glaze/dune)	0.91	496.13	2.30	1.00	0.56	1.01	1.03	22.12	67.76	2.84	101.61	17.26
ITASE-06/07 (glaze/dune)	0.51	433.64	1.70	1.24	0.59	0.85	0.99	20.62	50.74	2.18	60.92	10.92

Previous Studies												
EF_c	Sr	Cd	Cs	Ba	La	Ce	Pr	Pb	Bi	U	As	Li
Coats Land 1959-1990 [*Planchon et al.*, 2002]		133.00		0.80				56.00	127.00	4.00		
Law Dome 1898-1989 [*Vallelonga et al.*, 2004]	1.50	269.00						31.00	90.00	2.70		

Table 2.9. Enrichment factors for surface snow samples and previous studies. EFc = crustal enrichment factor; nss-EFc = non-sea-salt crustal enrichment factor.

Surface Snow EF_c (mean)	Al	S	Ca	Ti	V	Cr	Mn	Fe	Co	Na	Mg	K
ITASE-02	0.51	1517.20	2.38	0.79	4.24	14.99	1.83	0.63	5.10	52.88	255.03	9.72
ITASE-03 (non-glaze/dune)	0.28	1096.36	1.54	0.30	2.03	3.03	1.32	0.49	1.44	27.86	52.83	3.45
ITASE-03 (glaze/dune)	0.36	1865.58	2.21	0.28	1.61	4.11	1.52	0.56	2.55	52.28	58.48	3.36
ITASE-06/07 (non-glaze/dune)	1.36	1002.53	9.44	0.68	1.59	13.39	1.42	1.08	2.85	40.86	13.85	3.09
ITASE-06/07 (glaze/dune)	0.71	683.87	3.85	0.55	1.50	34.87	1.61	1.49	3.29	30.95	9.94	2.38

Surface Snow nss-EF_c (mean)	Al	S	Ca	Ti	V	Cr	Mn	Fe	Co	Na	Mg	K
ITASE-02	0.51	1418.48	0.89	0.79	4.24	15.01	1.84	0.63	5.11	7.99	245.25	8.25
ITASE-03 (non-glaze/dune)	0.28	1030.31	0.61	0.30	2.02	3.04	1.32	0.49	1.44	<0	46.15	2.47
ITASE-03 (glaze/dune)	0.36	1740.98	0.34	0.28	1.61	4.11	1.53	0.56	2.56	<0	45.77	1.50
ITASE-06/07 (non-glaze/dune)	1.36	876.17	7.60	0.68	1.58	13.39	1.42	1.08	2.85	<0	1.08	1.23
ITASE-06/07 (glaze/dune)	0.71	595.22	2.54	0.55	1.49	34.91	1.61	1.49	3.30	<0	0.98	1.07

Previous Studies EF_c	Al	S	Ca	Ti	V	Cr	Mn	Fe	Co	Na	Mg	K
Coats Land 1959-1990 [*Planchon et al.*, 2002]					1.30	16.00	3.00		6.00			
Law Dome 1898-1989 [*Vallelonga et al.*, 2004]					2.30		2.60		18.00			

Table 2.9 Continued. Enrichment factors for surface snow samples and previous studies. EFc = crustal enrichment factor; nss-EFc = non-sea-salt crustal enrichment factor.

Elements exhibiting highly-enriched $nssEF_c$ values are: Cd, Pb, Bi, As, Li, S, Cr, and Mg, suggesting additional source(s), in addition to the ocean and crust. Of these elements, Cd, Pb, Bi, As, Li, and S are highly enriched for all traverse years. Cr and Mg do not exhibit an $nssEF_c$ greater than 10 for the ITASE-03 and ITASE-06/07 traverse years, respectively (Table 2.9). The general pattern of enrichment for several of the highly enriched elements (Cd, Pb, Li and Cr) is such that the ITASE-03 $nssEF_c$ values are the lowest of the three traverse years. Cr, being the least highly-enriched of all the highly-enriched elements, does not exhibit $nssEF_c$ values higher than 10 for ITASE-03. Mg, however, exhibits highly-enriched $nssEF_c$ values for ITASE-02 and ITASE-03 for a more specific reason.

The Mg enrichment during the ITASE-02 and ITASE-03 traverse years is artificially high as a result of the following factors. The ITASE-06/07 surface snow samples were analyzed for all trace elements presented here during their first ICP-SFMS analysis. However, surface snow samples from the ITASE-02 and ITASE-03 traverse years were re-run on the ICP-SFMS (after sitting unfrozen for >1-year) in order to obtain Na, Mg, Li, and K data (these four elements were not measured on the ITASE-02 and ITASE-03 samples during their first ICP-SFMS analysis). The re-run Na and K data seem to be unaffected based upon the fact that the ICP-SFMS trace element concentrations are not higher than the original IC major ion data. Unfortunately, we do not have any IC analyses with which to compare the re-run Li data. However, the original ITASE-06/07 Li data exhibit similar concentrations and $nssEF_c$ values to the re-run ITASE-02 and ITASE-03 Li data, so we assume that the re-run Li is unaffected. The re-run ICP-SFMS Mg samples exhibit significantly higher concentrations than the IC major ion data, but the

original ITASE-06/07 ICP-SFMS Mg samples do not. There are two possible explanations: either the storage vials are leaching small amounts of Mg into the sample or a significant fraction of the total Mg is present in particulate form that takes longer than one week to dissolve in 1% HNO_3. The latter explanation is the more likely of the two.

Two recent studies [*Planchon et al.*, 2002; *Vallelonga et al.*, 2004] have published East Antarctic coastal firn EF_c data for Sr, Cd, Ba, Pb, Bi, U, V, Cr, Mn, and Co. All of our surface snow EF_c values fall within the range of these previous studies apart from the ITASE-02 EF_c data for elements Cd, Ba, and Bi, the ITASE-03 glaze/dune EF_c value for Sr, the ITASE-06/07 non-glaze/dune EF_c data for Sr, and the ITASE-06/07 glaze/dune EF_c data for Cr. The ITASE-02 Cd, Ba, and Bi exhibit EF_c values 2 to 5 times higher than previous studies (Table 2.9). As mentioned above, these elevated values may be a result of location differences. The ITASE-02 traverse samples are predominantly located on the West Antarctic plateau, while Law Dome and Coats Land are East Antarctic coastal locations. ITASE-06/07 glaze/dune Cr exhibits an EF_c slightly more than double the value from previous studies. This is probably a combined effect of the glaze/dune hiatus surfaces and their location close to the Transantarctic Mountains. Sr has a significant oceanic source, so we would expect this element to exhibit some enrichment relative to the crust. After the oceanic fraction is removed, Sr does not exhibit significant enrichment. Other elements that exhibit a significantly lower $nssEF_c$ compared to their EF_c (indicative of an oceanic source) include Ca, Na, Mg, and K, as expected. Several elements display only slightly lower $nssEF_c$ compared to their EF_c, suggesting a very small oceanic contribution. These include U, Li, and S.

2.4.4.4 Trace Element Volcanic Contribution

S in the Antarctic atmosphere is primarily of biogenic origin, but it also has a volcanic source comprising up to 10-15% [*Boutron and Patterson*, 1986; *Hur et al.*, 2007]. Previous studies have measured the ratio of sulfur to trace elements and heavy metals in volcanic emissions from around the world [*Hinkley et al.*, 1999; *Nriagu*, 1989]. We use the Hinkley et al. [1999] Element/S ratios (Table 2.10) for the highly enriched elements Cd, Pb, Bi, and As to calculate inputs from the global mean volcanic quiescent degassing background. We also use the Mount Erebus plume Element/S ratios (Table 2.10) from Zreda-Gostynska et al. [1997] to represent the local source contributions for Cd and As. Unfortunately, Zreda-Gostynska et al. do not measure Pb or Bi, and neither study measures Li.

Element	Global	Erebus
Cd	0.00006	0.000346183
Pb	0.00019	
Bi	0.00009	
As	0.00003	0.00097364

Table 2.10. Volcanic element-sulphur ratios. For the global mean volcanic quiescent degassing background [Hinkley et al., 1999] and the Mount Erebus plume [Zreda-Gostynska et al., 1997].

Prior to applying the volcanic calculation for each of the following elements, Cd, Pb, Bi, and As, we remove the oceanic fraction (as outlined above) and the crustal fraction, which is calculated according to the following: Crustal Fraction for element x (x_c = mean(r_{sample} * [$x_{upper\ crust}/r_{upper\ crust}$]), where r = Cs, La, Ce, Pr, V, and Mn). We are then left with the excess (excess = total – (oceanic + crustal)) elemental concentrations, from which we calculate the 10% (minimum) and 15% (maximum) S values to which we

apply the Hinkley et al. element/S ratios (Table 2.10) to obtain global volcanic background minimum (GVmin) and maximum (GVmax) concentrations.

Comparison between excess element concentrations, GVmin and GVmax (Table 2.11) reveals that, for As, the ITASE-02 global volcanic background contribution ranges from 4% to 7% of the mean excess As concentration. For ITASE-03 As, the global volcanic background contribution ranges from 3% to 4% over non-glaze/dune areas and from 4% to 6% over glaze/dune areas. For ITASE-06/07 As, the global volcanic background contribution ranges from 1% to 2% over glaze/dune and non-glaze/dune areas (Table 2.11). The spatial distribution of the As global volcanic background in our surface snow samples (Figure 2.11) reveals that contributions rarely ever get higher than the As detection limit and are therefore not considered a significant source for this element.

Antarctic Cd inputs from the global volcanic background are significant, with GVmax accounting for more than 50% of the mean excess Cd concentrations for ITASE-03. However, Cd GVmax is less significant for ITASE-02 and ITASE-06/07, with values of 21% and 15%, respectively (Table 2.11). Spatially, the distribution of the Cd GVmax input is highest in the glaze/dune areas (Figure 2.11) which suggests an alternate source must be responsible for the majority of the Cd in non-glaze/dune areas.

Pb contributions from the global volcanic background reach maximum values of only 8%, 9%, and 6% in the ITASE-02, ITASE-03 and ITASE-06/07 non-glaze/dune areas, respectively (Table 2.11). In the ITASE-03 and ITASE-06/07 glaze/dune areas, respective GVmax values reach 17% and 5% which suggests an alternate source is responsible for the majority of the Pb reaching Antarctica.

a)

ITASE-02 (mean)	As (ng/L)	Cd (ng/L)	Pb (ng/L)	Bi (ng/L)
Excess Concentration	0.513	0.319	2.879	0.172
Global Volcanic min	0.023	0.046	0.144	0.068
Global Volcanic max	0.034	0.068	0.217	0.103

ITASE-03 (mean)	As (ng/L)	Cd (ng/L)	Pb (ng/L)	Bi (ng/L)
Excess Concentration (non-glaze/dune)	1.725	0.269	4.846	0.195
Global Volcanic min (non-glaze/dune)	0.047	0.093	0.296	0.140
Global Volcanic max (non-glaze/dune)	0.070	0.140	0.444	0.210
Excess Concentration (glaze/dune)	2.488	0.351	5.641	0.219
Global Volcanic min (glaze/dune)	0.099	0.198	0.628	0.298
Global Volcanic max (glaze/dune)	0.149	0.298	0.942	0.446

ITASE-06/07 (mean)	As (ng/L)	Cd (ng/L)	Pb (ng/L)	Bi (ng/L)
Excess Concentration (non-glaze/dune)	3.025	0.706	5.882	0.139
Global Volcanic min (non-glaze/dune)	0.035	0.070	0.223	0.106
Global Volcanic max (non-glaze/dune)	0.053	0.106	0.334	0.158
Excess Concentration (glaze/dune)	2.786	1.121	7.453	0.164
Global Volcanic min (glaze/dune)	0.038	0.075	0.238	0.113
Global Volcanic max (glaze/dune)	0.056	0.113	0.357	0.169

b)

ITASE-02 (mean)	As (ng/L)	Cd (ng/L)
Remaining Concentration	0.479	0.256
Mean Erebus Volcanic min	0.222	0.079
Mean Erebus Volcanic max	0.370	0.132

ITASE-03 (mean)	As (ng/L)	Cd (ng/L)
Remaining Concentration (non-glaze/dune)	1.952	0.121
Erebus Volcanic min (non-glaze/dune)	0.303	0.108
Erebus Volcanic max (non-glaze/dune)	0.758	0.269
Remaining Concentration (glaze/dune)	2.073	0.086
Erebus Volcanic min (glaze/dune)	0.644	0.229
Erebus Volcanic max (glaze/dune)	1.609	0.572

ITASE-06/07 (mean)	As (ng/L)	Cd (ng/L)
Remaining Concentration (non-glaze/dune)	2.973	0.602
Erebus Volcanic min (non-glaze/dune)	0.215	0.077
Erebus Volcanic max (non-glaze/dune)	0.538	0.191
Remaining Concentration (glaze/dune)	2.729	1.008
Erebus Volcanic min (glaze/dune)	0.252	0.090
Erebus Volcanic max (glaze/dune)	0.631	0.224

Table 2.11. Volcanic minimum and maximum contributions. a) Excess element concentrations and global mean volcanic quiescent degassing background minimum and maximum contributions. b) Remaining element concentrations and Mount Erebus volcanic plume minimum and maximum contributions.

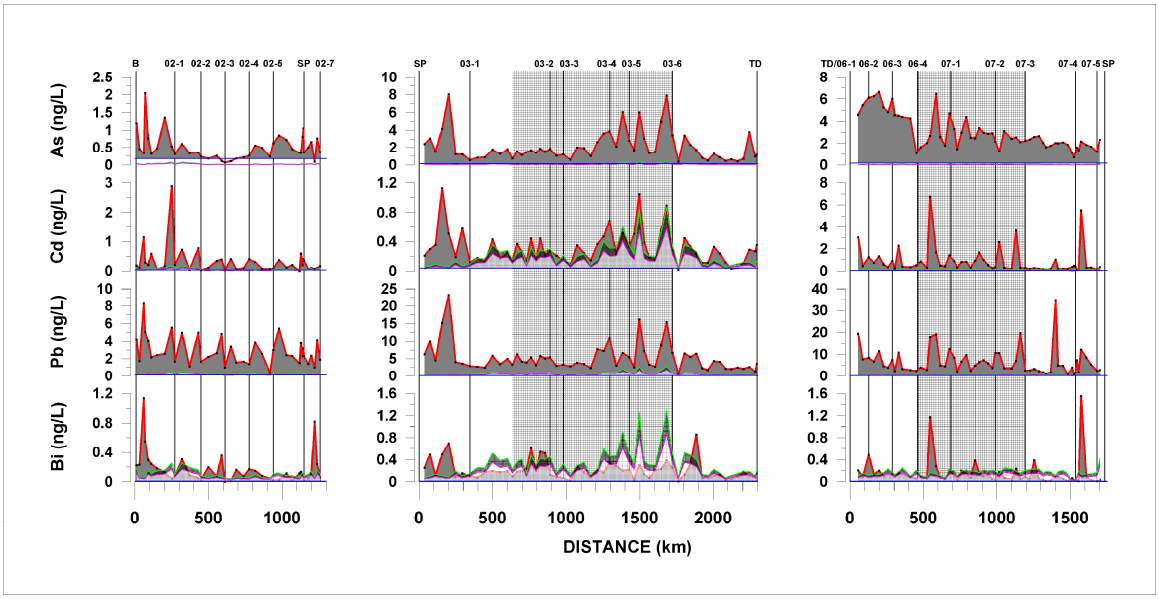

Figure 2.11. Surface snow excess element concentration (red) and global mean volcanic quiescent degassing background contributions. Minimum (pink) and maximum (green) contributions versus distance for the ITASE-02 (left), ITASE-03 (middle) and ITASE-06/07 (right) traverses. Vertical lines indicate the locations of firn section collection sites along each traverse; B = Byrd; SP = South Pole; TD = Taylor Dome. Large vertical shaded areas behind plots highlight glaze/dune regions. Horizontal (blue) lines signify detection limits. Note that scales may vary between traverse years.

The mean global volcanic background accounts for more than 100% of the Bi input for both ITASE-03 and ITASE-06/07, it also accounts for 60% of the Bi input for ITASE-02 (Table 2.11). However, GVmax Bi input is highest in the glaze/dune areas and overestimates several ITASE-03 glaze/dune values significantly (Figure 2.11). Elsewhere in Antarctica, GVmax input does not account for significant Bi peaks observed in the surface snow samples, specifically, the large double peak between South Pole and 03-1 and the large peak near Byrd (Figure 2.11).

Previous studies have shown that the Mount Erebus (77º 33’ S, 167º 10’ E, 3794m asl) plume is enriched in halogens and may therefore be an important source to the Antarctic atmosphere [*Kyle et al.*, 1990; *Zreda-Gostynska et al.*, 1993; *Zreda-*

Gostynska et al., 1997]. The Erebus plume also contains a variety of elements such as Na, Al, Cl, K, Ca, Sc, Ti, V, Cr, Mn, Fe, Co, Ni, Cu, Zn, As, Se, Br, Rb, Mo, Cd, In, Sb, Cs, La, Ce, Sm, Eu, Yb, Hf, Ta, W, and Au in varying amounts [*Zreda-Gostynska et al.*, 1997]. Of particular interest to this study are the Erebus Cd and As emissions because these elements exhibit enrichment in all of our samples.

Assuming the Erebus plume is homogeneous over Antarctica, which is likely an oversimplification, we use the Mount Erebus plume Element/S ratios (Table 2.10) from Zreda-Gostynska et al. [1997] to calculate the potential Erebus volcanic contributions of Cd and As to our surface snow samples. We subtract the GVmax Cd and As contributions from our excess Cd and As concentrations to obtain the remaining concentrations for Cd and As (Figure 2.12).

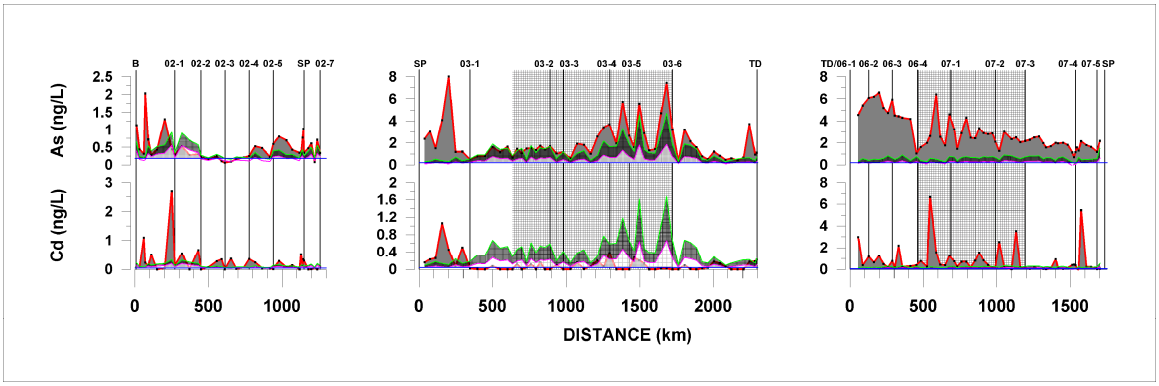

Figure 2.12. Surface snow remaining element concentration (red) and Mount Erebus volcanic plume contributions. Minimum (pink) and maximum (green) contributions versus distance for the ITASE-02 (left), ITASE-03 (middle) and ITASE-06/07 (right) traverses. Vertical lines indicate the locations of firn section collection sites along each traverse; B = Byrd; SP = South Pole; TD = Taylor Dome. Large vertical shaded areas behind plots highlight glaze/dune regions. Horizontal (blue) lines signify detection limits. Note that scales may vary between traverse years.

We calculate the Erebus volcanic contribution for Cd and As using the same method that we used for the global volcanic contribution, except we use 3% (EVmin) and 5% (EVmax) S values in the calculation of the Zreda-Gostynska et al. [1997] element/S ratios (Table 2.10).

Contributions from the Erebus plume potentially account for 77% and 51% of the ITASE-02 mean remaining As and Cd values, respectively (Table 2.11). Spatial data reveal that significant concentrations of As and Cd remain above the Erebus input, specifically, samples located closer to the coast and near South Pole (Figure 2.12).

ITASE-03 EVmax values of As contribute 39% and 78% of the mean remaining As concentration for non-glaze/dune and glaze/dune areas, respectively. ITASE-03 EVmax Cd contributions account for >200% and >600% of the mean remaining Cd concentrations in non-glaze/dune and glaze/dune areas (Table 2.11). Like the global volcanic background contributions, Erebus volcanic plume contributions of both As and Cd are highest in the glaze/dune areas but fail to account for the large peaks observed between South Pole and 03-1 (Figure 2.12).

The Erebus volcanic plume accounts for no more than 23% and 32% of the mean remaining As and Cd concentrations (Table 2.11). This suggests an alternate source/sources for the majority of the As and Cd reaching Antarctica.

2.5 Conclusions

This is the first study to measure 25+ chemical constituents in surface snow and firn across extensive regions of East and West Antarctica and may also be the first to provide total-Cs concentration data. Previous studies [*Faure and Lee*, 1999; *Pourchet et*

al., 2003; *Pourchet et al.*, 1997; *Sbrignadello et al.*, 1994; *Woodward*, 1964] have focused on only one isotope, ^{137}Cs, either as a measure of fallout from anthropogenic nuclear activities or as a dating tool for ice cores. Researchers usually measure ^{137}Cs fallout in Antarctic soils and sediments to gauge its impact on ecosystems, and when using Cs as a dating tool, researchers generally focus on ^{137}Cs concentrations around the time of the 1955 and 1965 bomb-activity peaks. As a result, data regarding total-Cs concentrations in recent Antarctic snow and firn are rare.

Comparisons between surface snow and multi-year firn values of Na^+ (winter-spring input) and SO_4^{2-} (summer input) suggest that the majority of these samples represent average summer surface snow concentrations (Figure 2.5). The majority of the surface snow trace element concentrations presented here are in the region of, or below, concentrations measured in previous studies and the multi-year means calculated from firn sections (Table 2.6 and Figure 2.7, 2.8, & 2.9). Therefore, the values presented here are conservative estimates of Antarctic mean trace element concentrations and may be used as a baseline for an Antarctic spatial chemical concentration framework. However, one must bear in mind that samples from glaze/dune areas represent multi-year values of unknown age.

Based upon backscatter and grain size values, in addition to physical and chemical concentration EOFs, we have shown that East Antarctic glaze/dune areas tend to increase the magnitude and variability of chemical concentrations in the snow, likely precluding these areas from containing a straightforward interpretation of chemical climate records. Backscatter and grain size measurements, good indicators of glaze/dune

extent in East Antarctica, may be extremely valuable during the site location phase of Antarctic climate-related ice coring sites.

Glazed, non-dune regions also adversely affect the chemical signature of surface snow and firn, although not as severely as glaze/dune regions. The average grain size in a typical glazed, non-dune region is not as large as that in well-developed glaze/dune region (Figure 2.3). However, glazed, non-dune regions may be identified by their high (greater than -10) backscatter values (Figure 2.3). Although the ITASE-03 and ITASE-06/07 traverses are the only ones shown to pass through extensive glaze/dune areas (Figure 2.1), we think that all of our traverse routes pass through at least some glazed, non-dune areas based upon backscatter values, field observations, chemical concentrations, and EOF results.

It is interesting to note that in all areas and during all traverse years the $\delta^{18}O$, elevation and mean annual temperature are always strongly related (Table 2.3). This is likely a result of Antarctic elevations, and hence temperatures, being strongly associated with distance from the coast and therefore the precipitation source. In West Antarctica (ITASE-02) the grain size and accumulation are strongly related to elevation and temperature while in central East Antarctica (ITASE-03) only the accumulation retains this strong relationship. Closer to the Transantarctic Mountains (ITASE-06/07), the accumulation is less strongly associated with elevation and temperature and inversely associated with backscatter and grain size. This pattern of accumulation behavior is most likely an outcome of the traverse passing through well-developed glaze/dune areas in addition to glazed, non-dune areas for significant portions of both the ITASE-03 and ITASE-06/07 traverse routes.

The elements Cd, Pb, Bi, As, Li, and S are significantly enriched across Antarctica relative to both the oceanic and crustal elemental compositions (Table 2.9). A significant fraction of Antarctic S comes from marine biological activity. However, a significant fraction (10-20%) is attributed to volcanism. Unfortunately, we do not have any volcanic contribution data for Li. However, global volcanic outgassing contributions account for a significant fraction of the Bi in both East and West Antarctica. Global volcanic outgassing also accounts for a significant fraction of the Cd in East Antarctica, but mainly in the glaze/dune areas (Figure 2.11). Global volcanic outgassing cannot account for the observed concentrations of Pb or As in any area of Antarctica. Significant excess chemical concentration peaks for Cd, Pb, Bi, and As in other areas of Antarctica suggest that alternate source/sources exists for these elements (Figure 2.11).

Volcanic outgassing from Mount Erebus can account for a significant fraction of the As and Cd in parts of West Antarctica and East Antarctica (Figure 2.12). Yet, as with the global volcanic outgassing, Erebus plume contributions account for a significantly smaller fraction of these two elements in non-glaze/dune areas, likely a result of non-volcanic S enrichment in glaze/dune areas (Figure 2.12). After accounting for potential volcanic contributions from global and local sources, concentrations of As remain high near coastal West Antarctica and Taylor Dome (Figure 2.12) suggesting either a marine source or a lower-atmospheric transport pathway for As.

The As and Cd concentration peaks between South Pole and 03-1 remain unexplained by the combination of crustal, oceanic, global volcanic and local volcanic source contributions (Figure 2.12). Additionally, the Bi and Pb concentration peaks between South Pole and 03-1 remain unexplained by the combination of crustal, oceanic

and global volcanic source contributions (Figure 2.11). One possible explanation for these peaks is increased anthropogenic activity at the South Pole Station during the summer months. Possible alternate sources for the remaining excess concentration peaks are marine biogenic and/or more distant anthropogenic sources from industrialized regions of the Southern Hemisphere and possibly the Northern Hemisphere. The latter source seems most likely for Cd, Pb and Bi because a marine biogenic source would cause a pattern more like S, with higher concentrations near the West Antarctic coast, which is not the case.

Future work will involve further research into the possible sources and input timing of previously unreported enriched elements, such as Li and As. Examination of the enriched-element time-series will help in this respect. Additional work to differentiate between non-glaze/dune and glazed, non-dune areas will be valuable. Expanding the scope of this research to achieve full-coverage of Antarctica will require the incorporation of external data, such as aerosol monitoring sites, and collaboration with other research groups in similar fields.

Most importantly, our study provides a robust framework for monitoring future changes in the chemistry of the atmosphere over Antarctica. With the ITASE surface snow and firn chemistry framework, it is now possible to more-accurately select sites that capture specific chemical changes of interest. For example, when monitoring changes in S deposition across Antarctica, this framework clearly shows that one need not sample the glaze/dune areas, particularly those on the East Antarctic Plateau. The framework highlights exactly where one need not sample. This level of sampling accuracy will prove particularly important in the future as we continue to monitor Antarctic atmospheric

chemical deposition. Potential changes in atmospheric chemistry are inevitable as Antarctica continues to warm and as Southern Hemisphere industrial activity intensifies.

Chapter 3

AN ICE CORE PROXY FOR NORTHERLY AIR MASS INCURSIONS (NAMI) INTO WEST ANTARCTICA

3.1 Chapter Summary

A 200-year proxy for Northerly Air Mass Incursions (NAMI) into central and western West Antarctica is developed from the examination of 19 shallow (21m – 150m deep) Antarctic ice core non-sea-salt (nss) Ca^{2+} concentration records. The NAMI proxy reveals a significant rise in recent decades. This rise is unprecedented for at least the last 200 years and is coincident with anthropogenically-driven changes in other large-scale Southern Hemisphere (SH) environmental phenomena such as greenhouse gas (GHG) induced warming, ozone depletion and the associated intensification of the SH westerlies. The Hysplit trajectory model is used to examine air mass transport pathways into West Antarctica. Empirical Orthogonal Function analysis, in combination with trajectory results, suggests that atmospheric circulation is the dominant factor affecting nssCa^{2+} concentrations throughout central and western West Antarctica. Ozone recovery will likely weaken the spring-summer SH westerlies in the future. Consequently, Antarctica could lose one of its best defenses against SH GHG warming.

3.2 Introduction

Globally record-breaking warming, glacier retreat, and ice shelf collapse on the Antarctic Peninsula reveal the consequences of anthropogenic source greenhouse gas (GHG) warming and ozone depletion coupled with the natural magnifying capacity of ocean ice cover removal [*ACCE*, 2009; *Lubin et al.*, 2008; *Rignot et al.*, 2004; *Scambos et al.*, 2004; *Turner et al.*, 2006; *van den Broeke*, 2005]. To the south, West Antarctica has undergone significant (>0.1ºC/decade since 1950) warming in recent decades [*Steig et al.*, 2009] and weak yet statistically significant warming trends are beginning to emerge at some East Antarctic interior and coastal stations since 1992 [*Monaghan et al.*, 2008]. Much of the foregoing is linked to the behavior of the Southern Annular Mode (SAM) [*Schneider et al.*, 2004; *Thompson and Solomon*, 2002]. The SAM is the dominant pattern of Southern Hemisphere (SH) atmospheric variability south of 20ºS and its index describes the relative anomalies in the meridional pressure gradient between the sub-Antarctic and middle latitudes. Since instrumental records began, in the 1950s, the SAM has been trending into a positive high-index state [*Marshall*, 2003; *Thompson et al.*, 2000]. Since the late 1970s there has been a rise in the rate of increase as a consequence of the thermal gradient amplification induced by ozone depletion and GHG warming [*ACCE*, 2009; *Thompson et al.*, 2000]. As a result, there has been contraction of the Antarctic Circumpolar Vortex (ACV), the large-scale cyclonic circulation of the troposphere centered over Antarctica, and intensification of the SH westerlies that form at the edge of the ACV [*Crook et al.*, 2008; *Randel and Wu*, 1999; *Thompson and Solomon*, 2002]. This intensification has thus far isolated most of Antarctica from the impacts of GHG warming [*ACCE*, 2009] and has probably led to a deepening of the Amundsen Sea

Low (ASL) pressure system [*Turner et al.*, 2009]. The more positive SAM has also weakened katabatic winds over much of East Antarctica resulting in a less turbulent heat flux into the surface [van den Broeke and van Lipzig, 2004]. Understanding how long these conditions persist and how rapidly the westerlies' barrier can be invaded is critical in assessing the future of SH climate and sea level rise.

To begin to address these questions we examine an ice core record array that reveals increases in extra-Antarctic source dust-laden air masses into coastal and central West Antarctica during the last century and a rapid rise in the rate of increase during the last three decades (Figure 3.1). These dust records offer a proxy for the relative intensity of extra-Antarctic continental source air mass incursions (storms) into West Antarctica, and by association the strength of the SH westerlies and Amundsen Sea Low that spawn these storms. Hereafter we will refer to this as the Northerly Air Mass Incursion (NAMI) proxy.

3.3 Methods

Previous work demonstrates that statistically significant correlations exist between glaciochemical concentrations and instrumented climate records in and around Antarctica. Examples of this include strong associations between ice core Na^+ concentrations and the ASL pressure system [*Kaspari et al.*, 2004; *Kreutz et al.*, 2000b], ice core methanesulphonic acid concentrations and sea ice extent [*Abram et al.*, 2007; *Curran et al.*, 2003; *Meyerson et al.*, 2002; *Welch et al.*, 1993], ice core stable isotopes and temperature [*Schneider et al.*, 2004; 2006], and the ice core non-sea-salt-Ca^{2+} (nssCa) concentrations used as a NAMI proxy in this study.

Figure 3.1. Polar stereographic shaded relief map of Antarctica showing NAMI cores and decadal contour plots showing the spatio-temporal distribution of normalized nssCa concentrations. Inset) Antarctic location map. EAIS = East Antarctic Ice Sheet, WAIS = West Antarctic Ice Sheet, RIS = Ross Ice Shelf, FRIS = Filchner-Ronne Ice Shelf, RS = Ross Sea, AS = Amundsen Sea, BS = Bellingshausen Sea, WS = Weddell Sea. Area denoted by yellow dashed line indicates geographic location of boxes shown below.
Boxes: decadal contour plots showing the spatio-temporal distribution of normalized nssCa concentrations from the suite of 19 cores. Black dots within each contour box indicate which ice cores were used to construct the plot. Note: 1990 contour box is smaller because the 03-1 core is not used for that decade.

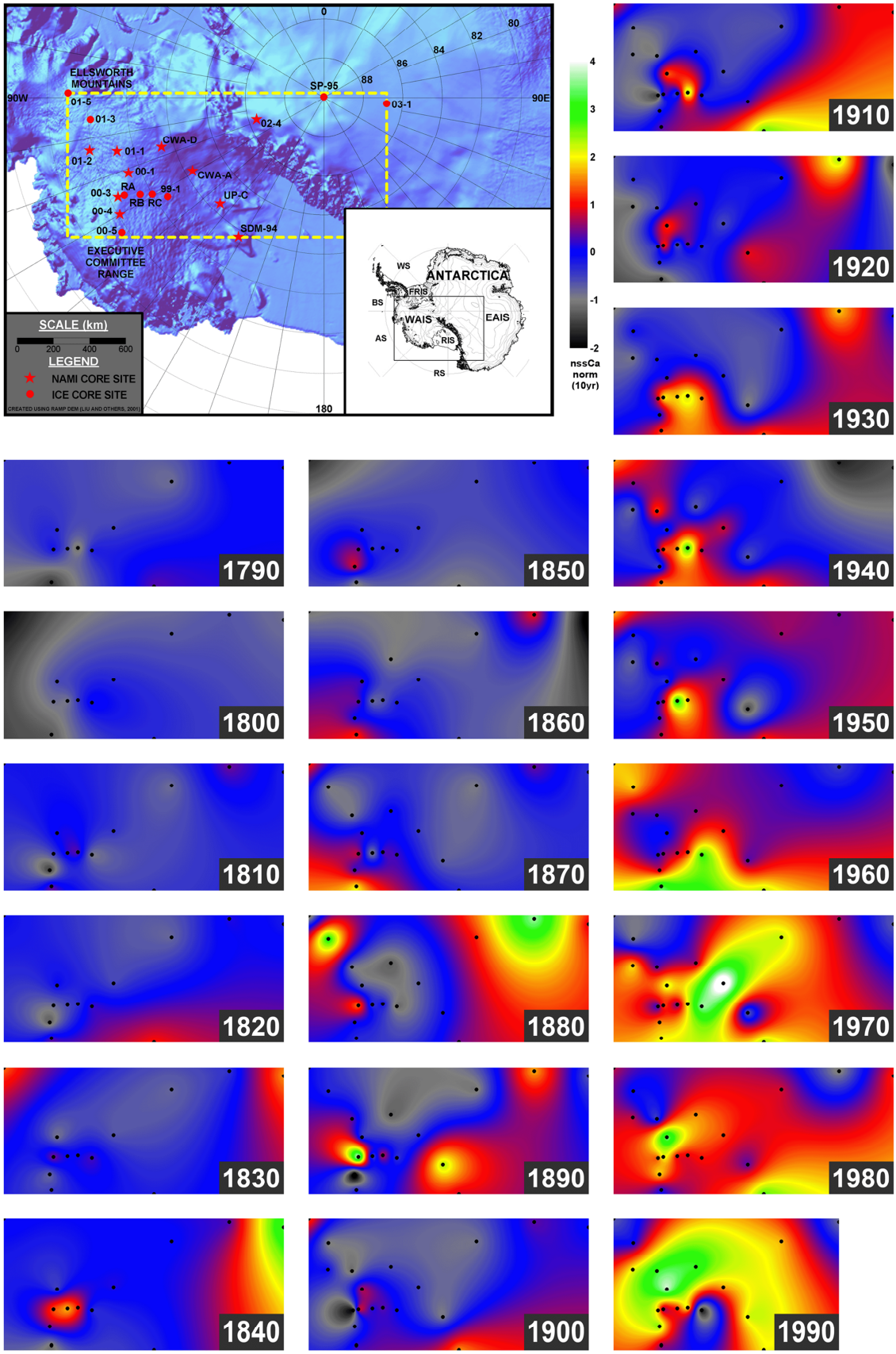
0
80
82
84
86
88
90W
90E
180
ELLSWORTH MOUNTAINS
EXECUTIVE COMMITTEE RANGE
SP-95
01-5
01-3
02-4
03-1
CWA-D
01-1
01-2
00-1
CWA-A
RA
00-3
99-1
RB
RC
UP-C
00-4
00-5
SDM-94
SCALE (km)
0 200 400 600
LEGEND
NAMI CORE SITE
ICE CORE SITE
CREATED USING RAMP DEM (LIU AND OTHERS, 2001)
ANTARCTICA
WS
FRIS
BS
WAIS
EAIS
AS
RIS
RS
4
3
2
1
0
-1
-2
nssCa norm (10yr)
1910
1920
1930
1790
1850
1940
1800
1860
1950
1810
1870
1960
1820
1880
1970
1830
1890
1980
1840
1900
1990

A previous ice core nssCa study [*Yan et al.*, 2005] established that a statistically significant positive relationship exists between the strength of SH westerlies and nssCa concentrations in two West Antarctic ice cores (SDM-94 and 00-1) from 1948 – 2002. In this study we expand these findings using an array of 19 ice core nssCa records that include the original SDM-94 and 00-1 sites (Figure 3.1) and expand the significance of the proxy based on investigation of the sources and transport pathways of nssCa.

The 19 ice cores used to produce our NAMI proxy range in depth from 21m to 150m and span the time period AD 850 – AD 2000 (Table 3.1). The majority of the cores (99-1, 00-1, 00-3, 00-4, 00-5, 01-1, 01-2, 01-3, 01-5, 02-4, and 03-1) used in this study were collected during seven US ITASE (International Trans Antarctic Scientific Expedition) field seasons [*Mayewski et al.*, 2009; *Mayewski et al.*, 2005b]. The US ITASE cores were melted using the University of Maine continuous melter system [*Osterberg et al.*, 2006] and are sub-annually sampled (except for 03-1) for their entire depth (see Table 3.1 for more information). This sampling resolution captures the clear seasonal signal that is present in several of the glaciochemical series and allows determination of a relative dating accuracy of better than one year [*Dixon et al.*, 2004; *Steig et al.*, 2005].

All samples were measured for Na^+, K^+, Mg^{2+}, Ca^{2+}, Cl^-, NO_3^-, SO_4^{2-} using a Dionex® DX-500 ion chromatograph coupled to a Gilson® autosampler. To determine anion (Cl^-, SO_4^{2-} and NO_3^-) and cation (Na^+, Ca^{2+}, Mg^{2+}, and K^+) concentrations we used an IonPac AS-11 Hydroxide-Selective Anion-Exchange Column, and an IonPac CS-12A Cation-Exchange Column, respectively. Ca^{2+} concentrations have an accuracy of better than 0.1 μg/l. nssCa concentrations were calculated using the standard seawater ratio

[*Holland*, 1978] of Na^+, K^+, Mg^{2+}, Ca^{2+}, Cl^-, and SO_4^{2-} after the method outlined by O'Brien *et al.* [1995] that performs an iterative test against each species to determine the most conservative seasalt indicator per sample.

Location (Core)	Latitude (ºN)	Longitude (ºE)	Elevation (m)	Depth (m)	Core Age (Year AD)	Mean Acc. Rate (cm weq)	References
99-1	-80.6200	-122.6300	1350	58	1988-1713	13	[*Dixon et al.*, 2004]
00-1	-79.3831	-111.2390	1791	105	1997-1651	21.8	[*Dixon et al.*, 2004]
00-3	-78.4330	-115.9172	1742	60	1999-1888	38.9	This Study
00-4	-78.0829	-120.0764	1697	58	1999-1799	19	[*Dixon et al.*, 2004]
00-5	-77.6830	-123.9950	1828	60	1995-1708	13.6	[*Dixon et al.*, 2004]
01-1	-79.1597	-104.9672	1842	73	2000-1857	33.7	This Study
01-2	-77.8436	-102.9103	1336	71	2000-1890	42.9	[*Dixon et al.*, 2004]
01-3	-78.1202	-95.6463	1620	71	2000-1859	32.6	[*Dixon et al.*, 2004]
01-5	-77.0593	-89.1376	1239	114	2000-1781	38.9	[*Dixon et al.*, 2004]
02-4	-86.5025	-107.9903	2586	72	1997-1593	11	This Study
03-1	-86.8400	95.3100	3124	21	(1982-1800)	4.6	This Study
SP-95	-90.0000	0.0000	2850	71	1990-1487	7.3	[*Meyerson et al.*, 2002]
SDM-94	-81.6480	-148.7900	620	150	1995-1890 (850)	11.9	[*Kreutz et al.*, 1997]
UP-C	-82.4391	-135.9719	525	28	1996-1870	12.1	This Study
CWA-A	-82.3671	-119.2855	950	93.5	1994-1934 (1741)	13.2	[*Reusch et al.*, 1999]
CWA-D	-81.3723	-107.2750	1930	50.5	1994-1952 (1851)	19.9	[*Reusch et al.*, 1999]
RIDS-A	-78.7300	-116.3300	1740	150	1996-1831 (1507)	23.3	[*Kreutz et al.*, 2000a]
RIDS-B	-79.4600	-118.0500	1603	60	1996-1925 (1691)	15	[*Kreutz et al.*, 2000a]
RIDS-C	-80.0100	-119.4300	1530	60	1996-1905 (1594)	11.2	[*Kreutz et al.*, 2000a]

Table 3.1. Data for ice cores. Note that ice core ages in brackets show full core age including multi-annual data (2.5-year), numbers without brackets in this column indicate the part of the core that is sampled sub-annually. Mean Acc. Rate = mean annual accumulation rate for the length of each sub-annual record (cm weq = cm of water equivalent depth).

The chemical concentration of each sample is reported rather than flux (flux = concentration * accumulation rate) because dry deposition rates for inland Antarctica are not well constrained and there is no significant correlation between nssCa concentration and accumulation rate to justify a flux correction [*Dixon et al.*, 2004]. Further, the use of a flux calculation would only serve to enhance the observed signal because nssCa concentrations are already higher close to the coast and would be higher still if multiplied by coastal accumulation rates (as coastal values are higher than those inland).

To better assess the spatio-temporal variability of the nssCa concentrations at each site all nssCa time series were normalized and the results contoured by decade from

1790 – 1990 (Figure 3.1). The contour maps highlight the relative magnitude of the nssCa variability from site to site through time. Each decadal value is the mean of the 5 years either side of it, e.g. the 1990 decadal value is calculated from all values between 1985 and 1995. As Table 3.1 shows, some cores do not have data all the way up to 1995 (03-1, SP-95, CWA-A, and CWA-D). For these cores we calculate the 1990 value using the available data for each core between 1985 and 1995. For the 03-1 core we use the available data to calculate a 1980 value and do not use the core in the 1990 contour plot. Two of the cores (99-1 and Up-C) contain data gaps. In the case of Up-C, the gaps are less than one year and temporally distributed enough that we do not consider them to alter the decadal values significantly. However, in the case of 99-1 the data gaps are more extensive with values missing for the following time periods: 1995 to 1988.4, 1963.7 to 1962.4, and 1957 to 1943. This results in ~6.6 years of data missing from the 1990 decadal value calculation, ~3.3 years missing from the 1960 value, 2 years missing from the 1940 value, and no value at all for 1950. For construction of the contour plots we use all available 99-1 data for the decadal values, but could not use the core for the 1950 plot.

3.4 Ice Core nssCa

Many of the ice core records exhibit nssCa concentration increases during the last century (Figure 3.1). In the last two to three decades, nssCa concentrations in several of these cores (in particular 00-1, 00-3, 00-4, 01-1, and SDM-94) increase more than 100% above their mean 1800-1900 values (Table 3.2). These sites are located in central and western West Antarctica directly inland from the Ross Ice Shelf and the Amundsen Sea embayment. Three cores further inland also show similar concentration increases (02-4,

CWA-A, and CWA-D). Cores from the East Antarctic interior (03-1 and SP-95) and the eastern segment of West Antarctica (01-3 and 01-5) exhibit no significant change throughout the 1900s. Several sites inland between the main West Antarctic ice divide and the Ross Ice Shelf (00-5, RIDS-A, -B, -C, and 99-1) exhibit a fairly high degree of concentration variability throughout the 1900s with no apparent trends.

Core	1990	1980	1970	1960	1950	1940	1930	1920	1910	1900
03-1	-	1.3	0.8	1.0	1.2	0.5	1.0	0.5	1.3	1.0
02-4	4.6	3.2	5.4	2.3	2.9	1.7	1.1	1.6	1.0	0.5
01-1	2.2	1.0	1.3	1.3	1.4	1.6	1.2	1.0	0.9	0.8
01-2	1.7	1.3	1.7	1.1	0.7	0.7	0.7	0.6	0.7	1.0
01-3	0.9	0.9	0.7	1.5	0.9	1.1	0.9	0.8	0.7	0.6
01-5	0.9	1.2	0.9	1.5	1.5	1.5	0.8	0.9	1.3	1.4
00-1	3.7	3.6	2.6	1.1	0.9	0.9	1.2	2.0	2.1	1.6
00-3	3.9	3.4	2.6	2.6	2.6	2.6	3.0	2.2	1.3	1.0
00-4	2.1	1.9	1.8	1.5	1.3	1.0	1.2	1.1	1.1	1.0
00-5	1.2	1.0	1.8	2.4	1.3	1.6	1.5	0.5	1.1	1.1
99-1	0.5	1.5	2.4	2.1	-	1.3	1.7	1.0	1.0	1.1
RIDS-A	0.9	1.7	1.3	0.9	0.9	1.3	1.6	1.3	0.9	1.1
RIDS-B	1.8	1.7	1.4	1.6	3.0	2.0	2.2	0.7	0.8	1.2
RIDS-C	1.8	1.3	1.8	1.4	1.6	2.2	1.8	1.2	2.0	1.1
CWA-A	10.4	8.8	24.6	7.7	5.6	6.7	1.7	0.3	0.4	0.6
CWA-D	4.8	3.3	2.3	2.3	1.5	1.1	1.5	2.0	1.6	1.2
SDM-94	1.9	2.2	2.1	2.0	1.5	1.6	1.6	1.3	2.2	1.7
UP-C	1.6	1.1	0.7	1.1	0.5	0.8	0.7	1.2	1.0	0.7
SP-95	0.7	0.7	1.0	0.8	1.0	0.5	1.2	1.4	1.1	1.0

Table 3.2. Relative nssCa concentration rise. Decadal nssCa concentrations where each decadal value is divided by the 1800-1900 mean value for that core.

The major source of nssCa in polar ice is crustally-derived dust [*Legrand and Mayewski*, 1997]. Previous work has shown that the sources of nssCa to West Antarctica are the circum-Antarctic SH continents and ice-free regions within Antarctica [*Bertler et al.*, 2005; *Gayley and Ram*, 1985; *Shaw*, 1979; *Tuncel et al.*, 1989]. However, only ~2% of Antarctica is ice-free and the majority of these ice-free areas are located in the Transantarctic Mountains. The Ellsworth Mountains contain a significant ice free area, but only two of our cores, 01-5 and 01-3, are located close enough for this source to be considered of potential significance.

The Pacific sector of the West Antarctic coastline contains only a tiny ice-free fraction. Tropospheric storm-track pathways into West Antarctica pass over only a limited section of the aforementioned ice-free areas. Since change in the extent of these ice-free areas has not been reported and they offer a minimal source region we do not consider the coastal West Antarctic ice-free areas to be a significant contributor to dust loading over the region encompassing the majority of cores used in this study.

3.5 Southern Hemisphere Dust Sources and Trajectories

The primary SH dust source regions feeding West Antarctica, in order of importance, are Australia, South America, and South Africa [*De Deckker et al.*, 2010; *Li et al.*, 2008; *Mahowald et al.*, 2010; *Prospero et al.*, 2002] Thirty-day forward trajectories (FT) originating from the southernmost dust source region on each of these SH continents, except Antarctica (Figure 3.2) were calculated using the NOAA Hysplit Model v.4.8 [*Draxler and Rolph*, 2003] in conjunction with the NCEP/NCAR global atmospheric reanalysis datasets archived on the READY website (ftp://www.ready.noaa.gov/pub/archives/reanalysis/).

The Hysplit model control file included: (i) starting locations = 7 (each location with a slightly different latitude and longitude, up to ±2° from the center of each dust source area), (ii) altitude of each starting location = 100 m, (iii) top of the model = 30,000 m (agl), and (iv) vertical motion = data (default value, uses meteorological model's vertical velocity fields).

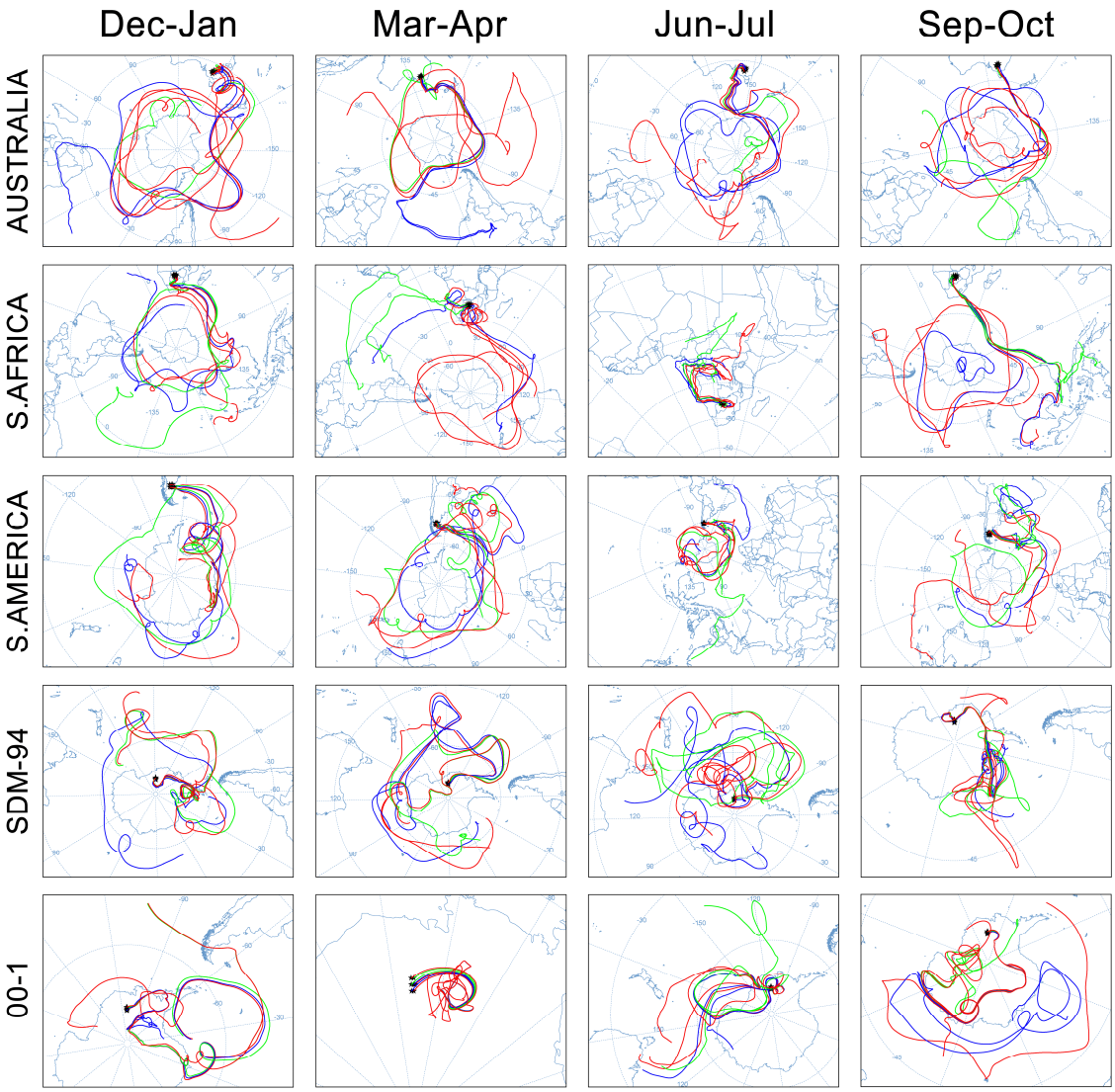

Figure 3.2. Thirty-day forward trajectories for 1996 originating from the southern-most dust source in Australia, South Africa, and South America. Thirty-day back trajectories for 1996 originating from the SDM-94 and 00-1 ice core sites in West Antarctica. Trajectories calculated using the NOAA Hysplit Model (version 4.8) in conjunction with the NCEP/NCAR atmospheric reanalysis (ftp://www.ready.noaa.gov/pub/archives/reanalysis/).

The FT was run for each of the four seasons for four different years (1980, 1989, 1996, and 1999) with seasonal starting times as follows: Dec 15th, Mar 15th, Jun 15th, and Sep 15th. These years were chosen to represent the last three decades whilst overlapping the most highly-resolved model data.

In each model run the dust-laden air parcels generally circulate southward from each dust source whereupon they are incorporated into, and circulate around Antarctica embedded in the ACV. Only Australia and South America commonly spawn air masses that reach the Antarctic continent within 30 days of transport from source. We show the 1996 model output for representative SH air mass transport pathways (Figure 3.2).

Thirty-day back trajectories (BT) from the SDM-94 and 00-1 ice core sites were also calculated using the same NOAA Hysplit Model in conjunction with NCEP/NCAR atmospheric reanalysis (Figure 3.2). The BT are based on identical model control file setups to the FT runs, the only difference being the start times: Jan 15th, Apr 15th, Jul 15th, and Oct 15th, in order to cover approximately the same 30-day period as the FT. The BT runs demonstrate that 30 days prior to arrival, air masses approaching SDM-94 and 00-1 frequently travel in a broadly similar pattern; the air masses originate somewhere within the ACV and circulate around the Antarctic continent until they are diverted inland, as synoptic storms, across the Ross, Amundsen, and Bellingshausen Seas. In some cases, the air masses reach West Antarctica after being diverted across the Weddell Sea and traveling over the Filchner-Ronne Ice Shelf. After moving inland, the air masses can circulate over the continent for some time before arrival at the core sites and in rare cases circulate randomly over the continent for 30 days or more before arrival. These FT and BT model runs show that dust reaching the West Antarctic ice core sites in this study is not directly related to a single dust source region. It is a blend from all SH sources that feed into the ACV.

3.6 Constructing the NAMI Proxy

Some site-to-site variability of nssCa concentrations results from the relatively chaotic behavior of air masses during their transit, via storm incursions, from the ACV to the ice core sites. To reduce the effects of this variability a NAMI proxy was developed by stacking annually averaged, normalized 02-4, 01-1, 01-2, 00-1, 00-3, 00-4, CWA-A, CWA-D, SDM-94, and Up-C nssCa concentration records. We chose these sites for a number of reasons, in order of importance: 1) they all correlate positively to the NCEP/NCAR reanalysis, Jan to Dec, 850mb zonal wind field in the area of the ACV, 2) they exhibit recent nssCa concentration increases with 1980-1990 values >100% above their 1800-1900 means (except Up-C and 01-2), and 3) they are directly in line with lower tropospheric air mass pathways into West Antarctica (except 02-4).

The Up-C and 01-2 cores exhibit slightly weaker recent nssCa concentration increases, 60% and 70% respectively, and the 02-4 core is not directly in line with lower tropospheric air mass pathways into West Antarctica. However, all three correlate positively to the NCEP/NCAR reanalysis, Jan to Dec, 850mb zonal wind field in the area of the ACV and were included primarily for this reason. Ten cores are used to construct the NAMI proxy and their nssCa records begin and end on different years. We consider the NAMI proxy valid as long as 50% or more of the cores are being utilized for a given year. When constructed from sub-annual nssCa data only, the NAMI proxy spans 1870-1997 (Figure 3.3a & 3.3b). For a longer perspective we can use 2.5-year nssCa data, the resulting NAMI then spans 1800-1995 (Figure 3.3c).

Of the 19 cores used in this study, 10 are suitable for constructing the NAMI proxy (they all exhibit positive associations in addition to the main reasons outlined

above), thus highlighting the importance of using a suite of ice cores. The remaining cores (03-1, 01-3, 01-5, 00-5, 99-1, RIDS-A, -B, -C, and SP-95) were not used for the NAMI proxy for a number of reasons, the most important being their lack of correlation to the NCEP zonal wind field. The signals of interest in these cores are likely confounded for a number of reasons. Sites 03-1 and SP-95 are located high on the East Antarctic Plateau, far from the influence of lower tropospheric storms. Sites 01-3 and 01-5 are located in the eastern sector of West Antarctica, near the Ellsworth Mountains and probably receive a confounding dust input from there. Site 00-5 is protected from incoming storms by its location behind the Executive Committee Mountains, which tend to divert storms away from the site. Sites RIDS-A, -B, -C, and 99-1 are situated leeward of the main West Antarctic ice divide, in a storm shadow zone, and as a result receive less consistent precipitation input than core sites located windward of the ice divide. The CWA-A, SDM-94, and Up-C cores are also located leeward of the main West Antarctic ice divide, however, the elevation and location of these three ice core sites is such that they still receive input from storms travelling inland across the Ross Ice Shelf.

3.7 Results and Discussion

The NAMI proxy for West Antarctica (Figure 3.3) reveals intensification starting between 1960 and 1970 with an abrupt increase in the rate of intensification, well above the range of natural variability, around 1980. The NAMI proxy exhibits an increasing trend similar to both the SAM [*Marshall*, 2003] from 1957-1997, and the total column ozone record (inverted) from above Halley station, Antarctica [*Shanklin*, 2009] from 1956-1997 (Figure 3.3a).

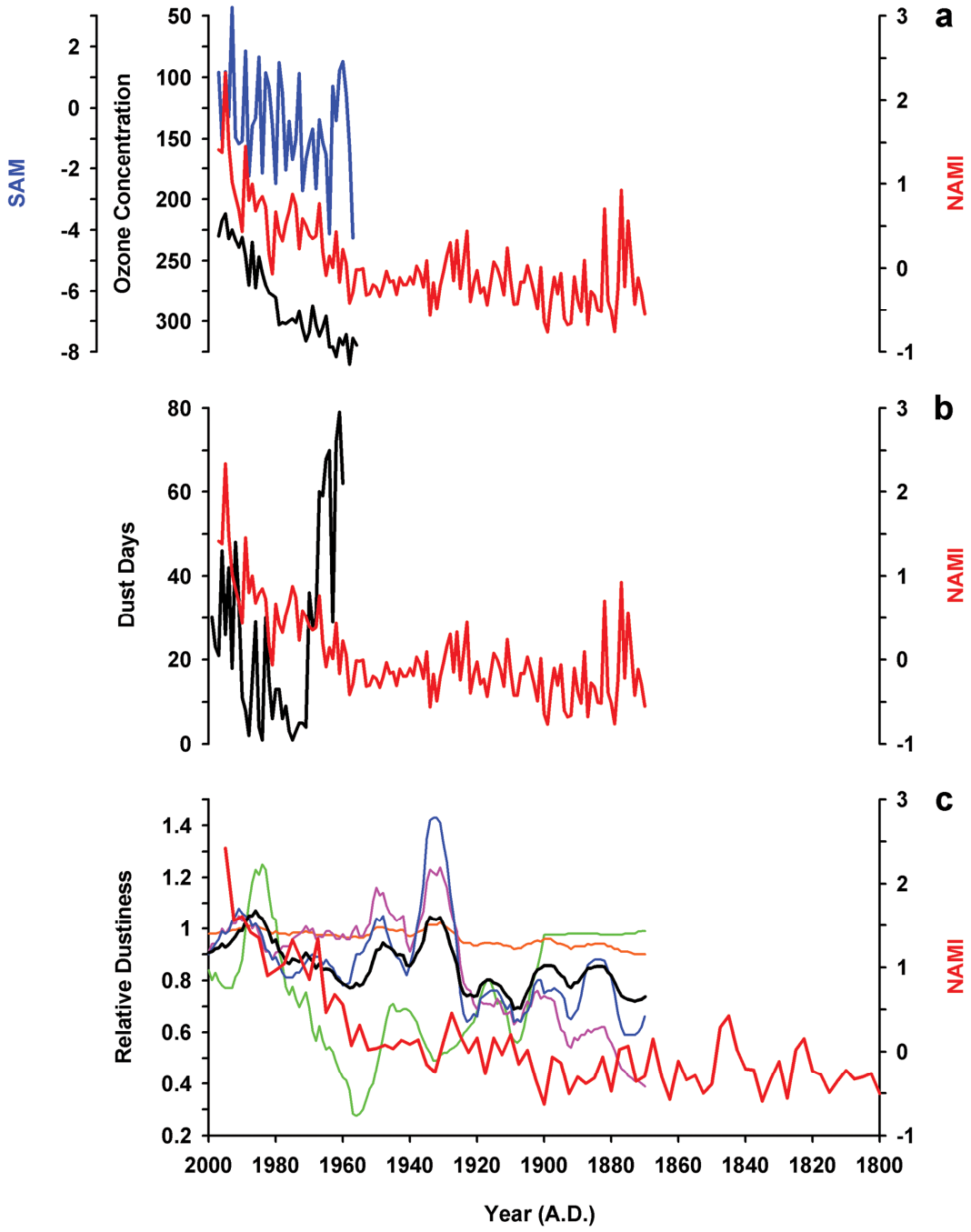

Figure 3.3. Annual and 2.5-year NAMI proxy with ozone, SAM, Australian dust, and SH relative dustiness data. a) & b) Annual NAMI proxy 1870-1997 (red). c) 2.5-year NAMI proxy 1800-1995 (red). Also shown, a) Total column ozone concentrations (inverted) above Halley British Antarctic Station 1956-1997 (black; [Shanklin, 2009]). Southern Annular Mode (SAM) 1957-1997 (blue; [Marshall, 2003]) b) Eastern Australian dust 1960-1999 (black; [BoM, 2005]). c) SH relative dustiness data 1870-2000 (black = SH dust stack, blue = Eastern Australia, purple = South America, orange = South Africa, green = North Africa; [Mahowald et al., 2010]).

Thus, the timing of the NAMI proxy increase coincides with recent intensification of the SH westerlies attributed to changes in the thermal gradient produced by modern ozone depletion and also GHG rise [*ACCE*, 2009; *Randel and Wu*, 1999; *Thompson and Solomon*, 2002].

3.7.1 NAMI and Australian Dust

The increases observed in our NAMI proxy are likely a product of changes in transport and/or emission strength (dustiness at source). To demonstrate which of these processes might dominate we compared the NAMI proxy to an instrumental record of dust from Eastern Australia [*BoM*, 2005] and to several SH dust time series extracted from a global reconstruction of dustiness [*Mahowald et al.*, 2010].

Two major dust pathways have been identified from the eastern and south-eastern seaboards of the Australian continent [*Ekstrom et al.*, 2004; *Marx et al.*, 2005; *McTainsh et al.*, 1998]. One pathway is associated with a strengthened mid-latitude westerly airstream coupled with a synoptic deep-low pressure system over south-eastern Australia and the Tasman Sea, that is typically related to a negative SAM climate pattern. This synoptic type transports dust east and south-east across the Tasman Sea and deposits Australian provenance dust in New Zealand, particularly the South Island [*Marx et al.*, 2009]. The second pathway is associated with a weakened westerly circulation over the mid-latitudes in the Australian region, with a poleward sub-tropical ridge and embedded high pressure system over south-eastern Australia, the southern Tasman Sea and New Zealand. This produces northerly winds over south-eastern Australia and transports Australian dust southwards towards the drifting low pressure systems in the westerlies

and is typically associated with positive SAM circulation patterns [*De Deckker et al.*, 2010]. These dust transporting synoptic types are particularly dominant in the Austral summer and spring, the FT analyses shown in Figure 3.2 support these observations.

An Australian Bureau of Meteorology dust record [*BoM*, 2005] from 1960 to 1999 comprises days per month of dust activity. We summed the monthly dust activity data to generate annual time series for 1960 to 1999, data are shown in Figure 3.3b for the combined eastern Australia Mulga and Darling River basins. The eastern Australian dust trend generally declines since the 1960's, dips in the 1970's, and then rises into the 1990's. As evidenced also by the FT, factors affecting dust entrainment and transport [*Ekstrom et al.*, 2004] from continental Australia are extremely variable, and correlations between the eastern Australian dust records and the NAMI proxy are not statistically significant. Despite lacking a statistically significant correlation, it should be noted that the trend of eastern Australian dust activity flips in the middle 1970's and from that point onwards both it and the NAMI proxy exhibit a positive trend. This is consistent with the observed increasing pressure anomaly associated with increased blocking high activity over the Tasman Sea and New Zealand region during spring. This is a major anomaly in the 1st EOF of the Southern Hemisphere pressure field over the past few decades, described by the SAM [*Hall and Visbeck*, 2002] and has also been identified in GCM's as a signature of anthropogenic climate change [*Cai et al.*, 2003].

3.7.2 Relative Dustiness in the Southern Hemisphere

Mahowald et al. [2010] use a combination of model provenance and geochemical provenance studies to produce a global dataset of dustiness from 1870-2000. Four dust

time series from the Mahowald et al. dataset representing North Africa, South Africa, South America, and eastern Australia appear in Figure 3.3c. North Africa is included because the inter-hemispheric transport of dust from the Northern Hemisphere to the Southern Hemisphere is significant, particularly for dust reaching Antarctica [*Li et al.*, 2008]. The latter three overlap the locations covered by the FT used in this study. A fifth time series is constructed by averaging the four aforementioned dust time series. This averaged series is used to represent relative dustiness in the SH atmosphere (Figure 3.3c). None of the dust series exhibit comparable variability to the NAMI proxy. This lends further support to the idea that the NAMI proxy is dominated by atmospheric circulation and storm intensity rather than change in dust source conditions or emissions.

A separate study of dust concentrations from a northern Antarctic Peninsula ice core [*McConnell et al.*, 2007] suggests dust concentrations starting to rise around 1900, coincident with Patagonian warming. However, this increase occurs ~60 years before any such rise in the NAMI proxy. Li et al. [2008] conduct a model-based investigation of dust transport in the SH using the GFDL atmospheric model. They suggest that Patagonian dust is transported primarily through the boundary layer of the atmosphere and dominates the half of the hemisphere comprising the Atlantic and Indian oceans, thus making it highly unlikely to be a significant source for most of West Antarctica. Further, Li et al. show that Australian dust is transported primarily through the mid-troposphere, dominates the Pacific sector, and is the most significant dust source for West Antarctica and for the whole SH in general.

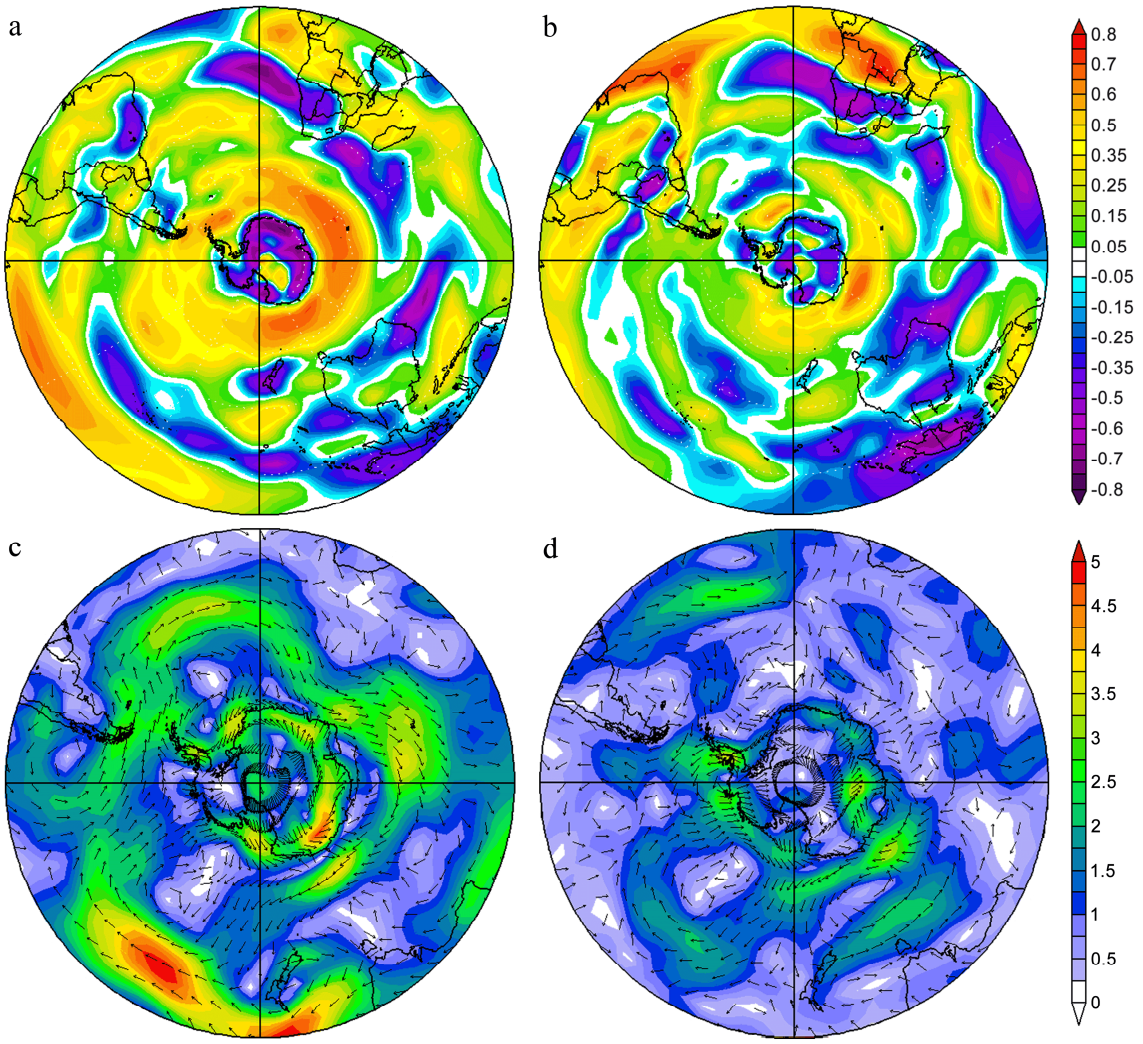

Figure 3.4. Correlation field between the annually averaged composite nssCa time series and the NCEP/NCAR reanalysis. For a) 1948-1997, and b) 1980-1997, Jan to Dec, 850mb zonal wind field (r-values above 0.37 and 0.59 represent significance above 99% respectively). September, 850mb vector wind composite mean for c) 1990s minus 1950s, and d) 1990s minus 1980s. (Images provided by the NOAA-ESRL Physical Sciences Division, Boulder Colorado from their Web site at http://www.cdc.noaa.gov/). Upper scale represents r-values for a) & b). Lower scale represents winds speeds for c) & d).

De Deckker et al. [2010] reinforce the conclusions of Li et al. [2008] by using atmospheric observations and model runs to show that Australia is the primary source of dust to West Antarctica, particularly during interglacial periods. Whilst we cannot break the NAMI proxy record down into seasonal components, due to lack of significant

seasonality in the nssCa signal, it is possible that increasing frequencies of mid-latitude blocking highs in association with an expanded Hadley circulation (a signature of anthropogenic climate change in the Australian/South-West Pacific region, as shown in AR4 [*IPCC*, 2007] models), particularly in the austral summer, are increasing dust transport to the high latitudes.

3.7.3 Correlation with the NCEP Zonal Wind Field

The NAMI proxy curve exhibits a significant ($r = >0.45$, $p = <0.01$) correlation with the NCEP/NCAR reanalysis 1948-1997, Jan to Dec, 850mb zonal wind field in the area of the ACV (Figure 3.4a). We use 850mb because it is a good approximation for the lower troposphere over the study region. Using the more recent period of the NCEP record (1980-1997), which is considered to be more reliable [*Hines et al.*, 2000], results in a similar correlation field, although reduced in strength and with lower significance ($r = >0.4$, $p = <0.1$) due to the reduced number of samples (Figure 3.4b). The spatial distribution of the r-values in Figure 4a and 4b (annular bands arranged more-or-less latitudinally) imply that westerly wind speeds around Antarctica increase concurrently with West Antarctic nssCa concentrations. Investigation of atmospheric circulation around Antarctica using the 850mb vector wind from the NCEP/NCAR reanalysis (subtracting the 1980s from the 1990s, Figure 3.4d, and subtracting the 1950s from the 1990s (with the caveat that the record is more reliable since 1980 onwards), Figure 3.4c) reveals, in recent decades, an increase in the strength of onshore winds along the West Antarctic coastline. These onshore winds impact the NAMI ice core proxy sites inland by increasing their exposure to, and hence concentration of, Southern Hemisphere dust.

West Antarctica is a region impacted by cyclonic storm incursions. The sub-annual nssCa time series that ultimately comprise our NAMI proxy do not display a particular seasonality, hence our proxy represents relative intensity related to storms entering West Antarctica throughout the year.

3.7.4 EOF Analysis

To further determine the relative significance of competing influences on our NAMI proxy we conduct Empirical Orthogonal Function (EOF) analyses using three different time series representing various aspects of SH climate. We use the SAM [*Marshall*, 2003] to represent the strength of westerly wind around Antarctica, the second principal component of 850 hPa geopotential height anomalies south of 20º S [*Thompson and Wallace*, 2000] to represent the dominant behavior of the ASL, and the four Mahowald et al. [2010] dust records, averaged, to represent relative dustiness of the SH atmosphere. We run two separate EOFs, one using non-detrended and another using detrended data. We run the latter EOF, with detrended data, to specifically exclude time series associations caused by long-term trends. In each case we use annually derived data.

3.7.4.1 Non-Detrended Data

Using the non-detrended data, ~75% of the NAMI proxy is represented by EOF 1 along with ~26% of the SAM and ~67% of the SH dust, all positively associated (Table 3.3a). Plotting the EOF 1 loading pattern next to the SAM, SH dust, and NAMI reveals a similar increasing trend exhibited by all. However, the trend of SH dustiness reverses

during the mid-1980s and decreases into the late 1990s. This declining trend in SH dustiness since the mid-1980s is not mirrored by the NAMI or the SAM (Figure 3.5a).

a)

Non-Detrended	EOF 1
% Variance	42.4
NAMI	74.6
SAM	25.6
ASL	-2.0
SH Dust	67.4

b)

Detrended	EOF 2
% Variance	29.4
NAMI	77.1
SAM	0.0
ASL	-35.8
SH Dust	-4.9

Table 3.3. EOF tables for a) non-detrended, and b) detrended data. % Variance = percent variance explained of total data. SAM = Southern Annular Mode. ASL = Amundsen Sea Low. SH Dust = Southern Hemisphere Dust Stack.

3.7.4.2 Detrended Data

Using the detrended data, ~77% of the NAMI proxy is represented by EOF 2 along with ~36% of the ASL (Table 3.3b). The ASL is negatively correlated with the NAMI indicating that as the ASL deepens, more dust is transported into West Antarctica (Table 3.3b). Plotting the EOF 2 loading pattern with the NAMI and ASL highlights this association (Figure 3.5b).

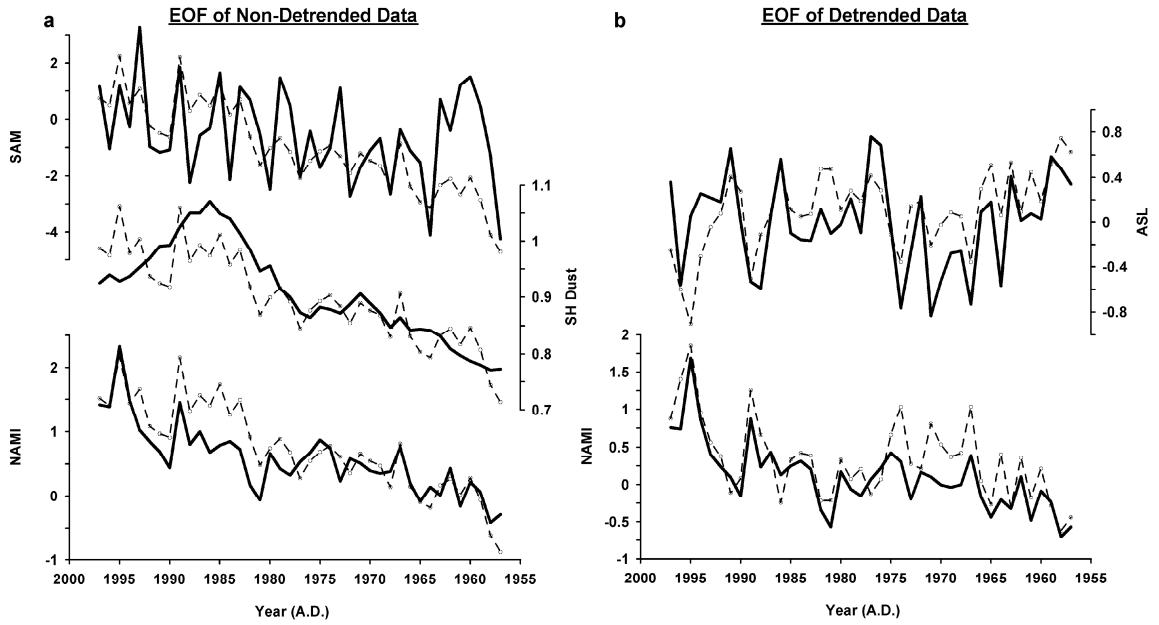

Figure 3.5. EOF loading patterns of a) non-detrended, and b) detrended data. In both cases the EOF is the dashed black line with circles. b) top EOF is inverted.

3.8 Conclusions

It is probable that large variations in dustiness at the primary SH dust source areas, particularly Australia, impact West Antarctic nssCa concentrations. However, as demonstrated above, our findings suggest that SH westerlies and ASL storm intensity are the dominant factors influencing annual variability in nssCa concentrations at the central and western West Antarctic ice core sites used in this study.

The decadal trend in the SAM, since the 1950s, is reflected by the trend of the non-detrended NAMI proxy. However, the detrended NAMI proxy is more closely associated with the annual variability of ASL. Turner et al. [2009] find that the trend towards stronger cyclonic circulation over the Amundsen Sea since the late 1970s is primarily a result of strengthened autumn wind speeds around the continent caused by stratospheric ozone depletion. Despite the ozone hole being an austral spring phenomena,

its impact on lower atmospheric flow is greatest during summer and autumn [*Turner et al.*, 2009]. Supported by our EOF results, this finding highlights the fact that nssCa concentrations in central West Antarctica are primarily influenced by changes in SH atmospheric circulation intensity as opposed to dust source emissions.

The ice core nssCa-based NAMI proxy suggests that the recent intensification of the SH westerlies and associated increase in ASL storm intensity is unprecedented for at least the last 200 years, underscoring the impact of CFC-induced ozone destruction. The implications of ozone recovery on an already warming Antarctic continent are worrisome [*Perlwitz et al.*, 2008]. The modern ozone hole over Antarctica acts to increase the thermal gradient between the Pole and the mid-latitudes by cooling the polar stratosphere. The ozone depletion-induced thermal gradient increase strengthens the westerlies and shields interior East Antarctica from the bulk of SH warming and in addition cools East Antarctica by reducing heat flux into the surface via weakened katabatic winds. Anderson *et al.* [2009] link intensification of the SH westerlies at the end of the last glacial period to an increase in atmospheric CO_2 concentrations through upwelling of CO_2-rich deep ocean water. This mechanism, although currently weak, is likely to further enhance rise of atmospheric CO_2. Mayewski et al. [2004a] propose changes in temperature and atmospheric circulation over coastal West Antarctica coincident with the rise in CO_2.that may mark the earliest impact of human activity on the climate of Antarctica.

Ozone recovery will likely weaken the SH westerlies, particularly during the Austral spring-summer. Consequently, Antarctica could lose one of its best defenses against SH GHG warming. This potential consequence is similar to the impact humans

have had in the Northern Hemisphere where sulfate aerosols temporarily reduced the warming effects of GHG rise from the 1940s-1970s.

Chapter 4

CONCLUSIONS

4.1 Chapter 2 Summary

This is the first time >25 chemical constituents (major ions, trace elements, and stable isotopes) have been measured in the surface snow and firn across extensive regions of East and West Antarctica. It is probably also the first to provide total-Cs concentration data. All samples (surface snow and firn sections) are analyzed using an ion chromatograph (IC) for their soluble major ion content (Na^+, K^+, Mg^{2+}, Ca^{2+}, Cl^-, NO_3^-, SO_4^{2-}, $CH_3SO_3^-$ (Methylsulfonate: MS^-)). The surface snow samples are additionally analyzed for their stable oxygen isotopes ($\delta^{18}O$) by isotope ratio mass spectrometry (IRMS). All surface snow samples and several firn sections (02-1, 02-5, South Pole, 03-1, 03-3, 06-2, 07-4, and 07-5; Table 2.1) are also analyzed for a suite of trace elements (Sr, Cd, Cs, Ba, La, Ce, Pr, Pb, Bi, U, As, Al, Ti, V, Cr, Mn, Fe, Co, and Li) by inductively coupled plasma sector field mass spectrometry (ICP-SFMS). The ICP-SFMS also measures the total Na, K, Mg, Ca, and S concentrations in each sample.

The majority of the trace element concentrations presented here are conservative estimates of Antarctic mean summer values, the remainder represent mean annual or glaze/dune values. In East Antarctic glaze/dune areas the magnitude and variability of chemical concentrations in the surface snow and firn is typically higher than the mean summer and mean annual values. This is an effect of the multi-decadal to multi-centennial hiatus surfaces present throughout the glazed areas of glaze/dune regions and likely precludes these areas from containing straightforward chemical climate records.

Glazed, non-dune regions also increase the magnitude and variability of chemical concentrations in surface snow and firn, although not as severely as glaze/dune regions. This may be a result of shorter-duration hiatus surfaces in these regions.

The elements Cd, Pb, Bi, As, Li, and S are significantly enriched across Antarctica relative to their expected ratios in both oceanic and crustal elemental material (Table 2.9). Volcanic outgassing contributions account for almost all the Bi in both East and West Antarctica and for a significant fraction of the Cd in East Antarctica (Figure 2.9). The remaining excess cadmium in Antarctic precipitation is likely related to anthropogenic activities, such as mining, in the Southern Hemisphere.

The volcanic contributions of enriched elements are always greatest in glaze/dune areas. This is most likely a direct effect of S enrichment. The S enrichment in glaze/dune areas is probably a result of the concentrating effect of the hiatus surfaces combined with their proximity to the stratospheric SO_4^{2-} background reservoir. The stratospheric SO_4^{2-} background reservoir is potentially composed of nonexplosive volcanic SO_4^{2-}, an admixture of sources that reside in polar stratospheric clouds (PSC), and continental SO_4^{2-} from sources such as anthropogenic emissions and dust. The volcanic contribution calculation for enriched elements assumes that a fixed percentage of the total S in the atmosphere is of volcanic origin. However, the volcanic contribution calculation frequently overestimates the element concentrations in glaze/dune areas. This suggests that the percentage of volcanic S in the volcanic contribution calculation is set too high and/or significant S input from other sources occurs over timescales comparable in length to the glaze/dune hiatus.

Despite apparent overestimations in glaze/dune areas, global volcanic outgassing cannot account for observed concentrations of Pb or As in any area of Antarctica. Previous studies [*Wolff and Suttie*, 1994] have revealed anthropogenic activity as the primary source of excess Antarctic Pb levels. However, excess Antarctic As concentrations exhibit a pronounced annual signal, particularly in West Antarctica, and are most likely associated with photochemical and/or biogenic activity.

The Bi, Cd, Pb, and As concentration peaks between South Pole and 03-1 remain unexplained by the combination of crustal, oceanic, global volcanic and local volcanic source contributions (Figure 2.11 and 2.12). The proximity of these peaks to South Pole suggests that local contamination from Amundsen-Scott Station may be responsible.

4.2 Chapter 3 Summary

A suite of 21 shallow firn/ice cores are used to develop a robust proxy for northerly air mass incursions into central and western West Antarctica. These findings suggest that concentrations of nssCa in central and western West Antarctica are primarily influenced by changes in SH atmospheric circulation (SH westerlies and ASL storm intensity) as opposed to dust source emissions. The NAMI proxy reveals that the recent increase in the strength of the Southern Hemisphere westerly winds [*Marshall*, 2003; *Thompson and Solomon*, 2002; *Thompson et al.*, 2000] is unprecedented for at least the last 200 years [*Dixon et al.*, in press].

The modern ozone hole over Antarctica acts to increase the thermal gradient between the Pole and the mid-latitudes by cooling the polar stratosphere [*Thompson et al.*, 2000]. The ozone depletion-induced thermal gradient increase strengthens the

westerlies and shields interior East Antarctica from the bulk of SH warming [*ACCE*, 2009]. By allowing the polar stratosphere to warm and thus reducing the thermal gradient between the Pole and the mid-latitudes, ozone recovery will likely weaken and/or lead to poleward contraction of the SH westerlies, particularly during the austral spring-summer. Consequently, Antarctica could lose one of its best defenses against SH GHG warming. This potential consequence is similar to the impact humans have had in the Northern Hemisphere where sulfate aerosols temporarily reduced the warming effects of GHG rise from the 1940s-1970s.

4.3 Implications and Recommendations for Future Work

Future research planned for the ITASE cores includes further verification of the sources and input timing of elements exhibiting a previously unreported enrichment, such as Li and As. Expanding the scope of this research to achieve full-coverage of Antarctica will require the incorporation of additional data, such as aerosol monitoring sites. Work on an Antarctic sea ice proxy is currently underway, utilizing ITASE cores in combination with all other available Antarctic ice core chemistry data.

These studies provide a robust baseline for monitoring future changes in the chemistry of the atmosphere over Antarctica. With the ITASE surface snow and firn chemistry framework, it is easier to select a sampling site that captures a non-convoluted climate record. The framework highlights where one need not or ought to sample. This ability will prove useful in the future as we continue to monitor Antarctic atmospheric chemical deposition. Potential changes in atmospheric chemistry are inevitable. Tracking

these changes is more important than ever as Antarctica continues to warm and as Southern Hemisphere industrial activity intensifies.

REFERENCES

Abram, N. J., R. Mulvaney, E. W. Wolff, and M. Mudelsee (2007), Ice core records as sea ice proxies: An evaluation from the Weddell Sea region of Antarctica, *Journal of Geophysical Research-Atmospheres*, *112*(D15), D15101.

ACCE (2009), Antarctic Climate Change and the Environment, *978-0-948277-22-1*, 555 pp, Scientific Committee on Antarctic Research, Cambridge, UK.

Albert, M., C. Shuman, Z. Courville, R. Bauer, M. Fahnestock, and T. Scambos (2004), Extreme firn metamorphism: impact of decades of vapor transport on near-surface firn at a low-accumulation glazed site on the East Antarctic plateau, in *Annals of Glaciology, Vol 39, 2005*, edited by J. Jacka, pp. 73-78.

Anderson, R. F., S. Ali, L. I. Bradtmiller, S. H. H. Nielsen, M. Q. Fleisher, B. E. Anderson, and L. H. Burckle (2009), Wind-Driven Upwelling in the Southern Ocean and the Deglacial Rise in Atmospheric CO2, *Science*, *323*(5920), 1443-1448.

Barbante, C., C. Turetta, G. Capodaglio, and G. Scarponi (1997), Recent decrease in the lead concentration of Antarctic snow, *International Journal of Environmental Analytical Chemistry*, *68*(4), 457-477.

Barbante, C., G. Cozzi, G. Capodaglio, K. van de Velde, C. Ferrari, C. Boutron, and P. Cescon (1999), Trace element determination in alpine snow and ice by double focusing inductively coupled plasma mass spectrometry with microconcentric nebulization, *Journal of Analytical Atomic Spectrometry*, *14*(9), 1433-1438.

Bertler, N., et al. (2005), Snow chemistry across Antarctica, *Annals of Glaciology*, *41*, 167-179.

Black, H. P., and W. Budd (1964), Accumulation in the region of Wilkes, Wilkes Land, Antarctica, *Journal of Glaciology*, *5*(37), 3-15.

Bohlander, J., and T. Scambos (2005), Outlines of Antarctic megadunes regions, *Boulder, Colorado USA: National Snow and Ice Data Center*, Unpublished data.

BoM (2005), Climate Data: Australia, version 2.2, edited, Australian Government, Bureau of Meteorology.

Boutron, C. F., and C. C. Patterson (1986), Lead concentration changes in Antarctic ice during the Wisconsin Holocene transition, *Nature*, *323*(6085), 222-225.

Boutron, C. F., and C. C. Patterson (1987), Relative levels of natural and anthropogenic lead in recent Antarctic snow, *Journal of Geophysical Research-Atmospheres*, *92*(D7), 8454-8464.

Cai, W., P. H. Whetton, and D. J. Karoly (2003), The Response of the Antarctic Oscillation to Increasing and Stabilized Atmospheric CO2, *Journal of Climate*, *16*(10), 1525-1538.

Carleton, A. M. (2003), Atmospheric teleconnections involving the Southern Ocean, *Journal of Geophysical Research-Oceans*, *108*(C4).

Crook, J. A., N. P. Gillett, and S. P. E. Keeley (2008), Sensitivity of Southern Hemisphere climate to zonal asymmetry in ozone, *Geophysical Research Letters*, *35*(7), L07806.

Curran, M. A. J., T. D. van Ommen, V. I. Morgan, K. L. Phillips, and A. S. Palmer (2003), Ice core evidence for Antarctic sea ice decline since the 1950s, *Science*, *302*(5648), 1203-1206.

Dansgaard, W., et al. (1993), EVIDENCE FOR GENERAL INSTABILITY OF PAST CLIMATE FROM A 250-KYR ICE-CORE RECORD, *Nature*, *364*(6434), 218-220.

De Deckker, P., M. Norman, I. Goodwin, A. Wain, and F. Gingele (2010), Lead isotopic evidence for an Australian source of aeolian dust to Antarctica at times over the last 170,000 years, *Palaeogeography, Palaeoclimatology, Palaeoecology*, *285*(3-4), 205-223.

Dixon, D., P. A. Mayewski, S. Kaspari, S. Sneed, and M. Handley (2004), A 200 year sub-annual record of sulfate in West Antarctica, from 16 ice cores, *Annals of Glaciology*, *39*, 545-556.

Dixon, D. A. (2008), Antarctic Mean Annual Temperature Map, edited, Boulder, Colorado USA: National Snow and Ice Data Center.

Dixon, D. A., P. A. Mayewski, I. D. Goodwin, G. J. Marshall, R. Freeman, K. A. Maasch, and S. B. Sneed (in press), An ice core proxy for northerly air mass incursions (NAMI) into West Antarctica, *International Journal of Climatology*.

Draxler, R. R., and G. D. Rolph (2003), HYSPLIT (HYbrid Single-Particle Lagrangian Integrated Trajectory) Model, edited, NOAA Air Resources Laboratory, Silver Spring, MD.

Duce, R. A., G. L. Hoffman, and W. H. Zoller (1975), Atmospheric trace-metals at remote northern and southern-hemisphere sites - pollution or natural?, *Science*, *187*(4171), 59-61.

Eisen, O., et al. (2008), Ground-based measurements of spatial and temporal variability of snow accumulation in east Antarctica, *Reviews of Geophysics*, *46*(1).

Ekstrom, M., G. H. McTainsh, and A. Chappell (2004), Australian dust storms: Temporal trends and relationships with synoptic pressure distributions (1960-99), *International Journal of Climatology*, *24*(12), 1581-1599.

Fahnestock, M. A., T. A. Scambos, C. A. Shuman, R. J. Arthern, D. P. Winebrenner, and R. Kwok (2000), Snow megadune fields on the East Antarctic Plateau: extreme atmosphere-ice interaction, *Geophysical Research Letters*, *27*(22), 3719-3722.

Faure, G., and G. Lee (1999), Occurrence of cesium-137 and other radionuclides in the surface layers of soil in Ohio and Antarctica, *Ohio Journal of Science*, *99*(5), 111-113.

Frezzotti, M., S. Gandolfi, and S. Urbini (2002a), Snow megadunes in Antarctica: Sedimentary structure and genesis, *Journal of Geophysical Research-Atmospheres*, *107*(D18).

Frezzotti, M., S. Gandolfi, F. La Marca, and S. Urbini (2002b), Snow dunes and glazed surfaces in Antarctica: new field and remote-sensing data, in *Annals of Glaciology, Vol 34, 2002*, edited by J. G. Winther and R. Solberg, pp. 81-88.

Gabrielli, P., C. Barbante, C. Boutron, G. Cozzi, V. Gaspari, F. Planchon, C. Ferrari, C. Turetta, S. M. Hong, and P. Cescon (2005), Variations in atmospheric trace elements in Dome C (East Antarctica) ice over the last two climatic cycles, *Atmospheric Environment*, *39*(34), 6420-6429.

Gabrielli, P., et al. (2010), A major glacial-interglacial change in aeolian dust composition inferred from Rare Earth Elements in Antarctic ice, *Quaternary Science Reviews*, *29*(1-2), 265-273.

Gayley, R. I., and M. Ram (1985), Atmospheric dust in polar ice and the background aerosol, *Journal of Geophysical Research-Atmospheres*, *90*(D7), 2921-2925.

Giovinetto, M. B. (1963), Glaciological studies on the McMurdo-South Pole traverse, 1960-1961, 83 pp, The Ohio State University Research Foundation, Columbus 12, Ohio.

Goodwin, I. D. (1990), Snow accumulation and surface-topography in the katabatic zone of eastern Wilkes Land, Antarctica, *Antarctic Science*, *2*(3), 235-242.

Gorlach, U., and C. F. Boutron (1992), Variations in heavy-metals concentrations in Antarctic snows from 1940 to 1980, *Journal of Atmospheric Chemistry*, *14*(1-4), 205-222.

Hall, A., and M. Visbeck (2002), Synchronous variability in the southern hemisphere atmosphere, sea ice, and ocean resulting from the annular mode, *Journal of Climate*, *15*(21), 3043-3057.

Hamilton, G. S., and V. B. Spikes (2004), Evaluating a satellite altimeter-derived digital elevation model of Antarctica using precision kinematic GPS profiling, *Global and Planetary Change*, *42*(1-4), 17-30.

Haran, T., J. Bohlander, T. Scambos, T. Painter, and M. Fahnestock (2005), MODIS mosaic of Antarctica (MOA) image map, edited, Boulder, Colorado USA: National Snow and Ice Data Center.

Hines, K. M., D. H. Bromwich, and G. J. Marshall (2000), Artificial surface pressure trends in the NCEP-NCAR reanalysis over the southern ocean and Antarctica, *Journal of Climate*, *13*(22), 3940-3952.

Hinkley, T. K., P. J. Lamothe, S. A. Wilson, D. L. Finnegan, and T. M. Gerlach (1999), Metal emissions from Kilauea, and a suggested revision of the estimated worldwide metal output by quiescent degassing of volcanoes, *Earth and Planetary Science Letters*, *170*(3), 315-325.

Holland, H. D. (1978), *The Chemistry of the Atmosphere and Oceans*, 369 pp., John Wiley & Sons Inc, New York.

Hong, S., A. Lluberas, G. Lee, and J. K. Park (2002), Natural and anthropogenic heavy metal deposition to the snow in King George Island, Antarctic Peninsula, *Ocean and Polar Reseach*, *24*(3), 279-287.

Hur, S. D., X. Cunde, S. M. Hong, C. Barbante, P. Gabrielli, K. Y. Lee, C. F. Boutron, and Y. Ming (2007), Seasonal patterns of heavy metal deposition to the snow on Lambert Glacier basin, East Antarctica, *Atmospheric Environment*, *41*(38), 8567-8578.

IPCC (2007), Climate Change 2007: the Physical Science Basis, in *Contribution of Working Group 1 to the Fourth Assessment Report of the Intergovernmental Panel on Climate Change*, edited by S. Solomon, D. Qin, M. Manning, M. Marquis, K. Averyt, M. M. B. Tignor, H. L. Miller and Z. Chen, p. 996, Cambridge University Press, Cambridge, United Kingdom and New York, NY, USA.

Jezek, K., J. Curlander, F. Carsey, C. Wales, and R. Barry (2002), RAMP AMM-1 SAR Image Mosaic of Antarctica, edited, Fairbanks, AK: Alaska SAR Facility, in association with the National Snow and Ice Data Center, Boulder, CO.

Jezek, K. C. (1999), Glaciological properties of the Antarctic ice sheet from RADARSAT-1 synthetic aperture radar imagery, in *Annals of Glaciology, Vol 29, 1999*, edited by T. H. Jacka, pp. 286-290.

Jouzel, J., G. Raisbeck, J. P. Benoist, F. Yiou, C. Lorius, D. Raynaud, J. R. Petit, N. I. Barkov, Y. S. Korotkevitch, and V. M. Kotlyakov (1989), A comparison of deep Antarctic ice cores and their implications for climate between 65,000 and 15,000 years ago, *Quaternary Research*, *31*(2), 135-150.

Justice, C. O., J. R. G. Townshend, E. F. Vermote, E. Masuoka, R. E. Wolfe, N. Saleous, D. P. Roy, and J. T. Morisette (2002), An overview of MODIS Land data processing and product status, *Remote Sensing of Environment*, *83*(1-2), 3-15.

Kaspari, S., P. A. Mayewski, D. A. Dixon, V. B. Spikes, S. B. Sneed, M. J. Handley, and G. S. Hamilton (2004), Climate variability in West Antarctica derived from annual accumulation-rate records from ITASE firn/ice cores, *Annals of Glaciology*, *39*, 585-594.

Kaufman, Y. J., D. D. Herring, K. J. Ranson, and G. J. Collatz (1998), Earth Observing System AM1 mission to Earth, *Geoscience and Remote Sensing, IEEE Transactions on*, *36*(4), 1045-1055.

Knusel, S., D. E. Piguet, M. Schwikowski, and H. W. Gaggeler (2003), Accuracy of continuous ice-core trace-element analysis by inductively coupled plasma sector field mass spectrometry, *Environmental Science & Technology*, *37*(10), 2267-2273.

Koffman, B. G., K. Kreutz, M. Handley, M. Wells, A. Kurbatov, and P. Mayewski (2008), A snowpit record of atmospheric Fe deposition in West Antarctica at the WAIS Divide site, *Geochimica Et Cosmochimica Acta*, *72*(12), A487-A487.

Krachler, M., J. Zheng, D. Fisher, and W. Shotyk (2005), Analytical procedures for improved trace element detection limits in polar ice from Arctic Canada using ICP-SMS, *Analytica Chimica Acta*, *530*(2), 291-298.

Kreutz, K. J., and P. A. Mayewski (1999), Spatial variability of Antarctic surface snow glaciochemistry: implications for palaeoatmospheric circulation reconstructions, *Antarctic Science*, *11*(1), 105-118.

Kreutz, K. J., P. A. Mayewski, L. D. Meeker, M. S. Twickler, and S. I. Whitlow (2000a), The effect of spatial and temporal accumulation rate variability in West Antarctica on soluble ion deposition, *Geophysical Research Letters*, *27*(16), 2517-2520.

Kreutz, K. J., P. A. Mayewski, L. D. Meeker, M. S. Twickler, S. I. Whitlow, and Pittalwala, II (1997), Bipolar changes in atmospheric circulation during the Little Ice Age, *Science*, *277*(5330), 1294-1296.

Kreutz, K. J., P. A. Mayewski, Pittalwala, II, L. D. Meeker, M. S. Twickler, and S. I. Whitlow (2000b), Sea level pressure variability in the Amundsen Sea region inferred from a West Antarctic glaciochemical record, *Journal of Geophysical Research-Atmospheres*, *105*(D3), 4047-4059.

Kyle, P. R., K. Meeker, and D. Finnegan (1990), Emission rates of sulfur-dioxide, trace gases and metals from Mount Erebus, Antarctica, *Geophysical Research Letters*, *17*(12), 2125-2128.

Legrand, M., and P. Mayewski (1997), Glaciochemistry of polar ice cores: A review, *Reviews of Geophysics*, *35*(3), 219-243.

Li, F., P. Ginoux, and V. Ramaswamy (2008), Distribution, transport, and deposition of mineral dust in the Southern Ocean and Antarctica: Contribution of major sources, *Journal of Geophysical Research*, *113*(D10).

Lide, D. R. (2005), Abundance Of Elements In The Earth's Crust And In The Sea, in *CRC Handbook of Chemistry and Physics, Internet Version 2005*, edited by D. R. Lide, CRC Press, Boca Raton, FL.

Lister, H., and G. Pratt (1959), Geophysical Investigations of the Commonwealth Trans-Antarctic Expedition, *The Geographical Journal*, *125*(3/4), 343-354.

Liu, H., K. Jezek, B. Li, and Z. Zhao (2001), Radarsat Antarctic Mapping Project digital elevation model version 2, *Boulder, CO: National Snow and Ice Data Center.*, *Digital media*, http://nsidc.org/data/nsidc-0082.html.

Lubin, D., R. A. Wittenmyer, D. H. Bromwich, and G. J. Marshall (2008), Antarctic Peninsula mesoscale cyclone variability and climatic impacts influenced by the SAM, *Geophysical Research Letters*, *35*(2), L02808.

Mahowald, N. M., et al. (2010), Observed 20th century desert dust variability: impact on climate and biogeochemistry, *Atmospheric Chemistry and Physics*, *10*(22), 10875-10893.

Marino, F., V. Maggi, B. Delmonte, G. Ghermandi, and J. R. Petit (2004), Elemental composition (Si, Fe, Ti) of atmospheric dust over the last 220 kyr from the EPICA ice core (Dome C, Antarctica), in *Annals of Glaciology, Vol 39, 2005*, edited by J. Jacka, pp. 110-118.

Marshall, G. J. (2003), Trends in the southern annular mode from observations and reanalyses, *Journal of Climate*, *16*(24), 4134-4143.

Marteel, A., et al. (2008), Changes in atmospheric heavy metals and metalloids in Dome C (East Antarctica) ice back to 672.0 kyr BP (Marine Isotopic Stages 16.2), *Earth and Planetary Science Letters*, *272*(3-4), 579-590.

Marx, S. K., B. S. Kamber, and H. A. McGowan (2005), Provenance of long-travelled dust determined with ultra-trace-element composition: a pilot study with samples from New Zealand glaciers, *Earth Surface Processes and Landforms*, *30*(6), 699-716.

Marx, S. K., H. A. McGowan, and B. S. Kamber (2009), Long-range dust transport from eastern Australia: A proxy for Holocene aridity and ENSO-type climate variability, *Earth and Planetary Science Letters*, *282*(1-4), 167-177.

Masson, V., et al. (2000), Holocene climate variability in Antarctica based on 11 ice-core isotopic records, *Quaternary Research*, *54*(3), 348-358.

Mayewski, P. A., and M. Bender (1995), The GISP2 ice core record - paleoclimate highlights, *Reviews of Geophysics*, *33*, 1287-1296.

Mayewski, P. A., and I. D. Goodwin (1997), International Trans Antarctic Scientific Expedition (ITASE) "200 Years of Past Antarctic Climate and Environmental Change", Science and Implementation Plan 1996, *PAGES Workshop Report Series 97-1*, 48 pp.

Mayewski, P. A., L. D. Meeker, S. Whitlow, M. S. Twickler, M. C. Morrison, R. B. Alley, P. Bloomfield, and K. Taylor (1993a), The atmosphere during the Younger Dryas, *Science*, *261*(5118), 195-197.

Mayewski, P. A., L. D. Meeker, M. C. Morrison, M. S. Twickler, S. I. Whitlow, K. K. Ferland, D. A. Meese, M. R. Legrand, and J. P. Steffensen (1993b), Greenland ice core signal characteristics - an expanded view of climate-change, *Journal of Geophysical Research-Atmospheres*, *98*(D7), 12839-12847.

Mayewski, P. A., et al. (2004a), A 700 year record of Southern Hemisphere extratropical climate variability, *Annals of Glaciology*, *39*, 127-132.

Mayewski, P. A., et al. (2005a), Solar forcing of the polar atmosphere, *Annals of Glaciology*, *41*, 147-154.

Mayewski, P. A., et al. (2004b), Holocene climate variability, *Quaternary Research*, *62*(3), 243-255.

Mayewski, P. A., et al. (2009), State of the Antarctic and Southern Ocean climate system, *Rev. Geophys.*, *47*(1), RG1003.

Mayewski, P. A., et al. (2005b), The International Trans-Antarctic Scientific Expedition (ITASE): an overview, *Annals of Glaciology*, *41*, 180-185.

McConnell, J. R., A. J. Aristarain, J. R. Banta, P. R. Edwards, and J. C. Simoes (2007), 20th-Century doubling in dust archived in an Antarctic Peninsula ice core parallels climate change and desertification in South America, *Proceedings of the National Academy of Sciences of the United States of America*, *104*(14), 5743-5748.

McTainsh, G. H., A. W. Lynch, and E. K. Tews (1998), Climatic controls upon dust storm occurrence in eastern Australia, *Journal of arid environments*, *39*(3), 457-466.

Meyerson, E. A., P. A. Mayewski, K. J. Kreutz, L. D. Meeker, S. I. Whitlow, and M. S. Twickler (2002), The polar expression of ENSO and sea-ice variability as recorded in a South Pole ice core, *Annals of Glaciology*, *35*, 430-436.

Monaghan, A. J., D. H. Bromwich, W. Chapman, and J. C. Comiso (2008), Recent variability and trends of Antarctic near-surface temperature, *Journal of Geophysical Research-Atmospheres*, *113*(D4), D04105.

Monaghan, A. J., et al. (2006), Insignificant change in Antarctic snowfall since the International Geophysical Year, *Science*, *313*(5788), 827-831.

Nriagu, J. O. (1989), A global assessment of natural sources of atmospheric trace-metals, *Nature*, *338*(6210), 47-49.

Obrien, S. R., P. A. Mayewski, L. D. Meeker, D. A. Meese, M. S. Twickler, and S. I. Whitlow (1995), Complexity of Holocene climate as reconstructed from a Greenland ice core, *Science*, *270*(5244), 1962-1964.

Osterberg, E. C., M. J. Handley, S. B. Sneed, P. A. Mayewski, and K. J. Kreutz (2006), Continuous ice core melter system with discrete sampling for major ion, trace element, and stable isotope analyses, *Environmental Science & Technology*, *40*(10), 3355-3361.

Parish, T. R., and D. H. Bromwich (1997), On the forcing of seasonal changes in surface pressure over Antarctica, *Journal of Geophysical Research-Atmospheres*, *102*(D12), 13785-13792.

Perlwitz, J., S. Pawson, R. L. Fogt, J. E. Nielsen, and W. D. Neff (2008), Impact of stratospheric ozone hole recovery on Antarctic climate, *Geophysical Research Letters*, *35*(8), L08714.

Picciotto, E. E., W. De Breuck, and G. Crozaz (1970), Snow accumulation along the South Pole-Dronning Maud Land Traverse, *International Association for Scientific HydroIogy*, *86*, 18-22.

Planchon, F. A. M., C. F. Boutron, C. Barbante, G. Cozzi, V. Gaspari, E. W. Wolff, C. P. Ferrari, and P. Cescon (2002), Changes in heavy metals in Antarctic snow from Coats Land since the mid-19th to the late-20th century, *Earth and Planetary Science Letters*, *200*(1-2), 207-222.

Pourchet, M., O. Magand, M. Frezzotti, A. Ekaykin, and J. G. Winther (2003), Radionuclides deposition over Antarctica, *Journal of Environmental Radioactivity*, *68*(2), 137-158.

Pourchet, M., S. K. Bartarya, M. Maignan, J. F. Pinglot, A. J. Aristarain, G. Furdada, V. M. Kotlyakov, E. Mosley-Thompson, N. Preiss, and N. W. Young (1997), Distribution and fall-out of Cs-137 and other radionuclides over Antarctica, *Journal of Glaciology*, *43*(145), 435-445.

Prospero, J. M., P. Ginoux, O. Torres, S. E. Nicholson, and T. E. Gill (2002), Environmental characterization of global sources of atmospheric soil dust

identified with the Nimbus 7 Total Ozone Mapping Spectrometer (TOMS) absorbing aerosol product, *Reviews of Geophysics*, *40*(1), 1002.

Randel, W. J., and F. Wu (1999), Cooling of the arctic and antarctic polar stratospheres due to ozone depletion, *Journal of Climate*, *12*(5), 1467-1479.

Reusch, D. B., P. A. Mayewski, S. I. Whitlow, Pittalwala, II, and M. S. Twickler (1999), Spatial variability of climate and past atmospheric circulation patterns from central West Antarctic glaciochemistry, *Journal of Geophysical Research-Atmospheres*, *104*(D6), 5985-6001.

Rignot, E., G. Casassa, P. Gogineni, W. Krabill, A. Rivera, and R. Thomas (2004), Accelerated ice discharge from the Antarctic Peninsula following the collapse of Larsen B ice shelf, *Geophysical Research Letters*, *31*(18), L18401.

Sbrignadello, G., S. Degetto, G. A. Battiston, and R. Gerbasi (1994), Distribution of 210Pb and 137Cs in Snow and Soil Samples from Antarctica, *International Journal of Environmental & Analytical Chemistry*, *55*(1), 235-242.

Scambos, T., and R. Bauer (2006), GPR and GPS data: characteristics of snow megadunes and their potential effect on ice core interpretation, edited, Boulder, Colorado USA: National Snow and Ice Data Center.

Scambos, T. A., J. A. Bohlander, C. A. Shuman, and P. Skvarca (2004), Glacier acceleration and thinning after ice shelf collapse in the Larsen B embayment, Antarctica, *Geophysical Research Letters*, *31*(18), L18402.

Scambos, T. A., T. M. Haran, M. A. Fahnestock, T. H. Painter, and J. Bohlander (2007), MODIS-based Mosaic of Antarctica (MOA) data sets: Continent-wide surface morphology and snow grain size, *Remote Sensing of Environment*, *111*(2-3), 242-257.

Schneider, D. P., E. J. Steig, and J. C. Comiso (2004), Recent climate variability in Antarctica from satellite-derived temperature data, *Journal of Climate*, *17*(7), 1569-1583.

Schneider, D. P., E. J. Steig, T. D. van Ommen, D. A. Dixon, P. A. Mayewski, J. M. Jones, and C. M. Bitz (2006), Antarctic temperatures over the past two centuries from ice cores, *Geophysical Research Letters*, *33*(16), L16707.

Shanklin, J. D. (2009), Total column ozone record from above Halley station, Antarctica, edited, British Antarctic Survey, Madingley Road, Cambridge, England. CB3 0ET.

Shaw, G. E. (1979), Considerations on the origin and properties of the Antarctic aerosol, *Reviews of Geophysics*, *17*(8), 1983-1998.

Shaw, G. E. (1982), On the residence time of the Antarctic ice-sheet sulfate aerosol, *Journal of Geophysical Research-Oceans and Atmospheres*, *87*(NC6), 4309-4313.

Siggaard-Andersen, M. L., P. Gabrielli, J. P. Steffensen, T. Stromfeldt, C. Barbante, C. Boutron, H. Fischer, and H. Miller (2007), Soluble and insoluble lithium dust in the EPICA DomeC ice core - Implications for changes of the East Antarctic dust provenance during the recent glacial-interglacial transition, *Earth and Planetary Science Letters*, *258*(1-2), 32-43.

Steig, E. J., D. P. Schneider, S. D. Rutherford, M. E. Mann, J. C. Comiso, and D. T. Shindell (2009), Warming of the Antarctic ice-sheet surface since the 1957 International Geophysical Year, *Nature*, *457*(7228), 459-462.

Steig, E. J., et al. (2005), High-resolution ice cores from USITASE (West Antarctica): development and validation of chronologies and determination of precision and accuracy, *Annals of Glaciology*, *41*, 77-84.

Suttie, E. D., and E. W. Wolff (1992), Seasonal input of heavy-metals to Antarctic snow, *Tellus Series B-Chemical and Physical Meteorology*, *44*(4), 351-357.

Swithinbank, C. (1988), Antarctica, in *Satellite image atlas of glaciers of the world*, edited by R. S. Williams, jr and J. G. Ferrigno, U.S. Government Printing Office, 1-139, Washington, DC.

Thompson, D. W. J., and J. M. Wallace (2000), Annular modes in the extratropical circulation. Part I: Month-to-month variability, *Journal of Climate*, *13*(5), 1000-1016.

Thompson, D. W. J., and S. Solomon (2002), Interpretation of recent Southern Hemisphere climate change, *Science*, *296*(5569), 895-899.

Thompson, D. W. J., J. M. Wallace, and G. C. Hegerl (2000), Annular modes in the extratropical circulation. Part II: Trends, *Journal of Climate*, *13*(5), 1018-1036.

Tuncel, G., N. K. Aras, and W. H. Zoller (1989), Temporal variations and sources of elements in the South-Pole atmosphere .1. Nonenriched and moderately enriched elements, *Journal of Geophysical Research-Atmospheres*, *94*(D10), 13025-13038.

Turner, J., T. A. Lachlan-Cope, S. Colwell, G. J. Marshall, and W. M. Connolley (2006), Significant warming of the Antarctic winter troposphere, *Science*, *311*(5769), 1914-1917.

Turner, J., J. C. Comiso, G. J. Marshall, T. A. Lachlan-Cope, T. Bracegirdle, T. Maksym, M. P. Meredith, Z. M. Wang, and A. Orr (2009), Non-annular atmospheric circulation change induced by stratospheric ozone depletion and its role in the recent increase of Antarctic sea ice extent, *Geophysical Research Letters*, *36*, L08502.

Vallelonga, P., J. P. Candelone, K. Van de Velde, M. A. J. Curran, V. I. Morgan, and K. J. R. Rosman (2003), Lead, Ba and Bi in Antarctic Law Dome ice corresponding to the 1815 AD Tambora eruption: an assessment of emission sources using Pb isotopes, *Earth and Planetary Science Letters*, *211*(3-4), 329-341.

Vallelonga, P., C. Barbante, G. Cozzi, V. Gaspari, J. P. Candelone, K. Van de Velde, V. I. Morgan, K. J. R. Rosman, C. F. Boutron, and P. Cescon (2004), Elemental indicators of natural and anthropogenic aerosol inputs to Law Dome, Antarctica, *Annals of Glaciology*, *39*, 169-174.

Van de Velde, K., P. Vallelonga, J. P. Candelone, K. J. R. Rosman, V. Gaspari, G. Cozzi, C. Barbante, R. Udisti, P. Cescon, and C. F. Boutron (2005), Pb isotope record over one century in snow from Victoria Land, Antarctica, *Earth and Planetary Science Letters*, *232*(1-2), 95-108.

van den Broeke, M. (2005), Strong surface melting preceded collapse of Antarctic Peninsula ice shelf, *Geophysical Research Letters*, *32*(12), L12815.

van den Broeke, M. R., and N. P. M. van Lipzig (2004), Changes in Antarctic temperature, wind and precipitation in response to the Antarctic Oscillation, *Annals of Glaciology*, *39*, 119-126.

Vaughan, D. G., J. L. Bamber, M. Giovinetto, J. Russell, and A. P. R. Cooper (1999), Reassessment of net surface mass balance in Antarctica, *Journal of Climate*, *12*(4), 933-946.

Watanabe, O. (1978), Distribution of surface features of snow cover in Mizuho Plateau, *Memoirs of National Institute of Polar Research*, *Special Issue*(7), 44-62.

Wedepohl, K. H. (1995), The composition of the continental crust, *Geochimica Et Cosmochimica Acta*, *59*(7), 1217-1232.

Welch, K. A., P. A. Mayewski, and S. I. Whitlow (1993), Methanesulfonic-acid in coastal Antarctic snow related to sea-ice extent, *Geophysical Research Letters*, *20*(6), 443-446.

Wolff, E. W., and D. A. Peel (1985), Closer to a true value for heavy metal concentrations in recent Antarctic snow by improved contamination control, *Annals of Glaciology*, *7*, 61-69.

Wolff, E. W., and E. D. Suttie (1994), Antarctic snow record of southern-hemisphere lead pollution, *Geophysical Research Letters*, *21*(9), 781-784.

Wolff, E. W., E. D. Suttie, and D. A. Peel (1999), Antarctic snow record of cadmium, copper, and zinc content during the twentieth century, *Atmospheric Environment*, *33*(10), 1535-1541.

Woodward, R. N. (1964), Strontium-90 and Caesium-137 in Antarctic Snows, *Nature*, *204*(4965), 1291-1291.

Xiao, C. D., D. H. Qin, T. D. Yao, J. W. Ren, and Y. F. Li (2000), Global pollution shown by lead and cadmium contents in precipitation of polar regions and Qinghai-Tibetan Plateau, *Chinese Science Bulletin*, *45*(9), 847-853.

Yan, Y. P., P. A. Mayewski, S. C. Kang, and E. Meyerson (2005), An ice-core proxy for Antarctic circumpolar zonal wind intensity, *Annals of Glaciology*, *41*, 121-130.

Zreda-Gostynska, G., P. R. Kyle, and D. L. Finnegan (1993), Chlorine, fluorine, and sulfur emissions from Mount Erebus, Antarctica and estimated contributions to the Antarctic atmosphere, *Geophysical Research Letters*, *20*(18), 1959-1962.

Zreda-Gostynska, G., P. R. Kyle, D. Finnegan, and K. M. Prestbo (1997), Volcanic gas emissions from Mount Erebus and their impact on the Antarctic environment, *Journal of Geophysical Research-Solid Earth*, *102*(B7), 15039-15055.

Appendix A

CONCURRENT RELATED PUBLICATIONS

High-resolution ice cores from US ITASE (West Antarctica): development and validation of chronologies and determination of precision and accuracy

Eric J. STEIG,[1] Paul A. MAYEWSKI,[2] Daniel A. DIXON,[2] Susan D. KASPARI,[2] Markus M. FREY,[3] David P. SCHNEIDER,[1] Steven A. ARCONE,[3] Gordon S. HAMILTON,[2] V. Blue SPIKES,[2] Mary ALBERT,[3] Deb MEESE,[3] Anthony J. GOW,[3] Christopher A. SHUMAN,[4] James W.C. WHITE,[5] Sharon SNEED,[2] Joseph FLAHERTY,[1] Mark WUMKES[7]

[1]*Department of Earth and Space Sciences, Box 351310, University of Washington, Seattle, WA 98195-1310, USA*
E-mail: steig@ess.washington.edu
[2]*Climate Change Institute, University of Maine, 303 Bryand Global Sciences Center, Orono, ME 04469-5790, USA*
[3]*Department of Hydrology and Water Resources, PO Box 210011, The University of Arizona, Tucson, AZ 85271-0011, USA*
[4]*US Army Cold Regions Research and Engineering Laboratory, 72 Lyme Road, Hanover, NH 03755-1290, USA*
[5]*NASA Goddard Space Flight Center, Code 971, Greenbelt, MD 20771, USA*
[6]*Institute of Arctic and Alpine Research, University of Colorado, Boulder, CO 80309-0450, USA*
[7]*Glacier Data, 750 Spudwood Road, Fairbanks, AK 99712, USA*

ABSTRACT. Shallow ice cores were obtained from widely distributed sites across the West Antarctic ice sheet, as part of the United States portion of the International Trans-Antarctic Scientific Expedition (US ITASE) program. The US ITASE cores have been dated by annual-layer counting, primarily through the identification of summer peaks in non-sea-salt sulfate ($nssSO_4^{2-}$) concentration. Absolute dating accuracy of better than 2 years and relative dating accuracy better than 1 year is demonstrated by the identification of multiple volcanic marker horizons in each of the cores, Tambora, Indonesia (1815), being the most prominent. Independent validation is provided by the tracing of isochronal layers from site to site using high-frequency ice-penetrating radar observations, and by the timing of mid-winter warming events in stable-isotope ratios, which demonstrate significantly better than 1 year accuracy in the last 20 years. Dating precision to ±1 month is demonstrated by the occurrence of summer nitrate peaks and stable-isotope ratios in phase with $nssSO_4^{2-}$, and winter-time sea-salt peaks out of phase, with phase variation of <1 month. Dating precision and accuracy are uniform with depth, for at least the last 100 years.

1. INTRODUCTION

The International Trans-Antarctic Scientific Expedition (ITASE) program is an international effort to improve our spatial picture of the Antarctic ice sheet. ITASE places emphasis on the surface and near-surface characteristics of the ice sheet, complemented by deep ice radar profiling and atmospheric sampling at altitudes upwards of 20 km. The first phase of the United States' effort has focused on the West Antarctic ice sheet (WAIS), and has completed four field seasons comprising oversnow traverses that included ice coring, atmospheric sampling, surface horizontal and vertical velocity measurements, and radar observations of near-surface stratigraphy, ice-sheet internal layering and bed topography. The traverses covered a total distance of >5000 km and comprise an unprecedented sampling of the Antarctic ice sheet that, when combined with data from other ITASE projects, will result in a comprehensive spatial and temporal map of Antarctic climate, atmospheric chemistry and ice-sheet surface mass balance.

As part of US ITASE, ice cores were obtained from 23 sites across the WAIS, between the Antarctic Peninsula, South Pole and the Ross Sea and Amundsen Sea ice drainages. At 21 of these sites, cores reaching to depths between ~50 and ~300 m were obtained, providing continuous records of snow chemistry covering at most sites at least 200 years, a benchmark time frame in the original ITASE implementation plan (Mayewski and Goodwin, 1996). These cores greatly expand the inventory, and widen the spatial coverage, of ice-core records available from earlier projects in West Antarctica, which include the long ice cores at Byrd (Johnsen and others, 1972) and Siple Dome (Taylor and others, 2004a), and shorter records from Siple Station and Dyer Plateau (Mosley-Thompson and others, 1990; Thompson and others, 1994) and in the Ross Ice drainage area (Kreutz and others, 2000a).

Ice-core records of past snow properties and near-surface atmospheric chemistry are widely used as proxy records of past climate conditions and as constraints for ice-sheet surface mass balance and ice deformation studies. The importance of obtaining multiple ice cores is that a single ice core, like a single weather station, will be representative only at some local or regional spatial scale, depending on the timescale of interest. This is particularly true in West Antarctica, because the spatial coherence of interannual climate variability is relatively small, and ice-sheet topography is sufficiently complex that there may also be significant microclimatic effects. Results from recent deep coring projects suggest that on longer timescales as well, significant climate changes appearing in one location in

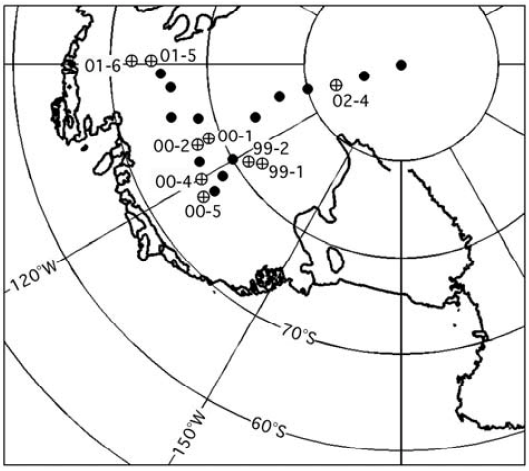

Fig. 1. Map of West Antarctica showing the location of US ITASE cores collected between 1999 and 2003. Locations specifically discussed in the text are named and shown by white circles with crosses.

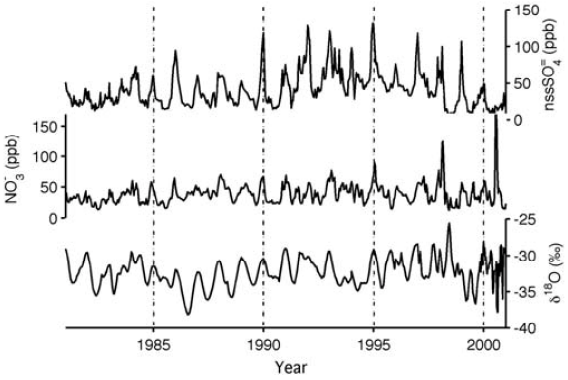

Fig. 2. Profiles of non-sea-salt sulfate ($nssSO_4^{2-}$), nitrate (NO_3^-) and oxygen isotope ratios ($\delta^{18}O$) in US ITASE core 2000-1, from 1981 to 2001. Note the distinct rise in sulfate levels beginning in 1991/92, due to the Pinatubo eruption. Dashed lines are for reference and show 1 January of selected years.

West Antarctica may not necessarily be felt at another (e.g. Siple Dome vs Byrd; see Taylor and others, 2004a). In contrast, the East Antarctic ice sheet appears to be quite uniform on both short (Schneider and Steig, 2002; Schneider and others, 2004) and long timescales (Jouzel and others, 2001; Watanabe and others, 2003).

The use of multiple ice cores and the measurement of multiple parameters can provide complementary information about the atmospheric and surface conditions that are being sampled. Consistently accurate and precise dating of ice cores is critical to the success of this approach. Placing Antarctica in the context of global climate variability requires ice cores that can be rigorously calibrated against direct meteorological observations on the same timescales. In this paper, we discuss the methods used for developing depth vs age relationships for the US ITASE cores, and we quantify the accuracy and precision of the resulting chronologies through several independent methods. Application of the resulting, highly resolved records to climatological and ice-sheet surface studies, based on these results, is the subject of several other papers (e.g. Dixon and others, 2004; Kaspari and others, 2004, 2005; Rick and Albert, 2004; Spikes and others, 2004; Schneider and others, 2005).

2. SITE SELECTION, ICE CORING AND ANALYSIS

West Antarctica has the specific advantage over East Antarctica as an ice-core drilling location that snow accumulation rates are generally high (>8 cm ice equivalent; e.g. Vaughan and others, 1999). However, West Antarctic temperatures are high enough at lower elevations that problems associated with surface melting or diffusive changes of chemical properties may be a concern. Selection of coring sites took this into account and traverse routes were therefore restricted largely to the high-plateau portion of the WAIS. Some areas were avoided for purely logistical reasons, most importantly the presence of crevasses. Target coring depths were chosen with the goal of obtaining at least 200 years of climate history from each core, combined with efficiency of field operations. In practice, this meant that we obtained deeper cores (>60 m) only where it was deemed necessary due to the high accumulation rates, though at selected sites longer records were obtained. Core locations are shown in Figure 1. Elevations, latitudes and longitudes of the US ITASE cores specifically discussed in this paper are given in the figure captions. Additional details on core depths and locations for all the US ITASE cores are archived at the US National Snow and Ice Data Center (www.nsidc.org).

Cores were retrieved using two different mechanical drilling systems. For the main ice core at each site, we used an Icefield Instruments Eclipse™ drill that obtains 1 m sections of 82 mm diameter cores. The drill was mounted on a sled and transported by snowmobile as a field-ready unit, saving drill set-up time. The Eclipse has the disadvantage of requiring that firn be excavated to allow space for the vertically swinging drill arm; thus the upper 1 m of snow cannot be sampled with the drill. In the first two field seasons we sampled the upper 1–2 m separately, after excavation for drill access, to obtain a continuous record up to the surface. In the third and fourth seasons we replaced firn-pit sampling with shallow coring, using a new system from Glacier Data™. The Glacier Data design is similar to that of the Eclipse but is considerably lighter and can drill directly from the surface; 50 mm diameter cores are obtained. We tested this drill to 40 m depth at Byrd Station and are confident that it can achieve much greater depths. Details on the drill designs are available from Icefield Instruments (www.icefield.yk.ca) and Glacier Data (www.glacierdata.com) respectively.

Core loss

In general, the 82 mm cores were packaged in the field and sampled later at the US National Ice Core Laboratory in Colorado; the 50 mm cores were either analyzed on-site or subsampled in the field and placed in cleaned sample containers, kept frozen until ready for analysis in the laboratory. All sampling was done by a team wearing Tyvek clean suits, masks and polypropylene gloves to prevent contamination. In the laboratory, established procedures were followed for clean chemical sampling using melter

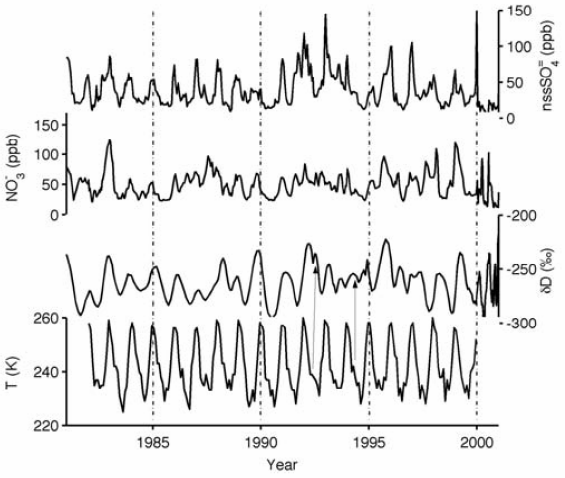

Fig. 3. Same as Figure 2, but for US ITASE core 2000-4, and also showing surface temperature from the Advanced Very High Resolution Radiometer (AVHRR) satellite. Arrows show suggested correlations between mid-winter warming events and mid-winter isotope (deuterium/hydrogen = δD) anomalies.

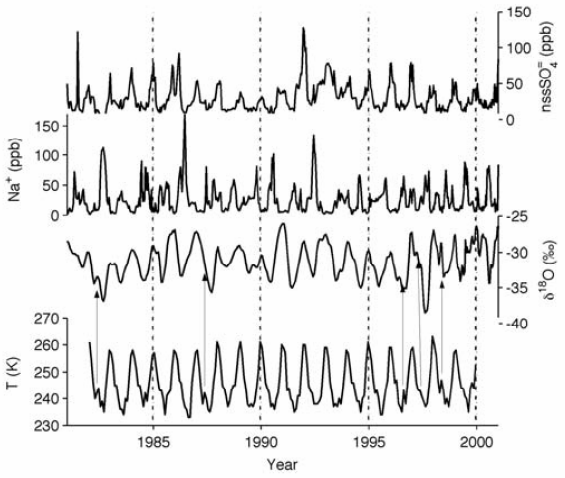

Fig. 4. Same as Figure 3, but for US ITASE core 2001-5, and showing sodium concentrations (Na^+) in place of nitrate. Arrows show suggested correlations between mid-winter warming events and mid-winter oxygen isotope anomalies.

heads designed to separately sample the outside and inside of the core. Concentrations of hydrogen peroxide, formaldehyde and selected major ions were measured by continuous flow analysis using the fluorescence or photometric detection methods (Röthlisberger and others, 2000) at the University of Arizona; stable-isotope concentrations ($\delta^{18}O$ and δD) were analyzed by mass spectrometry using CO_2 equilibration and Cr reduction at the University of Washington; all other geochemical measurements were conducted at the University of Maine using ion chromatography. Details of the sampling and measurement procedures used are given in Buck and others (1992) and Frey and others (in press).

3. ESTABLISHMENT OF DEPTH–AGE RELATIONSHIPS FROM SEASONAL VARIATIONS

Figures 2–6 show selected geochemical profiles from three sites (US ITASE 2000-1, 2000-4, and 2001-5) to illustrate the most important findings with respect to ice-core dating at US ITASE sites in West Antarctica. Other core profiles are similar and support the conclusions derived from these examples. We refer to these figures in this and in subsequent sections of the paper.

For the relatively high-accumulation sites we selected, geochemical and physical properties of the US ITASE cores show that there is excellent preservation of seasonal cycles in virtually all geochemical parameters and in grain-size variations that mark the transitions from summer to fall and winter to spring. This is a prerequisite for obtaining high-quality timescales. We also found that agreement between results from the 82 mm ice cores, which generally start ~1 m below the surface, and from the overlapping shallower snow pits and 50 mm cores, is excellent. Exceptions to the general rule of unambiguous seasonal indicators in the US ITASE cores are:

1. at the lowest-elevation/warmest sites (1999-1 and 1999-2), diffusion of the more mobile species, notably hydrogen peroxide (H_2O_2), water stable-isotope ratios ($\delta^{18}O$, δD) and nitrate (NO_3^-), preclude the detection of seasonal cycles in these species beyond the upper ~10 m of firn;
2. at most sites, we found that wind crusts in the physical stratigraphy were not reliably correlated with other indicators of annual snow accumulation; in general, we found more than one such layer in most years.

We established initial age vs depth relationships for the US ITASE cores through the identification of seasonal peaks from all the major geochemical time series considered together (SO_4^{2-}, Na^+, Ca^{2+}, Cl^-, Mg^{2+}, K^+ and NO_3^-), coupled with visual stratigraphy, but not including stable-isotope ratios and hydrogen peroxide. In practice, we find that the least ambiguous seasonal variations are in the sulfate concentrations, and in particular the derived parameter $nssSO_4^{2-}$ (non-sea-salt sulfate, also referred to as 'excess sulfate', determined by applying a standard sea-water ratio of 30.61 (Na^+), 1.1 (K^+), 3.69 (Mg^{2+}), 1.16 (Ca^{2+}), 55.04 (Cl^-) and 7.68 (SO_4^{2-}) to the ion concentrations in each sample; see O'Brien and others (1995) and Dixon and others (2004) for details). Sulfate deposition in West Antarctica reflects both sea-salt and non-sea-salt sources, with a strong altitude dependence on their relative importance. At lower elevations, the biogenic-source SO_4^{2-} fractions may overwhelm volcanic signals. This appears to be important at Siple Dome (elevation 600 m), which when combined with the rapid diffusion of stable isotopes (Cuffey and Steig, 1998) and somewhat ambiguous visual stratigraphy, has made dating to the interannual level problematic at this site (Taylor and others, 2004b). In the case of the US ITASE cores, there is a fairly small difference between the SO_4^{2-} and $nssSO_4^{2-}$ data; however, using the latter has the advantage of narrowing the width of the seasonal maxima, and of accentuating anomalously large peaks that are identified with large, globally significant explosive volcanic events.

On the basis of two independent influences on seasonal sulfate concentrations, we assigned the $nssSO_4^{2-}$ peaks to

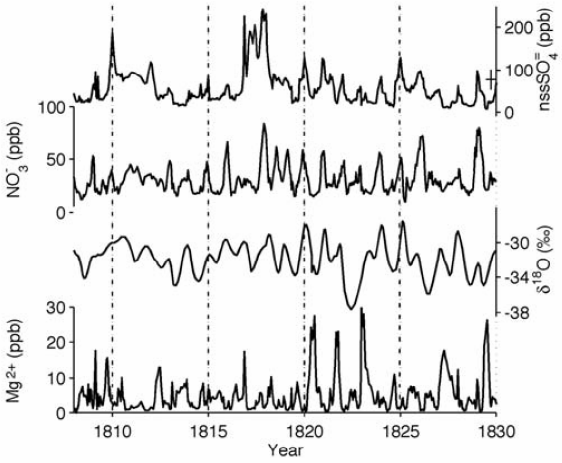

Fig. 5. Same as Figure 4, but showing the years 1808–30 in US ITASE core 2001-5, and showing NO_3^- in place of Na^+, and showing magnesium concentrations (Mg^{2+}) in the bottom panel. Cross on right side of upper panel shows mean and standard deviation of SO_4^{2-} concentrations measured in fresh snow during summer at core site 2001-6. Note significantly elevated sulfate levels in ~1816–17, due to the Tambora eruption, and in 1810–11.

early summer (nominally 1 January) of each year (Figs 2–5). The primary source of $nssSO_4^{2-}$ is the oxidation of various sulfur compounds beginning with dimethyl sulfide (DMS) which is produced by phytoplankton, with blooms generally beginning in December as sea-ice melt-induced surface water stratification becomes established, and peaking in early January (Arrigo and others, 1999; Kettle and others, 1999). The secondary source for $nssSO_4^{2-}$ is input from the upper troposphere and lower stratosphere, representing both volcanic inputs, and anthropogenic and additional biogenic sulfur from extrapolar regions (Delmas, 1982; Legrand and Mayewski, 1997). The peak input of this secondary source is also expected to occur in early austral summer, due to the spring-time break-up of the polar vortex. In addition to this a priori reasoning, numerous ice-core studies support the assignment of the $nssSO_4^{2}$ peak to early summer (Whitlow and others, 1992; Wagenbach and others, 1998; Kreutz and Mayewski, 1999). Also, measurements of optical depth from the atmosphere at South Pole place the maxima precisely in early January (Bergin and others, 1998). Finally, we note that $nssSO_4$ concentrations in fresh snow from a late December snowstorm in 2001, near site US ITASE 2001-6, are indistinguishable from the typical ice-core $nssSO_4$ maxima (Fig. 5).

4. ACCURACY OF TIMESCALES

Having established timescales for the cores that are based on seasonal variations alone, with $nssSO_4^{2-}$ providing the nominal assignment of calendar dates, i.e. time of year, we used several independent measures to validate the timescales. The validation procedures provide a means to estimate both the precision and accuracy of the timescales.

The identification of volcanic marker horizons provides a particularly important validation tool. In each of the US ITASE cores that have been analyzed for sulfate concentrations (US ITASE 1999-1, 2000-1, 2000-4, 2000-5, 2001-2, 2001-3, 2001-5) and in several additional West Antarctic cores, Dixon and others (2004) identified elevated $nssSO_4^{2-}$ levels at times consistent with the known dates of eruption of the following volcanoes (dates given in parentheses): Tambora, Indonesia (1815); Cosiguina, Nicaragua (1835); Krakatau, Indonesia (1883); Agung, Indonesia (1963); Pinatubo, Philippines, and Cerro Hudson, Chile (1991). An 'unknown' event, which has an established age of 1808/09 from Greenland ice cores and other evidence (Zielinski and others, 1994; Chenoweth, 2001), was also identified. Specifically, elevated levels of $nssSO_4^{2-}$ begin in 1810, 1816, 1837, 1885, 1964 and 1992. These ages, from the independent layer counting, are consistently 1–2 years after the eruption date of the volcanoes assigned to them, consistent with the typical stratospheric transport time across the circumpolar vortex. For the most recent volcanoes, we know from satellite observations that the stratospheric SO_4^{2-} clouds from Cerro Hudson and Pinatubo were centered over the South Pole in September and November 1991 (Cacciani and others, 1993; Saxena and others, 1995). Because the seasonal cycle in SO_4^{2-} begins to rise in September, it is difficult to demonstrate that the volcanic signal is registered precisely at the expected time. However, the background levels clearly begin to rise no earlier than 1991 and no later than 1992 in all cores (Figs 2–4), and the most prominent summer peak in all of the cores, after the 1964 peak attributed to Agung, occurs in January 1992.

On the basis of the seasonal ion-chemistry data and the volcanic marker horizons, a conservative estimate for the absolute dating accuracy for the US ITASE cores is $<\pm 2$ years. Strictly, this applies only at the times of the identified horizons. A concern that arises in assigning this value to the entire length of the cores is the possibility that, while the length of time between different volcanic horizons may be correct, there may be some timescale variation within these intervals that is greater than 1 year, particularly for the longer interval 1886–1963 when no volcanic horizons were identified. Indeed, in examining the $\delta^{18}O$ record from site 2001-5, we noted one year (1893) in which there appeared to be a 'missing' $\delta^{18}O$ annual cycle. Subsequent review of the $nssSO_4^{2-}$ profile also showed a weak $nssSO_4^{2-}$ peak at this time, suggesting that this year *may* have been misidentified as a summer peak. No such differences were observed in the other cores analyzed. Based on this comparison, we consider the overall, absolute dating accuracy to be conservatively ± 2 years overall, and much better than ± 1 year in the most recent (last ~20 years) parts of the US ITASE cores.

We can further demonstrate that the *relative* dating accuracy is in general no worse than 1 year. In particular, this higher level of accuracy applies for all the cores at those depths at which volcanic horizons (or total beta measurements that reveal known atomic bomb test events) have been identified, since all of these horizons occur in the same year in all of the cores analyzed (Dixon and others, 2004). For two of the cores, we can further demonstrate a relative dating accuracy of ± 1 year throughout the entire length of the records. Spikes and others (2004) showed, using shallow radar stratigraphy, that it was possible to unambiguously trace lines from the 2000-4 site to the 2000-5 site and to obtain identical ages ± 1 year at each. Arcone and others (2005) have also traced layers between sites 2000-4 and 2000-2, and place the 1991 summer layer at 10.1 m depth at 2000-2. While core 2000-2 remains to be processed for

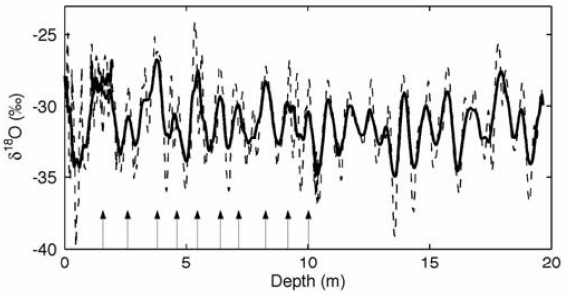

Fig. 6. Oxygen isotope ($\delta^{18}O$) record from US ITASE core 2000-2. Dashed line is measured data; bold line shows 19-point smoothed data. Arrows show inferred annual summer peaks between the surface (2001) and the depth of the radar reflector, independently attributed to the year 1991 from correlation with US ITASE core 2000-4.

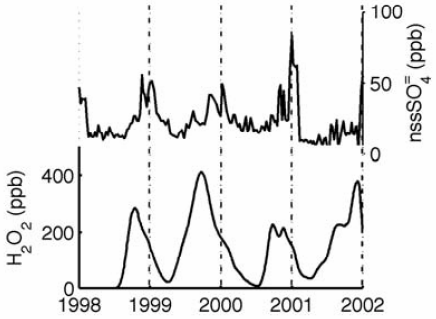

Fig. 7. Comparison of $nssSO_4^{2-}$ and H_2O_2 concentrations in US ITASE core 2001-5, between 1998 and 2002.

most geochemical measurements, from the stable-isotope profile (Fig. 6) we obtain 10.2 m for summer 1991, amounting to a difference of ~1 month at this high-accumulation site (estimated 46 g cm^{-2} a^{-1} mean for the past decade). The hydrogen peroxide record also indicates a depth of 10.2 m for late spring 1990 (Frey and others, in press).

Additional information from the stable-isotope and hydrogen peroxide concentrations further supports the estimated ±1 year accuracy. Seasonal $\delta^{18}O$, δD and H_2O_2 cycles in these cores, which were not used in the original layer counting, provide an independent check on the assumption that the $nssSO_4^{2-}$ variations are seasonal. For most cores, the $\delta^{18}O$ cycles are unambiguously seasonal through at least AD 1900, except for cores 1999-1 and 1999-2 where rapid isotope diffusion eliminates the seasonal variations at much shallower depths. In some cores the seasonal variations are detectable through the entire length (e.g. sites 2001-5 (Fig. 5) and 2002-4 (Jacobel and others, 2005)). For the most recent 20 years, the stable-isotope ratios provide an especially robust indicator of accuracy, because of the strong link between stable-isotope ratios and temperature. Schneider and others (2005) show that the correlation between climatological monthly mean stable-isotope values in these cores and local monthly temperature anomalies from AVHRR satellite observations is $r = 0.98$. (The 'climatological monthly mean' is the mean of all Januarys, all Februarys, etc. for 1982–99.) There is a distinctive mid-winter warming period that appears at some sites in some years in the temperature records. We find that there are elevated isotope values at the corresponding sites in the correct years (Figs 3 and 4). Shuman and others (1995) found a similar correspondence in Greenland ice cores. We cannot demonstrate this for all the cores; in US ITASE core 2000-1, for example, diffusion has eliminated sub-seasonal variations. Importantly, though, while there are some years in which the isotope anomalies do not appear, there are no years in which the mid-winter isotope values are elevated without a corresponding mid-winter warming seen in the temperature records. This is particularly clear at the highest-accumulation site, in core 2001-5 (Fig. 4). These results indicate that the correct years have been identified with no uncertainty for at least the last 20 years, i.e. the length of the satellite records.

5. PRECISION OF TIMESCALES

We now consider the dating precision of the US ITASE cores. By precision, in this context, we mean the uncertainty in correct assignment of calendar months for individual years in the records. The annual-layer counts are defined in terms of peak-to-peak intervals between nominally 'summer' values of geochemical measurements. In all cases, we used simple linear interpolation to define the timescale between these nominal 1 January values. The precision of the timescales thus depends on the precision of the assumptions (1) that the $nssSO_4^{2-}$ peaks actually coincide with 1 January and (2) that net snow accumulation is uniform throughout the year.

While there is no direct way to test these assumptions in the past, we noted above that there is independent evidence that the $nssSO_4^{2-}$ peaks in early January (Bergin and others, 1998), and that this timing reflects a combination of sea-ice melt and the break-up of the polar vortex. Analyses of sea surface DMS concentrations (Kettle and others, 1999), sea-ice variations (personal communication from C. Bitz, 2004), and stratospheric temperatures from US National Centers for Environmental Prediction (NCEP)/US National Center for Atmospheric Research (NCAR) re-analysis data (Waugh and others, 1999) indicate that all vary by <1 month, which would suggest that the maximum in $nssSO_4^{2-}$ peak also varies by about this amount except during volcanic events. We also have some direct evidence that it is reasonable to attribute the midpoint in seasonal $nssSO_4^{2-}$ to 'winter' (nominally 1 July by linear interpolation). As shown in Figures 4 and 7, maxima in sodium (Na^+) and minima in hydrogen peroxide (H_2O_2) and stable isotopes all occur within 1–2 months of the nominal midpoint of the year, consistent with previous observations suggesting these are all winter signatures. As noted above, the occurrence of some mid-winter warming events in the stable-isotope records further indicates correct identification of winter layers to within ~1 month (Figs 3 and 4). The H_2O_2 data provide perhaps the most robust evidence for the timing of mid-winter, since the predominant source of atmospheric H_2O_2 is of photochemical origin, limiting production to the sunlit season. The only existing set of all-year-round measurements of H_2O_2 in the Antarctic troposphere stems from a coastal site and shows a distinct seasonal cycle, with a minimum around the winter solstice (Riedel and others, 2000). Year-round snow sample studies at the South Pole provide evidence that the same annual cycle is recorded in the surface snow and preserved at depth as a function of

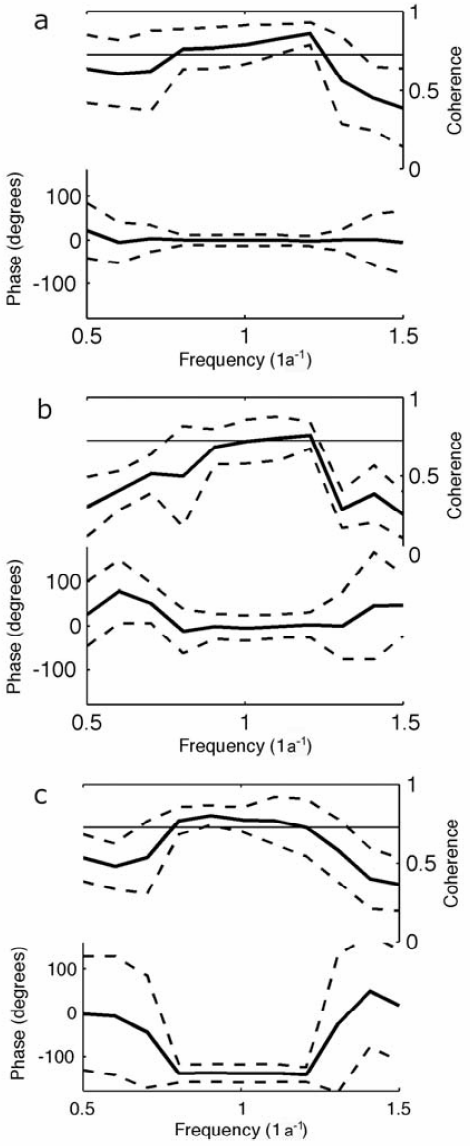

Fig. 8. Coherence and phase for non-sea-salt sulfate (SO_4^{2-}) compared with (a) NO_3^- in US ITASE core 2001-5; (b) $\delta^{18}O$ in core 2000–5; and (c) Na^+ in core 2000-4. The bandwidth is ~0.1 months. Bold lines show mean value; dashed lines are one standard deviation based on 10 year increments. Horizontal solid line in each upper panel is the 95% confidence limit for coherence.

accumulation rate and temperature (McConnell and others, 1998). Hydrogen peroxide shows preservation of the seasonal signature at all core sites with more than approximately 30 g cm^{-2} a^{-1} of annual accumulation down to depths >60 m (Frey and others, in press). Unfortunately, strong diffusional loss to the atmosphere and redistribution within the firn preclude a precise attribution of mid-winter at low-accumulation sites (<15 g cm^{-2} a^{-1}) beyond the upper ~10 m of the firn (Frey and others, in press).

On the basis of the above discussion, we suggest that a precision of ±1 month is a conservative estimate for the US ITASE cores, at least for the most recent years where we have independent calibration from the satellite-based temperature data. To verify that this stated precision is applicable to the full length of the records, we quantitatively examined the timing of nssSO_4^{2-} relative to other seasonal markers. To do this, we determined the variability in the coherence and phase of nssSO_4^{2-} vs NO_3^-, Na^+ and stable isotopes in each of the cores. We calculated the Thompson multi-taper (Thomson, 1982; Percival and Walden, 1993) phase and coherence spectra using three tapers over successive 10 year intervals from AD 1900 to 2000 to determine the mean and standard deviation of the phase. In all cases, greatest coherence is (as expected) at the annual cycle (i.e. frequency = 1 a^{-1}), and the phase at this frequency varies by <1 month. There is no temporal trend in either phase or coherence (though we restricted our analysis to the interval 1900–2000 because of diffusion of the seasonal $\delta^{18}O$ variations). As illustrated in Figure 8a, NO_3^- is in phase (0.0 ± 0.4 months) with nssSO_4^{2-}, consistent with the evidence that, like nssSO_4^{2-}, its variability is influenced by input from the upper troposphere/lower stratosphere (Mayewski and Legrand, 1990; Mulvaney and Wolff, 1993). Stable isotopes (Fig. 8b) are closely in phase with nssSO_4^{2-} as well, with a slight lead of 0.1 months (±0.9 month), consistent with the timing of warmest temperatures and the high seasonal isotope/temperature correlation (Schneider and others, 2005). Finally, Na^+ (Fig. 8c) leads nssSO_4^{2-} by ~5 ± 0.7 months, consistent with other evidence that Na^+ peaks in late winter (Bergin and others, 1998; Kreutz and others 2000b). Given that advection to the ice sheet of sea-salt aerosols by both summer and winter storms can lead to enhanced Na^+ concentrations, as expressed in relatively noisy Na^+ records with multiple peaks in a given year (Fig. 4), the consistency of phase is remarkable, and further attests to the consistency in the seasonal timing of the nssSO_4^{2-} peaks. This suggests that the identification of 'winter' in our records (nominally 1 July) is also precise to ±1 month. This in turn implies that snowfall throughout the year in West Antarctica is reasonably uniform: there is apparently insufficient variability in the seasonal timing of snowfall to influence the phase relationships by more than 1 month. Preservation of all annual layers further indicates that wind erosion or sublimation is insufficient in magnitude to remove annual snow accumulation. Both of these inferences are consistent with the precipitation modeling analyses of Bromwich and others (2004), which indicate a seasonal variation in snowfall amounts in West Antarctica of <25% and sublimation over precipitation ratios of <15%.

6. DISCUSSION

Recent work using paleoclimate proxy data has highlighted the importance of obtaining multiple, well-dated records at annual or better resolution, that can be used in calibration against the spatially comprehensive, but temporally very short, instrumental record of climate. Many analyses have emphasized tree ring records, primarily because the dating accuracy is excellent, and also because such records are available from nearly all continents and can therefore provide a representative sampling of climate variability (e.g. Mann and others, 1998; Jones and Widmann, 2003). As a general rule, available ice-core records have been too spatially sparse, and insufficiently resolved to contribute significantly to quantitative paleoclimate syntheses (Mann

and Jones, 2003), except where the longest timescales are concerned. Yet the polar regions, and Antarctica in particular, represent a large area that is inaccessible to such methods unless ice cores are used. An additional hindrance is that the instrumental record in Antarctica is particularly sparse and short, essentially limited to the last ~40 years.

One of the major goals of the overall ITASE program is to document Antarctic climate variability in the recent past (the last 200–2000 years) by obtaining highly resolved ice-core records distributed across the Antarctic ice sheet. Obtaining both high resolution and a high level of accuracy and precision is critical if we are to use multiple ice cores together as stacked records to reduce noise, or in multivariate regression models that are calibrated directly against the instrumental climate record (e.g. Schneider and others, 2005). The accuracy and precision obtained for the US ITASE cores recovered and analyzed from West Antarctica represent a significant contribution toward these efforts.

Importantly, for the period of overlap with the instrumental data (~40 years, and only ~20 years for satellite data), the absolute accuracy is demonstrably better than 1 year, and precision is well below the length of a season, allowing for calibration against both annually averaged and seasonal indicators of climate variability from the instrumental record. For longer-term records, the estimated relative accuracy of ±1 year is very promising, as any systematic errors would affect all the cores together and therefore be negligible for these cores taken as a group. We further emphasize that we consider our estimates of absolute accuracy (<±2 years) to be quite conservative, given the relative accuracy of <±1 year from the radar analyses. In section 3, we raised the point that we cannot rule out systematic biases in the cores between the stratigraphic tie points provided by the volcanic horizons. However, we suggest that it is in fact quite unlikely that the same number of years have been misidentified in multiple ice cores. That the ice-core-based age of the Tambora eruption is identical in all of the records is suggestive of an absolute accuracy of <±1 year. It is further notable that, in general, dating accuracy in layer-counted ice cores is expected to decrease with depth (age), since errors in layer counting will be cumulative. In the case of the US ITASE cores, however, the accuracy should be approximately uniform in distribution, because there is a roughly even distribution of well-dated volcanic layers throughout the cores.

Accurate and precise dating of paleoclimate proxy records is a critical step in using such records to extend our knowledge of climate and environmental change prior to the time period covered by the instrumental record. Our analyses suggest that the use of multiple Antarctic ice cores for quantitative investigation of climate variability on timescales significantly shorter than decadal is feasible with existing data. Complete spatial coverage of the Antarctic continent will be important. The spatial coverage of well-dated ice cores from West Antarctica, plus published data from East Antarctica, appears to be sufficient to reconstruct Antarctic mean temperature over the last ~100–200 years (Schneider and others, 2005), and may be adequate for reconstruction of interannual variations in the 'Southern Annular Mode' (Thompson and Wallace, 2000), but may be insufficient to reconstruct higher-order patterns of variability, such as the Pacific South America (Schneider and others, 2005) or 'Antarctic Dipole' (Yuan and Martinson, 2001) patterns in temperature, sea-ice and geopotential height anomalies. It will therefore be important to combine records from the US ITASE cores with those from other ITASE projects, and with existing highly resolved cores such as Law Dome in East Antarctica (Masson-Delmotte and others, 2003) and the Dyer Plateau on the Peninsula (Thompson and others, 1994). Care must be taken to ensure that consistent standards of accuracy and precision are used in all datasets.

ACKNOWLEDGEMENTS

We gratefully acknowledge the support of the US Antarctic Research Program, the New York Air National Guard 109th Airborne Division, the staff of Raytheon Polar Services and A. Zielinski at the University of Maine for help in, and getting to, the field. The first author was supported by grant OPP 0196105 from the US National Science Foundation. Suggestions by R. Mulvaney and two anonymous reviewers led to improvements to the manuscript.

REFERENCES

Arcone, S.A., V.B. Spikes and G.S. Hamilton. 2005. Phase structure of radar stratigraphic horizons within Antarctic firn. *Ann. Glaciol.*, **41** (see paper in this volume).

Arrigo, K. *and 6 others*. 1999. Phytoplankton community structure and the drawdown of nutrients and CO_2 in the Southern Ocean. *Science*, **283**(5400), 365–367.

Bergin, M.H., E.A. Meyerson, J.E. Dibb and P.A. Mayewski. 1998. Relationship between continuous aerosol measurements and firn core chemistry over a 10-year period at the South Pole. *Geophys. Res. Lett.*, **25**(8), 1189–1192.

Bromwich, D.H., Z. Guo, L. Bai and Q. Chen. 2004. Modelled Antarctic precipitation. Part I: spatial and temporal variability. *J. Climate*, **17**(3), 427–447.

Buck, C.F., P.A. Mayewski, M.J. Spencer, S. Whitlow, M.S. Twickler and D. Barrett. 1992. Determination of major ions in snow and ice cores by ion chromatography. *J. Chromatogr.*, **594**(1–2), 225–228.

Cacciani, M., P. di Girolamo, A. di Sarra, G. Fiocco and D. Fua. 1993. Volcanic aerosol layers observed by lidar at South Pole, September 1991–June 1992. *Geophys. Res. Lett.*, **20**(9), 807–810.

Chenoweth, M. 2001. Two major volcanic cooling episodes derived from global marine air temperature, AD 1807–1827. *Geophys. Res. Lett.*, **28**(15), 2963–2966.

Cuffey, K.M. and E.J. Steig. 1998. Isotopic diffusion in polar firn: implications for interpretation of seasonal climate parameters in ice-core records, with emphasis on central Greenland. *J. Glaciol.*, **44**(147), 273–284.

Delmas, R. 1982. Antarctic sulphate budget. *Nature*, **299**(5885), 677–678.

Dixon, D., P.A. Mayewski, S. Kaspari, S. Sneed and M. Handley. 2004. A 200-year sub-annual record of sulfate in West Antarctica from 16 ice cores. *Ann. Glaciol.*, **39**, 545–556.

Frey, M.M., R.C. Bales and J.R. McConnell. In press. Climate sensitivity of the century-scale hydrogen peroxide (H_2O_2) record preserved in 23 ice cores from West Antarctica. *J. Geophys. Res.*

Jacobel, R., B.C. Welch, E. Steig and D. Schneider. 2005. Glaciological and climatic significance of Hercules Dome, Antarctica – an optimal site for deep ice core drilling. *J. Geophys. Res.*, **110**(F1), F01015. (10.1029/2004JF000188.)

Johnsen, S.J., W. Dansgaard, H.B. Clausen and C.C. Langway, Jr. 1972. Oxygen isotope profiles through the Antarctic and Greenland ice sheets. *Nature*, **235**(5339), 429–434.

Jones, J.M. and M. Widmann. 2003. Instrument- and tree-ring-based estimates of the Antarctic oscillation. *J. Climate*, **16**(21), 3511–3524.

Jouzel, J. *and 12 others*. 2001. A new 27 ky high resolution East Antarctic climate record. *Geophys. Res. Lett.*, **28**(16), 3199–3202.

Kaspari, S. *and 6 others*. 2004. Climate variability in West Antarctica derived from annual accumulation rate records from ITASE firn/ice cores. *Ann. Glaciol.*, **39**, 585–594

Kaspari, S., P.A. Mayewski, D.A. Dixon, S.B. Sneed and M.J. Handley. 2005. Sources and transport pathways of marine aerosol species into West Antarctica. *Ann. Glaciol.*, **41** (see paper in this volume).

Kettle, A.J. *and 31 others*. 1999. A global database of sea surface dimethyl sulfide (DMS) measurements and a procedure to predict sea surface DMS as a function of latitude, longitude, and month. *Global Biogeochemical Cycles*, **13**(2), 399–444.

Kreutz, K.J. and P.A. Mayewski. 1999. Spatial variability of Antarctic surface snow glaciochemistry: implications for paleo-atmospheric circulation reconstructions. *Antarct. Sci.*, **11**(1), 105–118.

Kreutz, K.J., P.A. Mayewski, L.D. Meeker, M.S. Twickler and S.I. Whitlow. 2000a. The effect of spatial and temporal accumulation rate variability in West Antarctica on soluble ion deposition. *Geophys. Res. Lett.*, **27**(16), 2517–2520.

Kreutz, K.J., P.A. Mayewski, I.I. Pittalwala, L.D. Meeker, M.S. Twickler and S.I. Whitlow. 2000b. Sea level pressure variability in the Amundsen Sea region inferred from a West Antarctic glaciochemical record. *J. Geophys. Res.*, **105**(D3), 4047–4059.

Legrand, M. and P. Mayewski. 1997. Glaciochemistry of polar ice cores: a review. *Rev. Geophys.*, **35**(3), 219–243.

Mann, M.E. and P.D. Jones. 2003. Global surface temperatures over the past two millennia. *Geophys. Res. Lett.*, **30**(15), 1820. (10.1029/2003GL017814.)

Mann, M.E., R.S. Bradley and M.K. Hughes. 1998. Global-scale temperature patterns and climate forcing over the past six centuries. *Nature*, **392**(6678), 779–787.

Masson-Delmotte, V. *and 6 others*. 2003. Recent southern Indian Ocean climate variability inferred from a Law Dome ice core. *Climate Dyn.*, **21**(2), 153–166. (10.1007/s00382-003-0321-9.)

Mayewski, P.A. and I.D. Goodwin. 1996. International Trans-Antarctic Scientific Expedition (ITASE) '200 years of past Antarctic climate and environmental change'. Science and implementation plan, 1996. *PAGES Workshop Report* 97-1.

Mayewski, P.A. and M. Legrand. 1990. Recent increase in nitrate concentration of Antarctic snow. *Nature*, **346**(6281), 258–260.

McConnell, J.R., R.C. Bales, R.W. Stewart, A.M. Thompson, M.R. Albert and R. Ramos. 1998. Physically based modeling of atmosphere-to-snow-to-firn transfer of H_2O_2 at South Pole. *J. Geophys. Res.*, **103**(D9), 10,561–10,570.

Mosley-Thompson, E., L.G. Thompson, P.M. Grootes and N. Gundestrup. 1990. Little Ice Age (neoglacial) paleoenvironmental conditions at Siple Station, Antarctica. *Ann. Glaciol.*, **14**, 199–204.

Mulvaney, R. and E.W. Wolff. 1993. Evidence for winter/spring denitrification of the stratosphere in the nitrate record of Antarctic firn cores. *J. Geophys. Res.*, **98**(D3), 5213–5220.

O'Brien, S.R., P.A. Mayewski, L.D. Meeker, D.A. Meese, M.S. Twickler and S.I. Whitlow. 1995. Complexity of Holocene climate as reconstructed from a Greenland ice core. *Science*, **270**(5244), 1962–1964.

Percival, D.B. and A.T. Walden. 1993. *Spectral analysis for physical applications: multitaper and conventional univariate techniques*. Cambridge, Cambridge University Press.

Rick, U.K. and M.R. Albert. 2004. Microstructure and permeability in the near-surface firn near a potential U.S. deep drilling site in West Antarctica. *Ann. Glaciol.*, **39**, 62–66.

Riedel, K., R. Weller, O. Schrems and G. König-Langlo. 2000. Variability of hydrogen peroxide and methylhydroperoxide in the Antarctic troposphere. *Atmos. Environ.*, **34**, 5225–5234.

Röthlisberger, R. *and 6 others*. 2000. Technique for continuous high-resolution analysis of trace substances in firn and ice cores. *Environ. Sci. Technol.*, **34**(2), 338–342.

Saxena, V.K., J. Anderson and N.H. Lin. 1995. Changes in Antarctic stratospheric aerosol characteristics due to volcanic eruptions as monitored by the Stratospheric Aerosol and Gas Experiment II satellite. *J. Geophys. Res.*, **100**(D8), 16,735–16,751.

Schneider, D.P. and E.J. Steig. 2002. Spatial and temporal variability of Antarctic ice sheet microwave brightness temperatures. *Geophys. Res. Lett.*, **29**(20), 1964. (10.1029/2002GL015490.)

Schneider, D.P., E.J. Steig and J.C. Comiso. 2004. Recent climate variability in Antarctica from satellite-derived temperature data. *J. Climate*, **17**(7), 1569–1583.

Schneider, D.P., E.J. Steig and T. van Ommen. 2005. High-resolution ice-core stable-isotopic records from Antarctica: towards interannual climate reconstruction. *Ann. Glaciol.*, **41** (see paper in this volume).

Shuman, C.A., R.B. Alley, S. Anandakrishnan and C.R. Stearns. 1995. An empirical technique for estimating near-surface air temperature trends in central Greenland from SSM/I brightness temperatures. *Remote Sens. Environ.*, **51**(2), 245–252.

Spikes, V.B., G.S. Hamilton, S.A. Arcone, S. Kaspari and P. Mayewski. 2004. Variability in accumulation rates from GPR profiling on the West Antarctic plateau. *Ann. Glaciol.*, **39**, 238–244.

Taylor, K.C. *and 13 others*. 2004a. Abrupt late glacial climate change in the Pacific sector of Antarctica. *Quat. Sci. Rev.*, **23**(1), 7–15.

Taylor, K.C. *and 13 others*. 2004b. Dating the Siple Dome (Antarctica) ice core by manual and computer interpretation of annual layering. *J. Glaciol.*, **50**(170), 453–461.

Thompson, D.W.J. and J.M. Wallace. 2000. Annular modes in the extratropical circulation. Part I: Month-to-month variability. *J. Climate*, **13**(5), 1000–1016.

Thompson, L.G. *and 7 others*. 1994. Climate since AD 1510 on Dyer Plateau, Antarctic Peninsula: evidence for recent climate change. *Ann. Glaciol.*, **20**, 420–426.

Thomson, D.J. 1982. Spectrum estimation and harmonic analysis. *Proc. IEEE*, **70**, 1055–1096.

Vaughan, D.G., J.L. Bamber, M.B. Giovinetto, J. Russell and A.P.R. Cooper. 1999. Reassessment of net surface mass balance in Antarctica. *J. Climate*, **12**(4), 933–946.

Wagenbach, D. *and 7 others*. 1998. Sea-salt aerosol in coastal Antarctic regions. *J. Geophys. Res.*, **103**(D9), 10,961–10,974.

Watanabe, O., J. Jouzel, S. Johnsen, F. Parrenin, H. Shoji and N. Yoshida. 2003. Homogeneous climate variability across East Antarctica over the past three glacial cycles. *Nature*, **422**(2805), 509–512.

Waugh, D.W., W.J. Randel, S. Pawson, P.A. Newman and E.R. Nash. 1999. Persistence of the lower stratospheric polar vortices. *J. Geophys. Res.*, **104**(D22), 27,191–27,201.

Whitlow, S., P.A. Mayewski and J.E. Dibb. 1992. A comparison of major chemical species seasonal concentration and accumulation at the South Pole and Summit, Greenland. *Atmos. Environ.*, **26A**(11), 2045–2054.

Yuan, X. and D.G. Martinson. 2001. The Antarctic dipole and its predictability. *Geophys. Res. Lett.*, **28**(18), 3609–3612.

Zielinski, G.A. *and 8 others*. 1994. Record of volcanism since 7000 B.C. from the GISP2 Greenland ice core and implications for the volcano–climate system. *Science*, **264**(5161), 948–952.

Snow chemistry across Antarctica

N. BERTLER,[1] P.A. MAYEWSKI,[2] A. ARISTARAIN,[3] P. BARRETT,[1] S. BECAGLI,[4] R. BERNARDO,[5] S. BO,[6] XIAO C.,[7*] M. CURRAN,[8] QIN D.,[9] D. DIXON,[2] F. FERRON,[5] H. FISCHER,[10] M. FREY,[11] M. FREZZOTTI,[12] F. FUNDEL,[10] C. GENTHON,[13] R. GRAGNANI,[12] G. HAMILTON,[2] M. HANDLEY,[2] S. HONG,[14] E. ISAKSSON,[15] KANG J.,[6] REN J.,[9] K. KAMIYAMA,[16] S. KANAMORI,[16] E. KÄRKÄS,[17] L. KARLÖF,[15] S. KASPARI,[2] K. KREUTZ,[2] A. KURBATOV,[2] E. MEYERSON,[2] Y. MING,[6] ZHANG M.,[9] H. MOTOYAMA,[16] R. MULVANEY,[18] H. OERTER,[10] E. OSTERBERG,[2] M. PROPOSITO,[12] A. PYNE,[1] U. RUTH,[10] J. SIMÕES,[5] B. SMITH,[8] S. SNEED,[2] K. TEINILÄ,[19] F. TRAUFETTER,[10] R. UDISTI,[4] A. VIRKKULA,[17] O. WATANABE,[16] B. WILLIAMSON,[2] J-G. WINTHER,[15] LI Y.,[6] E. WOLFF,[18] LI Z.,[9] A. ZIELINSKI[2]

[1]*Antarctic Research Centre, Victoria University, PO Box 600, Wellington, New Zealand*
E-mail: Nancy.Bertler@vuw.ac.nz
[2]*Climate Change Institute, University of Maine, Orono, ME 04469, USA*
[3]*Laboratorio de Estratigrafia Glaciar y Geoquimica del Agua y de la Nieve – Conicet, CC 131, 5500 Mendoza, Argentina*
[4]*Chemistry Department – Analytical Chemistry, Scientific Pole, University of Florence, Via della Lastruccia 3, I-50019 Sesto Fiorentino (Florence), Italy*
[5]*Núcleo de Pesquisas Antárticas e Climáticas, Universidade Federal do Rio Grande do Sul, Avenida Bento Gonçalves 9500, 91.501-970 Porto Alegre, Brazil*
[6]*Polar Research Institute of China, Shanghai 200129, China*
[7]*Institute of Climate and Environment, Chinese Academy of Meteorological Sciences, 46 Zhongguancun South Avenue, Beijing 100081, China*
[8]*Australian Antarctic Division/Antarctic Climate and Ecosystems CRC, Private Bag 80, Hobart, Tasmania 7001, Australia*
[9]*Cold and Arid Regions Environmental and Engineering Research Institute, Chinese Academy of Sciences, 260 Donggang West Road, Lanzhou 730000, China*
[10]*Alfred Wegener Institute for Polar and Marine Research, Columbusstrasse, D-27568 Bremerhaven, Germany*
[11]*Department of Hydrology and Water Resources, PO Box 210011, The University of Arizona, Tucson, AZ 85271-0011, USA*
[12]*ENEA, Progetto Clima, Centro Ricerche Casaccia, I-00060 S. Maria Galeria (Roma), Italy*
[13]*Laboratoire de Glaciologie et Géophysique de l'Environnement, 54 rue Molière, BP 96, 38402 Saint-Martin-d'Hères Cedex, France*
[14]*Korea Polar Research Institute, Korea Ocean Research and Development Institute, PO Box 29, Ansan, 425-600, Seoul, Korea*
[15]*Norwegian Polar Institute, Polarmiljøsenteret, NO-9296 Tromsø, Norway*
[16]*National Institute of Polar Research, Kaga, Itabashi-ku, Tokyo 173-8515, Japan*
[17]*Division of Geophysics, Department of Physical Sciences, PO Box 64, University of Helsinki, FIN-00014 Helsinki, Finland*
[18]*British Antarctic Survey, Natural Environment Research Council, Madingley Road Cambridge CB3 0ET, UK*
[19]*Finnish Meteorological Institute, Air Quality Research, Sahaajankatu 20E, FIN-00810 Helsinki, Finland*

ABSTRACT. An updated compilation of published and new data of major-ion (Ca, Cl, K, Mg, Na, NO_3, SO_4) and methylsulfonate (MS) concentrations in snow from 520 Antarctic sites is provided by the national ITASE (International Trans-Antarctic Scientific Expedition) programmes of Australia, Brazil, China, Germany, Italy, Japan, Korea, New Zealand, Norway, the United Kingdom, the United States and the national Antarctic programme of Finland. The comparison shows that snow chemistry concentrations vary by up to four orders of magnitude across Antarctica and exhibit distinct geographical patterns. The Antarctic-wide comparison of glaciochemical records provides a unique opportunity to improve our understanding of the fundamental factors that ultimately control the chemistry of snow or ice samples. This paper aims to initiate data compilation and administration in order to provide a framework for facilitation of Antarctic-wide snow chemistry discussions across all ITASE nations and other contributing groups. The data are made available through the ITASE web page (http://www2.umaine.edu/itase/content/syngroups/snowchem.html) and will be updated with new data as they are provided. In addition, recommendations for future research efforts are summarized.

[*]Also at: Cold and Arid Regions Environmental and Engineering Research Institute, Chinese Academy of Sciences, 260 Donggang West Road, Lanzhou 730000, China.

INTRODUCTION

'Ice cores provide the most direct and highly resolved records of (especially) atmospheric parameters for the last 1,000,000 years' (EPICA community, 2004). While ice-core chemistry analyses have revolutionized our knowledge on the working of the climate system and its variability through time (Legrand and Mayewski, 1997; Mayewski and White, 2002), an improved understanding of the fundamental factors that ultimately control the chemistry of a snow or ice sample will allow even more detailed and accurate interpretation of glaciochemical records reconstructing past climate conditions with near-instrumental quality.

To reach this understanding, it is necessary to determine individual sources and pathways of aerosols, mechanisms that control precipitation efficiency as well as post-depositional effects (Legrand and Mayewski, 1997). Comparing snow chemistry at different sites and investigating the processes leading to spatial differences in snow chemistry help to improve our understanding of temporal variability and teleconnections. Here, we provide an updated summary of available data from 520 sites in Antarctica, developed by the International Trans-Antarctic Scientific Expedition (ITASE), with the goal of providing this new dataset along with research recommendations to the wider ice-core community, in order to stimulate and focus the discussion towards a more comprehensive data interpretation.

BACKGROUND

ITASE has as its primary aim 'the collection and interpretation of a continental-wide array of environmental parameters assembled through the coordinated efforts of scientists from several nations' (Science and Implementation Plan, 1990, http://www2.ume.maine.edu/itase/content/scie_plan/intro.html). During the Seventh International Symposium on Antarctic Glaciology, in Milan, Italy, in 2003, the ITASE community established seven synthesis groups, of which this group – the ITASE Chemistry Synthesis group – is coordinating the compilation and interpretation of the spatial variability in snow and ice chemistry across the continent to address the knowledge gap on factors governing the variability of ice-core chemistry in Antarctica. A two-step approach was adopted. Firstly, broad patterns in Antarctic snow chemistry are investigated using all available reliable data (this paper). This will allow the strategy to be formulated for the second step, in which the group will focus on individual time periods in order to investigate the causes for changes in chemistry patterns (future papers). This will be achieved by contrasting, for example, El Niño with La Niña years or studying the years before and after volcanic eruptions, such as the recent Pinatubo (Philippines) event.

In this first step, we summarize new and previously published data and provide recommendations for future common efforts. The new data are provided by the national ITASE programmes of Australia, Brazil, China, Germany, Italy, Japan, Korea, New Zealand, Norway, the United Kingdom, the United States and the national Antarctic programme of Finland.

DATA SELECTION CRITERIA

Previous glaciochemical surveys showed that careful data selection for an Antarctic-wide comparison is important (Mayewski and others, 1992; Mulvaney and Wolff, 1994; Wagenbach, 1996; Legrand and Mayewski, 1997; Wolff and others, 1998a, b; Kreutz and Mayewski, 1999; Kreutz and others, 1999; Stenberg and others, 1999). Data from 520 sites are summarized here and can be obtained from the ITASE Chemistry Synthesis group web page (http://www2.umaine.edu/itase/content/syngroups/snowchem.html). While the laboratory procedures of the individual groups are of high standard, no cross-evaluation has yet been undertaken. To obtain further information on individual datasets, contact details are provided along with the data.

Because Antarctic glaciochemistry shows large seasonal variability (Gow, 1965; Sigg and Neftel, 1988; Solomon and Keys, 1992; Legrand and Mayewski, 1997; Curran and others, 1998; Wolff and others, 1998a; Kreutz and others, 1999; Bertler and others, 2004b), it is desirable for any continent-wide comparison to use either well-dated (sub-annual) records or multi-year averages. The achievable level of age control of ice-core records is dependent on many factors, but particularly on annual accumulation (and sampling resolution) and therefore varies greatly across Antarctica. Of the 520 available data sources, 194 records are reliably identified as multi-year samples. The remaining records are predominantly surface snow samples collected along transects, and thus are an important contribution to determine aerosol sources. For the comparison of new ITASE data, however, we decided to aim in this first step for 5 year averages. This allows short records to be included while eliminating seasonal variability. A survey of ITASE metadata indicates that the 5 year interval most represented in the currently available dataset is 1992–97. At present, 45 sites provide well-dated chemistry measurements for this time period. This interval coincides with the Pinatubo volcanic eruption, and therefore provides an opportunity to study the effect of volcanic eruptions in future papers when time series are considered.

A second fundamental decision is whether to use concentration or flux data (Kreutz and others, 2000). Due to the spatially variable influence of dry and wet deposition across Antarctica and the difficulty of obtaining reliable, high-resolution annual snow accumulation measurements, concentration data are preferred over flux. However, as more accumulation data become available, the influence of spatially and temporally varying snow accumulation leading to varying contributions of wet vs dry deposition should be investigated further. This can be achieved by merging the data of this group with the currently compiled datasets of the ITASE/ISMASS (Ice Sheet Mass Balance and Sea Level programme) Mass Balance and Atmospheric Chemistry Synthesis groups.

In the metadata survey, information on all glaciochemical analyses has been compiled. Here, we focus on major ions: sodium (Na), magnesium (Mg), calcium (Ca), potassium (K), chloride (Cl), nitrate (NO_3), sulphate (SO_4) and methanesulfonate (MS). An Antarctic-wide comparison of other species, such as trace elements, organic acids, and particles, is hampered by the limited number of data points currently available. However, growing interest and improved analytical methods will enable us to incorporate such data in the near future.

DATA EVALUATION AND PRESENTATION

As Antarctica exhibits strong spatial contrasts, it is important to evaluate how well the sampled locations represent

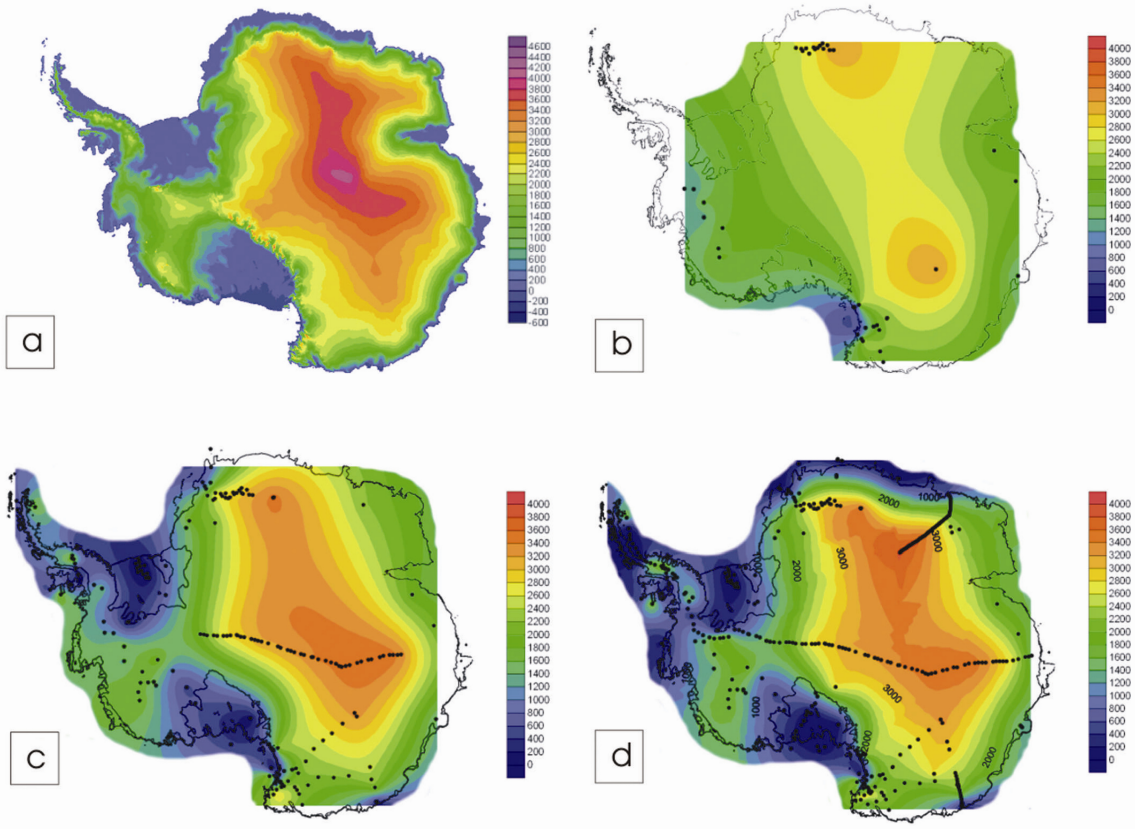

Fig. 1. Reconstructed topography of Antarctica, derived from (a) RAMP 5 km elevation model (Liu and others, 2001); (b) sample locations providing data for the period 1992–97; (c) sample locations providing multi-year averages; (d) all glaciological sample locations.

regional- to continent-scale gradients. Most parameters (e.g. elevation, distance from the sea, annual accumulation) change simultaneously along many transects and are therefore difficult to assess individually. The comparison between the Antarctic topography, as inferred by the RADARSAT Antarctic Mapping Project (RAMP) 5 km elevation model (Liu and others, 2001) (Fig. 1a), and the reconstructed surface using only elevation information from the sampled sites provides a means to evaluate how well Antarctic geographic features are represented by the sampled locations. The reconstructed surfaces in Figure 1b–d are calculated using the interpolation method of linear kriging between sampling sites. In Figure 1b the Antarctic surface is reconstructed using only sites that provide data from the chosen 1992–97 time period (45 data points). While the data are clustered and separated by large geographical gaps, they represent contemporary glaciochemical concentration, generally excluding time-driven factors, such as climate variability. The reconstructed topography lacks many of the significant Antarctic features (e.g. neither ice shelf nor the Antarctic Peninsula is yet represented). A number of sites provide 5 year averages for slightly different time periods or have an associated dating error of more than ±1 year. Incorporating these sites enlarges the database significantly. In Figure 1c the reconstructed topography using all multi-year data is shown (194 data points). While main geographical features, such as the East and West Antarctic ice sheets, the Ross and Filchner–Ronne Ice Shelves are represented, other significant details such as the Transantarctic Mountains, the Antarctic Peninsula and the Lambert Glacier system are poorly or not represented. The reconstructed topography in Figure 1d incorporates all available data (520 data points), including non-annual samples. This is the most comprehensive dataset currently available. As the data do not all represent the same time period or might represent only seasons, their interpretation in an Antarctic-wide comparison requires careful attention. Although the reconstructed map incorporating all available data is more detailed than Figure 1c, it still lacks important elements across large regions of the Antarctic continent. Overall, this comparison highlights the need for many more traverses to provide better coverage, especially of well-dated, multi-year, contemporary time series.

ION CONCENTRATION VS ELEVATION

As discussed above, many site physical characteristics influencing glaciochemistry change simultaneously, either geographically or temporally. These include annual accumulation, elevation and distance from the sea. Accurate, high-resolution annual accumulation data are difficult to obtain, as they require high-resolution dating and density measurements. Furthermore, there are no well-documented,

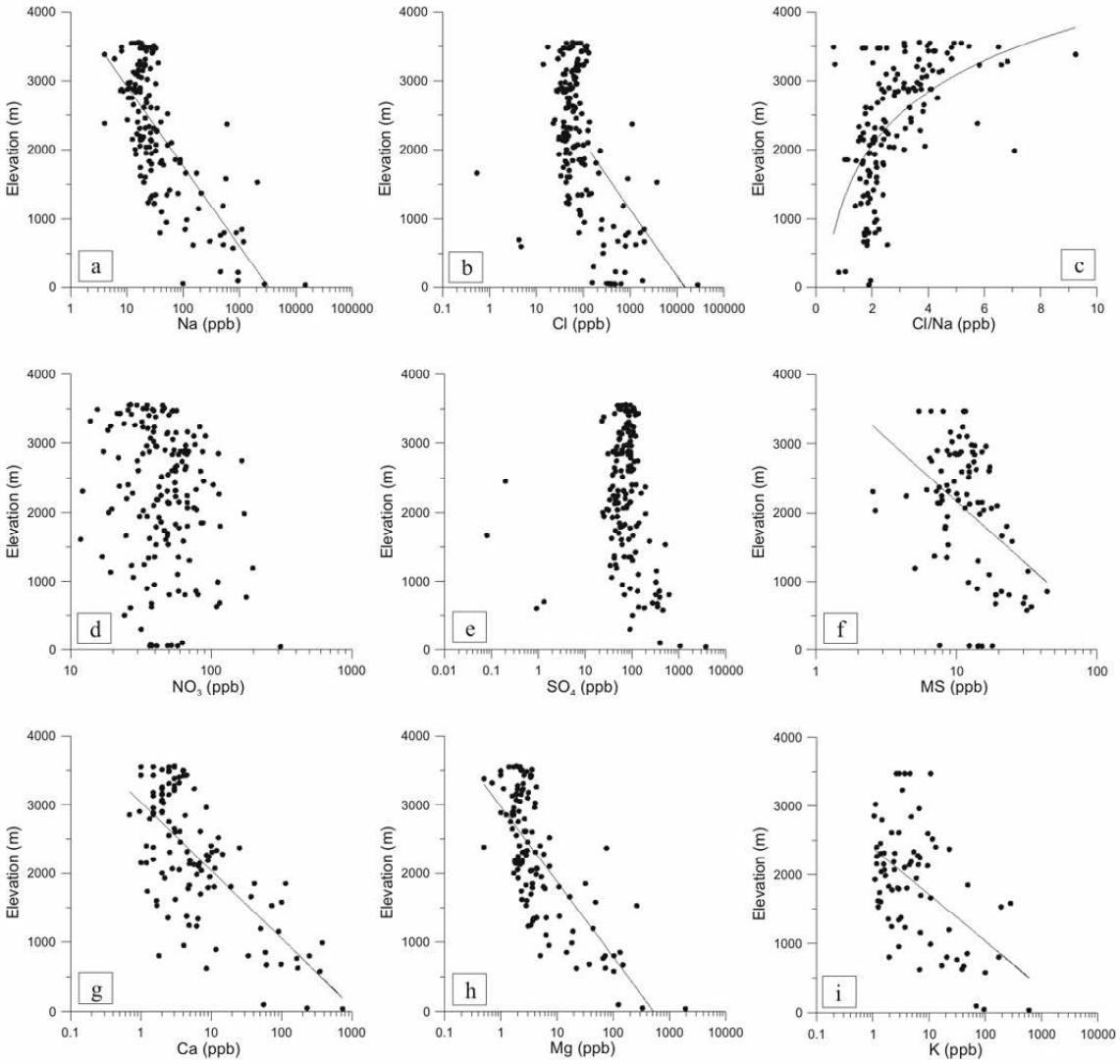

Fig. 2. Relationship between multi-year ion concentration data and elevation: (a) Na; (b) Cl; (c) Cl/Na ratio; (d) NO_3; (e) SO_4; (f) MS; (g) Ca; (h) Mg; and (i) K. All species are plotted on a logarithmic scale, except for (c) which is plotted on a linear scale. The logarithmic trends shown are significant on the 99.9% level.

straightforward linear associations between chemistry and accumulation rate. In order to determine distance from the sea, it is necessary to understand the pathway of the precipitating air mass for both wet and dry deposition. Local atmospheric circulation patterns can be highly variable and might change true distance to the sea from 10 km to 1000 km depending on the pathway of the air mass (e.g. Bertler and others, 2004a; Xiao and others, 2004; Kaspari and others, 2005). Furthermore, large seasonal changes in sea-ice cover further complicate the measurement of true distance to the sea. One parameter that is relatively easy to obtain and does not change significantly over short time periods is elevation.

However, as annual accumulation and distance from the sea exhibit a correlation with elevation in Antarctica, any observed patterns are likely to be caused by a varying combination of all three. Correlation between ion concentration and elevation is shown in Figure 2. Ion concentration variability across Antarctica exhibits an amplitude of up to four orders of magnitude. Therefore, ion concentrations are plotted on logarithmic scales, with the exception of the Cl/Na ratio.

The correlations between elevation and Na or Cl (Fig. 2a and b) show a statistically significantly inverse relationship (logarithmic) of decreasing ion concentration with increasing altitude of $r = -0.73$ and $r = -0.51$, respectively. Furthermore, the scatter in both datasets is larger at lower elevation than at higher locations. When correlating the Cl/Na ratio with elevation ($r = 0.56$), sites below 2000 m predominantly show values close to the marine ratio of ~1.8 (Warneck, 1988), while the scatter in the data increases significantly above 2000 m, reaching values of

up to 20 (Fig. 2c). This confirms that sites below 2000 m are predominantly influenced by sea salt, and also suggests no significant post-depositional aerosol loss or enrichment. The larger scatter with increasing elevation is indicative of a number of potential processes leading to relative enrichment or depletion of either species (Gayley and Ram, 1985; Mulvaney and Peel, 1988; Mulvaney and Wolff, 1994; De Angelis and Legrand, 1995; Yang and others, 1996a; Legrand and Mayewski, 1997; Kreutz and others, 1998; Stenberg and others, 1998; Wagenbach and others, 1998b; Wolff and others, 1998a, b; Kreutz and Mayewski, 1999; Udisti and others, 1999; Kreutz and others, 2000; Aristarain and Delmas, 2002; Proposito and others, 2002; Udisti and others, 2004; Becagli and others, 2005; Benassai and others, 2005).

No statistically significant correlation at the 99.9% significance level exists between elevation and NO_3 (Fig. 2d). NO_3 is predominantly a secondary aerosol, produced in the strato- and ionosphere. Processes leading to nitrate production in the higher atmosphere are thought to be stratospheric oxidation of N_2O, ionospheric dissociation of N_2, and polar stratospheric clouds via HNO_3. Additionally, lightening in the mid-latitudes produces the primary NO_3 aerosol in the troposphere (Parker and others, 1981, 1982; Parker and Zeller, 1980; McKenzie and Johnston, 1984; Evans and others, 1985; Legrand and Delmas, 1986; Toon and others, 1986; Legrand and Kirchner, 1990; Mayewski and others, 1990; Qin and others, 1992; Solomon and Keys, 1992; Clausen, 1995; Wolff, 1995; Yang and others, 1996a, b; Legrand and Mayewski, 1997; Wagenbach and others, 1998a; Palmer and others, 2001). Higher NO_3 concentrations are therefore expected within the boundary of the polar vortex due to the influence of upper atmospheric air masses. Furthermore, some post-depositional and photochemical mechanisms lead to NO_3 loss, especially at low-accumulation sites (De Angelis and Legrand, 1995; Legrand and Mayewski, 1997; Mulvaney and others, 1998; Wagnon and others, 1999; Röthlisberger and others, 2000, 2002; Jones and others, 2001; Wolff and others, 2002; Udisti and others, 2004), which partially offsets the trend towards higher NO_3 in the Antarctic interior. As this effect takes place in the upper few metres of the snowpack, it is particularly important to compare not only contemporary NO_3 data, but also samples derived from similar depths in the snow profile.

The correlation between SO_4 and elevation also shows no statistically significant trend at the 99.9% significance level. While concentration data exhibit a more scattered pattern at lower elevations, total SO_4 input seems largely independent of elevation. However, SO_4 has many sources (Delmas and others, 1982; Wolff and Mulvaney, 1991; Mayewski and others, 1992; Mulvaney and Wolff, 1994; Legrand, 1995; Legrand and Mayewski, 1997; Minikin and others, 1998; Udisti and others, 1998, 1999; Becagli and others, 2005), and individual SO_4 species might exhibit significant correlations with elevation. While primary aerosol SO_4 species (sea spray) and secondary marine-biogenic SO_4 should exhibit a rapid decrease with increasing elevation, volcanic SO_4 aerosols enters through the upper atmosphere and therefore should have a stronger signal in the Antarctic interior. Furthermore, the volcanic input of SO_4 often exceeds average SO_4 input (Mayewski and others, 1995; Zielinski and others, 1997; Dixon and others, 2004). Because data used in this comparison represent different time periods, samples containing volcanic SO_4 input have the potential to obscure an existing relationship, especially for the 1992–97 time period, which coincides with the Pinatubo 1991 eruption.

MS shows a statistically significant decrease with increasing elevation (Fig. 2f) of $r = -0.42$. While most ion species have multiple sources, MS is thought to have a single marine source and is derived via oxidation from plankton-produced DMS (dimethylsulfonate) in polar oceans (Mulvaney and others, 1992), which explains its anticorrelation with elevation. MS is observed to peak in summer, when biological activity is highest (Welch and others, 1993; Saltzman, 1995; Saltzman and others, 1997; Meyerson and others, 2002). Delmas and others (2003) and Weller and others (2004) describe a mechanism by which MS is lost to interstitial gaseous phase in the Antarctic interior, which might partially be responsible for the observed trend in Figure 3f. As for NO_3, it is therefore important to investigate MS data in relationship to snow depth of the sample.

Ca, Mg and K show an inverse relationship with decreasing concentration at higher-elevation sites (Fig. 3g and h), with $r = -0.70$ and $r = -0.73$, $r = -0.52$ respectively. Furthermore, the scatter in the datasets appears higher at lower-elevations sites, especially for Ca. These species have local and global terrestrial, as well as marine sources. In the vicinity of ice-free areas, such as the McMurdo Dry Valleys, ion concentration is influenced from those local sources (Gayley and Ram, 1985; Aristarain and Delmas, 2002; Bertler and others, 2004b). Elsewhere, the input is dominated by sea-salt and global dust input (Shaw, 1979), with the former producing orders-of-magnitude higher concentrations than the latter, thus explaining the overall inverse relationship with elevation.

SPATIAL ION CONCENTRATION VARIABILITY

To further investigate the relationships observed in Figure 2, the geographical variability is discussed in Figures 3–11. The data for each species have been clustered into colour-coded classes. Due to the large amplitude of variability in ion concentration, the classes are distributed, not linearly, but, rather, according to data distribution. This is necessary because coastal regions, for example, show Na concentrations four orders of magnitude higher than those in the Antarctic interior (Fig. 3). As a result, a linear scale would under-represent the variability, with only one class for the entire Antarctic interior or for coastal sites. To compare sites within the Antarctic interior, or various coastlines, it is necessary to tune the classes so that variability at both low and high concentrations can be observed. The legend shows the percentage and number of data points contained in each class. Furthermore, data have been distinguished into three groups: well-dated data representing the period 1992–97 (solid circles), all other multi-year samples (solid triangles) and undated or non-annual samples (crosses). The colour coding for concentration classes is the same for all three groups.

Spatial variability of Na concentration is shown in Figure 3, ranging from 2 to 14 680 ppb. As expected, the East Antarctic interior shows significantly lower values (~2–30 ppb) than the coastal sites (~75–14 680 ppb). However, high values have also been reported from Marie Byrd Land at high elevation, and low concentrations in the vicinity of the East Antarctic coastlines (Kaiser-Wilhelm II.

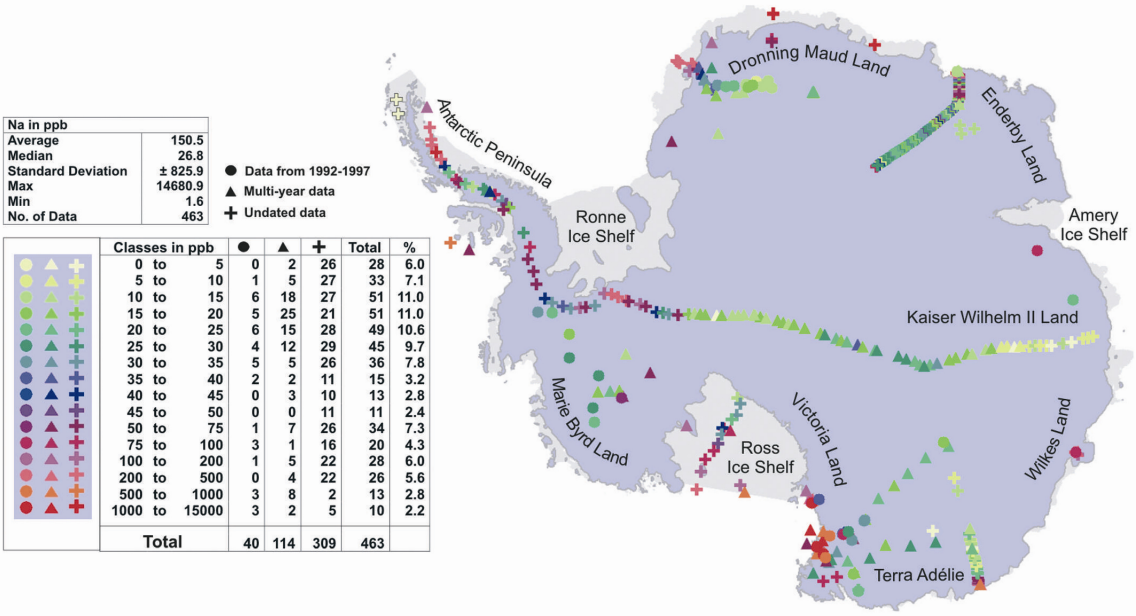

Fig. 3. Spatial variability of Na concentration measured in ppb. Solid circles represent 1992–97 data; solid triangles represent all other multi-year data. Crosses represent non-annual or undated samples.

Land and Terre Adélie). Furthermore, the change from very low to very high concentrations seems to occur within a narrow band in the vicinity of the coast. While high Na deposition is readily explained in coastal areas due to high sea-salt input, the narrow zone of marine air-mass intrusions (mesoscale cyclonic activity) coincides with the rapid decrease of Na concentrations in the Antarctic interior. Here the katabatic wind streams, transporting Na-depleted air masses from the interior towards the coast, compete with the Na-rich coastal air masses. In contrast, the Antarctic Peninsula shows overall high values and no trends, caused by strong sea-salt input all around and a secondary non-sea-salt contribution from ice-free mountain peaks I lowever, it is important to note that most of the data points located on the Antarctic Peninsula are surface samples representing winter snow. As Na peaks in most regions of Antarctica during winter, the higher Na concentrations reported from the Antarctic Peninsula are partially explained by this bias.

Cl variability exhibits a similar pattern to Na (Fig. 4), ranging from ~1 to 27 740 ppb. The highest values are observed at coastal sites (~150–27 740 ppb), and lower values in the interior (1 to ~150 ppb). The Antarctic Peninsula again shows overall high values and no significant trend with elevation. Furthermore, Cl shows high concentrations in the centre of the East Antarctic interior, which are also observed in the Na data, but to a lesser degree. In Figure 5 the spatial variability of the Cl/Na ratio is shown, ranging from 0.2 to 19.3. While most sites show a near-sea-water ratio of 1.8 (Warneck, 1988), in the Antarctic interior the ratio increases to an average value of 4.3, with data ranging from 2 to 9. Whereas coastal sites are likely to show sea-water Cl/Na ratios due to the direct input, elevated Cl/Na ratio in the low-accumulation zones of the Antarctic interior are suggestive of secondary Cl precipitation through HCl (De Angelis and Legrand, 1995), which might be partially offset by HCl re-emission from the upper layers of the snowpack (Udisti and others, 2004; Benassai and others, 2005). Overall, Antarctic interior Cl and Na concentrations are depleted in comparison to coastal values (Figs 3 and 4). However, in the East Antarctic interior, Cl seems relatively less depleted than Na, causing an increase in the Cl/Na ratio.

Figure 6 shows the spatial variability of NO_3, ranging from ~4 to ~800 ppb. Highest values can be observed in Enderby Land, Dronning Maud Land and Victoria Land, ranging from ~30 to 800 ppb. Intermediate values are reported from Marie Byrd Land, the Ronne Ice Shelf, the South Pole region and northern Victoria Land (~35–100 ppb), while the lowest values are observed on the Antarctic Peninsula and in Kaiser-Wilhelm-II. Land (~0–20 ppb). While NO_3 has been shown to be affected by post-depositional loss at low-accumulation sites (Mayewski and Legrand, 1990; De Angelis and Legrand, 1995; Legrand and Mayewski, 1997; Mulvaney and others, 1998), the lowest values for NO_3 have been observed at sites with relatively high annual accumulation, namely the Antarctic Peninsula and Kaiser-Wilhelm-II. Land. Samples from those sites were collected from the snow surface during August–September 1989 and February 1990, respectively, and contrast with snow surface samples from Enderby Land collected during October 1997, which show some of the highest values in the entire dataset. This suggests that post-depositional loss of NO_3 is strongly dependent on site-specific characteristics.

Spatial variability of SO_4 is shown in Figure 7. The data range from 0.1 to 3800 ppb. It is important to note that SO_4 is particularly prone to sporadic input through volcanic events. As the dataset represents different time periods, some of which coincide with volcanic eruptions, it is necessary

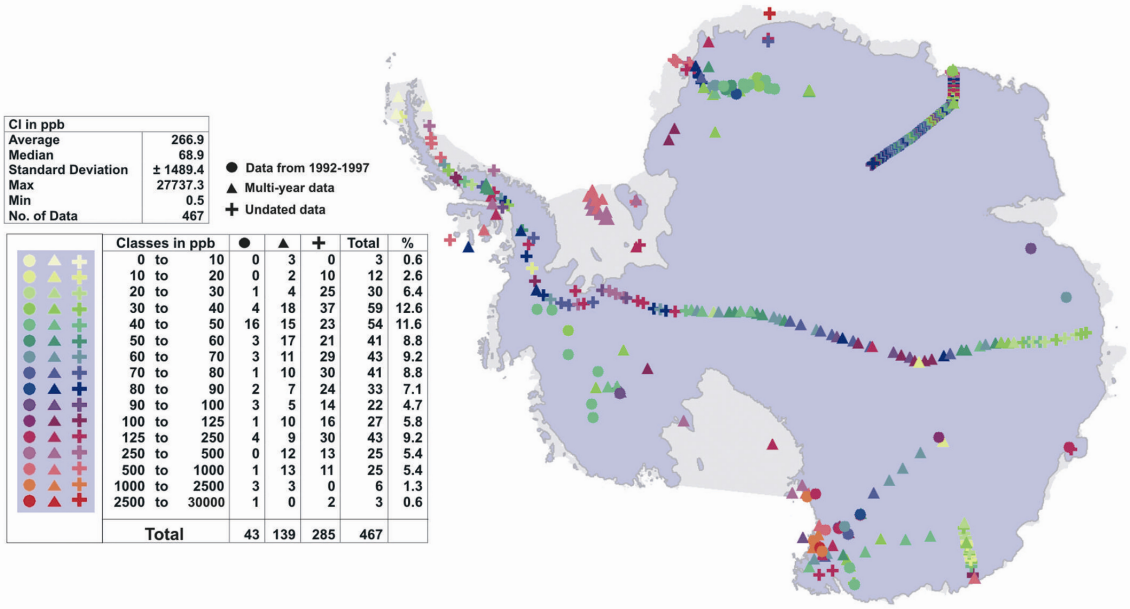

Fig. 4. Spatial variability of Cl concentration measured in ppb.

to interpret SO_4 variability carefully. However, many data points in Marie Byrd Land, Victoria Land and Dronning Maud Land are contemporary data from 1992–97 (Fig. 7, solid circles). The SO_4 concentrations of those data are higher in Victoria Land and Dronning Maud Land (~30–3800 ppb) than in Marie Byrd Land (~30–90 ppb). Furthermore, the transect leading from the Antarctic Peninsula to Kaiser-Wilhelm-II. Land shows large variability. The Antarctic Peninsula is characterized by low values (~10–30 ppb), with higher values only at coastal sites (~75–1000 ppb). The values from Kaiser-Wilhelm-II. Land are also relatively low, at 15–70 ppb. The central part of the transect,

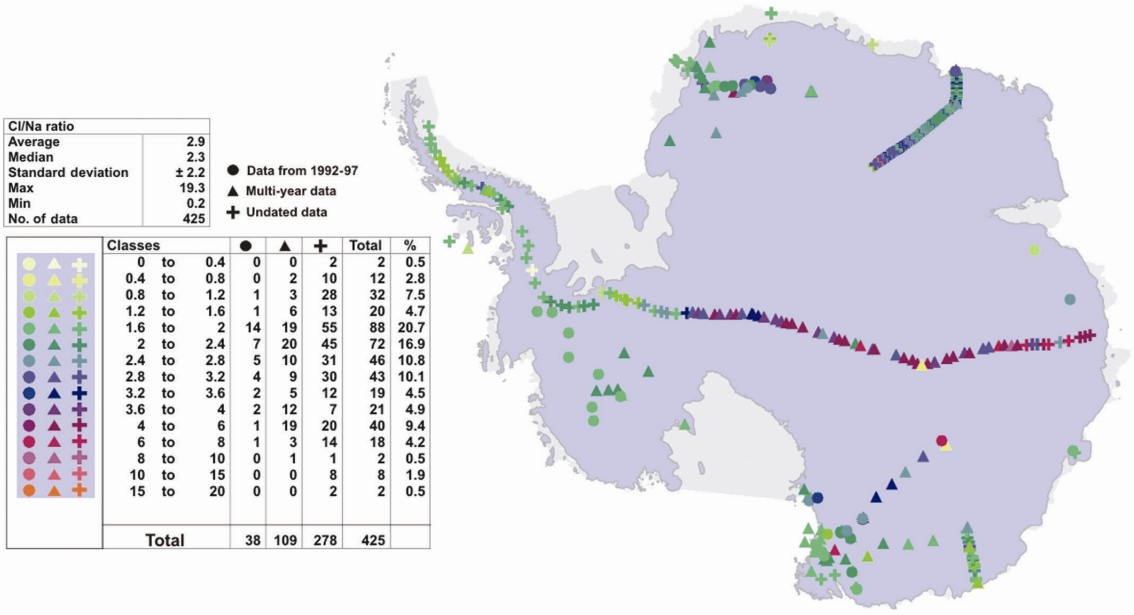

Fig. 5. Spatial variability of Cl/Na ratio.

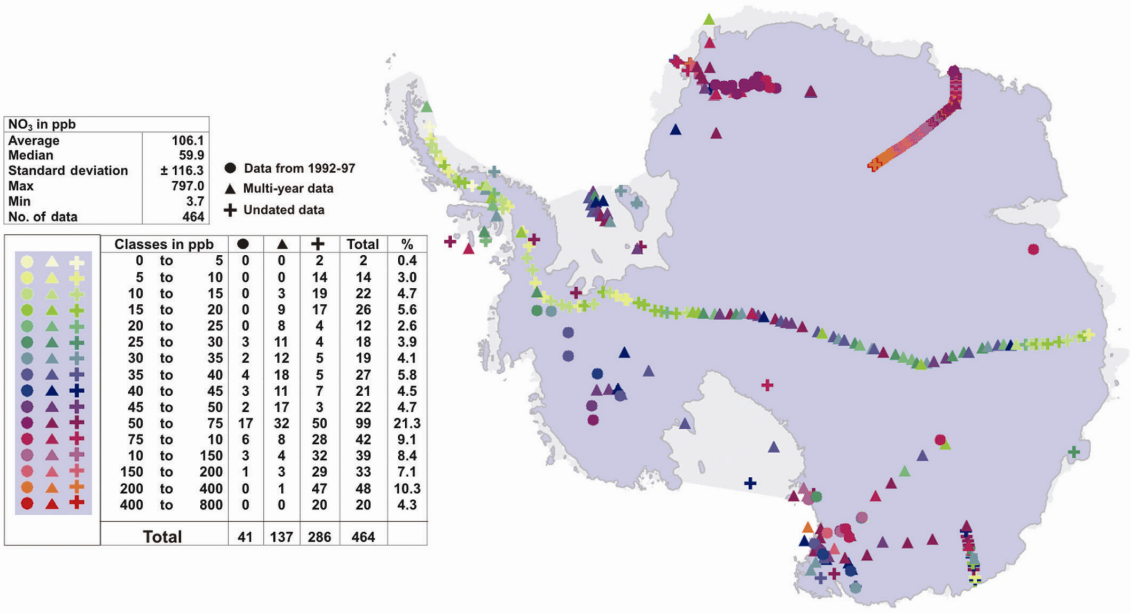

Fig. 6. Spatial variability of NO_3 concentration measured in ppb.

however, shows comparatively high values (~70–100 ppb). In addition, the Enderby Land transect shows an increase in SO_4 concentration with elevation (from ~10 ppb to 30 ppb). This could be influenced by local accumulation rates and variable SO_4 sources.

In Figure 8, spatial variability of MS data is shown, ranging from 3 to 166 ppb. In contrast to NO_3 and SO_4, MS is thought to be predominantly derived through wet deposition due to its high Henry constant (Udisti and others, 1998; Becagli and others, 2005). Overall, the data show highest concentration at coastal sites, with deceasing trends inland, except for two areas: the coastal sites at King George and Livingston Islands and the transect at Enderby Land. While MS concentrations in the former are unusually low compared to other coastal

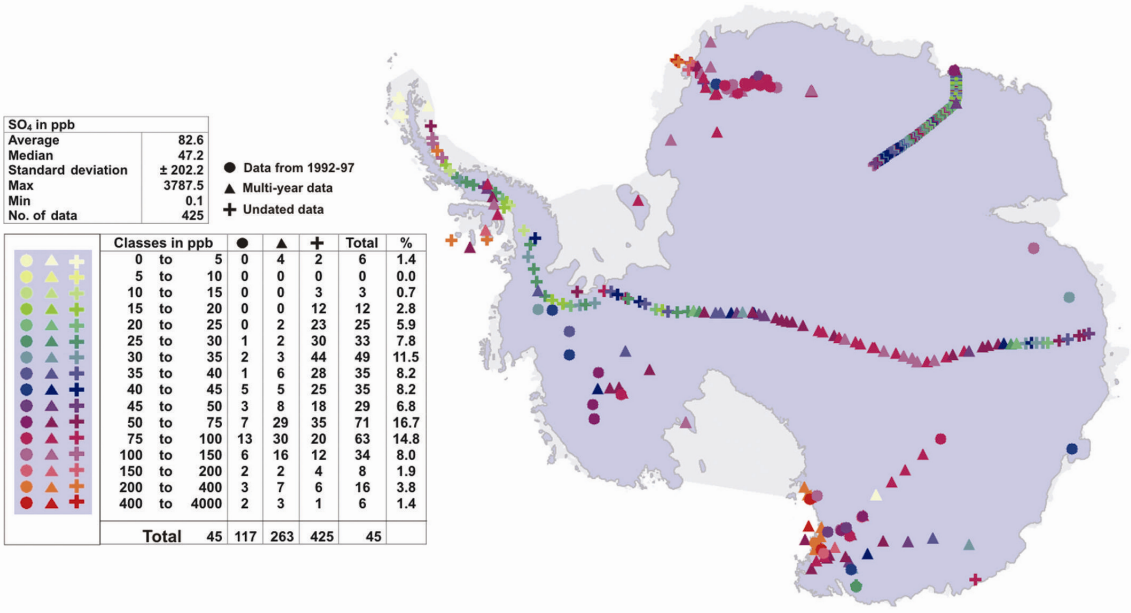

Fig. 7. Spatial variability of SO_4 concentration measured in ppb.

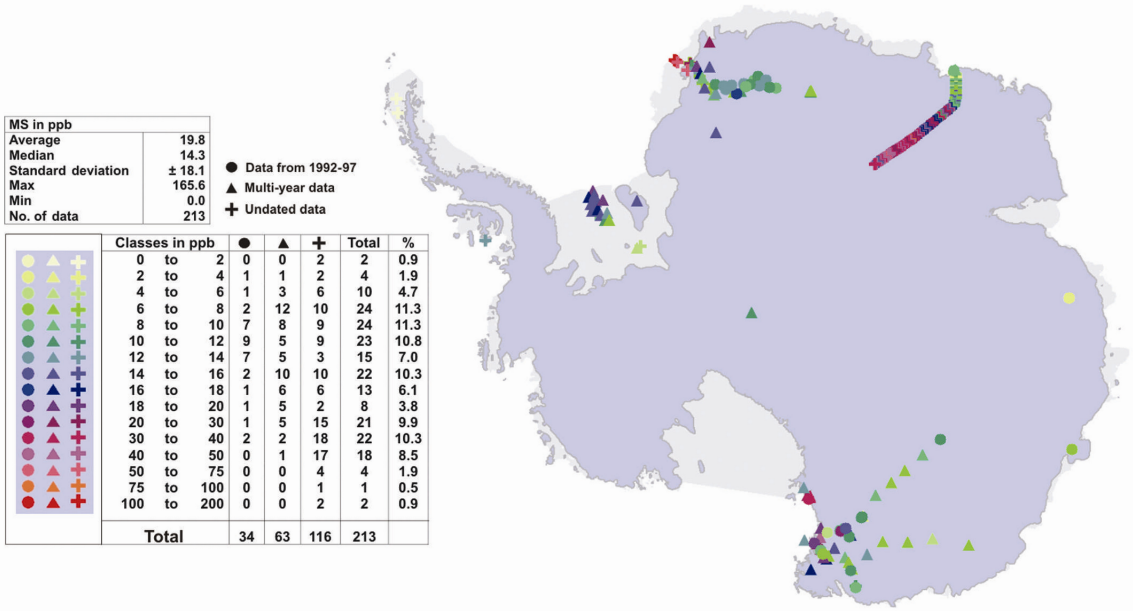

Fig. 8. Spatial variability of MS concentration measured in ppb.

sites (~0–2 ppb), the latter shows a trend from low MS values (0–14 ppb) at low elevation to high MS concentrations (14–50 ppb) further inland. A similar but less pronounced increase in concentration along the Enderby Land transect is also observed in the SO_4 and NO_3 data.

Ca, Mg and K are shown in Figures 9–11, respectively. Concentration values range from 0.1 to 740 ppb for Ca, from 0.2 to 1930 ppb for Mg, and from 0.1 to 600 ppb for K. All three species show overall low concentration values across Antarctica, with a few exceptions. Local dust sources such as the McMurdo Dry Valleys, a strong marine influence such as Terra Nova, or coastal sites at the Antarctic Peninsula cause orders-of-magnitude higher concentrations. Intermediate concentration levels are rare. The continent-wide

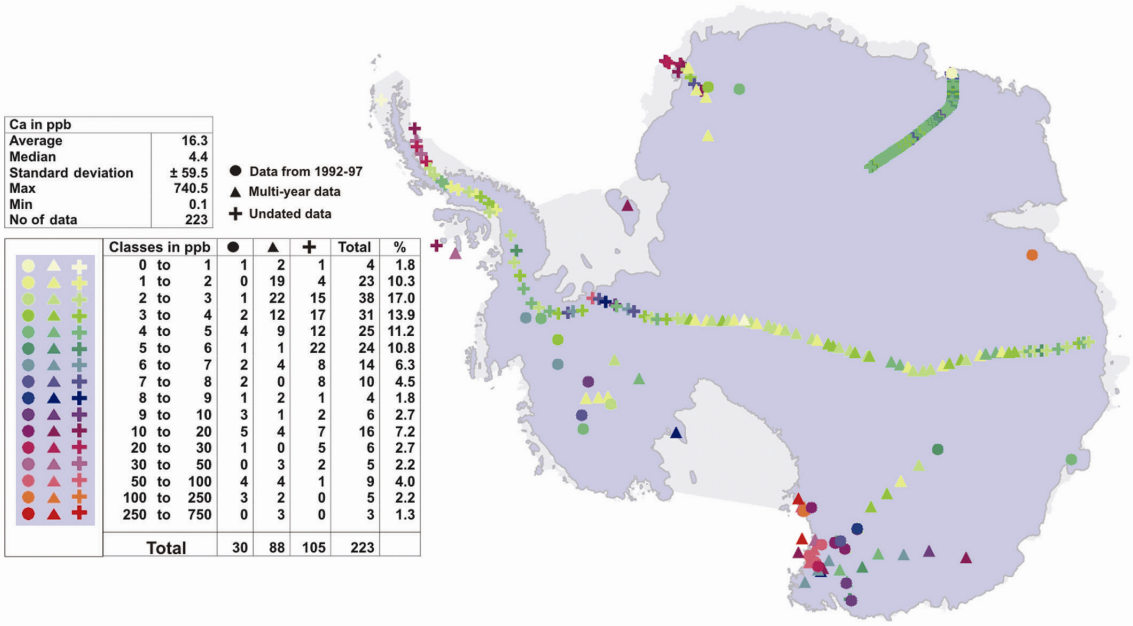

Fig. 9. Spatial variability of Ca concentration measured in ppb.

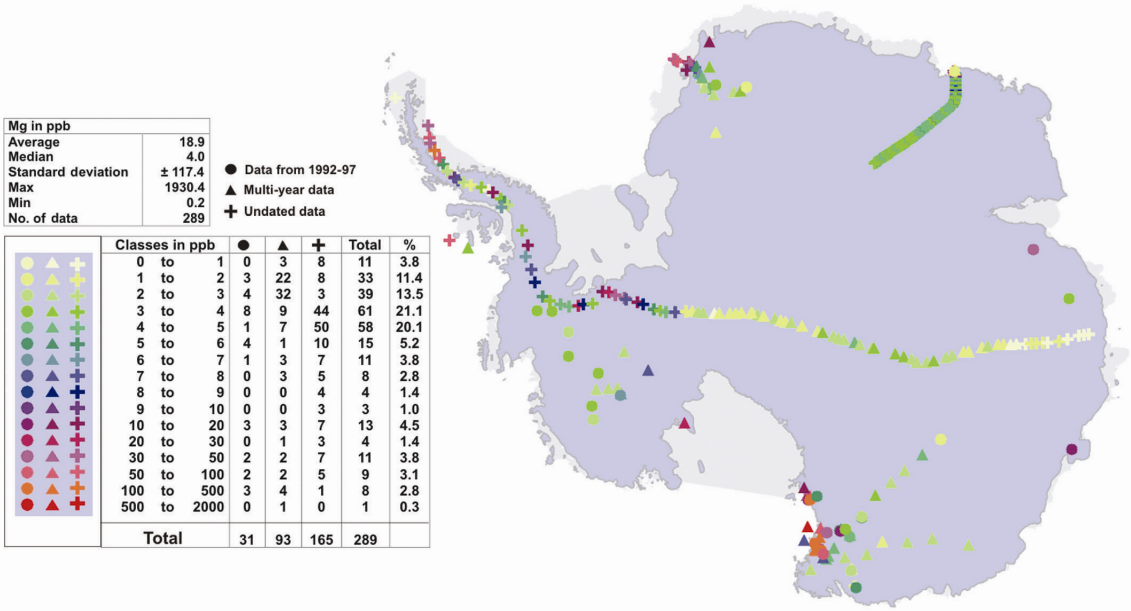

Fig. 10. Spatial variability of Mg concentration measured in ppb.

pattern might therefore be used to distinguish typical 'global' or hemispherical dust content from local Antarctic sources.

SUGGESTIONS FOR FUTURE WORK

The primary objectives of this paper are to provide an updated summary of available chemistry data from Antarctica and make recommendations for future efforts. The observed variability across Antarctica clearly shows the need for an improved understanding of the mechanisms that ultimately control the chemistry of a snow or ice sample. By making this dataset available, we invite and encourage the wider science community to participate in this continent-wide effort.

Based on our findings and on previous papers, we aim for the following research outputs as the next step for the ITASE Chemistry Synthesis group:

Investigation of the snow chemistry signal migration and spatial variability of significant climate events and oscillating and non-oscillating climate drivers

This can be achieved by intercontinental comparison of snow chemistry variability contrasting, for example, El Niño with La Niña years, high-index Antarctic Oscillation years with low-index years, and the snow chemistry signal before, during and after volcanic eruptions

Furthermore, cross–correlation of snow chemistry data with re-analysis data, such as NCEP/NCAR (US National Centers for Environmental Prediction/US National Center for Atmospheric Research) and ERA-40 (European re-analysis), will allow us to link characteristic geographic chemistry patterns to typical climate modes, establishing transfer functions, and to identify Antarctic teleconnections and their variability through time

Tuning general circulation models to reconstruct snow chemistry patterns in recurring synoptic and mesoscale climate events, using contemporary chemistry data as a training set, will allow us to use these models in reverse, to output climate events using chemistry data further back in time.

Investigation of the relationship between atmospheric aerosol loading and contemporary snow chemistry

Quantification of contemporary aerosol precipitation and deposition efficiency by linking surface snow chemistry concentration with atmospheric aerosol loading measurements can be established in collaboration with the ITASE Atmospheric Chemistry Synthesis group. Furthermore, this will assist in investigating the processes that lead to post-depositional ion concentration changes. It is important to compare samples of similar age as well as of similar snow depths

Investigation of dry vs wet deposition is particularly important when comparing coastal sites with the Antarctic interior. Here progress can be achieved in collaboration with the ITASE/ISMASS Mass Balance Synthesis group and the ITASE Atmospheric Chemistry Synthesis group

Incorporate new analytical techniques allowing the measurement of trace elements and their isotopic signatures, as well as organic acids, and particles.

Laboratory inter-comparison

We suggest a laboratory inter-comparison in order to demonstrate the compatibility of snow chemistry data across all laboratories.

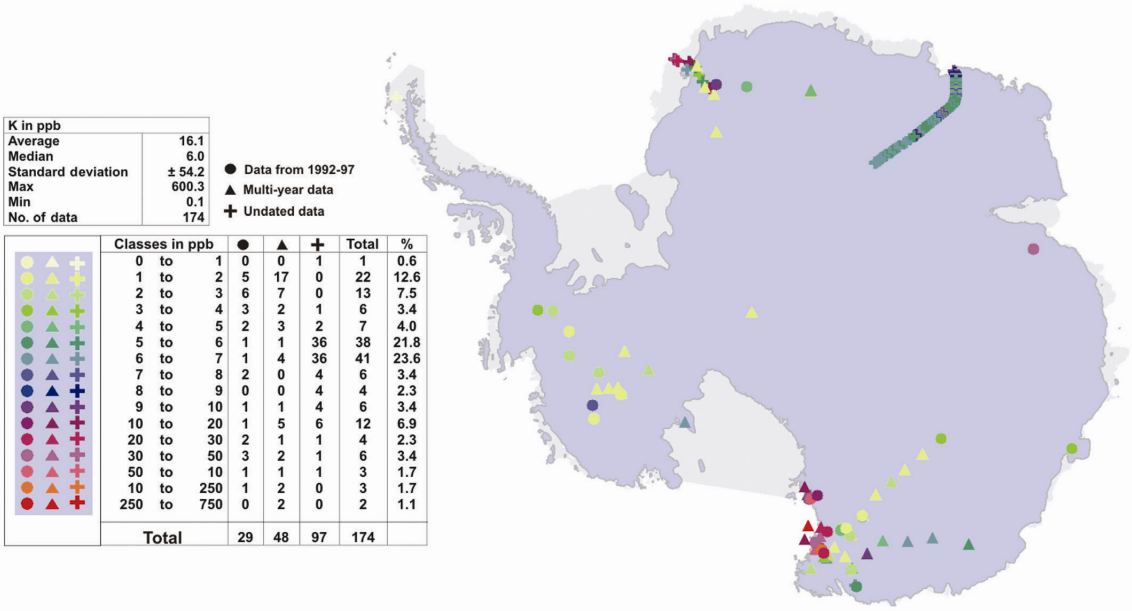

Fig. 11. Spatial variability of K concentration measured in ppb.

Data availability

The data described here are made available through the ITASE web page. The dataset will be updated as new data and datasets are provided.

ACKNOWLEDGEMENTS

We thank the Scientific Committee on Antarctic Research, the national Antarctic programmes and the national funding sources for their support. Two anonymous reviewers made helpful comments that improved the manuscript.

REFERENCES

Aristarain, A. and R.J. Delmas. 2002. Snow chemistry measurements on James Ross Island (Antarctic Peninsula) showing sea-salt aerosol modifications. *Atmos. Environ.,* **36**, 765–772.

Becagli, S. *and 12 others.* 2004. Chemical and isotopic snow variability in East Antarctica along the 2001/02 ITASE traverse. *Ann. Glaciol.,* **39**, 473–482.

Becagli, S. *and 6 others.* 2005. Spatial distribution of biogenic sulphur compounds (MSA, nssSO_4^{2-}) in the northern Victoria Land–Dome C–Wilkes Land area, East Antarctica. *Ann. Glaciol.,* **41** (see paper in this volume).

Benassai, S. *and 7 others.* 2005. Sea-spray deposition in Antarctic coastal and plateau areas from ITASE traverses. *Ann. Glaciol.*, **41** (see paper in this volume).

Bertler, N.A.N., P.J. Barrett, P.A. Mayewski, R.L. Fogt, K.J. Kreutz and J. Shulmeister. 2004a. El Niño suppresses Antarctic warming. *Geophys. Res. Lett.,* **31**(15), L15207. (10.1029/2004GL020749.)

Bertler, N.A.N., P.A. Mayewski, P.J. Barrett, S.B. Sneed, M.J. Handley and K.J. Kreutz. 2004b. Monsoonal circulation of the McMurdo Dry Valleys, Ross Sea region: signal from the snow chemistry. *Ann. Glaciol.,* **39**, 139–145.

Bertler, N.A.N., P.A. Mayewski, S.B. Sneed, T.R. Naish, U. Morgenstern and P.J. Barrett. 2005. Solar forcing recorded by aerosol concentrations in coastal Antarctic glacier ice, McMurdo Dry Valleys. *Ann. Glaciol.*, **41** (see paper in this volume).

Clausen, H.B. 1995. Group meeting on nitrate sources in Antarctica and Greenland. *In* Delmas, R.J., *ed. Ice core studies of global biogeochemical cycles.* Berlin, etc., Springer-Verlag, 247–248. (NATO ASI Series I: Global Environmental Change 30.)

Curran, M.A.J., T.D. van Ommen and V. Morgan. 1998. Seasonal characteristics of the major ions in the high-accumulation Dome Summit South ice core, Law Dome, Antarctica. *Ann. Glaciol.,* **27**, 385–390.

De Angelis, M. and M. Legrand. 1995. Preliminary investigations of post depositional effects of HCl, HNO_3, and organic acids in polar firn layers. *In* Delmas, R.J., *ed. Ice core studies of global biogeochemical cycles.* Berlin, Springer-Verlag, 361–381. (NATO ASI Series I: Global Environmental Change 30.)

Delmas, R.J., J.M. Barnola and M. Legrand. 1982. Gas-derived aerosol in central Antarctic snow and ice: the case of sulphuric and nitric acids. *Ann. Glaciol.,* **3**, 71–76.

Delmas, R.J., P. Wagnon, K. Goto-Azuma, K. Kamiyama and O. Watanabe. 2003. Evidence for the loss of snow-deposited MSA to the interstitial gaseous phase in central Antarctic firn. *Tellus,* **55B**(1), 71 79.

Dixon, D., P.A. Mayewski, S. Kaspari, S. Sneed and M. Handley. 2004. A 200 year sub-annual record of sulfate in West Antarctica from 16 ice cores. *Ann. Glaciol.,* **39**, 545–556.

EPICA community. 2004. Eight glacial cycles from an Antarctic ice core. *Nature,* **429**(6992), 623–628.

Evans, W.J.F., C.T. McElroy and I.E. Galbally. 1985. The conversion of N_2O_5 to HNO_3 at high latitudes in winter. *Geophys. Res. Lett.,* **12**(12), 825–828.

Gayley, R.I. and M. Ram. 1985. Atmospheric dust in polar ice and the background aerosol. *J. Geophys. Res.,* **90**(D7), 12,921–12,925.

Gow, A.J. 1965. On the accumulation and seasonal stratification of snow at the South Pole. *J. Glaciol.,* **5**(40), 467–477.

Jones, A.E. *and 6 others.* 2001. Measurements of NO_x emissions from the Antarctic snowpack. *Geophys. Res. Lett.,* **28**(8), 1499–1502.

Kaspari, S., P.A. Mayewski, D.A. Dixon, S.B. Sneed and M.J. Handley. 2005. Sources and transport pathways of marine aerosol species into West Antarctica. *Ann. Glaciol.,* **41** (see paper in this volume).

Kreutz, K.J. and P.A. Mayewski. 1999. Spatial variability of Antarctic surface snow glaciochemistry: implications for paleoatmospheric circulation reconstructions. *Antarct. Sci.,* **11**(1), 105–118.

Kreutz, K.J., P.A. Mayewski, S.I. Whitlow and M.S. Twickler. 1998. Limited migration of soluble ionic species in a Siple Dome, Antarctica, ice core. *Ann. Glaciol.,* **27**, 371–377.

Kreutz, K.J. *and 11 others.* 1999. Seasonal variations of glaciochemical, isotopic and stratigraphic properties in Siple Dome (Antarctica) surface snow. *Ann. Glaciol.,* **29**, 38–44.

Kreutz, K.J., P.A. Mayewski, L.D. Meeker, M.S. Twickler and S.I. Whitlow. 2000. The effect of spatial and temporal accumulation rate variability in West Antarctica on soluble ion deposition. *Geophys. Res. Lett.,* **27**(16), 2517–2520.

Legrand, M. 1995. Sulphur-derived species in polar ice: a review. *In* Delmas, R.J., *ed. Ice core studies of global biogeochemical cycles.* Berlin, Springer-Verlag, 91–119. (NATO ASI Series I: Global Environmental Change 30.)

Legrand, M. and R.J. Delmas. 1986. Relative contributions of tropospheric and stratospheric sources to nitrate in Antarctic snow. *Tellus,* **38B**(3–4), 236–249.

Legrand, M.R. and S. Kirchner. 1990. Origins and variations of nitrate in south polar precipitation. *J. Geophys. Res.,* **95**(D4), 3493–3507.

Legrand, M. and P. Mayewski. 1997. Glaciochemistry of polar ice cores: a review. *Rev. Geophys.,* **35**(3), 219–243.

Liu, H., K.C. Jezek, B. Li and Z. Zhao. 2001. *RADARSAT Antarctic Mapping Project digital elevation model version 2.* Boulder, CO, National Snow and Ice Data Center.

Mayewski, P.A. and M. Legrand. 1990. Recent increase in nitrate concentration of Antarctic snow. *Nature,* **346**(6281), 258–260.

Mayewski, P.A. and F. White. 2002. *The ice chronicles.* Hanover, NH, University Press of New England.

Mayewski, P.A., W.B. Lyons, M.J. Spencer, M.S. Twickler, C.F. Buck and S. Whitlow. 1990. An ice core record of atmospheric response to anthropogenic sulphate and nitrate. *Nature,* **346**(6284), 554–556.

Mayewski, P.A., M.J. Spencer and W.B. Lyons. 1992. A review of glaciochemistry with particular emphasis on the recent record of sulfate and nitrate. *In* Moore, B. and S. David, *eds. Proceedings of the 1988 OIED Global Change Institute: Trace Gases and the Biosphere.* Boulder, CO, University Corporation for Atmospheric Research/Office of Interdisciplinary Earth Studies, 177–199.

Mayewski, P.A. *and 11 others.* 1995. An ice-core-based, Late Holocene history for the Transantarctic Mountains, Antarctica. *In* Elliot, D.H. and G.L. Blaisdell, *eds. Contributions to Antarctic research IV.* Washington, DC, American Geophysical Union, 33–45. (Antarctic Research Series 67.)

McKenzie, R.L. and P.V. Johnston. 1984. Springtime stratospheric NO_2 in Antarctica. *Geophys. Res. Lett.,* **11**(1), 73–75.

Meyerson, E.A., P.A. Mayewski, K.J. Kreutz, L.D. Meeker, S.I. Whitlow and M.S. Twickler. 2002. The polar expression of ENSO and sea-ice variability as recorded in a South Pole ice core. *Ann. Glaciol.,* **35**, 430–436.

Minikin, A. *and 7 others.* 1998. Sulfur-containing species (sulfate and methanesulfonate) in coastal Antarctic aerosol and precipitation. *J. Geophys. Res.,* **103**(D9), 10,975–10,990.

Mulvaney, R. and D.A. Peel. 1988. Anions and cations in ice cores from Dolleman Island and the Palmer Land plateau, Antarctic Peninsula. *Ann. Glaciol.,* **10**, 121–125.

Mulvaney, R. and E.W. Wolff. 1994. Spatial variability of the major chemistry of the Antarctic ice sheet. *Ann. Glaciol.,* **20**, 440–447.

Mulvaney, R., E.C. Pasteur, D.A. Peel, E.S. Saltzman and P.Y. Whung. 1992. The ratio of MSA to non-sea-salt sulphate in Antarctic Peninsula ice cores. *Tellus,* **44B**(4), 295–303.

Mulvaney, R., D. Wagenbach and E. Wolff. 1998. Postdepositional change in snowpack nitrate from observation of year-round near-surface snow in coastal Antarctica. *J. Geophys. Res.,* **103**(D9), 11,021–11,031.

Palmer, A.S., T.D. van Ommen, M.A.J. Curran and V. Morgan. 2001. Ice-core evidence for a small solar-source of atmospheric nitrate. *Geophys. Res. Lett.,* **28**(10), 1953–1956.

Parker, B.C. and E.J. Zeller. 1980. Nitrogenous chemical composition of Antarctic snow and ice. *Antarct. J. US,* **15**(5), 79–81.

Parker, B.C., E.J. Zeller and A.J. Gow. 1981. Nitrogenous chemical composition of Antarctic snow and ice. *Antarct. J. US,* **16**(5), 79–81.

Parker, B.C., G.A.M. Dreschhoff, C.M. Laird and E.J. Zeller. 1982. Nitrates in South Pole snow. *Antarct. J. US,* **17**(5), 88–89.

Proposito, M. *and 9 others.* 2002. Chemical and isotopic snow variability along the 1998 ITASE traverse from Terra Nova Bay to Dome C, East Antarctica. *Ann. Glaciol.,* **35**, 187–194.

Qin, D., E.J. Zeller and G.A.M. Dreschhoff. 1992. The distribution of nitrate content in the surface snow of the Antarctic ice sheet along the route of the 1990 International Trans-Antarctic Expedition. *J. Geophys. Res.,* **97**(A5), 6277–6284.

Röthlisberger, R., M.A. Hutterli, S. Sommer, E.W. Wolff and R. Mulvaney. 2000. Factors controlling nitrate in ice cores: evidence from the Dome C deep ice core. *J. Geophys. Res.,* **105**(D16), 20,565–20,572.

Röthlisberger, R. *and 10 others.* 2002. Nitrate in Greenland and Antarctic ice cores: a detailed description of post-depositional processes. *Ann. Glaciol.,* **35**, 209–216.

Saltzman, E.S. 1995. Ocean/atmosphere cycling of dimethylsulfide. *In* Delmas, R.J., *ed. Ice core studies of global biogeochemical cycles.* Berlin, etc., Springer-Verlag, 65–90. (NATO ASI Series I: Global Environmental Change 30.)

Saltzman, E.S., P.Y. Whung and P. Mayewski. 1997. Methanesulfonate in the Greenland Ice Sheet Project 2 ice core. *J. Geophys. Res.,* **102**(C12), 26,649–26,657.

Shaw, G.E. 1979. Consideration on the origin and optical properties of the Antarctic aerosol. *Rev. Geophys. Space Phys.,* **17**(8), 1983–1998.

Sigg, A. and A. Neftel. 1988. Seasonal variations in hydrogen peroxide in polar ice cores. *Ann. Glaciol.,* **10**, 157–162.

Solomon, S. and J.G. Keys. 1992. Seasonal variations in Antarctic NO_x chemistry. *J. Geophys. Res.,* **97**(D8), 7971–7978.

Stenberg, M. *and 7 others.* 1998. Spatial variability of snow chemistry in western Dronning Maud Land, Antarctica. *Ann. Glaciol.,* **27**, 378–384.

Stenberg, M., M. Hansson, P. Holmlund and L. Karlöf. 1999. Variability in snow layering and snow chemistry in the vicinity of two drill sites in western Dronning Maud Land, Antarctica. *Ann. Glaciol.,* **29**, 33–37.

Toon, O.B., P. Hamill, R.P. Turco and J.O. Pinto. 1986. Condensation of HNO_3 and HCl in the winter polar stratospheres. *Geophys. Res. Lett.,* **13**(12), 1284–1287.

Udisti, R., R. Traversi, S. Becagli and G. Piccardi. 1998. Spatial distribution and seasonal pattern of biogenic sulphur compounds in snow from northern Victoria Land, Antarctica. *Ann. Glaciol.,* **27**, 535–542.

Udisti, R., S. Becagli, E. Castellano, R. Traversi, S. Vermigli and G. Piccardi. 1999. Sea-spray and marine biogenic seasonal contribution to snow composition at Terra Nova Bay, Antarctica. *Ann. Glaciol.,* **29**, 77–83.

Udisti, R. *and 7 others.* 2004. Atmosphere–snow interaction by a comparison between aerosol and uppermost snow layers composition at Dome C (East Antarctica). *Ann. Glaciol.,* **39**, 53–65.

Wagenbach, D. 1996. Coastal Antarctica: atmospheric chemical composition and atmospheric transport. *In* Wolff, E.W. and R.C. Bales, *eds. Chemical exchange between the atmosphere and polar snow.* Berlin, etc., Springer-Verlag, 173–199. (NATO ASI Series I: Global Environmental Change 43.)

Wagenbach, D., M. Legrand, H. Fischer, F. Pichlermayer and E. Wolff. 1998a. Atmospheric near-surface nitrate at coastal Antarctic sites. *J. Geophys. Res.,* **103**(D9), 11,007–11,020.

Wagenbach, D. *and 7 others*. 1998b. Sea-salt aerosol in coastal Antarctic regions. *J. Geophys. Res.,* **103**(D9), 10,961–10,974.

Wagnon, P., R.J. Delmas and M. Legrand. 1999. Loss of volatile acid species from upper firn layers at Vostok, Antarctica. *J. Geophys. Res.,* **104**(D3), 3423–3431.

Warneck, P. 1988. *Chemistry of the natural atmosphere*. San Diego, CA, Academic Press.

Welch, K., P.A. Mayewski and S.I. Whitlow. 1993. Methanesulfonic acid in coastal Antarctic snow related to sea-ice extent. *Geophys. Res. Lett.,* **20**(6), 443–446.

Weller, R., F. Traufetter, H. Fischer, H. Oerter, C. Peel and H. Miller. 2004. Post-depositional losses of methane sulfonate nitrate and chlorine at the EPICA deep-drilling site in Dronning Maud Land, Antarctica. *J. Geophys. Res.,* **109**(D7), D07301. (10.1029/2003JD004189.)

Wolff, E.W. 1995. Nitrate in polar ice. *In* Delmas, R.J., *ed. Ice core studies of global biogeochemical cycles*. Berlin, etc., Springer-Verlag, 195–224. (NATO ASI Series I: Global Environmental Change 30.)

Wolff, E.W. and R. Mulvaney. 1991. Reactions on sulphuric acid aerosol and on polar stratospheric clouds in the Antarctic stratosphere. *Geophys. Res. Lett.,* **18**, 1007–1010.

Wolff, E.W., M.R. Legrand and D. Wagenbach. 1998a. Coastal Antarctic aerosol and snowfall chemistry. *J. Geophys. Res.,* **103**(D9), 10,927–10,934.

Wolff, E.W., D. Wagenbach, E.C. Pasteur, R. Mulvaney, M. Legrand and J.S. Hall. 1998b. Relationship between chemistry of air, fresh snow and firn cores for aerosol species in coastal Antarctica. *J. Geophys. Res.,* **103**(D9), 11,057–11,070.

Wolff, E.W., J.S. Hall, R. Mulvaney, E.C. Pasteur, D. Wagenbach and M. Legrand. 2002. Modelling photochemical NO_x production and nitrate loss in the upper snowpack of Antarctica. *Geophys. Res. Lett.,* **29**(20), 1944. (10.1029/2002GL015823.)

Xiao, C., P.A. Mayewski, D. Qin, Z. Li, M. Zhang and Y. Yan. 2004. Sea level pressure variability over the southern Indian Ocean inferred from a glaciochemical record in Princess Elizabeth Land, east Antarctica. *J. Geophys. Res.,* **109**(D16), D16101. (10.1029/2003JD004065.)

Yang, Q., P.A. Mayewski, E. Linder, S. Whitlow and M. Twickler. 1996a. Chemical species spatial distribution and relationship to elevation and snow accumulation rate over the Greenland ice sheet. *J. Geophys. Res.,* **101**(D13), 18,629–18,637.

Yang, Q., P.A. Mayewski, G.A. Zielinski, M. Twickler and K.C. Taylor. 1996b. Depletion of atmospheric nitrate and chloride as a consequence of the Toba volcanic eruption. *Geophys. Res. Lett.,* **23**(18), 2513–2516.

Zielinski, G.A. *and 7 others*. 1997. Volcanic aerosol records and tephrochronology of the Summit, Greenland, ice cores. *J. Geophys. Res.,* **102**(C12), 26,625–26,640.

GROUND-BASED MEASUREMENTS OF SPATIAL AND TEMPORAL VARIABILITY OF SNOW ACCUMULATION IN EAST ANTARCTICA

Olaf Eisen,[1,2] Massimo Frezzotti,[3] Christophe Genthon,[4] Elisabeth Isaksson,[5] Olivier Magand,[4] Michiel R. van den Broeke,[6] Daniel A. Dixon,[7] Alexey Ekaykin,[8] Per Holmlund,[9] Takao Kameda,[10] Lars Karlöf,[11] Susan Kaspari,[7] Vladimir Y. Lipenkov,[8] Hans Oerter,[2] Shuhei Takahashi,[10] and David G. Vaughan[12]

Received 31 October 2006; revised 2 July 2007; accepted 25 September 2007; published 11 April 2008.

[1] The East Antarctic Ice Sheet is the largest, highest, coldest, driest, and windiest ice sheet on Earth. Understanding of the surface mass balance (SMB) of Antarctica is necessary to determine the present state of the ice sheet, to make predictions of its potential contribution to sea level rise, and to determine its past history for paleoclimatic reconstructions. However, SMB values are poorly known because of logistic constraints in extreme polar environments, and they represent one of the biggest challenges of Antarctic science. Snow accumulation is the most important parameter for the SMB of ice sheets. SMB varies on a number of scales, from small-scale features (sastrugi) to ice-sheet-scale SMB patterns determined mainly by temperature, elevation, distance from the coast, and wind-driven processes. In situ measurements of SMB are performed at single points by stakes, ultrasonic sounders, snow pits, and firn and ice cores and laterally by continuous measurements using ground-penetrating radar. SMB for large regions can only be achieved practically by using remote sensing and/or numerical climate modeling. However, these techniques rely on ground truthing to improve the resolution and accuracy. The separation of spatial and temporal variations of SMB in transient regimes is necessary for accurate interpretation of ice core records. In this review we provide an overview of the various measurement techniques, related difficulties, and limitations of data interpretation; describe spatial characteristics of East Antarctic SMB and issues related to the spatial and temporal representativity of measurements; and provide recommendations on how to perform in situ measurements.

Citation: Eisen, O., et al. (2008), Ground-based measurements of spatial and temporal variability of snow accumulation in East Antarctica, *Rev. Geophys.*, *46*, RG2001, doi:10.1029/2006RG000218.

1. INTRODUCTION

[2] The development of the Earth's climate is strongly linked to the state of the polar regions. In particular, the large ice sheets influence components of the climate system, including the global water cycle by locking up or releasing large amounts of fresh water; the radiation budget through the high albedo of ice- and snow-covered surfaces; and the thermohaline circulation through the amount of fresh water released to the ocean by melting or iceberg calving. Since the termination of the last glacial period, the only remaining large ice sheets are located in Antarctica and Greenland.

[3] The polar ice sheets are not only active participants in the global climate system (including being a major control on global sea level), but they also provide the only archive which gives direct access to the paleoatmosphere. *Ice cores* collected from polar regions and analyzed for atmospheric gases, stable isotopes, major ions, trace elements, etc.,

[1]Laboratory of Hydraulics, Hydrology and Glaciology, ETH Zurich, Zurich, Switzerland.
[2]Alfred Wegener Institute for Polar and Marine Research, Bremerhaven, Germany.
[3]Laboratory for Climate Observation, Italian National Agency for New Technologies, Energy and the Environment, Rome, Italy.
[4]Laboratoire de Glaciologie et Géophysique de l'Environnement, CNRS, University Joseph-Fourier, Grenoble, France.
[5]Norwegian Polar Institute, Tromsø, Norway.
[6]Institute for Marine and Atmospheric Research, Utrecht University, Utrecht, Netherlands.
[7]Climate Change Institute, University of Maine, Orono, Maine, USA.
[8]Arctic and Antarctic Research Institute, St. Petersburg, Russia.
[9]Department of Physical Geography and Quaternary Geology, Stockholm University, Stockholm, Sweden.
[10]Kitami Institute of Technology, Kitami, Japan.
[11]SWIX Sport AS, Lillehammer, Norway.
[12]British Antarctic Survey, Cambridge, UK.

8755-1209/08/2006RG000218$15.00
Paper number 2006RG000218

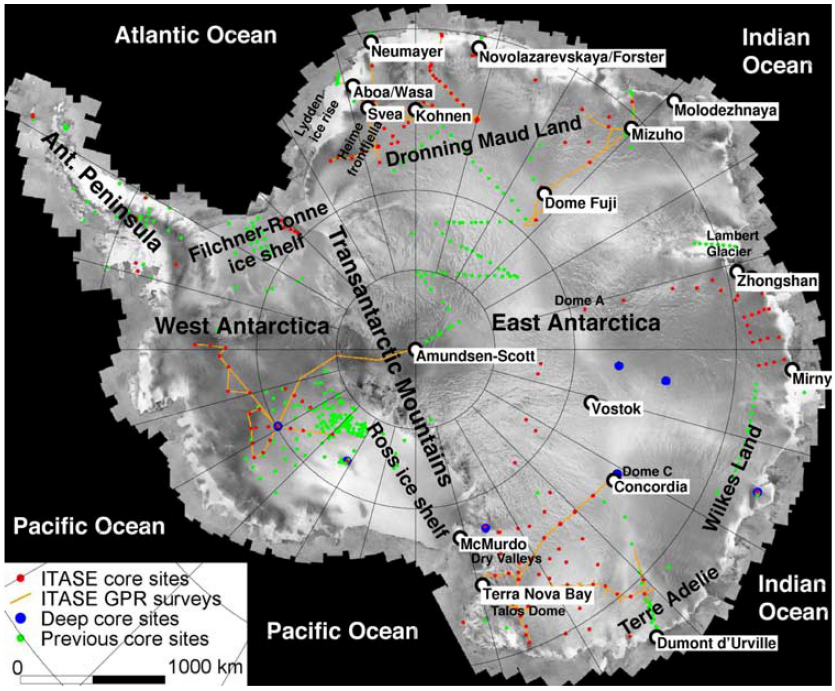

Figure 1. Map of Antarctica with some topographic names, drilling sites, radar profiles, and stations mentioned in the text (underlain by white rectangles), adapted from *Mayewski et al.* [2005] with permission of the International Glaciology Society. Radarsat mosaic in the background. ("Terra Nova Bay" station was renamed to "Mario Zucchelli station" in 2004.)

enable past climate conditions to be reconstructed [e.g., *Mayewski et al.*, 1993; *Dansgaard et al.*, 1993]. (Italicized terms are defined in the glossary, after the main text.) These records, currently spanning as far back in time as the past 800 ka [*Jouzel et al.*, 2007], are an important key to identification of the causes and forcing mechanisms of climate change.

[4] Understanding past conditions of the ice sheets and determining their present state are essential to predict their behavior under future climate conditions. The most important physical variable in assessing past and current ice sheet conditions is the *surface mass balance*. The current state-of-the-art ground-based techniques used to determine surface mass balance and its spatial and temporal characteristics in East Antarctica are the topic of this paper. Surface mass balance has been termed differently by many authors. Most completely, it is described as *mean net annual surface mass balance* and includes all terms that contribute to the solid, liquid, and gaseous transfer of water across the surface of the ice sheet. Hereafter, we will abbreviate this to "surface mass balance" (SMB) while maintaining the averaging implied by the full description. We also note that this term is the aggregate of many processes, such as precipitation from clouds and clear skies, the formation of hoarfrost at the surface and within the snowpack, sublimation, melting and runoff, wind scouring, and drift deposition.

1.1. Principal Processes

[5] Antarctica consists of West and East Antarctica, divided by the Transantarctic Mountains (Figure 1), and the Antarctic Peninsula. Whereas floating ice shelves form a considerable part of West Antarctica, the largest ones being the Filchner-Ronne and Ross ice shelves, East Antarctica is mainly formed by the inland ice sheet plateau, roughly comprising two thirds of the continent. Our main aim is to present the characteristics of SMB of the East Antarctic plateau area, which despite its apparent homogeneity shows large spatial variability. Nevertheless, we include findings based on data from West Antarctica and near-coastal sites as well for a larger context.

[6] On the *Antarctic ice sheet*, few places display a constantly negative SMB (e.g., *blue ice areas*) [e.g., *Bintanja*, 1999; *van den Broeke et al.*, 2006b]. Unlike in Greenland and the Antarctic Peninsula [*Vaughan*, 2006] where melting is an important process, wind erosion and sublimation are the key factors for negative SMB of the West and East Antarctica ice sheets. On the interior plateau of the Antarctic ice sheet, large areas have a mass balance close to zero, and negative mass balance has been reported for some areas [*Frezzotti et al.*, 2002b]. Nevertheless, annual SMB is generally positive in the long term. We will therefore use the term *accumulation* or accumulation rate synonymously to refer to a positive SMB.

[7] Solid atmospheric precipitation (snowfall or diamond dust) is deposited at the surface of the East Antarctic Ice Sheet. Atmospheric precipitation is homogeneous over tens to hundreds of kilometers. Wind erosion, wind redistribution, sublimation, and other processes during or after the precipitation event lead to a deposition at the surface which is spatially less homogeneous than the original precipitation. Variations in accumulation over tens of kilometers have been observed since the 1960s [*Black and Budd*, 1964; *Pettré et al.*, 1986]. These accumulation variations and surface processes result in surface features including sastrugi, longitudinal dunes [*Goodwin*, 1990], dunes on the 100-m scale [*Ekaykin*, 2003; *Karlöf et al.*, 2005b], and, most impressively, megadunes on a kilometer scale [*Fahnestock et al.*, 2000; *Frezzotti et al.*, 2002a]. Once the snow is permanently deposited, further accumulation is responsible for the submergence of surface layers. In the firn column, the snow densifies under the overburden weight, and the interplay with ice dynamics like advection begins to deform the surface layer.

[8] The spatial and temporal distribution of SMB is a primary concern for numerous issues: for determining the current state of the ice sheet and estimating mass balance changes over regional, basin-wide, and continental scales and the associated contribution to sea level change [e.g., *Joughin et al.*, 2005, and references therein]; for ice flow modeling of the age-depth relationship and subsequent application to ice cores; for calibration of remote sensing measurements of SMB; for understanding of the SMB–surface meteorology–climate relationship; and for improving, verifying, and validating various types of models, in particular, the climate models from which predictions (future) or reconstructions (paleoclimate) of accumulation are tentatively obtained. Unfortunately, there exists a discrepancy between assumptions and needs of these applications in terms of spatiotemporal coverage and resolution of SMB and the actual data characteristics available. For instance, dating of ice cores by flow modeling usually assumes rather smooth accumulation patterns, mainly formed by larger features, accumulation time series, and ice dynamical history. Surface accumulation, on the other hand, is not smooth in time and space. Because of interaction with surface features, such as varying surface slopes, significant surface accumulation variations occur on much smaller spatial scales than precipitation, as will be demonstrated here. Analysis of *firn cores* and meteorological observations integrated with validated model reanalysis data of European Centre for Medium Range Weather Forecasts 40-Year Reanalysis (ERA 40) pointed out high variability of snow accumulation at yearly and decadal scales over the past 50 years but without a statistically significant trend [*Monaghan et al.*, 2006].

1.2. General Difficulties

[9] While measurement of precipitation has been a routine part of worldwide observations for more than a hundred years, there is still no practical technique that can be used to measure SMB in East Antarctica in realtime as part of a meteorological measurement program. This is largely due to the technical difficulties involved in making measurements without disturbing natural patterns of snow drift and measuring changes at depth in the snowpack. Thus, knowledge of SMB seasonality, trends, and spatial variability is limited. For this reason, we rely heavily on after-the-fact measurements obtained from ice cores, snow accumulation stakes, etc. Acquiring information about surface accumulation on the ice sheets with adequate sampling intervals is thus labor intensive. Only along a few selected profiles (ITASE, EPICA, JARE, RAE) (ITASE, International Transantarctic Scientific Expedition; EPICA, European Project for Ice Coring in Antarctica; JARE, Japanese Antarctic Research Expedition; RAE, Russian Antarctic Expedition) and in certain areas has area-wide information on accumulation been obtained (Figure 1).

[10] SMB observations cannot be easily extrapolated in time and space because spatial variations in SMB amount to considerable percentages of the absolute values, and often exceed these; the magnitude of the temporal variations is small compared to spatial variability, depending on the considered timescale; and the structure of the SMB covariance is unknown. To overcome these limitations, two other important techniques are therefore used to achieve area-wide information: satellite remote sensing and numerical climate modeling.

1.3. Remote Sensing and Numerical Modeling

[11] Currently, there is no definitive way to determine SMB from remote sensing data. There are signals in some remote sensing fields that are related to SMB as has been discussed widely by *Zwally and Giovinetto* [1995], *Winebrenner et al.* [2001], *Bindschadler et al.* [2005], *Rotschky et al.* [2006], and *Arthern et al.* [2006], but these are not solely dependent on accumulation rate and are thus to some extent "contaminated" by other factors. For this reason, most authors have attempted to use remote sensing fields to guide interpolation of field measurements. The most recent attempt at this by *Arthern et al.* [2006], who used a formal scheme to incorporate estimates of uncertainty and models of covariance, probably provides the most defensible estimate of the remotely sensed broadscale pattern of SMB across East Antarctica (Figure 2a). The typical footprint of these compilations is 20 km horizontally.

[12] In contrast to measuring area-wide precipitation in situ, as attempted by *Bindschadler et al.* [2005], numerical models are used to simulate atmospheric processes and related accumulation features [e.g., *Gallée et al.*, 2005]. The first step for successful modeling is detailed understanding of the physical processes involved. The second step involves model validation. Because of computing resource limitations, there is currently no way to explicitly resolve processes that induce spatial variability of SMB at kilometer scales or less (e.g., sastrugi and dunes) with an atmospheric model run in climate mode, that is, over several years. Such features have to be at best statistically parameterized, or considered as noise, when comparing field data with model results [*Genthon et al.*, 2005]. Although most

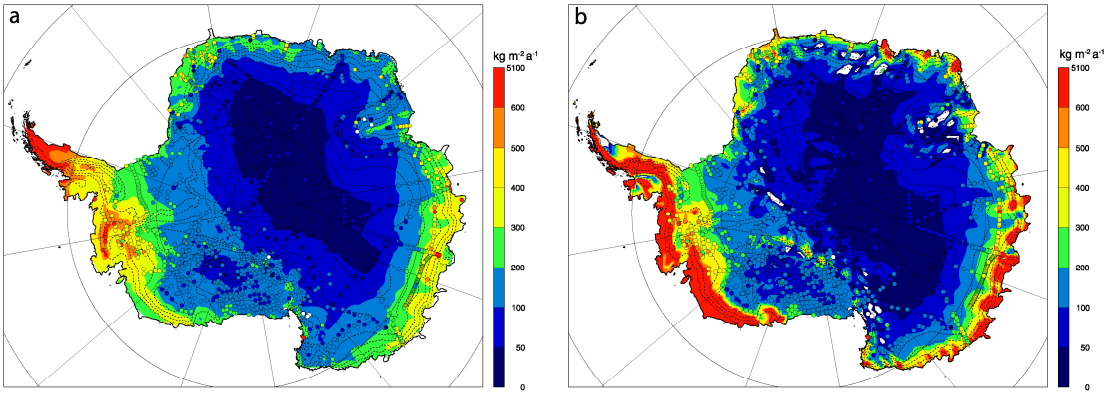

Figure 2. Examples for interpolated distributions of SMB (in kg m^{-2} a^{-1}) based on point observations (circles) in Antarctica. (a) Interpolation of SMB observations guided by passive microwave remote sensing (adapted from *Arthern et al.* [2006]); (b) numerical climate modeling of SMB (solid precipitation minus sublimation and melt) [*van den Broeke et al.*, 2006a] with ground-based SMB data collection indicated by circles [*van de Berg et al.*, 2006].

global models have spatial resolutions of 100 km and greater [*Genthon and Krinner*, 2001], grid stretching in global models [*Krinner et al.*, 2007] and regional climate modeling [*van Lipzig et al.*, 2004a; *van de Berg et al.*, 2006] allow resolutions on the order of 50–60 km that can better capture the mesoscale impacts of topography on SMB distribution such as diabatic cooling of air mass along slopes, air channeling, or barrier effects. Most of the boundary conditions needed to run global (including stretchable grid) and regional atmospheric models, such as topography, sea surface temperature and sea ice, and radiatively active gases and aerosols, are the same. On the other hand, regional models also need lateral boundary conditions such as temperature, winds, and moisture. This is generally provided by meteorological analyses for recent and present-day climate simulations, but data from global climate models are necessary to run realistic climate change experiments. In this respect, stretchable grid global models are self-consistent. As an example, Figure 2b shows mass balance from RACMO2/ANT for the period 1980–2004 [*van den Broeke et al.*, 2006a], with a horizontal resolution of 55 km, as well as a selection of observed mass balance values (updated from *Vaughan et al.* [1999b]). The model is clearly capable of reproducing the large-scale features of the Antarctic SMB (direct correlation with 1900 SMB observations yields $R = 0.82$) but cannot resolve the finer-scale features [*van de Berg et al.*, 2006] that are known to exist and that are one focus of the present paper. Double or triple nesting of models up to 3-km resolution is successfully used to improve weather forecasts in topographically complex regions, and could also be used to improve the model footprint of accumulation variability, once the governing processes (wind-driven snow redistribution) are properly parameterized [*Bromwich et al.*, 2003].

[13] One major use of SMB observations is to verify and validate climate models that are used to better understand the climate and SMB of Antarctica and to predict its future evolution. Therefore, using climate model results for driving interpolations and building maps of the Antarctic SMB from the field observations [*van de Berg et al.*, 2006] requires more care to avoid circular reasoning than for satellite data [*Vaughan et al.*, 1999b; *Arthern et al.*, 2006], as these are more independent from ground observations. However, the models do provide the means for hindcasting accumulation and may be used to identify areas where additional data or verification of existing data are most needed, such as areas where several models disagree with field reports or with interpolations [*Genthon and Krinner*, 2001; *van den Broeke et al.*, 2006a]. This approach has been used to select the sites of some of the recent Italian-French ITASE surveys, and the new data have confirmed problems with the previous estimates [*Magand et al.*, 2007].

[14] Despite significant advances in either discipline (remote sensing or numerical modeling), both techniques fail in detecting or explaining small-scale (<50 km) variability in SMB observations. The processes playing part in the ice sheet–climate–weather interaction act on a broad range of spatial and temporal scales. As mentioned in section 1.1, precipitation is homogeneous on scales of roughly 10^4 km^2, mainly on the plateau, and is subject to redistribution in the atmospheric boundary layer on scales of centimeters to kilometers. The scale of temporal variability increases from a scale related to the movement, dynamic, and lifetime of frontal systems on the order of days to seasonal variations and interannual variability. Partly related to larger-scale oscillatory atmospheric and oceanographic patterns are variations on interannual to decadal scales. Variations that occur over centuries and millennia are of relevance for climate conditions. The longest variations are on the timescale of glacial cycles with a period of 10^4–10^5 years (Table 1). The different techniques employed to observe these changes operate in a rather limited spatiotemporal window and with limited spatiotemporal resolution (Figure 3). Satellite sensors have

TABLE 1. Relevance and Scales of Surface Mass Balance Measurements

Target	Temporal Scales	Spatial Scales
Mass balance changes	1 to 10^5 years	basin to ice sheet
Climate-SMB relationship	hours to 100 years	centimeter to 100–1000 km
Climate models[a]	hours to 100 years 10^4–10^5 years in snapshots	10–100 km to ice sheet
Remote sensing[b]	hours to 30 years	submeter to ice sheet
Ice flow modeling[c]	10 to 10^5 years	100 m to ice sheet

[a]For (in)validation of models, the model output is compared with actual measurements. This permits judging the usability of models.
[b]Some remote sensing applications (altimetry, gravity, passive microwave, scatterometers, etc.) profit or even require data calibration for retrieval algorithms at specific test sites for correct interpretation and further extensions of the measurements to other areas. Validations are likewise important.
[c]Input of SMB to ice flow models is especially important for interpreting deep ice cores.

a comparably large range of footprint sizes and spatial coverage but are usually limited in temporal resolution and length of time series. Numerical models, in contrast, can cover temporal scales from hours to millennia, but their spatial coverage and resolution depend on each other in a reciprocal manner, thus yielding either low resolution at large spatial coverage or vice versa.

1.4. Outline

[15] With this background on surface accumulation in mind, the purpose of this review paper is to provide the glaciological community and those outside with a reference to measurement techniques of SMB and characteristics thereof in East Antarctica. We present the different types of measurements in section 2, including point measurements at the surface (*stakes* and *ultrasonic sounders*), point measurements at depth (*snow pits*, firn cores, and ice cores), and continuous lateral measurements (*ground-penetrating radar*). Sections 2.1–2.5 each contain a description of the mode of operation and type of analysis for the individual measurements, the basic measurement procedure for each technique and all required input quantities to derive the accumulation estimate, and an account of error estimates for each data type. We also present selected sample data to illustrate typical results obtained from these measurements and how the SMB data can form the input to other studies. Section 3 summarizes findings derived from the different measurement techniques, addresses their pros and cons, and judges the spatial and temporal representativity and limitation of SMB data. In section 4 we discuss the application of measurement data. We provide recommendations and principles for proper usage without stressing the data beyond physically justified limits to avoid misinterpretations. Additionally, we emphasize that observers in the field should be aware of end-users' needs.

2. MEASUREMENT TECHNIQUES

[16] Common for all measurements of SMB at the surface is the observation of deposited mass over a certain time period, or proxies thereof. The different methods not only cover a wide spectrum of technical modes of operation, they also yield information about mass balance for varying spatial and temporal scales and resolutions, as schematically illustrated in Figures 3, 4, and 5. SMB measurements derived from stakes, ultrasonic sounders, snow pits, and firn or ice cores provide information from a single point at the surface (Figure 4). In contrast, ground-penetrating radar (GPR) is carried out along profiles in such high resolution that it can be considered a quasi-continuous measurement. Whereas stakes and ultrasonic sounders have to be operated for a longer period to obtain a time series, snow pits, firn/ice cores, and GPR are able to provide a time series from a single deployment. One could thus classify the measurements into instantaneous and retrospective methods, with unclear boundaries. Owing to the different variables measured, the methods provide accumulation rates on very different timescales and resolution, as schematically illustrated in Figure 5. The detailed differences will be set forth in this section. Before introducing the individual methods, we first discuss the important role of snow density and how it is measured.

2.1. Prerequisite: Determination of Snow Density

[17] All techniques aimed at the determination of SMB perform some sort of difference-length measurement (height

Figure 3. Schemes to illustrate the (a) resolutions and (b) coverage of the different types of measurements in time (x axis) and space (y axis) used to derive surface mass balance. In Figure 3a, the rectangles indicate the typical resolutions of the various techniques. In addition to the characteristics of an individual measurement (e.g., a snow pit or a GPR profile), the combination of these with groups and larger entities are also displayed (e.g., stake lines or GPR grids). In this sense, "single snow pit" indicates the resolution within an individual pit, whereas "(snow pits at different sites)" refers to the distance between different snow pits. Likewise for ultrasonic sounders at different sites and GPR distance between different profiles. In Figure 3b, the rectangles indicate typical temporal and spatial coverage of measurements. For instance, stake lines may be hundreds of meters to more than 1000 km long. The time series derived from such a line could be just a year or up to several decades. In contrast, a single stake covers only an area of a few square centimeters. For implementing measurement programs, the question arises as to what can be achieved by a three- to four-person team in a single season. As logistics often impose the largest constraints in Antarctica, the resolution and coverage provided here could serve as a guideline to which combination of methods seems most effective.

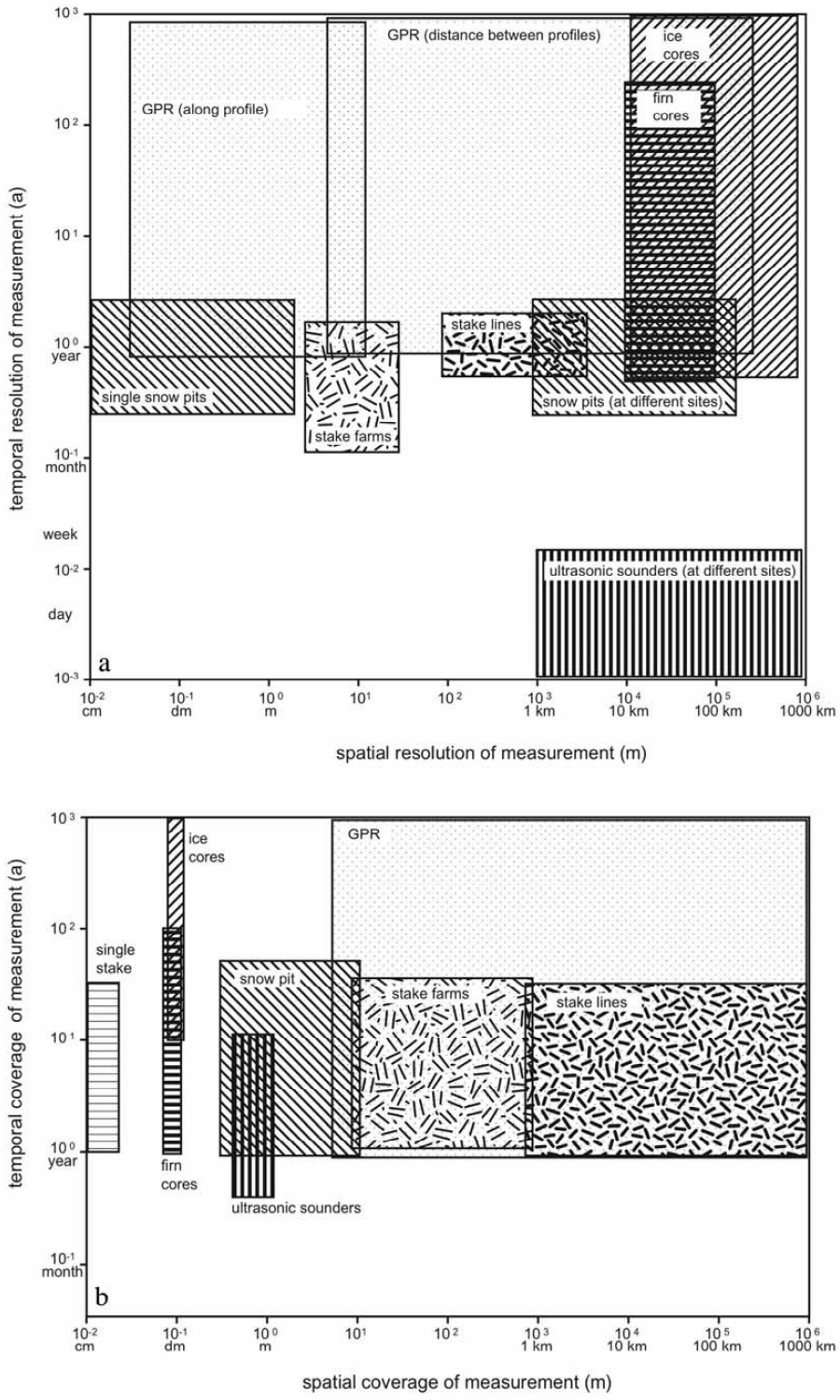
GPR (distance between profiles)
ice cores
firn cores
GPR (along profile)
stake lines
single snow pits
snow pits (at different sites)
stake farms
ultrasonic sounders (at different sites)
temporal resolution of measurement (a)
year
month
week
day
a
spatial resolution of measurement (m)
cm
dm
m
1 km
10 km
100 km
1000 km
GPR
ice cores
single stake
snow pit
stake farms
stake lines
firn cores
ultrasonic sounders
temporal coverage of measurement (a)
b
spatial coverage of measurement (m)

Figure 3

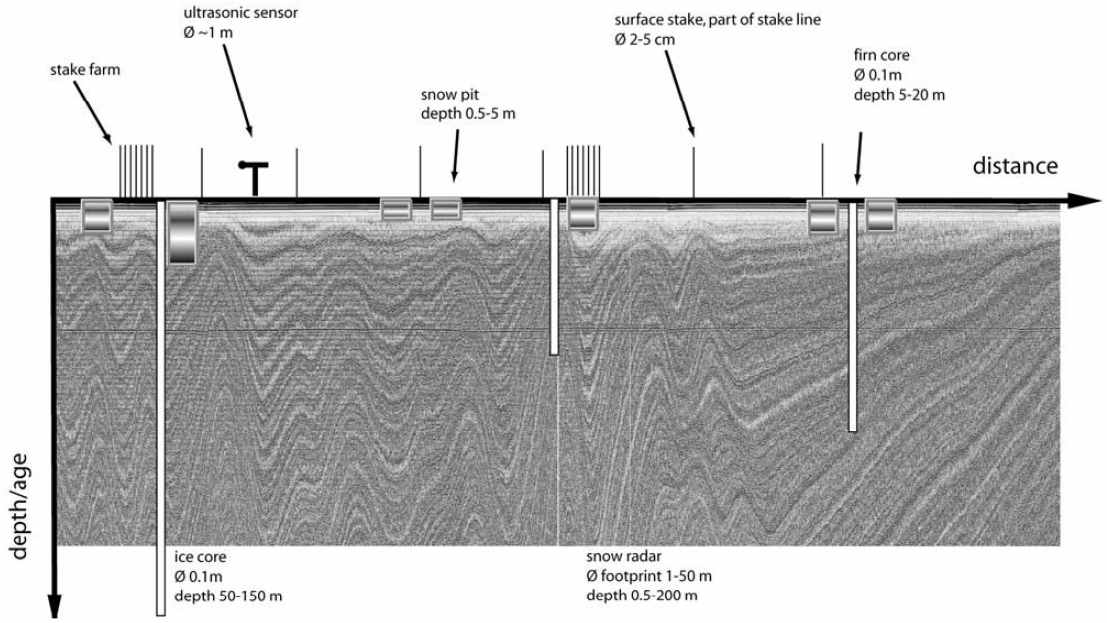

Figure 4. Scheme to illustrate spatial sampling interval and sample depths of different methods: stakes and ultrasonic sounders, at surface; snow pits, up to a few meters depth; firn cores, few tens of meters; ice cores, up to several tens to hundreds of meters, reaching below the firn-ice transition; GPR, tens to hundreds of meters. GPR data acquired along a 50-km profile [*Anschütz et al.*, 2007] are shown as background to illustrate the lateral variation. Continuous reflections present layers of equal age (isochrones). The canceled circle indicates the horizontal distance over which SMB is determined. (Note that ice core deep drilling is possible to some kilometers depths, but we are not concerned with that technique here.)

change, layer thickness, etc.) over certain time periods. To convert this length measurement to a SMB value, knowledge of the density distribution of the observed sample is fundamental. Determination of the snow density is usually more difficult and less accurate compared to the length measurements for a number of reasons. One of few exceptions for direct snow density measurements is the only recent adaptation of a neutron-scattering probe [*Morris and Cooper*, 2003; *Hawley et al.*, 2006].

[18] The classic method calculates density from snow sample volume and mass; however, accurately determining snow sample volume is a hard task under field conditions. The easiest method is to use a sampling probe with known volume. It is possible that each national Antarctic expedition uses different types of snow-sampling devices, which introduces additional uncertainties in the final values. A suitable field method for density measurements in snow pits is proposed in the ITASE guidelines by *Mayewski and Goodwin* [1997]. Because of the strong densification within the uppermost layers, density should be sampled at high vertical resolution. To avoid the risk of disturbing the underlying snow during sampling, the snow can be collected in a crossover pattern (see Figure 9c in section 2.4). Moreover, sampling snow pits from the bottom upward to the surface avoids the risk of contaminating the lower levels by snow falling down from previous sampling above. Depth control and minimizing depth error is most easily obtained by constantly leveling the sample depth with two adjacent rulers. Depending on the equipment used, the sample volume error is around several percent, and the error in the mass determination depends on the balance used. An optimistic volume error of ~1% and an accuracy of the balance of ±1 g would yield an uncertainty of about 1.4% for the density sampled in a snow pit [*Karlöf et al.*, 2005b]. The balance error increases to about ±5 g if spring scales are used.

[19] Density measurements are mainly made during the austral summer season (December or January), which may introduce additional errors because of seasonal changes in snow density that can result from numerous processes. For instance, surface density differs between snowfall events and precipitation-free periods, as wind can cause erosion, hardening, and redistribution of the snow. General factors causing seasonal density variations are changing wind speed and temperature, larger or smaller portions of low-density fresh snow, and vapor transfer between the surface, atmosphere, and deeper snow layers. It is not obvious which seasonal (or annual) density value best characterizes the "effective" annual density. These effects are different for snow density in the first meter in high-accumulation coastal areas (density on the order of 400 kg m^{-3}) compared to low-accumulation inland areas (around 300 kg m^{-3}). Sea-

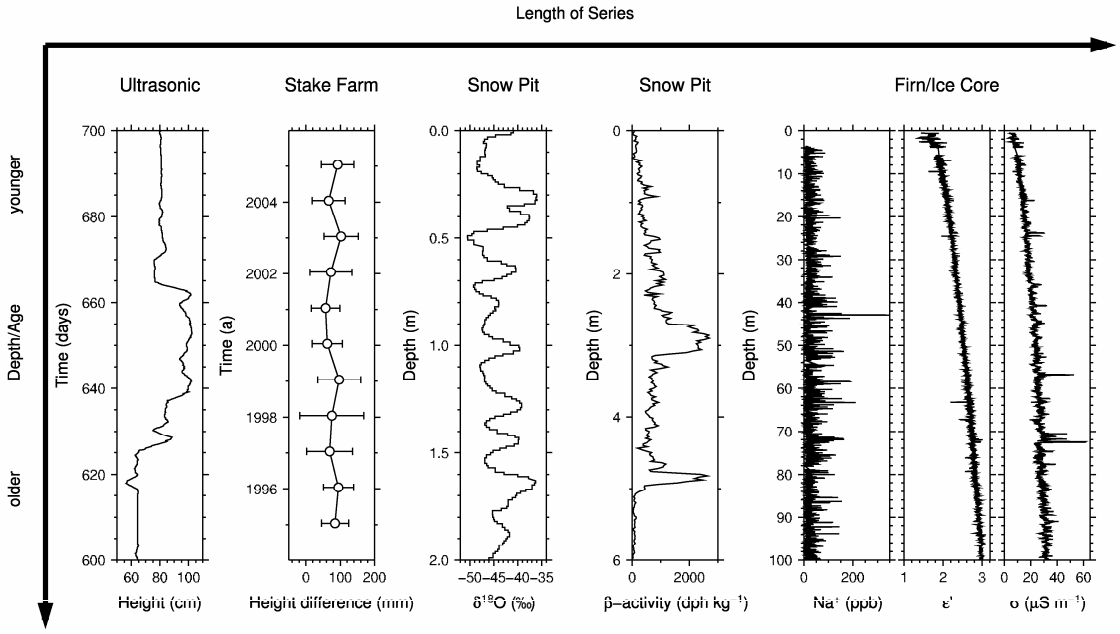

Figure 5. Data series obtained from various measurement techniques for single locations. The vertical axis indicates depth (for measurements made at depth) and time (for measurements made at the surface: ultrasonic sounders and stakes), respectively, increasing downward. The covered time/depth span differs between graphs. The temporal scale of the time/depth series lengths tentatively increases to the right. From left to right, 100 days of an ultrasonic sounder time series from the automatic weather station AWS9 (height above surface) [*van den Broeke et al.*, 2004b] at site DML05, near the EPICA deep drilling at Kohnen station in Dronning Maud Land (DML), illustrating the accumulation of snow and subsequent partly erosion; 11-year time series of measured height differences to previous year from a stake farm at Dome Fuji [*Kameda et al.*, 2008]. The circle indicates the average of 36 stakes, and the bar indicates the spatial standard deviation of the measurements; the oxygen stable isotope record is from a 2-m-deep snow pit (DML25 [*Oerter*, 2005, available at http://doi.pangaea.de/10.1594/PANGAEA.264585; *Oerter et al.*, 2004]), spanning roughly 10 years. Annual cycles are clearly visible; β activity record is from a 6-m-deep snow pit at the South Pole from 1978 [*Pourchet et al.*, 1983] spanning several decades; example of chemistry measurements (Na^+ content) [*Sommer et al.*, 2000b] and dielectric profiling record (relative permittivity ε' and conductivity σ) is from core B32 at site DML05 [*Wilhelms*, 2000] near the EPICA deep drilling in DML. The shown depth section corresponds to an 1100-year period from A.D. 883 to 1997.

sonally varying density is especially a problem for SMB measurements performed at the surface (introduced in sections 2.2 (stakes) and 2.3 (ultrasonic sounders)), in which case, density variations should be tracked in the snow layer accumulated during the given period of time (month or year). Unfortunately, almost no data are available that describe the seasonal change of the near-surface snow density and thus the actual density for the measured height difference, e.g., in the case of ultrasonic sounders. Although density values can be taken from adjacent snow pit studies, the question then arises as to which depth of the surface snow best approximates the average density. For instance, Vostok mean annual snow accumulation is only 7 cm on average (varying from negative values to more than 20 cm on individual stakes). A study of density in 17 snow pits showed that snow density does not change much with depth in the uppermost 20 cm of the snow. Consequently, the mean density from this layer is used for converting snow accumulation to SMB at Vostok. Nevertheless, at Vostok the mean density of the uppermost 20 cm changes between 310 kg m^{-3} in winter and 330 kg m^{-3} in summer, which means that the uncertainty related to this source of errors may be as much as 6%.

2.2. Point Measurements at the Surface: Stakes

[20] The easiest way to measure SMB is based on stakes planted in the snow by simply measuring the amount of accumulation over a certain time period. Despite its simplicity, this method is valuable as it allows a rough estimate of the local or regional distribution of SMB. Sources of error include the conversion of the accumulated snow to SMB, density measurements (see section 1.1), and the subsidence of the stake bottom. This simple technique is

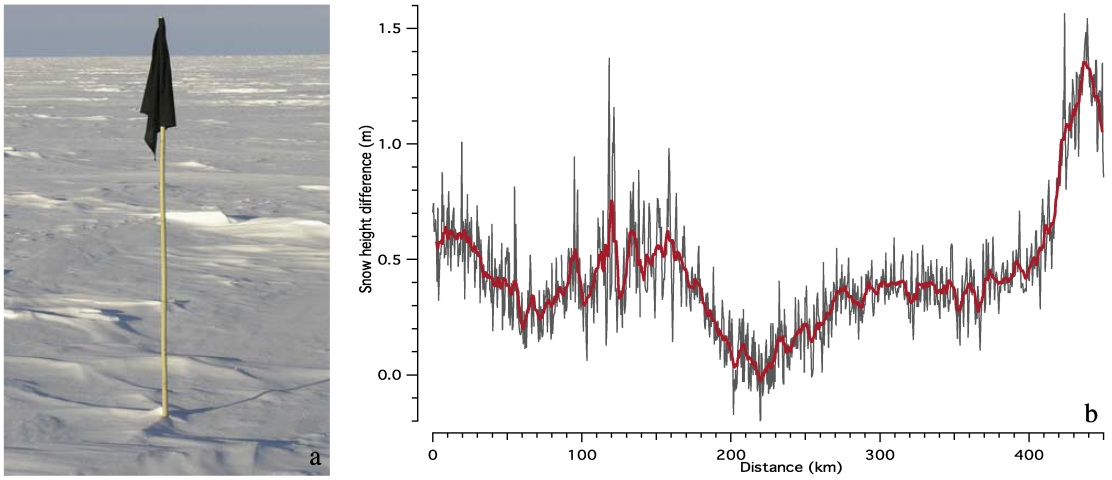

Figure 6. (a) Typical bamboo stake with a fabric flag at the top. Note the microrelief surrounding the stake base, which complicates height readings. (b) One year (2003) of sample data from the 450-km stake line from Neumayer station to Kottasberge, Heimefrontfjella, in DML; grey, single measurements every 500 m; bold, moving average over 5 km.

used by almost every nation in Antarctica. Examples are given in section 2.2.4.

[21] In addition to single stakes, *stake lines* and *stake farms* have also been used. Stake farms are more common at year-round stations, whereas stake lines may be established along traverse routes which are visited in more than one season. A stake farm gives single measurements for a well-defined small area, e.g., on the order of 10^4–10^6 m^2 (tens of meters to kilometer side length) which are averaged to produce a single accumulation value. By using several stakes the small-scale depositional noise can be reduced. Additionally, continuous monitoring of stake farms provides a record of the buildup of the snow cover during the year and information on seasonal variations [see, e.g., *Fujii*, 1981; *Mosley-Thompson et al.*, 1999; *Schlosser et al.*, 2002], an important fact further explained in section 2.2.4. Measurements in stake farms are influenced by a slight disturbance of the natural snow deposition through the stakes themselves, the disturbance of the snow surface when people have to pass through the stake farm for measuring the stakes, and the accuracy of the height measurements itself. Stake readings are usually done on the leeward side of the prevailing wind direction to minimize the effect of footprints on the snow surface.

[22] Single stakes of a stake line are usually used primarily as markers for way points. They provide one value for each stake but over a larger distance (Figure 6). These measurements are helpful in measuring the spatial distribution of accumulation with a spacing on the order of kilometers. Single measurements are still affected by small-scale depositional noise, but because the time span for reading these lines is normally 1 year or more, the noise is a small source of error compared to the measured accumulation. The use of Global Positioning System (GPS) receivers for positioning the stakes is an important tool to relocate the stakes. Stake locations can also be used to calculate surface velocities. In the case of traverse routes, the stakes are regularly replaced over the years and placed back in the original position. Determination of the accumulation rate from the stake observations consists of two types of observations: stake height measurements (allowing to determine the accumulation over a given time period) and density measurements.

2.2.1. Stake Height and Correction for Densification

[23] Stake height measurements are only possible if the stake bottom is immobile relative to the surrounding snow layer. This can be achieved by fixing the stake bottom on a horizontal slab, or by fixing it on a natural hard layer (wind slab). Usually, it is assumed that the stake bottom is firmly anchored in the snow and the stakes move down with the snow layer on which the stake bottom is fixed. Using a light weight stake, of which the bulk density is close to that of near-surface snow (e.g., commonly used bamboo stakes, 250–350 kg m^{-3}, 2–3 cm in diameter and 2.5 m in length), this condition is fulfilled in a first approximation. In the past, aluminum and bamboo stakes have been used, but they frequently have failed because of blizzard winds or melting due to solar radiation in coastal areas. Polycarbonate snow poles (50 mm diameter, 6 mm wall diameter), which have recently been used, are less fragile than bamboo and aluminum poles but are more expensive. However, the logistical costs of deployment and resurvey of stakes are much higher, and stake loss due to extreme environmental conditions is a critical issue. The maximum stake height for strong wind is around 4 m, being initially buried about 1.5 m in the snow (a ratio of about 35%). Additional factors that can cause uncertainty in reading the height appear if wind scouring or sastrugis with strong microrelief occur

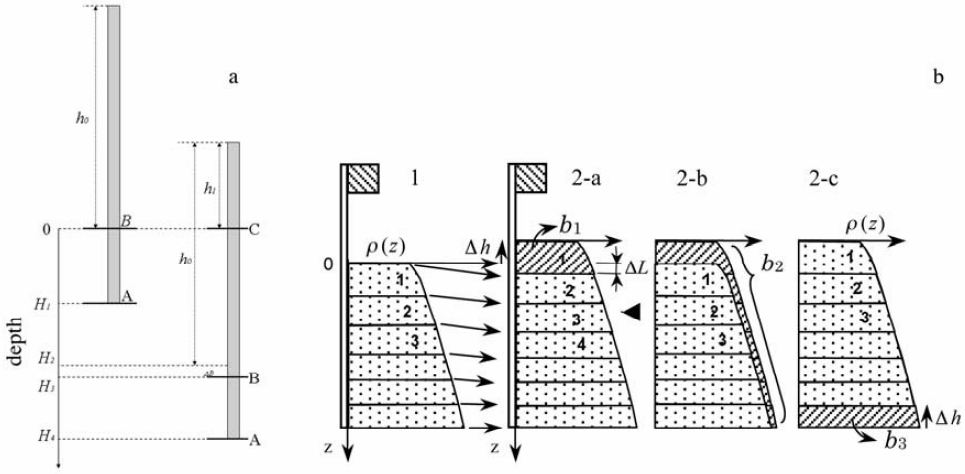

Figure 7. (a) Position of a stake in two moments in time. (b) Schematic diagram of the density-depth profile at Dome Fuji with flag stake for first (1, dotted area) and second year (2-a, 2-b, 2-c) to illustrate the effect of compaction and accumulation for determination of SMB from changes in stake height (redrawn from *Takahashi and Kameda* [2007] with permission of the International Glaciology Society). The mass accumulated in the second year is shown as the hatched areas b_1, b_2, and b_3 (with $b_1 = b_2 = b_3$) in the second year's panels; previous layers are labeled 1–3 from the surface downward. In diagram 2-a, the first year's surface is lowered by ΔL due to compaction. Δh is the change in stake height from first to second year. New snow layer is labeled 1, while the first year's layer 1 becomes layer 2, likewise for layers 2 and 3. Accumulation is thus the layer b_1 of thickness $\Delta h + \Delta L$. In diagram 2-b, density-depth profiles for first year (dotted) in respect to first year's surface and first year's layer numbering, overlaid on profile from second year in respect to second year's surface. Assuming Sorge's law and a firmly anchored stake bottom, the density-depth profiles in both years have the same shape. Accumulation is then the (hatched) area b_2 between both density profiles. 2-c: Shifting the first year's density profile upward by Δh to overlap with the second year's profile to the same surface level, the accumulation appears to be the hatched area at the stake base of thickness Δh.

around the stake (Figure 6a), and if a flexible stake is used, it can become bent.

[24] Accumulation values obtained as a difference of stake height at two moments in time must then be corrected for snow settling (densification), illustrated in Figure 7. In Figure 7 the same stake is shown at two moments in time. In the beginning, the stake bottom is fixed in the snow layer A at the depth H_1, while snow layer B is located at the surface. The stake height above the surface is h_0. Some time later, the stake has apparently sunk into the snow due to accumulation, and the new stake height is h_1. However, the actual accumulation is higher than the difference $h_0 - h_1$ due to the snow densification (note the thinning of the AB layer). The correction ΔB is the difference between the thickness of the AB layer in the beginning and in the end ($H_3 - H_2$ in Figure 7a). In order to calculate the corrected snow accumulation, we have to define the snow mass in the BC layer (i.e., layer accumulated during the given period of time), which is equal to the difference of the mass in AC layer and AB layer. The latter masses can be easily determined as soon as we know the snow density profile to the depth of H_4. This approach is only valid when two conditions are met: (1) the density profile is stable in time (known as Sorge's law) and (2) the snow mass between two fixed snow layers is constant (i.e., vapor mass transport is negligible).

[25] One can derive the equation for the correction of annual snow accumulation (the length measurement):

$$\Delta(\Delta h) = \dot{b}\left(\frac{1}{\rho_0} - \frac{1}{\rho_b}\right), \tag{1}$$

where $\dot{b}$ is the mean annual SMB, ρ_b is the snow density at the depth of stake bottom, and ρ_0 is the density of surface snow. From equation (1) it is seen that the correction value is positively related to the vertical gradient of snow density (Figure 7).

[26] Similar studies have been made by *Takahashi and Kameda* [2007]. They showed that the snow density at the stake bottom should be used for SMB calculations as

$$\dot{b} = \bar{\rho}_b \Delta h, \tag{2}$$

where Δh is the difference in stake height between two measurements, which is the same as the change of stake bottom depth; $\bar{\rho}_b$ is the average snow density between the two depths of the stake bottom, assuming a stable density profile. This correction is 1 – 27% of the annual snow accumulation at inland sites like Vostok and Dome

TABLE 2. Some Error Sources of SMB Estimates for Different Methods[a]

Source	Type of Error	Affects
Stakes		
Length measurement	height	mass
Anchoring/submergence	height	mass
Surface roughness	height	mass
Density	mass	mass
Ultrasonic Sounders		
Air temperature and profile	sound velocity	mass
Sound velocity	height	mass
Density	mass	mass
Fallen rime	height	mass
Anchoring/submergence	height	mass
Surface roughness	height	mass
Drifting snow	height	mass
Cores		
Annual cyclicity	ambiguities in age	time
Hiatus (erosion)	ambiguities in age	time
Time markers	time of deposition	time
Density from weighing	mass, core volume	mass
Density from profiling	mass, core volume	mass
Dynamic layer thinning	layer thickness	mass
GPR		
IRH resolution and tracking	traveltime	time, mass
Wave speed profile	depth	time, mass
Age-depth profile	age	time
Transfer of age to IRH	age	time
Density measurements	mass, wave speed	time, mass
Extrapolating wave speed	depth error	time, mass
Interpolating/extrapolating density	mass	mass
Dynamic layer thinning	layer thickness	mass

[a]The source is the determined property or the assumption being made. The type of error indicates which error is physically being made. Finally, the affects indicate which of the three properties of SMB (mass per area and time) are affected by the error. For stakes and ultrasonic sounders, the date of measuring is known best, so time is not affected. For cores, the annual cyclicity is variation in signals used for counting years. For GPR, tracking is the uncertainty when following a reflection horizon along the profile, and extrapolation is estimation of density and wave speed profile between different core locations.

Fuji and cannot be neglected. Information on density is not always available (particularly for older records); thus conversion of changed snow height to mass may not be possible or will have a large uncertainty.

2.2.2. Accumulation Uncertainties From Stakes

[27] The uncertainty of the stake-based accumulation determination consists of two main sources: (1) measurement errors, briefly described in section 2.2.1 for accumulation and density measurements and (2) natural noise predominantly caused by the small-scale relief-related spatial variability of snow accumulation and density (Table 2). Apparent accumulation uncertainties for field data are based on all possible sources of error; however, natural noise is the largest source of error, with all other sources at least 1 order of magnitude less. It is worth noting that the uncertainty is inversely related to the number of stakes and the period of observation. As an example, the standard deviation of accumulation, as measured at an individual stake in terms Δh, is $\sigma(\Delta h) = 5.3$ cm, i.e., nearly equal to the mean annual accumulation at Vostok. The corresponding standard deviation for the surface (at 20 cm depth) snow density is $\sigma(\rho) = 33$ kg m^{-3}, i.e., about 10% of the mean. This means that the density is a comparatively less noisy parameter than the height measurement. The standard error in accumulation (calculated from the equation $\sigma(\dot{b})/\dot{b} = \sigma(\Delta h)/h + \sigma(\rho)/\rho$) from a single stake is thus 18 kg m^{-2} a^{-1}, or about 85% of the mean annual accumulation at Vostok. This means that a single-stake observation in low-precipitation areas of central Antarctica provides practically no information about the mean accumulation rate. The standard error of annual accumulation decreases as the period of observations increases. One could expect that the error would follow the known equation $\sigma(\dot{b}) = \sigma(\dot{b}_i)/\sqrt{n}$, where $\sigma(\dot{b}_i)$ is the standard error of accumulation for a 1-year period and n is the number of 1-year observation periods. Thus, after 30 years of observations the error must be about 3 kg m^{-2} a^{-1}. Instead, previous research (not published) showed that the standard accumulation rate error for a single stake in a stake farm at Vostok after a 30-year period of observations is as low as 1.7 kg m^{-2} a^{-1}. This is related to the fact that as the observation period becomes longer, the given stake becomes representative for a wider area and thus the accumulation at the adjacent stakes becomes correlated. In this case, the uncertainty versus time function shown above becomes closer to linear: $\sigma(\dot{b}) = \sigma(\dot{b}_i)/n$. The uncertainty in the 1-year accumulation value from the whole stake farm is inversely proportional to the number of stakes k: $\sigma_k(\dot{b}) = \sigma(\dot{b})/\sqrt{k}$. For the Vostok Station stake network ($k = 79$) we can expect that the error for accumulation is 0.6 cm. In fact, this value may be slightly higher because, as we showed before, the accumulation at the adjacent stakes is not completely independent. Corresponding errors for density and accumulation values are 3 kg m^{-3} and 2.0 kg m^{-2} a^{-1}. The error of the mean annual accumulation value from the Vostok Station stake network is difficult to evaluate properly, but on the basis of the data discussed here we estimate it as $1.7/\sqrt{79} = 0.2$ kg m^{-2} a^{-1}. This value is less than the 0.8 kg m^{-2} a^{-1} determined from the time series of annual accumulation values over the last 30 years, but the latter value also includes the natural temporal variability of accumulation. In general, only long-term observations will result in reliable accumulation values. Spectral analyses of accumulation measurements from single stakes with respect to annual average accumulation of a stake farm in the Dome C drainage area show that single stakes or cores are not representative on an annual scale. Even for a site with high accumulation (250 kg m^{-2} a^{-1}), sastrugi with a height of about 20 cm cause significant noise in the individual measurements [*Frezzotti et al.*, 2007].

2.2.3. Optimal Parameters for Stake Farms and Lines

[28] When planning to set up a stake network in Antarctica, the first question to be addressed after defining the accumulation scale aimed at, is "What are the optimal parameters of the network (in terms of data quality, effort needed to make the measurements) for this particular area?" Large networks containing more stakes will produce more accurate results, but more time and effort are required to make the measurements. The network size and stake number also depend on the temporal and spatial scales of

accumulation one is interested in. A trade-off has to be made between the error of the estimated accumulation mean (decreasing with the number of stakes) and the size of the area for which the estimate is representative. The distance between stakes is determined by the size of the stake farm or line and is often restricted by logistic constraints. Unfortunately, the best sampling strategy for a specific area is often made clear only after measurements of the stake farm have already been made.

[29] As an example, optimal parameters (see Appendix A) have been determined for the Vostok area from a stake farm [*Barkov and Lipenkov*, 1978]. For comparatively small (within first hundred meters) stake farms the accuracy of the obtained accumulation values is much more dependent on the size of the farm than on the number of stakes, which is due to the influence of microrelief of the snow surface. Keeping the same amount of stakes but increasing the size of the stake network rapidly decreases the standard error of the accumulation value. At the size of 500–1000 m a saturation value is achieved. This value depends on the dominant larger-scale glacier relief forms. For example, in the megadune areas the saturation value must be of the order of the megadune length, i.e., less than 5 km. Further increasing the stake network dimensions does not significantly change the accuracy, although it does increase the represented area.

2.2.4. Examples for Long-Term Measurements and Current Approaches

[30] In Wilkes Land, the Indian-Pacific sector of Antarctica, stake measurements have been performed for half a century. An early overview of measurements and results is presented by *Young et al.* [1982]. Stake measurements of Antarctic SMB by the Russian (Soviet at that time) Antarctic Expedition (RAE) began with the opening of the first Russian base, Mirny (in 1956). Subsequently, stake networks were established at all permanent Russian stations (Vostok, Novolazarevskaya, Molodezhnaya, Bellingshausen, Leningradskaya; for a list of Antarctic stations see the Scientific Committee on Antarctic Research (SCAR) Web site http://www.scar.org), with varying network shapes, size, and number of stakes to obtain optimal setups. The most extensive data were obtained at Molodezhnaya (~11 stake networks and profiles operating from 1966 to 1981) and Novolazarevskaya. Stake lines were established along the RAE routes (Pionerskaya–Dome C, Komsomolskaya–Dome B, Mirny–Vostok). The best results were achieved from the permanent 1410-km-long Mirny–Vostok traverse, where about 800 stakes were set up in intervals of 0.5–3 km, as summarized by *Lipenkov et al.* [1998]. In addition, seven stake farms (1×1 km^2, 20–40 stakes each) were organized along the traverse in the 1970s and annually visited until the 1980s. The stake network at Vostok was set up in 1970 and is still in operation. Monthly observations allow for a robust characterization of SMB in this region and provide a prototype for the extremely low accumulation areas of central Antarctica. Results were obtained on the interannual and seasonal variability of SMB and responsible mechanisms [*Barkov and Lipenkov*, 1996; *Ekaykin*, 2003]. Among these results are the exclusion of temporal trends of mean accumulation rate (22 kg m^{-2} a^{-1}) over the observation period and the identification of different relief forms of intermediate scale, between microrelief and megadunes, called mesodunes [*Ekaykin*, 2003]. Migration of these mesodunes causes a relief-related (nonclimatic) temporal variability of SMB at a single point with periods of up to 20–30 years [*Ekaykin et al.*, 2002]. In eastern Wilkes Land, seasonal surface observations of stakes and relief forms were carried out by Australian expeditions [*Goodwin*, 1991].

[31] Since the International Geophysical Year (1957–1958), a variety of stake networks have been established at South Pole Station. These include a 42-stake pentagon and an 11-km cross consisting of six arms with a stake interval of 300 m. Details are summarized by *Mosley-Thompson et al.* [1995]. Remeasurements were carried out at irregular intervals. In November 1992, Ohio State University (OSU) set up a network of 236 stakes radiating outward from South Pole Station as six 20-km-long arms, at an interval of ~500 m. Remeasurements are performed annually in November. Results from the first 5 years of measurements indicate that earlier estimates, that one in 10 years has negative SMB [*Gow*, 1965; *Mosley-Thompson and Thompson*, 1982], are probably too high. At least in recent times at the South Pole [*Mosley-Thompson et al.*, 1999], less than 1% of all observations revealed zero or negative SMB. Moreover, the same study by *Mosley-Thompson et al.* [1999] reveals that the net accumulation of about 85 kg m^{-2} a^{-1} during the period 1965–1994 is the highest 30-year average of the last 1000 years at the South Pole.

[32] *Pettré et al.* [1986] report SMB data along a transect from the coast near Dumont d'Urville to Dome C. Most of the data are from stakes, with the stakes from the coast to 32 km inland being surveyed over as long as 21 years (1971–1983). During the old Dome C deep ice core drilling, a stake farm was measured during 1978–1980 to study spatiotemporal variability of a single core [*Palais et al.*, 1982; *Petit et al.*, 1982]. Between 1998 and 2001, at Talos Dome and along the traverse in the Dome C drainage area [*Magand et al.*, 2004; *Frezzotti et al.*, 2005, 2007], 17 stake farms were set up by the Italian Antarctic Programme, each including from 30 to 60 stakes at 100-m intervals in the shape of a cross within an area of 4 km^2, each centered on a core site. Measurements were carried out annually at four sites where automatic weather stations (AWS) have been installed. Other stake farms have been remeasured only 2–4 times. Stake farm readings show that accumulation hiatuses (no accumulation or even ablation) can occur at sites with average accumulation rates below 120 kg m^{-2} a^{-1}.

[33] In the Lambert Glacier Basin (LGB) area, stake measurements were performed by the Australian and Chinese National Antarctic Research Expeditions (ANARE, CHINARE). Results of early stake lines (1960s and 1970s) along the ANARE LGB traverse routes are summarized by *Morgan and Jacka* [1981] and *Budd and Smith* [1982]. Later measurements included stake networks (1983–1993) and multiannual combinations of networks and stakes (2 km interval) (about 1989–1994), comple-

mented by cores [*Goodwin et al.*, 1994; *Ren et al.*, 1999, 2002; *Goodwin et al.*, 2003; *Xiao et al.*, 2005]. Extension of earlier routes with 2-km stake intervals provides a continuous line over 1100 km from Zhongshan station to Dome A (1996–1999 [*Qin et al.*, 2000]).

[34] Farther to the west a number of stake lines and farms have been and are still being operated along the Dronning Maud Land coast. In eastern Dronning Maud Land, the Japanese Antarctic Research Expeditions (JAREs) deployed stakes since 1968 [*Takahashi and Watanabe*, 1997]. Stakes spaced at 2-km intervals were set from the coastal area to inland sites at Dome Fuji over a distance of more than 1000 km. Eleven stake farms were set en route from Dome Fuji to the plateau (e.g., 6×6 at 20 m intervals, 50 rows of stakes over 100 m; see *Kameda et al.* [2007] for details). Six stake farms from the coast to Mizuho were established in 1971. Most of these stakes and stake farms have been surveyed at least once per year. Results are given by *Takahashi and Watanabe* [1997], *Takahashi et al.* [1994], *Fujiwara and Endoh* [1971], *Endo and Fujiwara* [1973], and *Kameda et al.* [1997, 2008].

[35] At the former Georg Forster station (GDR), three stake lines, each 85–115 km in length with stake spacings of 1–5 km, were operated from 1988 to 1993 in an area of strongly differing accumulation regimes containing blue ice areas [*Korth and Dietrich*, 1996]. Other examples are the stake farm operated near the German Georg-von-Neumayer station 1981–1993 and near Neumayer station since 1992 [*Schlosser et al.*, 2002]. Measurements were extended by a 450-km stake line (500-m interval) between Neumayer station at the coast and the Heimefrontfjella (Figure 6) [see *Rotschky et al.*, 2006] (half of the traverse route to the EPICA deep drilling at Kohnen station), which has been revisited annually since 1996. A stake line between the Swedish stations Svea and Wasa was established in January 1988 [*Stroeven and Pohjola*, 1991] and partly surveyed until 1998 [*Isaksson and Karlén*, 1994]. A new 300-km profile was established in 2002/2003 for a long-term SMB monitoring [*Swedish Antarctic Research Programme*, 2003]. Shorter lines, also partly in conjunction with GPR, were investigated near the Finnish Aboa station [*Isaksson and Karlén*, 1994; *Sinisalo et al.*, 2005] and on Lydden ice rise (Brunt ice shelf) [*Vaughan et al.*, 2004]. In blue ice areas occurring in mountain regions of East Antarctica, stake networks were surveyed to gain information on *ablation* rates and to study meteorite traps [*Bintanja*, 1999; *Folco et al.*, 2002]. The data suggest that ablation rates decrease with increasing distance from the ice sheet edge, with values from 350 to 30 kg m^{-2} a^{-1}.

[36] An example of a contemporary integrated SMB approach is the Les Glaciers, un Observatoire du Climat (GLACIOCLIM) Surface Mass Balance of Antarctica (SAMBA, see http://www-lgge.obs.ujf-grenoble.fr/~christo/glacioclim/samba) observation system, a French-Italian cooperation. The French GLACIOCLIM glacier observation system consists of a ~1-km^2 stakes network (50-m interval) located on the coast of Adélie Land, with year-round surveys performed monthly. Additionally, various meteorological instruments in the area are used to study the warm/ablating region to develop an understanding of SMB genesis and to verify local modeling capabilities in such a region. An ~100-km stake line (interval 0.5–2.5 km with annual observations), recently extended to 150 km from the coast toward Dome C, is used for sampling the coast to plateau transition and sampling spatial scales consistent with climate models and with satellite data. Along the stake lines, two AWS are deployed, one of which is accompanied by a 1-km^2 stake network (250-m interval). Aiming at the sampling of both small and large scales of accumulation (model, satellite), three 1-km^2 stake networks (40-m interval) were set up in the Dome C area in 2005/2006, with the stake farms located 25 km apart. This network is surveyed at least once a year and may be surveyed more frequently now that the Concordia station is permanently inhabited. Meteorological data are available from the station. The focus of future projects is the short-term variability at various sites by measuring precipitation with spectronivometers and accumulation with ultrasonic sounders. The observation system and monitoring are expected to last at least 10 years. Examination of the data should allow us to address the climate–accumulation interaction as well as climate–model validation on subannual to multiannual scales, which will also enable analysis of interannual variations and processes.

2.3. Point Measurements at the Surface: Ultrasonic Sensors

[37] A relatively recent (~10–15 years) technique for monitoring SMB in East Antarctica is tracking surface height changes by way of ultrasonic height rangers. These sensors determine the vertical distance to the snow surface by measuring the elapsed time between emission and return of an ultrasonic pulse. An air temperature measurement is required to correct for variations of the speed of sound in air.

[38] Until quite recently, ultrasonic height rangers were mainly used to study the growth and decay of the seasonal snowpack in the Northern Hemisphere. As the design evolved (for instance, by including a multiple echo processing algorithm that stores several reflected signals to improve operational efficiency and to decrease the problem of obstacles), ultrasonic height rangers also found their way into mass balance research of high-altitude/high-latitude ice masses, such as Alpine and Arctic valley glaciers [*Oerlemans*, 2003; *Klok et al.*, 2005] and the Greenland ice sheet [*Steffen and Box*, 2001; *Van de Wal et al.*, 2005; *Smeets and van den Broeke*, 2008]. With rugged housing and improved low-temperature specification (nowadays typically down to −45°C), application of ultrasonic height rangers in Antarctic mass balance studies has become widespread. They are deployed in a wide range of climate settings, such as the McMurdo Dry Valleys [*Doran et al.*, 2002], the high accumulation coastal zone of East Antarctica [*McMorrow et al.*, 2001] and West Antarctica [*van Lipzig et al.*, 2004b], and the dry East Antarctic interior [*Reijmer and Broeke*, 2003; *van den Broeke et al.*, 2004b] as well as in the intermediate

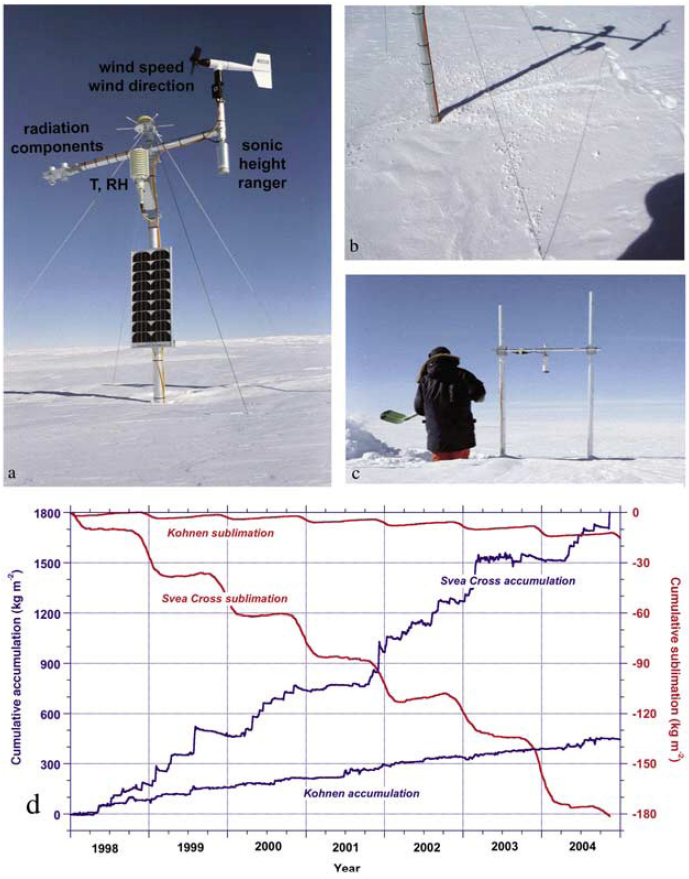

Figure 8. (a) Picture of AWS9 (near EPICA deep drilling in DML at Kohnen station), taken 4 years after installation, i.e., after about 1 m of snow has accumulated. The data logger and pressure sensor are buried in the snow. (b) Rime from the mast fallen on the ground might cause artificial accumulation. (c) Picture of stand-alone ultrasonic height meter, near AWS9. The data logger and pressure sensor are buried in the snow [*van den Broeke et al.*, 2004b]. (d) Sample data from ultrasonic sounders: scale on left side is cumulative accumulation at AWS6 (Svea Cross) and AWS9 (Kohnen station) for the period 1998–2004; scale on right side is cumulative sublimation as calculated from AWS data. Note different *y* axis scales.

katabatic wind zone [*Helsen et al.*, 2005] and on the ice shelves [*Braaten*, 1994].

[39] In East Antarctica and elsewhere, it is advantageous to mount the ultrasonic height ranger on or next to an automatic weather station (AWS, Figure 8). The AWS usually observes a range of atmospheric variables such as air pressure, air and snow temperature, air relative humidity, air velocity, and occasionally also radiation components [*van den Broeke et al.*, 2004a]. This means that surface height changes can be interpreted in a mass balance framework, including sublimation from the surface and from drifting snow particles [*Fujii and Kusunoki*, 1982; *Kaser*, 1982; *Clow et al.*, 1988; *Stearns and Weidner*, 1993; *King et al.*, 1996, 2001; *Bintanja*, 2003]. Moreover, ultrasonic height data can be accepted/rejected on the basis of prevailing meteorological conditions (see section 2.3.4). Finally, the ultrasonic height ranger can be coupled to the AWS's power and data logging system. If more information is required on the spatial variability of accumulation, several ultrasonic height rangers can be deployed in stand-alone mode, using a dedicated energy/data logger system (Figure 8c).

2.3.1. Typical Sensor Specifications

[40] As a typical example, here we list the specifications of a widely used ultrasonic height ranger, the SR50 produced by Campbell in Canada. Its limited dimensions (length 31 cm, diameter 7.5 cm, and weight 1.3 kg) make it convenient for use in AWS. With an operating temperature range down to −45°C and proven working capacity down to −70°C [*van den Broeke et al.*, 2004b] it is suitable for operation in most parts of East Antarctica. The power requirement is 9–16 Vdc (volts direct current), so that it can be powered by the data logger's 12-Vdc power supply that is standard equipment on most AWS. The low power consumption (250 mA during measurement peaks) is favorable for operation on unmanned remote platforms. The measurement range (0.5–10 m) is suitable for operation in

accumulation as well as in ablation areas. The beam acceptance (maximum deviation from the vertical) of ~22° poses no problem, as ablation-induced tilt of the mast normally does not occur in East Antarctica. The measurement accuracy is ±1 cm or 0.4% of the distance to the surface, whichever is greatest, and data can be stored at a maximum resolution of 0.1 mm. To account for the temperature-dependent speed of sound, a correction for the deviation of the mean layer air temperature from a fixed calibration temperature (273 K) must be applied.

2.3.2. Advantages of Ultrasonic Height Rangers for Mass Balance Studies

[41] The obvious advantage of ultrasonic height rangers in comparison to stakes, snow pits, and cores is that individual accumulation/ablation events are unambiguously dated. This means that the temporal variability (e.g., the seasonal cycle or the summer and winter balance) of accumulation/ablation can be quantified. This has important applications in ice core paleoclimatology: if, for instance, a significant seasonal cycle in accumulation is present that changes in time, this introduces a bias in the climate signal extracted from cores. Case studies of chemical and physical anomalies in the firn can be based on individual accumulation events identified in the ultrasonic time series. In combination with AWS data, the accumulation/ablation time series of ultrasonic height rangers can also be used to force snowpack models at their upper boundary or serve as a starting point for atmospheric trajectory calculations [*Noone et al.*, 1999; *Reijmer et al.*, 2002; *Helsen et al.*, 2004]. Moreover, the temporal distribution of accumulation/ablation events is essential for validation of meteorological and/or mass balance models [*Gallée et al.*, 2001; *van Lipzig et al.*, 2004a]. Finally, for accurate energy balance calculations from single or multilevel AWS data it is desirable to know the exact height of the wind speed, temperature, and humidity sensors above the surface, as well as the depth of snow temperature sensors [*van den Broeke et al.*, 2004b].

2.3.3. Technical Problems

[42] The ultrasonic height ranger needs to be mounted on a rack or mast so that its beam is perpendicular to the surface and is not obstructed. In accumulation areas, such as in East Antarctica, the sensor needs to be kept at least 0.5 m from the surface. This requires regular, expensive, servicing visits, the frequency of which depends on the rate of accumulation, the battery, and data storage capacity. In practice, the servicing interval will typically be once per year for coastal East Antarctica and once every 2–3 years for the interior plateau.

[43] Ultrasonic height rangers are susceptible to failure from ageing, corrosion, or freeze-thaw delaminating of the acoustic membrane. Membrane failure rate has been observed to increase with age. Therefore, regular replacement of the acoustic membrane as a preventive measure should be considered for each visit. The proximity of open sea and/or an effective transport of sea salt to the observation site significantly reduce the lifetime of the acoustic membrane. In East Antarctica, this is usually not a big problem, and lifetimes of the membranes are typically 5 years or more.

[44] A common problem that prevents correct operation of the ultrasonic height sensor is that the acoustic membrane becomes obstructed by snow/rime. Sometimes mounting a cone around the sensor can prevent this, but this carries with it the risk of spurious ice accretion on the cone and subsequent structural failure of the mast. Riming problems are considerably reduced on the ice sheet slopes, away from the flat domes in the interior and the flat ice shelves near the coast. The reason is that along these slopes, semipermanent katabatic winds heat and dry the lower atmosphere resulting in a continuous flow of subsaturated air past the sensor, keeping it free of rime.

2.3.4. Data Interpretation Problems and Uncertainties

[45] Measurements from an ultrasonic height ranger performed at a single site suffer from the same problems of poor spatial representativity as single core or stake measurements (see section 2.1). These problems can be partly solved by using the same solutions as for the other techniques, i.e., operating a farm of stakes (or drilling several shallow cores) in the surroundings of the ultrasonic height sensor or deploying several sensors.

[46] Naturally, the measuring site should be far enough upwind from obstacles to avoid spurious lee accumulation or snow erosion on a flat surface. In East Antarctica, it is usually easy to find an upwind measurement site with a large fetch because surface conditions are usually very homogeneous and (katabatic) wind direction is exceptionally constant [*van den Broeke and van Lipzig*, 2003]. Dominant sastrugi orientation from surface or aerial surveys or a modeled wind field [*van Lipzig et al.*, 2004a] can help in determining the prevailing wind direction if no local meteorological data are available.

[47] Once a suitable spot is found, raw distance data should be collected and the temperature-dependent speed of sound correction applied after data collection. In-sensor temperature measurements on older sensor types should preferably not be used because the sensor can overheat significantly under low wind speed/strong insolation conditions, fouling the surface height data. It is best to measure the air temperature independently with a ventilated dedicated sensor placed approximately halfway between the ultrasonic height ranger and the surface. A more elaborate alternative is to measure temperature at sensor height and at the surface (e.g., using a longwave radiation sensor), to calculate the temperature profile (using similarity theory and appropriate stability functions [e.g., *Andreas*, 2002; *Holtslag and Bruijn*, 1988]) and to take the mean temperature of the air layer. In East Antarctica, it is worthwhile to spend some effort to correctly perform the temperature correction because the radiation balance at the surface is often negative so that the temperature difference between the ultrasonic height ranger and the surface in the stably stratified surface layer can be considerable, up to 5–10 K in the first couple of meters during calm, clear conditions.

[48] At sites where riming occurs frequently, rime collected on the mast structure can fall off and collect at the surface, leading to artificially enhanced accumulation

(Figure 8b). This will only affect low-accumulation sites on the interior plateau.

[49] Once the wind speed exceeds a certain threshold, snowdrift occurs in the near surface air layer [*Li and Pomeroy*, 1997; *Mann et al.*, 2000]. This can lead to an erroneous height reading from a reflection from a dense drifting snow layer. Usually, AWS data can be used to detect snowdrift events so that these readings can be discarded.

[50] The technical and operational difficulties described in this section and section 2.3.3 (see also Table 2) reduce the 1-cm accuracy under laboratory conditions to an operational accuracy of typically 2–3 cm. This accuracy is sufficient for high-accumulation sites, but it is not good enough to detect the often much smaller precipitation events that are common on the interior plateau of East Antarctica. Here, small events (<1 kg m^{-2}) make up most of the total accumulation [*Reijmer et al.*, 2002].

[51] A large uncertainty is introduced when converting instantaneous height changes from the ultrasonic ranger to mass changes. In practice, continuously measured height changes are converted to mass changes through multiplication by the average density of the accumulated snowpack since the last visit, as measured in a snow pit or firn core (see section 2.1). Although this yields a correct value of the total accumulation integrated over the time interval between the pit studies, the sometimes considerable density variations in the upper firn layers result in an uncertainty of up to 20% or worse for mass changes on the event timescale.

[52] Another problem affecting ultrasonic height measurements in East Antarctica is the depth and temperature dependence of the firn densification rate. Under idealized steady state conditions, assuming continuous accumulation and a constant temperature, the vertical speed in the firn depends only on the local density (Sorge's law). Under these assumptions, knowing the anchor depth of the structure holding the ultrasonic height ranger and the density profile suffices to correct for this. Unfortunately, accumulation is not a continuous, steady state process: after a stepwise increase in surface height due to an accumulation event, the densification rate of a freshly fallen snow layer decreases with time. In addition, the densification process depends on temperature, causing accelerated summertime densification of the upper snowpack [*Dibb and Fahnestock*, 2004; *Li and Zwally*, 2002] and on the microstructure [*Freitag et al.*, 2004]. The summer heat wave slowly penetrates the firn, locally enhancing firn densification rates when it passes. This implies that only time-dependent firn densification modeling along the lines of *Li and Zwally* [2004], at least taking into account temperature, can account for the differential densification effect in a physically realistic way.

2.3.5. A Data Example From East Antarctica

[53] The following data example demonstrates both the great value and the problems of using ultrasonic height ranger data in East Antarctic mass balance research. Figure 8d shows 7 years (1998–2004) of accumulation derived from ultrasonic height ranger data from two AWS sites in western Dronning Maud Land (DML; left scale). The first AWS is located at Svea Cross (74°28.9′S, 11°31.0′W, 1160 m above sea level (asl)), at the foot of the Heimefrontfjella in the katabatic wind zone. The second is located adjacent to Kohnen station (75°00.2′S, 0°00.4′E, 2892 m asl, see Figure 8) on the Amundsenisen of the flat East Antarctic plateau. In addition to surface height changes, the AWSs measure wind speed and direction, temperature, relative humidity, shortwave and longwave radiation fluxes, air pressure, and snow temperatures. The sampling frequency typically is 6 min from which 1-h averages are calculated and stored in a Campbell CR10 data logger with separate memory module.

[54] The ultrasonic data (Figure 8d) have been corrected for temperature but not for differential firn densification. To convert height changes to mass changes, we applied a mean density of 396 kg m^{-3} at Svea Cross and 307 kg m^{-3} at Kohnen. Missing data, mainly due to riming (20% at Kohnen, <1% at Svea Cross), have been linearly interpolated. To remove some residual noise, a cubic spline fit was applied to the data. Applying linear fits to the cumulative mass balance curve yields values for the specific SMB of 243 kg m^{-2} a^{-1} at Svea Cross and 64 kg m^{-2} a^{-1} at Kohnen. These values agree with accumulation derived from shallow firn cores drilled at these sites.

[55] The data show that the measurement accuracy of the ultrasonic height ranger is insufficient to unambiguously resolve individual precipitation events at the low-accumulation site Kohnen. The record rather shows a continuous, slow accumulation interspersed with occasional larger events. No significant surface lowering is observed between accumulation events. At Kohnen, even during summer, temperatures are apparently too low to force strong sublimation and a seasonal cycle in the densification.

[56] This is very different at Svea Cross, where the accumulation occurs in large, well-defined events, some of which can also be found in the record of Kohnen. In between these accumulation events, dry periods lasting up to 8 months occur at Svea Cross. During these dry episodes, significant surface lowering occurs in the summer period (November–February). To determine which part of the surface lowering is caused by sublimation, AWS data were used to calculate the turbulent flux of latent heat [*van den Broeke et al.*, 2004b]. The scale on the right in Figure 8d indicates the resulting cumulative sublimation/deposition. As can be seen, sublimation dominates during summer, averaging typically 25 mm water equivalent (about 6.5 cm of snow) at Svea Cross and about 10 times less at Kohnen. At Svea Cross, this accounts for part but not all of the surface lowering that is observed during summer; enhanced summer densification of the firn layer enclosed by the AWS anchor depth and the surface accounts for the residual surface lowering.

2.4. Point Measurements at Depth: Snow Pits, Firn, and Ice Cores

[57] Snow pits and core drilling (Figure 9) are used to access older snow and ice below the surface. Their deployment retrieves sequences of buried snow and ice from only a single operation, as layers of different age are accessed at

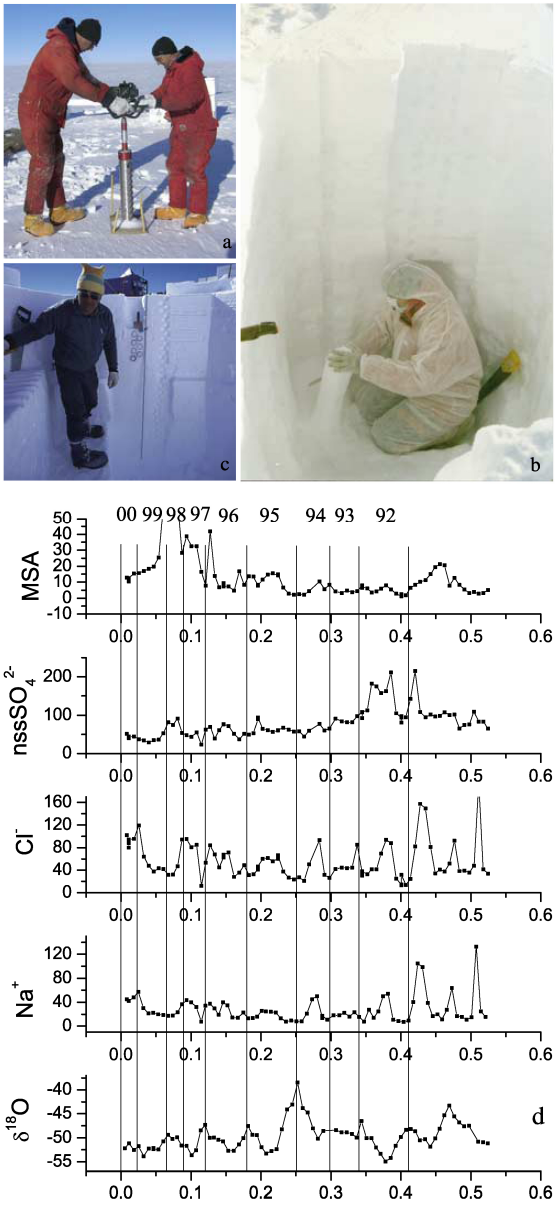

Figure 9. (a) Firn core drilling. Typical drill diameters are 3 inches (7.6 cm) and 4 inches (10.2 cm). The wooden board marks the reference level of the snow surface. (b) Taking samples in a 3-m-deep snow pit. To avoid sample contamination, the person wears a clean room suite. (c) Taking density measurements with tubes in a snow pit with a crossover pattern (visible to the left of the ruler in the center). (d) Example from pit MC in DML on how several different species have been used in dating the pits [*Karlöf et al.*, 2005b] (with permission of the International Glaciology Society). They mainly used the oxygen isotope data with support of ions to date the pits. Years (1992–2000) are indicated at the top; year transitions are marked with vertical lines.

once. Apart from accumulation, time series for a number of other parameters are established as well.

[58] The SMB corresponding to a sample in a certain depth interval (and thus age interval) is most generally derived from the ratio of mass (or water equivalent depth) of the considered sample to the time span that the sample range covers. As for stake and ultrasonic measurements, determination of density is thus one important key. In contrast to those methods, which monitor the surface and obtain time series of surface accumulation only by repeated observations of surface height at an accurately known point in time, the determination of the age as a function of depth is the other key parameter. One derives this function for instance by interpolating discrete *time markers* (e.g., *volcanic horizons*) or counting of layers of known origin, like annual signals [*Whitlow et al.*, 1992].

2.4.1. Density Measurements

[59] The techniques presented in sections 2.4.1.1–2.4.1.3, used to determine density as a function of depth along cores, complement the classic surface snow density measurement methods described in section 2.1.

2.4.1.1. Classic Technique

[60] Firn core density is most often determined by measuring core length and diameter and weighing each core section on an electronic scale directly after core retrieval in the field [*Isaksson et al.*, 1996; *Oerter et al.*, 1999; *Magand et al.*, 2004; *Frezzotti et al.*, 2005]. However, problems with this simple method are that the snow in the uppermost meter is usually poorly consolidated and loss of material is therefore unavoidable, reducing the accuracy of volume calculations. It is therefore common practice for firn core retrieval that density is measured in a pit (about 2 m depth) in direct connection to the drill site where stratigraphic studies and snow sampling can also be performed. Another problem is that the diameter of the core pieces changes depending on the snow type. For instance, less dense snow can be compacted or lost, resulting in an overestimation of density [*Karlöf et al.*, 2005b]. Cores with a wider diameter (e.g., 4 inch, 10.2 cm) reduce the uncertainty in density measurements. Core imperfections that can occur during drilling alter the volume of the core segment and can thus affect density measurements.

2.4.1.2. Radiation Attenuation Profiling

[61] Radiation attenuation profiling is based on the absorption and scattering of hard radiation to determine ice density. The ratio between transmitted and received ray intensity is a measure for absorption and scattering, which can be related to snow, firn, and ice density. Currently, three types of radiation are utilized: γ rays, X rays, and neutrons. In the case of γ attenuation profiling (GAP) [*Gerland et al.*, 1999; *Wilhelms*, 1996, 2000] the γ ray originates from a radioactive source (e.g., ^{137}Cs) and passes through the core in transverse direction to a detector. For monochromatic radiation the mass absorption coefficient is known with 0.1% relative error. The statistical intensity measurement error is determined by free-air reference. To reduce statistical errors, multiple (usually more than 10) measurements are averaged. The calibrated detector signal has to be

corrected for variations in core diameter. For high-quality cores, the diameter is accurate to $\leq$1 mm. The possible influence at maximum misalignment of the core within the measurement bench has to be accounted for, as well as cracks from core breaks at the end of an ice core. The precision of the GAP density measurements is typically around 10 kg m^{-3} for a 100-mm-diameter core. The depth resolution of GAP depends on the characteristics of the radioactive source, like ray diameter and dispersion characteristics. Typical resolution is on the order of 1 cm, with measurements carried for redundancy to the subcentimeter level.

[62] For X-ray attenuation profiling [*Hori et al.*, 1999], the accuracy is about 1%, the same as for the γ attenuation method. However, field measurements by the X-ray method are difficult since a large experimental system is required. It is therefore mostly applied in the laboratory.

[63] In contrast to these two methods, neutron probes (Walingford probe) [*Morris and Cooper*, 2003] are operated in the borehole instead of along the core. The neutron probe method thus has the advantage that only a (reasonably smooth) hole instead of a core is necessary for determining density profiles. The depth resolution, however, is physically limited to 10 cm. The uncertainty of the derived density is on the order of 10 kg m^{-3}.

2.4.1.3. Dielectric Profiling

[64] The complex dielectric constant is expressed as $\varepsilon^* = \varepsilon' - i\varepsilon''$. In the case of ice, the real part ε', the ordinary complex permittivity of the medium, mainly depends on density. The imaginary part ε'', the dielectric loss factor, is related to conductivity σ and radian frequency ω by $\varepsilon'' = \sigma(\varepsilon_0\omega)^{-1}$, where ε_0 is the permittivity of free space. Both parts of ε^* can be determined with dielectric profiling (DEP) [*Moore and Paren*, 1987]. A DEP device is essentially a calibrated and guarded scanning capacitor. The core is put between two semispheres. Its conductance and admittance are determined by applying alternating current potentials, typically at a single frequency of 10 kIIz to a few hundred kilohertz, which are then converted to ε^*. For accurate devices, the real and imaginary components can each be determined to within 1% [*Wilhelms*, 2000]. A widely used formula relating the ordinary relative permittivity ε' and density ρ is based on the approximation derived by *Looyenga* [1965] from theoretical consideration of air distributed in a dielectric medium, with spherical approximations of bubbles, $\varepsilon' = ((\rho/\rho_{ice})[\sqrt{[3]}\varepsilon'_{ice} - 1] + 1)^3$. Other approximations were derived from comparison of density and permittivity measurements, e.g., by *Robin et al.* [1969], *Tiuri et al.* [1984], or *Kovacs et al.* [1995]. The latter refined an empirical approximation, $\varepsilon' = (1 + 0.845\rho)^2$, which is now widely used for permittivity-density conversions [*Kovacs et al.*, 1995]. They obtained a standard error of $\pm$0.031 for ε'. Both of the above formulae take only the real part of ε^* into account, causing a mixing of the complex components [e.g., *Barnes et al.*, 2002]. Recently, *Wilhelms* [2005] demonstrated that neglect of complex mixing for the density-permittivity relation could result in errors in ε^* and suggested extension of Looyenga's formula into complex space. In general, integration of the density-depth profile to obtain cumulative mass results in a higher accuracy, as statistical uncertainties of abnormally high or low values are averaged out.

2.4.2. Age Estimates

[65] Two main methods are used to date firn and ice cores (from seasonal to century scales): counting of seasonal variations of various parameters (physical, chemical, isotopic) that show cyclic variations during the year (Figure 9d) and identifying prominent horizons of known age, such as acid layers from dated volcanic eruptions or radioactive fallout from atmospheric thermonuclear bomb tests. A third method exploits the natural decay of radioactive materials. The method used depends on the purpose of the study and the accumulation rate at the site; however, many studies utilize all three methods.

2.4.2.1. Seasonal and Annual Layer Counting

[66] 1. The stable isotope (δ^{18}O and δD) stratigraphy [*Dansgaard et al.*, 1973] is a method commonly used to determine annual layers [e.g., *Morgan et al.*, 1991] in areas with higher accumulation (above about 80–100 kg $m^{-2}a^{-1}$). The oxygen and hydrogen isotopic composition of polar snow is mainly related to the condensation temperature [*Dansgaard*, 1964]. One advantage of the stable isotope stratigraphy is that no special precautions during the sampling procedure are necessary to prevent sample contamination [*Legrand and Mayewski*, 1997]. However, at least seven to eight samples per year are needed to correctly resolve seasonal and thus annual signals. The seasonal cycle of δ^{18}O (or δD) is usually well developed only in the upper part (5–10 m) of the snowpack because of diffusion during densification [*Johnsen*, 1977; *Legrand and Mayewski*, 1997] in the postdepositional process. As few studies have been dedicated to the analysis of postdepositional effects on Antarctic snow composition, the possibility that wind-driven ablation [*Ekaykin et al.*, 2002; *Frezzotti et al.*, 2004] as well as sublimation [*Neumann and Waddington*, 2004; *Neumann et al.*, 2005; *Satake and Kawada*, 1997] may induce systematic effects on isotope levels has to be kept in mind. These could affect seasonal and annual signals [*Masson-Delmotte et al.*, 2008] and thus SMB measurements. As suggested by Masson-Delmotte et al., systematic measurements of water vapor and snow isotopic composition should provide a means of disentangling the effect of depositional and postdepositional processes and, as a consequence, allow a better understanding of their effect on SMB estimates.

[67] 2. Chemistry of discrete firn/ice core samples has been routinely analyzed for major ion content (e.g., via ion chromatography). Over the last decade, continuous flow analysis (CFA), high-resolution fast ion chromatography (FIC), and continuous melting discrete sampling (CMDS) methods have been improved such that a quasi-continuous record of a number of different species is measured simultaneously along a single core [*Fuhrer et al.*, 1993; *Sigg et al.*, 1994; *Fuhrer et al.*, 1996; *Röthlisberger et al.*, 2000; *Sommer et al.*, 2000b, 2000a; *Udisti et al.*, 2000; *Traversi et al.*, 2002; *Rasmussen et al.*, 2005; *Osterberg et al.*, 2006].

Typical markers for seasonal layer counting are methanesulphonic acid (MSA) and nonsea-salt (nss) sulphate (nss SO_4^{2-}), the main oxidation products of dimethylsulphide (DMS), which are mainly produced by marine biogenic activity [*Saigne and Legrand*, 1987]. Study of seasonal cycles of sulfur aerosol carried out in coastal Antarctica have shown that MSA and nss SO_4^{2-} exhibit a strong seasonal cycle characterized by summer maxima [*Jourdain and Legrand*, 2001; *Curran et al.*, 1998]. Another seasonal indicator is Na^+, a tracer of sea salt. Na^+ concentrations peak during the winter as a consequence of more frequent advection of marine air masses over the Antarctic ice sheet [*Legrand and Delmas*, 1984], with the strongest seasonal signal near the coast. Among the commonly used ions, sodium, nss sulphate, and nitrate often show well-developed seasonal variations on the polar plateau [*Isaksson et al.*, 1996; *Stenni et al.*, 2000, 2002; *Traufetter et al.*, 2004; *Kaspari et al.*, 2005; *Dixon et al.*, 2004; *Karlöf et al.*, 2005b]. Also for these species it is important to sample with high enough frequency to capture their variations, i.e., at least seven to eight samples per year [*Mayewski and Goodwin*, 1997]. However, it is worth keeping in mind that nitrate diffuses and is probably reemitted from the upper layers of the ice sheet [*Wolff et al.*, 1995; *Weller et al.*, 2004]. Nitrate reemission is inversely related to accumulation rate and usually obliterates its seasonal signature at low accumulation sites. Therefore, SO_4^{2-} and Na^+ provide the most robust annual peaks within cores. In order to avoid using occasional double peaks as dividing lines for years, multiple ions with different seasonal timings can be used to define the annual horizons [e.g., *Legrand and Mayewski*, 1997].

[68] 3. Some gases also display a seasonal cycle, in addition to isotopes and ions. One example is hydrogen peroxide (H_2O_2, e.g., measured via spectrofluorimeter methods), which is principally produced in the atmosphere by photochemistry in summer. Its maximum concentration occurs in the period of maximum solar radiation, from late spring to late summer [*Neftel*, 1991]. H_2O_2 is subject to postdepositional change, caused by reemission to the atmosphere, the same as some other species. Utilization of H_2O_2 for annual layer counting is thus restricted to high-accumulation areas (>200 kg m^{-2} a^{-1}).

[69] 4. For electrical methods, the varying concentrations of ions are a major cause of variations in alternating current (AC) and direct current (DC) electric conductivity. Two techniques are used to determine quasi-continuously the variation of conductivity along a core. The electric conductivity method (ECM) [*Hammer*, 1980] is a measure of the electrical current from which acidity concentration levels may be inferred in cores. ECM is performed in a cold room with stable temperature conditions as well as in the field. In contemporary systems, two to seven electrodes with an applied high voltage of several hundred volts (AC or DC) are moved along a freshly cut ice surface, and measurements are typically taken at millimeter resolution. The original method has been modified in various ways and is used by different groups [*Isaksson et al.*, 1996; *Kaczmarska et al.*, 2004; *Wolff et al.*, 1999; *Taylor and Alley*, 2004]. A direct current flowing between the electrodes is dominated by the acid content and the temperature of the ice [*Schwander et al.*, 1983; *Moore and Mulvaney*, 1989] but is only slightly dependent on the salt concentration under normal conditions [*Schwander et al.*, 1983; *Wolff et al.*, 1997]. For alternating currents, salts have an increasing effect on conductivity [*Barnes et al.*, 2002]. The imaginary part of the dielectric constant determined from DEP, ε'', already introduced in section 2.4.1.3 in the context of density measurements, likewise reveals variations in AC conductivity [*Moore and Mulvaney*, 1989]. As an alternating current technique, which is nondestructive as it does not require direct contact between the ice and the electrodes [*Wilhelms et al.*, 1998], it also responds to both the acidity and the total salt content in the ice [*Barnes et al.*, 2002]. Measurements are performed in millimeter to centimeter increments. There is evidence that the DEP and ECM electrical methods respond to different chemical compositions. *Minikin et al.* [1994] suggested that DEP peaks represent winter maxima of sea salts, while peaks in ECM respond mostly to summer maxima of nss sulphate and partly to high values of NO_3^-, MSA, and HCl^-. *Hammer et al.* [1994] and *Mulvaney et al.* [2002] confirm that ECM is a sufficient method for detecting both volcanic peaks and seasonal changes in acidity. Apart from identifying volcanic signals in conductivity, ECM is also used to analyze annual peaks if conditions are favorable enough.

[70] 5. Dating firn and ice cores via visual stratigraphy is based on visual differences in summer and winter snow due to changes in atmospheric conditions and radiative fluxes [*Alley et al.*, 1997]. To aid the identification of annual layers, the surface of the core is prepared with a microtome knife. The core is placed on a light table to identify seasonal variations in transparency and scattering associated with annual layering. Summer layers are characterized by coarse-grained, low-density hoar layers, whereas winter layers have higher density and finer grain size. Below the firn-ice transition, summer layers have fewer and larger bubbles compared to winter layers and can also be identified by the presence of summer melt layers in coastal regions. Because of annual layer thinning, annual layers become more difficult to identify with depth. In regions with low accumulation, postdepositional processes such as drifting and melting (e.g., near coastal blue ice areas or very low accumulation areas on the plateau) can preclude the presence of visible annual layers [*Taylor et al.*, 2004]. An advantage of visible stratigraphy is that it can also be applied in the field if stratigraphic changes are strong enough to be identified without preparation of the core. At least for higher accumulation sites, and thus favorable conditions, visual stratigraphy provides an initial approximation of annual accumulation rates [*Morgan et al.*, 1991], useful for later decisions on core processing (e.g., sampling resolution). Although the visual stratigraphy is commonly applied to derive on-site information in snow pits, accumulation rates derived from pit stratigraphy alone involve personal and subjective interpretation, which can lead to unreliable results, as pointed out by *Picciotto et al.* [1971].

[71] 6. New techniques build on the greater availability of more advanced chemical analysis instrumentation, such as inductively coupled plasma–mass spectrometry (ICP-MS), allows the accurate determination of many tens of chemical elements at the parts per billion, parts per trillion, and parts per quadrillion levels. Improved instrumentation coupled with advances in sample generation, e.g., by laser ablation [*Reinhardt et al.*, 2001], ultraclean sample analysis, and continuous sampling [*Knüsel et al.*, 2003; *Osterberg et al.*, 2006], will likely yield new firn and ice core dating methods. This would be particularly advantageous for dating ice cores from low-accumulation sites (such as the East Antarctic plateau).

2.4.2.2. Reference Horizons

[72] There are several valuable reference horizons that have been used in Antarctic accumulation studies for validating the depth-age scale developed from annual layer counting or for use as a time horizon, which can then be used for calculating the accumulation rate between horizons. Below we discuss the two most commonly used reference horizons (volcanic peaks and artificial radionuclides) and suggest additional horizons that could be worthwhile to explore further.

[73] 1. For volcanic peaks, sulphate (in the form of atmospheric H_2SO_4) is generally the dominant ion in high-altitude Antarctic snow, with the dominant source from marine biogenic emissions and sporadic input from volcanic activity. For the Antarctic polar plateau, historical volcanic eruptions such as Pinatubo 1991, Mount Hudson 1991, Mount Agung 1963, Krakatau 1883, and Tambora 1815 (plus an unknown eruption 1809) have been shown to be easily distinguishable peaks that can be used as unambivalent time markers, either from chemical analysis or conductivity measurements [e.g., *Cole-Dai et al.*, 1997; *Oerter et al.*, 1999; *Nishio et al.*, 2002; *Stenni et al.*, 2002; *Traufetter et al.*, 2004; *Dixon et al.*, 2004]. Because of oxidation of SO_2, H_2SO_4 forms within about 1 month following the eruption [*Coffey*, 1996]. Once in the stratosphere, the atmospheric residence time of SO_4^{2-} is a few years, during which it can be transported to the polar regions and subsequently scavenged by snowfall. An increase of nss SO_4^{2-} concentrations in polar snow is observed in a period up to 3 years after a major volcanic eruption [*Cole-Dai and Mosley-Thompson.*, 1999]. For example, the eruption of Tambora (located in Indonesia) occurred in April 1815. The rise of SO_4^{2-} above background noise is observed in late austral winter 1816, with maximum concentrations during the austral summer of 1816/1817 [*Cole-Dai et al.*, 1997; *Palmer et al.*, 2001] due to the lag between the eruption and nss SO_4^{2-} deposition in Antarctica. In several papers from the EPICA presite and ITASE surveys, attempts have been made to develop a useful volcanic chronology spanning the last millennium to aid in the correlation between cores [*Karlöf et al.*, 2000; *Traufetter et al.*, 2004; *Hofstede et al.*, 2004]. The Tambora double peak has served as the main time horizon for the dating of many firn cores in the ITASE program [*Isaksson et al.*, 1996, 1999; *Oerter et al.*, 1999, 2000; *Stenni et al.*, 1999, 2001; *Karlöf et al.*, 2000; *Ekaykin et al.*, 2004; *Dixon et al.*, 2004; *Karlöf et al.*, 2005b; *Frezzotti et al.*, 2005; *Steig et al.*, 2005]. The most prominent eruptions during the last millennium in addition to Tambora are the A.D. 1259 eruption suggested to be El Chichon [*Palais et al.*, 1992] and the A.D. 1452 eruption suggested to be Kuwae [*Delmas et al.*, 1992]. These eruptions have been identified in many Antarctic ice cores [i.e., *Moore et al.*, 1991; *Cole-Dai et al.*, 1997, 2000; *Watanabe et al.*, 1997]. However, the volcanic signal at high-accumulation, low-elevation sites located near the Ross Sea coast in West Antarctica has been overwritten by large amounts of biogenic SO_4 that is released by marine organisms [*Dixon et al.*, 2004]. This may be a problem at other low-elevation coastal sites that are situated close to polynyas, too. Currently, on the polar plateau (SMB < 70 kg m^{-2} a^{-1}), ~2.5-m-deep snow pits are deep enough to reach the 1991–1992 layer from the Mount Pinatubo and Mount Hudson eruptions. Attempts have been made to determine if dating horizons as shown in time series of DEP, ECM, and sulfate are significant with respect to natural and measurement-induced noise [*Cole-Dai et al.*, 1997; *Fischer et al.*, 1998; *Karlöf et al.*, 2005a, 2006; *Steig et al.*, 2005].

[74] 2. Time markers from artificial radionuclides are based on radioisotopes from atmospheric nuclear weapon tests (United States, United Kingdom, Soviet Union, France, China, and India) carried out between 1953 and 1980. They were deposited in Antarctica after transport in the upper atmosphere and stratosphere [*Picciotto and Wilgain*, 1963; *Wilgain et al.*, 1965; *Feely et al.*, 1966; *Picciotto et al.*, 1971; *Lambert et al.*, 1977; *Carter and Moghissi*, 1977; *Jouzel et al.*, 1979; *Kamiyama et al.*, 1989]. Since the signing of the Limited Nuclear Weapon Test Ban Treaty in 1963, the number of atmospheric nuclear weapon tests greatly decreased with tests being carried out mainly underground. Other sources of anthropogenic fallout post-1963 may be linked to the nuclear disaster in Chernobyl in 1986 [*Dibb et al.*, 1990]. Very sensitive analytical techniques and procedures have been developed and improved over the last 40 years to detect and measure both artificial and natural radionuclides present in the ice sheets [*Picciotto and Wilgain*, 1963; *Delmas and Pourchet*, 1977; *Pinglot and Pourchet*, 1979, 1994]. The high solubility of most fission products induces the formation of distinct and stable radioactive reference horizons in areas of dry snow facies or with moderate percolation of meltwater. Among the radioactive fallout, ^{90}Sr and ^{137}Cs radionuclides (referred to gross β activity), plutonium isotopes, and ^{241}Am [*Pourchet et al.*, 2003] are best suited for the formation of distinct radioactive horizons owing to their high production yield and their low volatility, which prevents vertical migration in the firn layers as long as they remain dry [*Picciotto et al.*, 1971]. Another artificial product, tritium (^{3}H), behaves differently during its injection into the global system (by thermonuclear explosions) and its deposition than the fission products previously cited [*Picciotto et al.*, 1971]. Nevertheless, very distinct radioactive peaks in continuous tritium profiles are also observed [*Jouzel et*

al., 1979; *Oerter et al.*, 1999; *Stenni et al.*, 2002; *Frezzotti et al.*, 2005]. The timing of radioactive deposition from the nuclear tests is well known in Antarctica [*Wilgain et al.*, 1965; *Feely et al.*, 1966; *Jouzel et al.*, 1979; *Oerter et al.*, 1999; *Pourchet et al.*, 1983, 1997, 2003; *Magand et al.*, 2004], with the maximum radioactivity peaks in 1954–1955 and 1965–1966 used as convenient horizons for dating snow and ice layers and measuring SMB. *Jouzel et al.* [1979] observed the largest tritium peak at the South Pole during 1966. On the basis of comparison between the tritium profile in snow layers at Dronning Maud Land and the tritium distribution at the Kaitoke (New Zealand) International Atomic Energy Agency (IAEA) station, *Oerter et al.* [1999] attributed the highest values to the 1964–1969 years. Best fit depth–time scales were used to transform the measured depth profiles to time series similar to the tritium content of precipitation at Kaitoke. In Antarctica, total β counting remains the most frequent radioactivity measurement [*Picciotto and Wilgain*, 1963; *Lambert et al.*, 1977; *Pourchet et al.*, 2003]. As a consequence, there is a great deal of data on the history of artificial radioactive fallout over Antarctica since the 1950s; thus total β activity is a well-constrained method used to identify radioactive reference horizons for estimating SMB in accumulation areas. In situ γ ray spectrometers for ice boreholes [*Pinglot and Pourchet*, 1981] enable a rapid determination of the mean annual accumulation from 1965 to present by measuring the radioactive fallout layers. This provides valuable information in the field to estimate the depth range necessary to reach dating horizons (like volcanic signals) as previously cited.

2.4.2.3. Radiochronology

[75] As in many geoscientific disciplines, the natural decay of radioactive isotopes can be used to determine the age of an investigated sample, commonly referred to as *radionchronology*. A common example for ice is ^{210}Pb, a natural β emitter. It is a long-lived daughter nuclide (half-life 22.3 years) belonging to the ^{238}U family [*Picciotto et al.*, 1971]. Its presence in the atmosphere is a result of the α radioactive decay of radon gas (^{222}Rn). The atmosphere is the major source of ^{210}Pb deposited on the Antarctic ice sheet. Many factors contribute to the low radon (and its daughter nuclide) concentrations in Antarctica [*Pourchet et al.*, 1997, 2003]. These include ice that prevents the escape of radon from the Antarctic geological basement, the surrounding ocean without radon emission, and the time required for air masses to move from continental areas (the main source of radon emission) to the south polar region. Very little ^{210}Pb was produced by the nuclear explosions during the 1960s.

[76] Studies carried out during this period show that the quantity of ^{210}Pb deposited at a given place, averaged over a year or more, appears to be constant and not to have changed significantly since the advent of H-bombs [*Bull*, 1971]. As a result, the natural ^{210}Pb continuous flux deposition over the Antarctic ice sheet could be used for dating purposes over periods of the past 100 years. Because of radioactive decay, the natural ^{210}Pb activity decreases with depth of the firn and ice layers. The age of a firn layer at z meters depth is thus given by

$$t = \frac{1}{\lambda} \ln \frac{A_0}{A_z}, \tag{3}$$

and the average rate of accumulation of snow above this depth is given by

$$\dot{b} = \frac{z\lambda}{\ln \frac{A_0}{A_z}}, \tag{4}$$

where A_0 and A_z are the ^{210}Pb activities per unit weight of snow at the surface and at a depth of z meters, respectively, and λ is the ^{210}Pb decay constant. The first attempts at dating firn or ice layers in the polar regions with the ^{210}Pb method were successfully validated by other direct measurements [*Goldberg*, 1963; *Picciotto et al.*, 1964; *Crozaz et al.*, 1964; *Nemazi et al.*, 1964; *Crozaz and Langway*, 1966]. We have to stress that accurate dating of snow by ^{210}Pb is only possible with the following assumptions: (1) The mean ^{210}Pb activity in precipitation has remained constant during the last two centuries, (2) the ^{226}Ra concentrations within the firn/ice samples are negligible, (3) no diffusion of air into the ice sheet occurs (bearing additional ^{222}Rn), and (4) ^{210}Pb remains at its initial place of deposition (no vertical transportation by water from melting snow). Even if none of these assumptions are perfectly fulfilled, we argue that a generally reliable determination of SMB over the past few decades is achievable by this method in areas exempt from melting, i.e., in accumulation zones [*Pourchet et al.*, 1997, 2003].

2.4.2.4. Optimal Strategies for Age Estimates

[77] Counting seasonal cyclicity of chemical/isotopic parameters (δ^{18}O, δD, H_2O_2, MSA, Na^+, NO_3^-, nss SO_4^{2-}, etc.) is the most precise dating method, but it is also the most time- and equipment-intensive method. A multiparameter approach using several high-resolution chemical records (as shown in Figure 9d) is therefore the most reliable way to derive annual dating. Because several atmospherically derived chemical species peak during different times of the year, it may thus be possible to ensure that no year is missing [e.g., *Udisti*, 1996; *Steig et al.*, 2005]. In general, however, seasonal cycles are difficult to observe at sites with low accumulation (below about 80–100 kg m^{-2} a^{-1}), such as the polar plateau, because the seasonally deposited chemical or physical signals often have been strongly erased or reworked by the action of wind at the surface. Applying these methods to discrete samples (as from snow pits) is ineffective in the inner part of East Antarctica, e.g., in the Dome C area, unless a high (subcentimeter) sampling resolution is used. At most low accumulation areas, high-resolution continuous electric (DEP and ECM) and chemical measurements (CFA, FIC, CMDS) and the simultaneous analysis of multiple-parameter records have to be performed in order to detect seasonal signals in the physical and chemical properties of cores and thus achieve annual dating. During the past decade, high-

resolution continuous methods have been used in many studies, such as for the EPICA presite surveying in Dronning Maud Land [*Sommer et al.*, 2000b]. Thus, it was possible to perform annual layer counting back several hundred years at several places on the East Antarctic plateau with SMB below 80 kg m^{-2} a^{-1}, e.g., at the South Pole [*Meyerson et al.*, 2002] or Dronning Maud Land [*Sommer et al.*, 2000a], and even below 50 kg m^{-2} a^{-1} from an ice core site located approximately 600 km south of Dome A (D. A. Dixon, personal communication). Such results imply that wind scouring does not suffice to erode annual signals at these sites. However, the identification of annual layers does not unequivocally imply the possibility of resolving accumulation history with representative values (±10%) of annual resolution [*Frezzotti et al.*, 2007]. When continuous sampling is not available, reference horizon dating may be the only available method at low accumulation sites. In such cases, only a mean accumulation rate between two reference horizons can be calculated. This precludes these records from studies interested in the interannual variability in accumulation, for instance, to assess changes in climate, to account for flux of chemical compounds, etc.

2.4.3. Accumulation Errors From Pit and Core Measurements

[78] Annual layer counting using seasonal cyclicity of multiparameters can be fine tuned using atmospheric thermonuclear bomb test layers and volcanic peaks as fixed time markers to achieve the best accuracy for the evaluation of snow accumulation in cores. Dating errors may arise from incorrect or nonidentification of seasonal signals (e.g., hiatus in accumulation or erosion) and from incorrect identification or errors in identification of historical volcanic or nuclear bomb layer markers. Dating errors could be ±1 year for the depth coincident with the marker, but they could be higher at points that are far from dated reference horizons [e.g., *Steig et al.*, 2005].

[79] The associated relative errors in accumulation $\dot{b}$ derived from snow pits, firn, and ice cores (Table 2) can be expressed as

$$\frac{\delta\dot{b}}{\dot{b}} \leq \sqrt{2\left(\frac{<0.5l}{\Delta z}\right)^2 + \left(\frac{\delta(\Delta t)}{\Delta t}\right)^2 + \left(\frac{\delta(\Delta m)}{\Delta m}\right)^2}, \qquad (5)$$

where l is sample length, Δz and Δt are the depth and age difference between the dating horizons used, and Δm is the mass difference of the two columns above the two dating horizons, sometimes expressed in meter water equivalent depth; $\delta(\ )$ is the uncertainty of the parenthesized variable, e.g., the error in the date of volcanic deposition. When the sample length is relatively large compared to the depth between dating horizons, the first term on the right-hand side is important. On the other hand, if the age–depth profile is derived from high-resolution measurements like electrical methods, the first term can be neglected. The error estimate only applies at the identified dating horizons. Any physical variation, i.e., change in accumulation, between the dating horizons is not captured by this error estimate. The typical error $\delta\dot{b}$ in $\dot{b}$ is less than 10% for both snow pits and cores.

[80] The extraction of snow accumulation values from cores requires estimating the effects of thinning due to ice dynamics (densification, compression, flow, etc.). Vertical thinning of surface layers is predictable from the sum of horizontal strain rates. As firn cores are relatively shallow (less than 50–100 m) in comparison to the total thickness of ice sheets (more than 1000 m), thinning could be assumed to be less than 5%, implying negligibility. In cold, large ice sheets like the one in East Antarctica, the strain rates are expected to be around 10^{-4} a^{-1}. On fast moving glaciers, ice streams, and ice shelves, they can sometimes get close to 10^{-2} a^{-1}, and as a result, cores that represent several hundred years can be significantly affected by thinning. As an example, consider a 100-year-old layer. If both horizontal strain rates are 10^{-4} a^{-1}, the 100-year-old layer should have thinned by only 2%, but if strain rates are 10^{-2} a^{-1}, the layer is thinned to 13% of its original thickness. For a 100-m core with around 200 kg m^{-2} a^{-1} accumulation, corresponding to 300 years of accumulation history, and at a strain rate of 10^{-3} a^{-1}, a 55% thinning of the original layer thickness should result. Whether layer thinning takes place or not has thus to be evaluated for each site individually.

2.5. Laterally Continuous Measurements: Ground-Penetrating Radar

[81] GPR maps the internal structure of the firn column along a profile from the surface. Variation in depth of continuous internal layers of equal age along the profile yields information about the accumulation pattern. Combining GPR with highly resolved ice core data is required to date the internal layers.

[82] Over the last few decades, a number of methodological studies have been carried out to investigate the suitability of high-resolution GPR for mapping accumulation rates along surface profiles. The results demonstrate that GPR profiling of firn stratigraphy, coupled with precise GPS measurements is capable of complementing traditional methods like stakes, snow pits, and cores to map accumulation rates and to improve the understanding of spatial accumulation patterns. In the literature, terms like GPR (traditionally used in engineering geophysics), ice-penetrating radar, snow radar, and sometimes radio echo sounding are used synonymously. Here, we stick to the first term and imply investigations with a phase-sensitive radar. Commercial and easily transportable GPR systems have become available and are widely used to survey the near-surface firn (<100–200 m). Over recent years this had the consequence that GPR was routinely employed during operational surveys to map the internal structure of the firn column and to determine regional surface accumulation, e.g., during most campaigns related to ITASE and EPICA [*Isaksson and Karlén*, 1994; *Richardson et al.*, 1997; *Richardson and Holmlund*, 1999; *Nereson et al.*, 2000; *Richardson-Näslund*, 2001; *Urbini et al.*, 2001; *Frezzotti et al.*, 2002b; *Frezzotti and Flora*, 2002; *Sinisalo et al.*, 2005; *Richardson-Näslund*, 2004; *Rotschky et al.*, 2004; *Karlöf*, 2004; *Spikes et al.*, 2004; *Eisen et al.*, 2005; *Frezzotti et al.*, 2005; *Arcone et al.*, 2005a, 2005b; *Jacobel et al.*, 2005; *Anschütz et al.*,

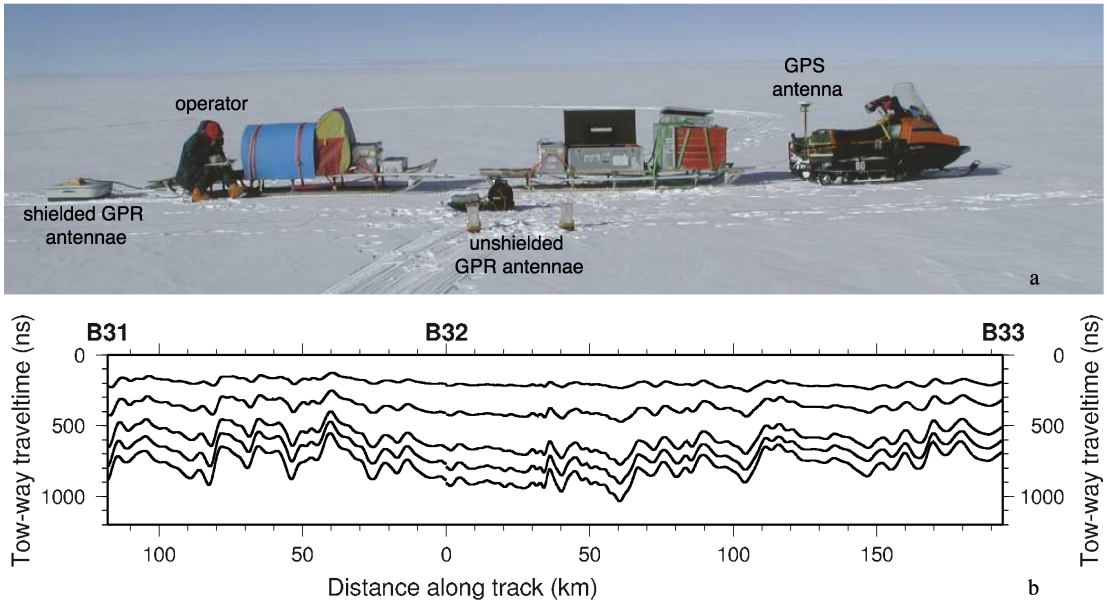

Figure 10. (a) Setup of GPR measurements: For common offset surveys, a shielded antenna (left) is pulled by a snowmobile. The GPS antenna is mounted at the rear of the vehicle (right). Common midpoint surveys utilize separate transmitter and receiver (front). (b) Sample profile of five internal horizons tracked in common offset GPR data over 300 km in Dronning Maud Land [*Eisen et al.*, 2004].

2007, 2008]. High-frequency GPR in the range of 100 MHz to 1 GHz is capable of imaging the structure of the upper tens to hundreds of meters of the ice column in high resolution. On the Antarctic inland plateau, this provides a means to derive information about the local SMB over the last tens of years to about 1000 years. It has thus become possible to map accumulation rates and their spatial variations along continuous profiles within the upper parts of the snowpack.

2.5.1. Technical Background and Functional Principle

[83] Application of GPR for imaging the snow and firn column at shallow depths usually utilizes a transmitter and receiver moved at a fixed distance from each other across the surface along the survey profile. This setup is called common offset (CO), referring to the constant distance between transmitter and receiver. The device is either towed by hand, snowmobile, or tractor, and the geographical position is usually obtained from kinematic GPS measurements (Figure 10a). At defined intervals, either at equal temporal or spatial increments, the transmitter emits an electromagnetic pulse into the snow column. Distances between consecutive measurements vary, depending on the system performance, between about 0.1 and 10 m. The pulse penetrates into the snow column and is partly reflected where the complex dielectric ε^* constant changes. The reflected signals travel back to the receiving antenna at the surface. The complete signal is recorded as a function of traveltime of the transmitted radar pulse.

[84] Three factors are known to change the dielectric constant in firn and ice: gradients in the real part, the permittivity, are mostly related to density; they dominate reflections in the upper hundreds of meters. Variations in the imaginary part are proportional to conductivity, are related to acidity, and depend on frequency. They are the governing reflection cause in deeper ice. A third mechanism, proposed by *Harrison* [1973], involves dielectric anisotropy of the crystal fabric, but it becomes significant only at the deeper levels (>500–1000 m) of the ice sheet where changes in anisotropic crystal fabrics could develop [*Fujita et al.*, 1999; *Matsuoka et al.*, 2003, 2004; *Eisen et al.*, 2007]. Other radar techniques are based on frequency-modulated continuous wave (FMCW) transmissions or stepped-frequency radars [*Kanagaratnam et al.*, 2001; *Corr et al.*, 2002]. Although the technical details on data acquisition and processing are different, the results are the same, an image of subsurface reflections along a profile (Figure 4).

[85] Studies of dielectric properties of ice and internal radar reflection horizons (IRHs, outlined in Figure 10b) show that most processes forming electromagnetic reflectors take place at the glacier surface at approximately the same time [*Gudmandsen*, 1975]. (Details on physical structure and processes related to the origin of reflections in firn are given by *Kohler et al.* [2003], *Eisen et al.* [2003a, 2003b], and *Arcone et al.* [2005a].) While some significant progress in understanding this process has been made in recent years [*Eisen et al.*, 2003b; *Arcone et al.*, 2005a], it is still not entirely clear how the GPR produces a continuous reflecting horizon in the ice, visible over hundreds to even thousands of kilometers. At present, there remains some uncertainty about how the material properties in firn combine to form the continuous reflecting horizons. It does

seem apparent that both density and chemical properties in the ice contribute, but since layers are visible even where the wavelength of the radar exceeds the annual layer thickness, it is clear that at least in the shallow regions some complex interference pattern is generally being observed. However, the isochronity of observed reflections has been proven heuristically by connecting firn and ice core drill sites [*Jacobel and Hodge*, 1995; *Spikes et al.*, 2004; *Eisen et al.*, 2004; *Frezzotti et al.*, 2005] and by comparing accumulation rates deduced from GPR with those measured along surface stake lines [*Vaughan et al.*, 2004]. The submergence rate of an isochrone surface is determined by interaction of the surface accumulation with the flow field [*Robin et al.*, 1969; *Gudmandsen*, 1975; *Clough*, 1977; *Millar*, 1981; *Bogorodsky et al.*, 1985; *Moore*, 1988]. Continuously moving the radar system along a surface profile and recording individual traces at high enough spatial repetition rates (on the order of decimeters to meters) makes it possible to continuously image the internal reflections along the profile (Figure 10b). As the continuous internal reflection horizon corresponds to an isochronous layer, the spatial variation of layer depth provides information on variations in the accumulation rate and changes due to ice sheet dynamics. The latter can mostly be neglected in the upper meters of the ice column in regions of slow flow (see previous discussion on accumulation errors from cores in section 2.4.2.3).

2.5.2. Accumulation Estimates From GPR

[86] On the Antarctic plateau, the isochronous reflections can be followed over hundreds of kilometers. The variation in depth of an individual reflector already provides a qualitative picture about the variation of surface accumulation along the profile. To determine quantitative accumulation estimates, several processing steps are necessary [*Arcone et al.*, 2005a; *Rotschky et al.*, 2004]: (1) track one or more internal reflections along the profile; (2) convert the radargram from time to depth domain along the whole profile; (3) date the isochrones at one or more points (the isochronity assures that the age can be distributed along the profile); (4) determine the cumulative mass as a function of depth from the surface to the reflector depth along the profile; and (5) calculate the average SMB by dividing the cumulative mass by the respective age of the reflector.

[87] These processing steps involve several other input properties. We now discuss details and peculiarities of each step.

2.5.2.1. Tracking Internal Reflections

[88] After digital data processing of the raw radar data (horizontal stacking, filtering, gain control), continuous reflections can be followed in the radargrams. Depending on data processing and display, it is possible to identify a single phase, for instance, the first break, and track that along the whole profile, or track the maximum amplitude when the signal envelope is used. Tracking can be performed manually, trace by trace, or semiautomatically. Semiautomatic tracking is implemented in a number of programs, mainly based on experiences in the seismic exploration industry. The tracking algorithm exploits the coherency of signal features (e.g., minimum, maximum, or zero amplitude) above noise level to automatically detect the same feature within a prescribed time window in adjacent traces and follows it as long as a similarity criterion is fulfilled. The tracking process is observed by the user and requires manual interaction in case of a low signal-to-noise ratio.

2.5.2.2. Time-to-Depth Conversion

[89] Knowledge of the variation of the electromagnetic wave speed with depth is necessary in order to be able to convert the observed reflections from time to depth domain. Some authors directly calculate water equivalent depth of a horizon to derive accumulation [*Vaughan et al.*, 1999b; *Spikes et al.*, 2004]. The wave speed is mainly a function of density; contributions from conductivity can be neglected at radio frequencies. Different methods were developed to determine the wave speed–depth function. The most direct method involves the measurement of the dielectrical properties along cores by means of DEP (see section 2.4.1) [*Moore and Paren*, 1987; *Wilhelms et al.*, 1998; *Karlöf*, 2004; *Wilhelms*, 2005], from which the interval velocities can be directly calculated. Instead of the dielectrical properties, density profiles from snow pits, firn, or ice cores are also often used to determine the electromagnetic wave speed from mixture models [*Robin et al.*, 1969; *Clough and Bentley*, 1970; *Kovacs et al.*, 1995; *Richardson et al.*, 1997; *Urbini et al.*, 2001; *Eisen et al.*, 2002; *Spikes et al.*, 2004; *Anschütz et al.*, 2006]. The downhole radar technique makes use of a drilled hole to record traveltimes as a function of depth of a reflecting target lowered in the hole [e.g., *Jezek and Roeloffs*, 1983; *Clarke and Bentley*, 1994]. Interval velocities can then be derived from the transmitter–target–receiver traveltime as a function of depth. An indirect method known from reflection seismic exploration is the common midpoint (CMP) survey technique [*Yilmaz*, 1987]. It is a special case of the radar wide-angle reflection and refraction measurement [*Annan and Davis*, 1976; *Jezek and Roeloffs*, 1983; *Morey and Kovacs*, 1985; *Bogorodsky et al.*, 1985] and has been widely applied for radar measurements in glaciology [e.g., *Blindow*, 1994; *Hempel et al.*, 2000; *Murray et al.*, 2000; *Eisen et al.*, 2002]. It makes use of a special setup of linear geometry, such that the points of reflection at a certain depth remain constant with increasing offset between transmitter and receiver. The velocity-depth function can be inferred from the increase of traveltime with offset, assuming near-horizontal reflectors.

2.5.2.3. Age Estimates of Reflection Horizons

[90] Dating IRHs is achieved by transferring age-depth distribution, as obtained from snow pit and cores as described in section 2.4.2, to the respective depth of the IRH at the location where the age-depth distribution was measured. This is usually achieved by mere comparison or correlation techniques in the depth domain. A new approach utilizes numerical forward modeling of radargrams, based on dielectric profiling of ice cores, to relate depth (and thus age) to the time domain of the radar data [*Eisen et al.*, 2004]. A problem related to the dating of snow layers by core analysis comes along with the spatial separation of GPR

profiles and coring sites. In several cases, the GPR soundings were not always made directly over the exact coring point or in the same year; in some cases, the distance between the coring site and the radar survey exceeded 10 m [*Richardson-Näslund*, 2001]. In other cases, it is not possible to follow isochrones all the way to a coring site, and thus it is not always possible to determine the age of a snow layer by direct comparison with core or pit data. Such a layer can still be dated indirectly using overlapping sections of other internal layers that could be dated directly against cores and pits. This method allows one to obtain approximate estimates of spatial variability in accumulation rate that would otherwise be unobtainable [*Richardson-Näslund*, 2001]. Even if absolute dating is not possible, a qualitative interpretation of spatial accumulation variability can still be achieved [*Vaughan et al.*, 2004].

2.5.2.4. Cumulative Mass

[91] Integration of measured density profiles yields the distribution of cumulative mass with depth. (For more details on density measurements, see section 2.1.) Generally, snow/firn density increases with increasing depth. Thus, the density-depth profile influences the wave speed–depth profile and cumulative mass value. Cumulative mass is usually calculated from the surface down to the depth of the radar reference layer. However, depending on the time interval of interest, it is also possible to calculate the mass difference between two internal reflectors to determine spatial variability of past accumulation rates, similar to firn and ice core studies.

[92] One question coming along with the spatial extent of radar profiles is the lateral homogeneity of density-depth distributions. Snow and firn densities in the dry zone are predominantly determined by overburden pressure, which is governed by local meteorological parameters: temperature, wind, and accumulation rate [*Craven and Allison*, 1998; *Kameda et al.*, 1994]. Depending on the study area, the distributions can be homogeneous over hundreds of kilometers on the polar plateau and in particular at ice divides and domes [*Frezzotti et al.*, 2004; *Richardson-Näslund*, 2004; *Rotschky et al.*, 2004; *Arcone et al.*, 2005b] or could vary considerably at places with high spatial accumulation variability due to strong wind erosion [*Richardson et al.*, 1997; *Spikes et al.*, 2004; *Frezzotti et al.*, 2005]. At Dome C and Talos Dome, dedicated density profile analyses from a number of cores and pits reveal no detectable geographical variation in density or compaction within a 50-km diameter of the dome areas [*Frezzotti et al.*, 2005, 2007; *Urbini et al.*, 2008]. In contrast, especially in coastal regions, variations on short distance scales can be significant [*Richardson-Näslund*, 2004; *Vaughan et al.*, 2004; *Frezzotti et al.*, 2005; *Anschütz et al.*, 2006]. In the latter case, density profiles need to be laterally interpolated to provide information along the GPR profiles. The largest variability in density is usually in the uppermost 3–20 m.

[93] Density data surveyed by core and pit are fitted with polynomial or logarithmic functions, usually yielding a correlation coefficient (R^2) of more than 0.9 for measured and computed densities [e.g., *Richardson et al.*, 1997; *Frezzotti et al.*, 2005]. Because of a change of density function with depth, the density profiles should cover the snow radar investigation depth. The uncertainties associated with each cumulative mass measurement vary with depth.

2.5.3. Errors of GPR-Based Accumulation Estimates

[94] A number of factors determine the final uncertainty of an accumulation estimate based on GPR (Table 2). They can be separated by errors related to determining the depth of the reflector, the age of the reflector, and the cumulative mass above the reflector. Other errors arise by spatially interpolating or extrapolating the density information along a radar profile. Depending on the region of investigation, the density–depth and thus the mass–depth and wave speed–depth distributions can be very homogeneous, e.g., in undisturbed regions on the Antarctic plateau, or very inhomogeneous, as near coastal sites and slope areas.

[95] The operation frequency of the radar system and the characteristic of the source signal determines the possible vertical resolution of a reflector. Theoretically, a quarter of the wavelength is the highest resolution that can be achieved. Another consideration is the ability to separate two neighboring reflectors. According to the Ricker criterion, they can be separated when the traveltime difference in the reflected signals is larger than half the cycle duration of the signal. However, most radars transmit a source signal which contains more than a single cycle, thus reducing the resolution. Two signals can then be separated when the traveltime difference exceeds half the pulse width. GPR is usually operated in a bistatic mode, which means separate antennae at a certain distance (dm to m, depending on frequency) for transmission and reception of the radar signal. This causes an error in estimated depth, especially for reflectors close to the surface (see *Pälli et al.* [2002] for a discussion).

[96] Accuracy of the traveltime–depth conversion depends on the source of information for the velocity profile (e.g., density measurement along a core or from common midpoint radar). Uncertainties in the age estimate of a reflector are caused by the initial uncertainty of the underlying age–depth scale (snow pit, firn, or ice core) and the transfer of the age information for, e.g., a core to the reflector. (For more details on age estimates, see section 2.4.2.) The error in accumulation depends finally on the accuracy of the depth-integrated density profile. Small-scale variations in density, like ice lenses or wind crusts, are averaged out by the integration, and neither cause large errors in cumulative depth or wave speed.

[97] *Spikes et al.* [2004] pointed out that uncertainties are based mainly on the three components: layer thinning due to ice advection, the procedure for depth calibration, and the isochronal accuracy of each horizon. Their results indicate that uncertainties at a firn depth of 10 m are about 4% of the calculated snow accumulation and decrease to 0.5% at a firn depth of 60 m. In general, conservative uncertainty estimates of SMB derived from GPR are some 5% on the polar plateau, most of which stems from the uncertainty in dating. A summary of factors contributing to errors is provided in Table 2.

2.5.4. Spatial Variability of SMB From GPR

[98] Along the Terra Nova Bay–Dome C traverse, standard deviation of variability decreases generally from the coast (47%) to the ice divide (3%) [*Frezzotti et al.*, 2004]. However, sites characterized by relatively complex surface morphology with abrupt changes in slope along wind direction show higher standard deviation (34–47%) than sites that have a low slope along wind direction (5–10%). High standard deviation in spatial variability is also observed inland in the areas of megadune fields (24% [*Frezzotti et al.*, 2002b, 2005]). The lowest values are observed at domes and ice divides (3–9%). Changes in spatial distributions have been observed over the last few centuries using GPR, with a decrease in SMB gradient along the wind direction at Talos Dome and a counterclockwise rotation of SMB distribution in the northern part of Dome C. Observations at Dome C reveal a significant increase in accumulation since the 1950s, which could correlate to altered snow accumulation patterns due to changes in snowfall trajectory. Snow accumulation mechanisms are different at the two domes: a wind-driven snow accumulation process operates at Talos Dome, whereas snowfall trajectory direction is the main factor at Dome C [*Urbini et al.*, 2008].

[99] Along the transect that crosses Talos Dome, analysis of spatial variability shows that in the coastal area, spatial variability reaches 200 kg m^{-2} a^{-1} over 1 km and wind-driven sublimation values may be as high as 260 kg m^{-2} a^{-1}. In the plateau area, spatial variability reaches 40 kg m^{-2} a^{-1} over 1 km, and wind-driven ablation is as high as 50 kg m^{-2} a^{-1} [*Frezzotti et al.*, 2007]. Redistribution processes are only present on a local scale; wind-driven sublimation values represent 20–75% of solid precipitation. Depositional features are very rare, related to the formation of transverse dunes and negligible in the SMB. The spatial variability of SMB at the kilometer scale is 1 order of magnitude higher than its temporal variability (20–30%) at the centennial timescale [*Frezzotti et al.*, 2004].

[100] The spatial variability at sites very close to the coast in Adélie Land is less than 10%. Along coastal and inland slopes the spatial standard deviation, also based on stake line data, increases from 20% to more than 50%. On the plateau the spatial variability varies up to about 20%, but in the undisturbed part of the plateau it was below 10%. Variations of the same order in the three regimes, coastal, transition, and plateau, are evident from stake line data [*Pettré et al.*, 1986], although measurements are less sound than GPR results.

[101] On the plateau in DML, the small-scale variation in accumulation is on the order of 5–15% of the mean accumulation [*Richardson-Näslund*, 2001; *Rotschky et al.*, 2004; *Eisen et al.*, 2005]. Small-scale means over distances of 10 km compare to mean values over 100 km. In the perimeter of the EPICA deep drilling site, accumulation variability is less than 15% on average, but accumulation gradients can be up to 2.5 kg m^{-2} a^{-1} over 1 km [*Eisen et al.*, 2005]. Averaged SMB values for the last 150 years decorrelated over a distance of about 10 km [*Rotschky et al.*, 2004]. In contrast, increased variability of up to 45% [*Richardson and Holmlund*, 1999] occurs on slopes and near the coast. At Camp Victoria, Amundsenisen (2400 m above sea level), and Camp Maudheimvidda (362 m asl), both in DML, *Holmlund et al.* [2000] performed 10–20 × 20 km^2 grid net studies to determine the spatial variability in an area with rather low ice flow velocities. They mapped the top 30–40 m and related the observed layers to the layer depth at a drilling spot at the center of the grid. At Maudheimvidda, the variation in layer depths amounted to 40 to 240% of the layer depth at the center of the grid. According to radar data, the pattern seen at the surface could be seen some tens of meters down into the snowpack. At altitudes around 2200–2500 m, at Camp Victoria, the variability was somewhat less pronounced but still on the order of 10%.

2.5.5. Point Measurements Versus GPR-Based SMB Estimates

[102] One could expect that point measurement and GPR yield principally different results because they sample different areas: the cores, stakes, and ultrasonic sensors sample centimeter-scale areas (2–10 cm), while GPR works at the meter scale. Accumulation rates derived by point measurements and GPR methods [*Richardson-Näslund*, 2001, 2004; *Rotschky et al.*, 2004; *Vaughan et al.*, 2004; *Frezzotti et al.*, 2005; *Anschütz et al.*, 2007; *Frezzotti et al.*, 2007] agree fairly well, the discrepancy ranged from a few percent to 20%, and the results do not indicate any systematic errors. *Frezzotti et al.* [2005] found major differences between point measurements and GPR (20%) along the Terra Nova Bay–Dome C traverse in regions of large spatial variability in SMB (47% over 15 km at maximum). At this site, two cores were drilled a few tens of meters apart and show a 13% difference in accumulation for the tritium/β marker horizons [*Frezzotti et al.*, 2005]. Detailed chemical studies in 16 × 6 m snow pits combined with GPR measurements on the polar plateau in DML found that the variability of snow layer thickness at the microscale was on average 9% [*Stenberg et al.*, 1999]. A qualitatively good comparison between stake line measurements and GPR layer architecture enabled *Vaughan et al.* [2004] to deduce that the observed IRH are isochrones. For layers several tens of meters deep, covering more than a century, a problem exists when comparing core and GPR measurements when GPR traverses pass several kilometers away from the core. Although values are still comparable, a detailed match is difficult [*Rotschky et al.*, 2004].

3. REPRESENTATIVITY AND LIMITATIONS

[103] Section 2 presented the different techniques carried out on the ground to determine accumulation, discussed difficulties associated with the measurements, and provided error estimates. Once values for the SMB are available, one asks what these values actually mean? Are they just valid for a short period of time, or just in the very vicinity of the measurement locations, or both? This brings us to the issue of the representativity, which is fundamental, as the inter-

pretation of SMB requires consideration of the climatic context, also on larger temporal and spatial scales. In this section we summarize important accumulation characteristics derived from the different measurement techniques and discuss the spatial and temporal representativity of the data.

[104] For the application of SMB data for the different purposes described in section 1, the three key questions are (1) What is the temporal representativity? (2) What is the spatial representativity? (3) Are spatial and temporal signals linked? Related issues are the stability of accumulation patterns in time. Do values at different locations with different mean SMB fluctuate synchronously, i.e., do they covary? Or do temporal changes, for instance, induced by short- and long-term local climate changes, also change the accumulation pattern, resulting in independent fluctuations? Likewise, the effect of ice flow has to be taken into account for core and GPR interpretations on longer timescales, as advection causes mixing of temporal signals with spatial information. For a reliable interpretation of SMB data, these factors have to be separated.

3.1. Temporal Representativity

[105] Time series obtained from stakes and ultrasonic measurements indicate a large interannual variability in accumulation, with variations of up to nearly 50% with respect to the 50-year average accumulation from firn cores [*Frezzotti et al.*, 2007]. *Monaghan et al.* [2006] combine model simulations and observations primarily from cores. They point out that yearly and decadal snowfall variability at local and continental scales is very large. Comparison between stake and core values makes it possible to measure the frequency distribution and thus to infer the probability of identifying missing layers and also the lowest and highest SMB values in cores. Significant differences between core and stake measurements have been observed at sites with SMB < 200 kg m^{-2} a^{-1} [*Frezzotti et al.*, 2007]. Reasons could be the misidentification of annual layers from seasonal signals and the consequent error in the definition of high and low values (values with differences >40% with respect to average value) or/and the slight variations in input timing of the chemical or isotopic composition (e.g., interannual variability in peak-input timing of sulphate could vary by weeks). The misidentification could be due to large annual peaks that could be interpreted as a double year or to two adjacent peaks that will not be stratigraphically detectable because they are sufficiently narrow and could therefore be interpreted as a single year. Signal noise is produced principally by postdepositional processes such as wind erosion, drift, and redeposition. Postdepositional noise primarily influences the high frequencies [*Fisher et al.*, 1985], and misidentification of an annual layer results in overestimation of accumulation in 1 year and to an underestimation in the preceding or following year. Both noise and error reduce the temporal representativeness of the time series.

[106] At the South Pole, the frequency distribution of stratigraphic layer thicknesses in cores and in a snow pit is not compatible with a significant number (between 1% and 5% probability) of missing layers associated with zero accumulation years inferred from measurements of stake heights. The original implication that a large percentage of years (about 10%) is missing from the ice core stratigraphy [*Van der Veen and Bolzan*, 1999; *Mosley-Thompson et al.*, 1995] has been found to be an overestimate [*Mosley-Thompson et al.*, 1999] (see also section 2.2.4). In general, stake or ultrasonic measurements are the only way to detect zero accumulation or erosion values on an annual or seasonal scale.

[107] Analysis of Gaussian distributions of accumulation versus SMB from stake farms shows that only sites with SMB > 750 kg m^{-2} a^{-1} have present values that are representative to within ±10% at an annual scale [*Frezzotti et al.*, 2007]. The SMB distribution shows that more than 80% of stakes at sites with low SMB around 80 kg m^{-2} a^{-1} and more than 40% of stakes at high SMB sites (~250 kg m^{-2} a^{-1}) present SMB differences of more than ±10% with respect to the mean. The temporal representativity increases with multiyear averages: for high SMB, values are representative at ±10% using three cumulative years; for a SMB of 80–150 kg m^{-2} a^{-1}, using 5–7 cumulative years is necessary [*Frezzotti et al.*, 2007]. *Goodwin et al.* [2003] propose that the 3-year running mean accumulation data from eastern Wilkes Land cores (235–570 kg m^{-2} a^{-1}) are representative for the precipitation minus evaporation signal rather than the local microrelief noise. The same timescale is found to be significant by wavelet analyses of electrical records by *Karlöf et al.* [2006]; that is, the correlation between different records is highest in the 1- to 3-year period. This is attributed to the fact that most material emitted by volcanic eruptions is removed from the atmosphere within 3 years of eruptions, including deposition on the ice sheets. Their study implies that the temporal and spatial representativity of SMB and the records from which it is derived are not necessarily the same. At the South Pole, *McConnell et al.* [1997] computed the average time (310 years) required to statistically ensure that each monthly SMB record within the year is adequately represented in the time average. They also pointed out that the averaging of adjacent cores would decrease the time window proportionally. *Van der Veen and Bolzan* [1999] pointed out that noise could be removed using a Gaussian weighting function with a standard deviation of about 5 years. At the coastal region of Adélie Land, reevaluation of older stake line data from *Pettré et al.* [1986] indicates interannual standard variations on the order of 45%.

[108] *Genthon* [2004] calculates the variability and the radius of decorrelation of precipitation and precipitation minus evaporation over Antarctica from climate models and meteorological analyses. Interannual variability ranges from 5 to 40% of the mean. On the century scale, however, a number of GPR studies (aiming at the spatial characteristics presented next) reveal that the accumulation patterns are stable in time.

3.2. Spatial Homogeneity and Variations

[109] Stake farms and lines have given an indication of the spatial variability in SMB on various scales, e.g., the quasi-uncorrelated annual accumulation caused by microrelief at low-accumulation sites on the plateau. Given the amount of resources required to deploy and maintain stake networks, however, the volume of data that they have produced is generally low. The emergence of GPR techniques has dramatically increased our ability to measure, and therefore understand, the spatial variability in SMB. A number of GPR surveys (see section 2.5.4) reveal that spatial variability of SMB at the kilometer scale can be up to 1 order of magnitude higher than its temporal variability (maximum 20–30%) at the multidecadal/secular and centennial timescale. Generally, the patterns of spatial variability are stable in time at least over a couple of decades to centuries. Stationary features are of comparable length scales (kilometers to tens of kilometers) [*Richardson-Näslund*, 2004; *Vaughan et al.*, 2004; *Frezzotti et al.*, 2004; *Eisen et al.*, 2005]. In rare cases, like the East Antarctic megadune fields, migrating accumulation patterns occur [*Frezzotti et al.*, 2002b]. Recently, migrating features on the 5-km scale were observed close to the coast [*Anschütz et al.*, 2006], although their variations are less pronounced and laterally extensive than megadunes.

[110] Several authors demonstrate the dependence of SMB on temperature, elevation, saturation vapor pressure, and distance from the open ocean [e.g., *Muszynski and Birchfield*, 1985; *Giovinetto et al.*, 1990; *Fortuin and Oerlemans*, 1990]. Although common, large-scale patterns are not always simple [e.g., *Smith et al.*, 2002]. The high spatial variability of SMB on the 1- to 10-km scale is mostly explained by wind-driven processes, being a function of surface slope [*King et al.*, 2004; *Frezzotti et al.*, 2004]. Likewise, the SMB of annual stake measurements is also related to morphology via the surface slope [*McConnell et al.*, 1997; *Frezzotti et al.*, 2005]. However, *Frezzotti et al.* [2004] point out that along some transects (Talos Dome, Dome C) the maximum value of snow accumulation is highly correlated with firn temperatures and represents the snow precipitation minus surface sublimation (ablation not induced by wind). The difference between the maximum and minimum SMB values at these sites represents mainly ablation processes driven by katabatic winds. These wind-driven sublimation phenomena, controlled by the slope along the prevalent wind direction, have considerable impact on the spatial distribution of SMB. They sublimate and export huge quantities of snow into the atmosphere and then into the ocean, leading to a nonnegligible term in continental SMB studies [*Frezzotti et al.*, 2004, 2007]. The direct snow redistribution process is local (e.g., sastrugi formation) and has a strong impact on the annual variability of accumulation at the annual/meter scale (i.e., noise in ice cores).

[111] Whereas SMB based on GPR and stake lines shows that decadally averaged spot measurements are only representative within a small area of a few square kilometers around the site (i.e., indicate relatively short correlation lengths), precipitation is much more homogeneous. On the basis of the analysis of climate models and meteorological data, the decorrelation length of precipitation and precipitation minus evaporation of about 500 km is comparatively large [*Genthon*, 2004]. Nevertheless, as for SMB features, large differences occur between the coast and the interior, with particularly low values on the ridges and domes. The correlation length for real SMB is much shorter than that of precipitation or precipitation minus evaporation due to depositional and postdepositional processes. However, by spatially smoothing the small-scale noise (e.g., as defined by *Genthon et al.* [2005]), one may expect a correlation with precipitation at the 100-km scale.

3.3. Associations Between Spatial and Temporal Variability

[112] The spatial scale of significance for a single firn or ice core record is a critical issue for the interpretation of the accumulation time series. Microrelief (sastrugis) introduces a high-frequency, quasi-stochastic variability into core records of annual layer thickness [*Fisher et al.*, 1985; *Van der Veen and Bolzan*, 1999]. Medium-scale undulations (wavelengths < 20 km) in surface topography up stream from a core-drilling site can cause variations in measured accumulation rates. One of the earliest results on this topic reveals that accumulation in troughs can be 30–50% more than on exposed surface crests [*Gow and Rowland*, 1965]. Meanwhile, as demonstrated in section 3.2, knowledge about the spatial variability has increased significantly. The stratigraphic record of a core is affected by the flow of ice, so the material at depth is slowly moved away from the original deposition site. If topographic features capable of changing the accumulation are located up stream of a core site, they can generate decadal to centennial long periods of accumulation consistently above or below the long-term mean because layers deeper in the record will have been deposited at these topographic troughs and crests [*Richardson and Holmlund*, 1999; *Kaspari et al.*, 2005; *Hamilton*, 2004]. The only way to really understand the significance of a core record is to know something about the spatial field of SMB surrounding the core and also to have a good idea of the rate of movement of the ice through this field. Analysis of these data would allow some separation of the spatial and temporal variability that the core represents. This is the only way to understand the true significance of accumulation rate histories in cores. Any core for which these data are not available, or that is collected on fast moving ice, or is sufficiently deep to have moved more than a fraction of the correlation length for SMB, contains an accumulation rate history that is a mixed signal and is likely not interpretable.

[113] *Richardson and Holmlund* [1999] demonstrate the importance of determining the spatial significance of cores and recommend radar surveys prior to drilling, as this is the easiest way to get this information. The timescale for which this influence is important depends on the specific SMB and flow velocities at the site. However, it is possible to resolve temporal signals if the effects of local topography and ice

flow are considered [*Spikes et al.*, 2004]. The length of periodic variations due to mesoscale relief and/or megadunes depend on ice velocity and SMB and can therefore vary in space and time. *Frezzotti et al.* [2005] point out that in megadune areas the distortion of records is characterized by a SMB periodicity of about 1500 years. In coastal areas with relatively large flow velocities and significant topographic variations, spatial SMB variations can influence temporal records on scales as short as a few decades [*Anschütz et al.*, 2006]. *Arcone et al.* [2005b] demonstrate how the same effect is present in the GPR data themselves and must be corrected for. Consequently, several techniques have been developed to deconvolve spatial from temporal effects by employing GPR data [*Hamilton*, 2004; *Arcone et al.*, 2005b; *Parrenin et al.*, 2006].

3.4. Spatial Interpolation

[114] There are probably several different length scales for coherence in the true field of SMB. There may be greater complexity in places, but in general, we might argue that the shortest length scale is governed by the sastrugi length (0.1–100 m), the next is governed by the topography over which the wind transport of snow occurs (10–10,000 m), and the longest is governed by the regional differences in the supply of precipitation governed by synoptic climate (100–4000 km). The efforts at interpolation on the continental scale have usually been focused on producing a map of the third correlation scale, accepting that there is variability on the other two length scales that are not represented (see treatment by *Vaughan et al.* [1999a]). Understood in this way, attempts to use local measurements to draw a continental-scale map make some sense, although they are fraught with pitfalls. Improved interpolation can also be achieved by subdividing data sets of local measurements in regions of comparable properties (e.g., coastal areas and plateau region) and then performing interpolation for each region separately [*Rotschky et al.*, 2007]. The complexity and quality of the efforts have undoubtedly increased in the last few decades, culminating with the explicit and formal treatment of uncertainty given by *Arthern et al.* [2006]. The map presented in their study will not be definitive in any sense but is a major step forward, since it includes a formal assessment of the uncertainty involved with the gridding process.

4. CONCLUSION AND RECOMMENDATIONS

[115] We have presented a summary of East Antarctic SMB characteristics and techniques used to acquire these. Our goal is to improve the knowledge of potential users about the difficulties associated with interpretation of measurements but also to highlight the need to perform more measurements and to use the ones currently available. We have demonstrated that SMB varies significantly in time and space on various scales. None of available measurement techniques are able to capture all scales simultaneously, neither can they be combined to provide area-wide measurements on basin scales, mainly as a result of logistical constraints. Nevertheless, regionally confined studies provide valuable information from which a number of recommendations for data acquisition and potential data users can be proposed:

[116] 1. Decadal SMB values decorrelate on the 1- to 10-km scale but covary over length scales of hundreds of kilometers. The recent discovery from GPR data that on this scale, there exists a static (topographically induced) pattern of SMB, which cannot be observed in or estimated from sparse point measurements of SMB, is of utmost importance. These observations clearly indicate the potential pitfalls of using isolated measurements as being representative of a larger region. These pitfalls can be avoided and point measurements (usually cores) given regional significance by the simple expedient of acquiring GPR data around the core location. Ideally, the GPR profiles should span several ice thicknesses up flow, down flow, and across flow and should be tuned to acquire layer information at least as deep as the core. A well-dated core combined with GPR data will allow independent calculation of spatial and temporal means and variations for the region, plus their errors. These are the parameters that need to be routinely acquired and used if we are to substantially advance our understanding of continent-wide patterns of SMB across the Antarctic ice sheet.

[117] 2. Spatial variability increases as topographic complexity increases, caused by wind deposition/erosion. It is important to consider aeolian processes in general but especially when selecting sites for firn and ice coring in areas with relatively complex topography. Slope variations of only a few meters per kilometer have a significant impact on wind-derived snow accumulation processes and also therefore on the accumulation records. To fully understand the dominant processes that affect SMB and to incorporate these into global climate reconstructions, high-resolution representativity of SMB from cores is needed. Statistically meaningful reconstructions at annual and/or seasonal scale can be produced using multiple cores for each "center of action."

[118] 3. The effective use of ultrasonic height ranger data in East Antarctic mass balance research requires that meteorological data are collected simultaneously and at the same location, so that the individual components of the SMB (sublimation, melt, snowdrift sublimation) can be quantified or at least estimated. Because of the operational accuracy of 2–3 cm, ultrasonic height ranger data are less useful to the study of individual accumulation events on the dry interior plateau of Antarctica. However, they are very valuable to to determination of intraannual variability and seasonal cycles, which at many places are not known, not even qualitatively.

[119] 4. A considerable problem, which presently remains unsolved, is the conversion of height to mass changes for both stakes and ultrasonic sounders. This needs urgent attention, especially if the use of ultrasonic height ranger and stake data increases in the future. Moreover, the spatial interpolation and extrapolation of density profiles require further input.

TABLE 3. Possible Usage of Ground Truth SMB Estimates[a]

Source	Estimated SMB Property	Ground Truth Application
Stake farm	decorrelation and covariance on (sub)annual and subkilometer scale	laser altimetry
Stake line	decorrelation and covariance on (sub)annual and kilometer scale	laser altimetry, gravimetry
Ultrasonic sounders	high temporal resolution of single events, covariance	regional climate modeling
Snow pits	high-resolution time series	regional climate modeling, microwave radiometry
Cores	high-resolution and long-term record	regional climate modeling, microwave radiometry
GPR	temporally averaged decorrelation	altimetry, gravimetry

[a]All methods provide estimates of SMB. Specific properties, however, can only be determined by specific methods.

[120] 5. An apparently trivial aspect is documentation. Experience with older data sets shows that documentation is essential but, unfortunately, often neglected and partly even missing. The documentation should contain an exact description of how the raw data sets (e.g., length measurements) were obtained, which auxiliary parameters (e.g., density) were determined, and how measured quantities were finally converted to SMB.

[121] 6. For subsurface measurements, it is a great advantage if one can determine in the field if a good dating horizon has been reached. This can be achieved by several nondestructive measurements, either in the hole, in the pit, or along the core. Cores should be drilled to a depth covering the period back to the eruption of Tambora in A.D. 1815 and the unknown eruption in A.D. 1809.

[122] 7. When retrieving a firn core, there is often some unrecoverable loss of core material. This occurs predominantly in the upper meters. A correction scheme similar to a procedure described by *Whillans and Bolzan* [1988] is recommended, with special attention to an accurate measurement of diameter. To facilitate the identification of overlap between the core and a snow pit, the pit should be deep enough to cover one dating horizon that can also be captured in the adjacent drilled core. This latter task, however, is difficult and not always possible.

[123] 8. Accumulation on the plateau is, in general, more "well behaved" in terms of spatial representativity (apart from megadune fields) than the transition region from the plateau to the coastal areas, where high katabatic winds occur frequently and the morphological variability is often high (e.g., nunataks, valley glaciers). We need more sampling in the coastal regions if we are to improve continental average assessments.

[124] Ground truthing is essential for methods like remote sensing and numerical modeling, which require (and provide) estimates of decorrelation lengths, covariance, and associated uncertainties. The serviceability depends on the type of field data and their usage (Table 3). As a suitable combination, stake farms and GPS surveys in 1 km^2 areas provide a reference for laser altimetry. Decadal measurements of stake lines provide covariance on an annual scale for gravimetry, and ultrasonic sounders provide single events for regional models. Pits, cores, and GPR provide longer-term records for regional- or continental-scale modeling as well as spatial characteristics for remote sensing.

[125] From the point of view of specific mass balance estimates, the potential that with increasing precipitation, the East Antarctic Ice Sheet could be the single largest ameliorator of sea level rise, and could balance a few tens of centimeters of sea level rise over the coming century, means that setting and understanding the baseline (current rates and trends in accumulation) are highly important. The accounting methods reviewed in this paper to determine the mean net annual SMB provide a significant contribution to this aim. Although they may never be suitable to infer the specific mass balance of the entire ice sheet, or even regions of it, by ground-based measurements alone, the records of SMB history and its spatial characteristics are definitely required to determine if the ice sheet's SMB is changing in a secular fashion and whether or not this pattern is related to anthropogenic climate change. Assessments of ice sheet surface elevation changes [*Davis et al.*, 2005; *Zwally et al.*, 2005] will continue to yield the most precise results for mass balance estimates of specific drainage basins or ice sheets as a whole. In the intermediate-term perspective, gravity measurements and related time series may potentially become more accurate than they are at present [e.g., *Chen et al.*, 2006; *Velicogna and Wahr*, 2006; *Ramillien et al.*, 2006], thus providing valuable contributions to other techniques.

[126] New airborne techniques for determining the internal layering near the surface of ice masses are currently being developed, mainly in the context of calibration and validation campaigns for satellite remote sensors. The Airborne Synthetic Aperture and Interferometric Radar Altimeter (ASIRAS) System [*Mavrocordatos et al.*, 2004] and the D2P (delay/Doppler phase monopulse) radar [*Stenseng et al.*, 2005], for instance, do not only operate as classical altimeters or synthetic aperture radar (SAR) but also utilize an interferometric SAR mode. They are basically a replicate of the SAR/Interferometric Radar Altimeter (SIRAL) instrument to be operated on board CryoSat-2. The systems provide vertical resolution comparable to high-frequency GPR. The larger footprints cause less horizontal resolution than GPR but allow a higher spatial coverage. The advantage lies in operating such a system from an airplane, covering a relatively large area with profiles over a short period of time. Recent ASIRAS results from the dry snow zone [*Hawley et al.*, 2006] and percolation zone [*Helm et al.*, 2007] of the Greenland ice sheet, accompanied by ground-based measurements [*Scott et al.*, 2006], indicate that annual layers can be continuously detected by this system, promising extended future measurements in Antarctica. The combination of satellite remote sensors with airborne surveys and

dedicated ground measurements will likely remain the primary line of action for the next decade to obtain mass balance estimates for large parts of the ice sheet.

APPENDIX A: OPTIMAL ESTIMATION OF STAKE INTERVAL

[127] By studying the accumulation correlation of nearby stakes as a function of distance, *Barkov and Lipenkov* [1978] evaluated the optimal distance between stakes (putting the stakes too close to each other will not significantly increase the accuracy due to accumulation correlation at the adjacent stakes) using a "structural function" $b_{\Delta h}(\lambda)$ as a measure of correlation:

$$b_{\Delta h}(\lambda) = 2\sigma^2_{\Delta h}(1 - r_{\Delta h}(\lambda)), \tag{A1}$$

with snow buildup Δh, its spatial variability $\sigma_{\Delta h}$, distance between stakes λ, and the correlation coefficient between snow buildup at two stakes $r_{\Delta h}$. The optimal distance is reached as soon as the correlation turns insignificant (and $b_{\Delta h}$ reaches a saturation value). They found that at Vostok Station the annual accumulation at two points is practically not correlated at the distance of 65 m. Thus, Vostok stake farm with its distance between adjacent stakes of 25 m is close to optimum and even slightly oversampled. This implies that for studies aiming at smaller scales, stake distances on the order of several tens of meters are sufficient. However, both optimal distance and the saturation values vary over Antarctica.

[128] The structural function is used to determine optimal parameters (stake farm size/profile length and amount of stakes) of the stake farm/profile [*Barkov and Lipenkov*, 1978]:

$$\sigma^2_{\bar{\Delta}h} = \sigma^2_{\Delta h} - \frac{1}{n^2}\sum_{i=1}^{n-1}(n-i)b_{\Delta h}(i\Delta l) \tag{A2}$$

where $\sigma_{\bar{\Delta}h}{}^2(l, n)$ is the total error of snow buildup depending on the length of the route (l) and amount of stakes (n); $\sigma^2_{\Delta h}$ is the spatial variability of snow buildup (standard deviation); i is the index number of a given stake; Δl is the interval between adjacent stakes; and $b_{\Delta h}(i\Delta l)$ is the value of the structural function for the distance $i\Delta l$. The optimal parameters of the stake farm correspond to the minimum value of $\sigma_{\bar{\Delta}h}{}^2(l, n)$. This method is well suited for a series, members of which are not independent, which is the case for the snow buildup spatial distribution.

GLOSSARY

Ablation: Negative surface mass balance.

Accumulation: Positive surface mass balance.

Antarctic ice sheet: Grounded part of the Antarctic polar ice cap, divided in the East and West Antarctic ice sheets.

Blue ice area: Area of negative surface mass balance, where ice formed up stream emerges to the surface. Because of the higher density of the ice this appears blue. Surrounding areas with positive mass balance appear white because of the lower density of firn and snow compared to ice.

Firn core: Core extracted from the upper tens of meters from the firn, above the pore close-off depth, where no bubbles are yet present.

Ground-penetrating radar: Geophysical tool that emits electromagnetic waves from the surface into the ground; measures the round-trip traveltime of the wave that is returned from reflecting horizons.

Ice core: Core extracted from below the pore close-off depth, where bubbles have formed and are enclosed by ice.

Mean net annual surface mass balance: Summary of terms contributing to the solid, liquid, and gaseous transfer of water across the surface of the ice sheet; commonly normalized to kg m^{-2} a^{-1} but often given in millimeters water equivalent.

Radiochronology: Determination of age from the natural decay of radioactive species.

Snow pit: Trench excavated in the snow, often of rectangular cross section, with a vertical wall on one side to investigate the stratigraphy and to take samples.

Stake: Pole put into the snow (often bamboo, sometimes aluminium or similar). The height above snow or ice surface is measured at intervals to determine mass balance.

Stake farm: Combination of stakes in a two-dimensional setup, often as a rectangular grid.

Stake line: Combination of stakes along a one-dimensional line, often hundreds of kilometers long.

Surface mass balance: Short for mean net annual surface mass balance.

Time marker: Unambiguously identifiable feature of known age in time series records.

Ultrasonic sounder: Device to measure the distance to the surface. Operates with sound wave at ultrasonic frequencies.

Volcanic horizon: Deposits from volcanic eruptions (acids, ash) identifiable in layers, which were deposited at the ice sheet surface, buried, and submerged over time.

[129] **ACKNOWLEDGMENTS.** Special thanks to Tas van Ommen for his encouragement and contributions to the initial kick-off of the paper and to Martin Sharp and Ian Goodwin for their reviews. Data contributed by Robert Arthern for Figure 2 are greatly acknowledged. The background of this work is based on decades of field measurements and generations of scientists, made possible by the different national polar research institutions. We acknowledge their long-term support for designing and organizing ground-based measurements of Antarctic surface mass balance and the efforts by logistics to making them real. This work, moreover, greatly profited from discussions with numerous colleagues at the different institutions, too many to list them all here. This research was partly funded by the Italian National Antarctic Research Program (PNRA) and the Deutsche Forschungsgemeinschaft through an "Emmy Noether" scholarship, grant EI 672/1, to O.E. The Editor responsible for this paper was Ian Fairchild. He thanks Ian Goodwin as the technical reviewer and Martin Sharp as the cross-disciplinary reviewer.

REFERENCES

Alley, R. B., et al. (1997), Visual-stratigraphic dating of the GISP2 ice core: Basis, reproducibility, and application, *J. Geophys. Res.*, *102*(C12), 26,367–26,381.

Andreas, E. L. (2002), Parameterizing scalar transfer over snow and ice: A review, *J. Hydrometeorol.*, *3*, 417–432.

Annan, A. P., and J. L. Davis (1976), Impulse radar sounding in permafrost, *Radio Sci.*, *11*(4), 383–394.

Anschütz, H., O. Eisen, W. Rack, and M. Scheinert (2006), Periodic surface features in coastal East Antarctica, *Geophys. Res. Lett.*, *33*, L22501, doi:10.1029/2006GL027871.

Anschütz, H., O. Eisen, H. Oerter, D. Steinhage, and M. Scheinert (2007), Investigating small-scale variations of the recent accumulation rate in Central Dronning Maud Land, East Antarctica, *Ann. Glaciol.*, *46*, 14–21.

Anschütz, H., D. Steinhage, O. Eisen, H. Oerter, M. Horwath, and U. Ruth (2008), Small-scale spatio-temporal characteristics of accumulation rates in western Dronning Maud Land, Antarctica, *J. Glaciol.*, in press.

Arcone, S. A., V. B. Spikes, and G. S. Hamilton (2005a), Phase structure of radar stratigraphic horizons within Antarctic firn, *Ann. Glaciol.*, *41*, 10–16.

Arcone, S. A., V. B. Spikes, and G. S. Hamilton (2005b), Stratigraphic variation within polar firn caused by differential accumulation and ice flow: Interpretation of a 400 MHz short-pulse radar profile from West Antarctica, *J. Glaciol.*, *51*(174), 407–422.

Arthern, R. J., D. P. Winebrenner, and D. G. Vaughan (2006), Antarctic snow accumulation mapped using polarization of 4.3-cm wavelength microwave emission, *J. Geophys. Res.*, *111*, D06107, doi:10.1029/2004JD005667.

Barkov, N. I., and V. Y. Lipenkov (1978), Nakoplenie snega v rayone stantsii Vostok v 1970–1973 (Snow accumulation in the area of Vostok Station in 1970–1973), *Inf. Bull. Sov. Antarct. Exped.*, *98*, 63–68.

Barkov, N. I., and V. Y. Lipenkov (1996), Nakoplenie snega v rayone stantsii Vostok, Antarktida, v 1970–1992 (Snow accumulation in the area of Vostok Station, Antarctica, in 1970–1992), *Mater. Glyatsiol. Issled.*, *80*, 87–88.

Barnes, P. R. F., E. W. Wolff, R. Mulvaney, R. Udisti, E. Castellano, R. Röthlisberger, and J.-P. Steffensen (2002), Effect of density on electrical conductivity of chemically laden polar ice, *J. Geophys. Res.*, *107*(B2), 2029, doi:10.1029/2000JB000080.

Bindschadler, R., H. Choi, C. Shuman, and T. Markus (2005), Detecting and measuring new snow accumulation on ice sheets by satellite remote sensing, *Remote Sens. Environ.*, *98*(4), 388–402.

Bintanja, R. (1999), On the glaciological, meteorological, and climatological significance of Antarctic blue ice areas, *Rev. Geophys.*, *37*, 337–359.

Bintanja, R. (2003), The mass balance of a dry snow surface during a snowstorm, *Ann. Glaciol.*, *38*, 79–83.

Black, H. P., and W. Budd (1964), Accumulation in the region of Wilkes, Wilkes Land, Antarctica, *J. Glaciol.*, *5*(37), 3–15.

Blindow, N. (1994), The central part of the Filchner-Ronne Ice Shelf, Antarctica: Internal structures revealed by 40 MHz monopulse RES, *Ann. Glaciol.*, *20*, 365–371.

Bogorodsky, V. V., C. R. Bentley, and P. E. Gudmandsen (1985), *Radioglaciology*, D. Reidel, Dordrecht, Netherlands.

Braaten, D. A. (1994), Instrumentation to quantify snow accumulation and transport dynamics at two locations on the Ross Ice Shelf, *Antarct. J. U.S.*, *29*(5), 86–87.

Bromwich, D. H., A. J. Monaghan, J. G. Powers, J. J. Cassano, H. L. Wei, Y. H. Kuo, and A. Pellegrini (2003), Antarctic mesoscale prediction system (AMPS): A case study from the 2000–01 field season, *Mon. Weather Rev.*, *131*, 412–434.

Budd, W. F., and I. N. Smith (1982), Large-scale numerical modelling of the Antarctic ice sheet, *Ann. Glaciol.*, *3*, 42–49.

Bull, C. (1971), Snow accumulation in Antarctica, in *Research in the Antarctic*, edited by L. Quam, pp. 367–421, Am. Assoc. for the Adv. of Sci., Washington, D. C.

Carter, M. W., and A. A. Moghissi (1977), Three decades of nuclear testing, *Health Phys.*, *33*, 55–71.

Chen, J. L., C. R. Wilson, D. D. Blankenship, and B. D. Tapley (2006), Antarctic mass rates from GRACE, *Geophys. Res. Lett.*, *33*, L11502, doi:10.1029/2006GL026369.

Clarke, T. S., and C. R. Bentley (1994), High-resolution radar on Ice Stream B2, Antarctica: Measurements of electromagnetic wave speed in firn and strain history from buried crevasses, *Ann. Glaciol.*, *20*, 153–159.

Clough, J. W. (1977), Radio echo sounding: Reflections from internal layers in ice sheets, *J. Glaciol.*, *18*(78), 3–14.

Clough, J. W., and C. R. Bentley (1970), Measurements of electromagnetic wave velocity in the East Antartic ice sheet, in *International Symposium on Antarctic Glaciological Exploration (ISAGE), Proceedings SCAR/IASH Symposium*, edited by A. J. Gow et al., *IAHS Publ.*, *86*, 115–128.

Clow, G. D., C. P. McKay, G. M. Simmons Jr., and R. A. Wharton Jr. (1988), Climatological observations and predicted sublimation rates at Lake Hoare, Antarctica, *J. Clim.*, *1*, 715–728.

Coffey, M. T. (1996), Observations of the impact of volcanic activity on stratospheric chemistry, *J. Geophys. Res.*, *101*(D3), 6767–6780.

Cole-Dai, J., and E. Mosley-Thompson (1999), The Pinatubo eruption in South Pole snow and its potential value to ice-core paleovolcanic records, *Ann. Glaciol.*, *29*, 99–105.

Cole-Dai, J., E. Mosley-Thompson, and L. G. Thompson (1997), Annually resolved Southern Hemisphere volcanic history from two Antarctic ice cores, *J. Geophys. Res.*, *102*(D14), 16,761–16,771.

Cole-Dai, J. H., E. Mosley-Thompson, S. P. Wight, and L. G. Thompson (2000), A 4100-year record of explosive volcanism from an East Antarctica ice core, *J. Geophys. Res.*, *105*(D19), 24,431–24,441.

Corr, H. F. J., A. Jenkins, K. W. Nicholls, and C. S. M. Doake (2002), Precise measurement of changes in ice-shelf thickness by phase-sensitive radar to determine basal melt rates, *Geophys. Res. Lett.*, *29*(8), 1232, doi:10.1029/2001GL014618.

Craven, M., and I. Allison (1998), Firnification and the effects of wind-packing on Antarctic snow, *Ann. Glaciol.*, *27*, 239–245.

Crozaz, G., and C. C. Langway Jr. (1966), Dating Greenland firn-ice cores with ^{210}Pb, *Earth Planet. Sci. Lett.*, *1*(4), 194–196.

Crozaz, G., E. Picciotto, and W. D. Breuck (1964), Antarctic snow chronology with ^{210}Pb, *J. Geophys. Res.*, *69*(12), 2597–2604.

Curran, M. A. J., G. B. Jones, and H. Burton (1998), Spatial distribution of dimethylsulfide and dimethylsulfoniopropionate in the Australasian sector of the Southern Ocean, *J. Geophys. Res.*, *103*(D13), 16,677–16,689.

Dansgaard, W. (1964), Stable isotopes in precipitation, *Tellus*, *16*, 436–468.

Dansgaard, W., S. J. Johnsen, H. B. Clausen, and N. Gundestrup (1973), Stable isotope glaciology, *Medd. Groenl.*, *197*(2), 53.

Dansgaard, W., et al. (1993), Evidence for general instability of past climate from a 250-kyr ice-core record, *Nature*, *364*, 218–220, doi:10.1038/364218a0.

Davis, C. H., Y. Li, J. R. McConnell, M. M. Frey, and E. Hanna (2005), Snowfall-driven growth in East Antarctic ice sheet mitigates recent sea-level rise, *Science*, *308*(5730), 1898–1901.

Delmas, R., and M. Pourchet (1977), Utilisation de filtres échangeurs d'ions pour l'étude de l'activité Béta globale d'un carottage glaciologique, *IAHS Publ.*, *118*, 159–163.

Delmas, R. J., S. Kirchner, J. M. Palais, and J. R. Petit (1992), 1000 years of explosive volcanism recorded at the South Pole, *Tellus, Ser. B*, *44*, 335–350.

Dibb, J. E., and M. Fahnestock (2004), Snow accumulation, surface height change, and firn densification at Summit, Greenland: Insights from 2 years of in situ observation, *J. Geophys. Res.*, *109*, D24113, doi:10.1029/2003JD004300.

Dibb, J. E., P. A. Mayewski, C. S. Buck, and S. M. Drummey (1990), Scientific correspondence: Beta radiation from snow, *Nature*, *345*, 25.

Dixon, D., P. A. Mayewski, S. Kaspari, S. Sneed, and M. Handley (2004), A 200-year sub-annual record of the primary sources of sulfate in West Antarctica, *Ann. Glaciol.*, *39*, 545–556.

Doran, P. T., C. P. McKay, G. D. Clow, G. L. Dana, A. G. Fountain, T. Nylen, and W. B. Lyons (2002), Valley floor climate observations from the McMurdo dry valleys, Antarctica, 1986–2000, *J. Geophys. Res.*, *107*(D24), 4772, doi:10.1029/2001JD002045.

Eisen, O., U. Nixdorf, F. Wilhelms, and H. Miller (2002), Electromagnetic wave speed in polar ice: Validation of the CMP technique with high resolution DEP and γ-density measurements, *Ann. Glaciol.*, *34*, 150–156.

Eisen, O., F. Wilhelms, U. Nixdorf, and H. Miller (2003a), Identifying isochrones in GPR profiles from DEP-based forward modelling, *Ann. Glaciol.*, *37*, 344–350.

Eisen, O., F. Wilhelms, U. Nixdorf, and H. Miller (2003b), Revealing the nature of radar reflections in ice: DEP-based FDTD forward modeling, *Geophys. Res. Lett.*, *30*(5), 1218, doi:10.1029/2002GL016403.

Eisen, O., U. Nixdorf, F. Wilhelms, and H. Miller (2004), Age estimates of isochronous reflection horizons by combining ice core, survey, and synthetic radar data, *J. Geophys. Res.*, *109*, B04106, doi:10.1029/2003JB002858.

Eisen, O., W. Rack, U. Nixdorf, and F. Wilhelms (2005), Characteristics of accumulation rate in the vicinity of the EPICA deep-drilling site in Dronning Maud Land, Antarctica, *Ann. Glaciol.*, *41*, 41–46.

Eisen, O., I. Hamann, S. Kipfstuhl, D. Steinhage, and F. Wilhelms (2007), Direct evidence for radar reflector originating from changes in crystal-orientation fabric, *Cryosphere Discuss.*, *1*(1), 1–16.

Ekaykin, A. A. (2003), Meteorological regime of central Antarctica and its role in the formation of isotope composition of snow thickness, Ph.D. thesis, Univ. Joseph Fourier, Grenoble, France.

Ekaykin, A. A., V. Y. Lipenkov, N. I. Barkov, J. R. Petit, and V. Masson-Delmotte (2002), Spatial and temporal variability in isotope composition of recent snow in the vicinity of Vostok Station: Implications for ice-core interpretation, *Ann. Glaciol.*, *35*, 181–186.

Ekaykin, A. A., V. Y. Lipenkov, I. N. Kuzmina, J. R. Petit, V. Masson-Delmotte, and S. J. Johnsen (2004), The changes in isotope composition and accumulation of snow at Vostok Station over the past 200 years, *Ann. Glaciol.*, *39*, 569–575.

Endo, Y., and K. Fujiwara (1973), Characteristics of the snow cover in East Antarctica along the route of the JARE South Pole Traverse and factors controlling such characteristics, *JARE Sci. Rep., Ser. C, Earth Sci.*, *7*, 38 pp.

Fahnestock, M. A., T. A. Scambos, C. A. Shuman, R. J. Arthern, D. P. Winebrenner, and R. Kwok (2000), Snow megadune fields on the East Antarctic Plateau: Extreme atmosphere-ice interaction, *Geophys. Res. Lett.*, *27*(22), 3719–3722.

Feely, H. W., H. Seitz, R. J. Lagomarsino, and P. E. Biscaye (1966), Transport and fallout of stratospheric radioactive debris, *Tellus*, *18*, 316–328.

Fischer, H., D. Wagenbach, and J. Kipfstuhl (1998), Sulfate and nitrate firn concentrations on the Greenland ice sheet: 2. Temporal anthropogenic deposition changes, *J. Geophys. Res.*, *103*(D17), 21,935–21,942.

Fisher, D. A., N. Reeh, and H. B. Clausen (1985), Stratigraphic noise in time series derived from ice cores, *Ann. Glaciol.*, *7*, 76–83.

Folco, L., A. Capra, M. Chiappini, M. Frezzotti, M. Mellini, and I. E. Tabacco (2002), The Frontier Mountain meteorite trap (Antarctica), *Meteorit. Planet. Sci.*, *37*, 209–228.

Fortuin, J. P. F., and J. Oerlemans (1990), The parameterization of the annual surface temperature and mass balance of Antarctica, *Ann. Glaciol.*, *14*, 78–84.

Freitag, J., F. Wilhelms, and S. Kipfstuhl (2004), Microstructure dependent densification of polar firn derived from X-ray microtomography, *J. Glaciol.*, *50*(169), 243–250.

Frezzotti, M., and O. Flora (2002), Ice dynamic features and climatic surface parameters in East Antarctica from Terra Nova Bay to Talos Dome and Dome C: ITASE Italian Traverse, *Terra Antarct.*, *9*(1), 47–54.

Frezzotti, M., S. Gandolfi, F. L. Marca, and S. Urbini (2002a), Snow dunes and glazed surfaces in Antarctica: New field and remote-sensing data, *Ann. Glaciol.*, *34*, 81–88.

Frezzotti, M., S. Gandolfi, and S. Urbini (2002b), Snow megadunes in Antarctica: Sedimentary structure and genesis, *J. Geophys. Res.*, *107*(D18), 4344, doi:10.1029/2001JD000673.

Frezzotti, M., et al. (2004), New estimations of precipitation and surface sublimation in East Antarctica from snow accumulation measurements, *Clim. Dyn.*, *23*(7–8), 803–813, doi:10.1007/s00382-004-0462-5.

Frezzotti, M., et al. (2005), Spatial and temporal variability of snow accumulation in East Antarctica from traverse data, *J. Glaciol.*, *51*(172), 113–124.

Frezzotti, M., S. Urbini, M. Proposito, C. Scarchilli, and S. Gandolfi (2007), Spatial and temporal variability of surface mass balance near Talos Dome, East Antarctica, *J. Geophys. Res.*, *112*, F02032, doi:10.1029/2006JF000638.

Fuhrer, K., A. Neftel, M. Anklin, and W. Maggi (1993), Continuous measurements of hydrogen peroxide, formaldehyde, calcium and ammonium concentrations along the new GRIP ice core from Summit, central Greenland, *Atmos. Environ., Part A*, *27*(12), 1873–1880.

Fuhrer, K., A. Neftel, M. Anklin, M. Staffelbach, and T. Legrand (1996), High-resolution ammonium ice core record covering a complete glacial-interglacial cycle, *J. Geophys. Res.*, *101*(D2), 4147–4164.

Fujii, Y. (1981), Formation of surface snow layer at Mizuho Station, Antarctica, *Mem. Nat. Inst. Polar Res. Spec. Issue*, *19*, 280–296.

Fujii, Y., and K. Kusunoki (1982), The Role of sublimation and condensation in the formation of ice sheet surface at Mizuho Station, Antarctica, *J. Geophys. Res.*, *87*(C6), 4293–4300.

Fujita, S., H. Maeno, S. Uratsuka, T. Furukawa, S. Mae, Y. Fujii, and O. Watanabe (1999), Nature of radio echo layering in the Antarctic ice sheet detected by a two-frequency experiment, *J. Geophys. Res.*, *104*(B6), 13,013–13,024.

Fujiwara, K., and Y. Endoh (1971), Preliminary report of glaciological studies, *Jpn. Antarct. Res. Exped. Sci. Rep., Special Issue*, *2*, 68–109.

Gallée, H., G. Guyomarch, and E. Brun (2001), Impact of snow drift on the Antarctic ice sheet surface mass balance: Possible sensitivity to snow surface properties, *Boundary Layer Meteorol.*, *99*, 1–19.

Gallée, H., V. Peyaud, and I. Goodwin (2005), Simulation of the net snow accumulation along the Wilkes Land transect, Antarctica, with a regional climate model, *Ann. Glaciol.*, *41*, 17–22.

Genthon, C. (2004), Space-time Antarctic surface mass balance variability from climate models, *Ann. Glaciol.*, *39*, 271–275.

Genthon, C., and G. Krinner (2001), Antarctic surface mass balance and systematic biases in general circulation models, *J. Geophys. Res.*, *106*(D18), 20,653–20,664.

Genthon, C., S. Kaspari, and P. A. Mayewski (2005), Interannual variability of the surface mass balance of West Antarctica from ITASE cores and ERA40 reanalyses, *Clim. Dyn.*, *24*, 759–770, doi:0.1007/s00382-005-0019-2.

Gerland, S., H. Oerter, J. Kipfstuhl, F. Wilhelms, H. Miller, and W. Miners (1999), Density log of a 181 m long ice core from Berkner Island, Antarctica, *Ann. Glaciol.*, *29*, 215–219.

Giovinetto, M. B., N. M. Waters, and C. R. Bentley (1990), Dependence of Antarctic surface mass balance on temperature, elevation, and distance to open ocean, *J. Geophys. Res.*, *95*(D4), 3517–3531.

Goldberg, E. D. (1963), Geochronology with lead-210, in *Radioactive Dating*, pp. 121–131, Int. At. Energy Agency, Vienna.

Goodwin, I. D. (1990), Snow accumulation and surface topography in the katabatic zone of eastern Wilkes Land, Antarctica, *Antarct. Sci.*, *2*(3), 232–235.

Goodwin, I. D. (1991), Snow-accumulation variability from seasonal surface observations and firn-core stratigraphy, eastern Wilkes Land, Antarctica, *J. Glaciol.*, *37*(127), 383–387.

Goodwin, I. D., M. Higham, I. Allison, and R. Jaiwen (1994), Accumulation variation in eastern Kemp Land, Antarctica, *Ann. Glaciol.*, *20*, 202–206.

Goodwin, I., M. de Angelis, M. Pook, and N. W. Young (2003), Snow accumulation variability in Wilkes Land, East Antarctica, and the relationship to atmospheric ridging in the 130°–170°E region since 1930, *J. Geophys. Res.*, *108*(D21), 4673, doi:10.1029/2002JD002995.

Gow, A. J. (1965), On the accumulation and seasonal stratification of snow at the South Pole, *J. Glaciol.*, *5*(40), 467–477.

Gow, A. J., and R. Rowland (1965), On the relationship of snow accumulation to surface topography at "Byrd Station", Antarctica, *J. Glaciol.*, *5*(42), 843–847.

Gudmandsen, P. (1975), Layer echoes in polar ice sheets, *J. Glaciol.*, *15*(73), 95–101.

Hamilton, G. (2004), Topographic control of regional accumulation rate variability at South Pole and implications for ice core interpretation, *Ann. Glaciol.*, *39*, 214–218.

Hammer, C. (1980), Acidity of polar ice cores in relation to absolute dating, past volcanism, and radio-echoes, *J. Glaciol.*, *25*(93), 359–372.

Hammer, C. U., H. B. Clausen, and C. C. Langway Jr. (1994), Electrical conductivity method (ECM) stratigraphic dating of the Byrd Station ice core, Antarctica, *Ann. Glaciol.*, *20*, 115–120.

Harrison, C. H. (1973), Radio echo sounding of horizontal layers in ice, *J. Glaciol.*, *12*(66), 383–397.

Hawley, R. L., E. M. Morris, R. Cullen, U. Nixdorf, A. P. Shepherd, and D. J. Wingham (2006), ASIRAS airborne radar resolves internal annual layers in the dry-snow zone of Greenland, *Geophys. Res. Lett.*, *33*, L04502, doi:10.1029/2005GL025147.

Helm, V., W. Rack, R. Cullen, P. Nienow, D. Mair, V. Parry, and D. J. Wingham (2007), Winter accumulation in the percolation zone of Greenland measured by airborne radar altimeter, *Geophys. Res. Lett.*, *34*, L06501, doi:10.1029/2006GL029185.

Helsen, M. M., R. S. W. van de Wal, M. R. van den Broeke, E. R. T. Kerstel, V. Masson-Delmotte, H. A. J. Meijer, C. H. Reijmer, and M. P. Scheele (2004), Modelling the isotopic composition of snow using backward trajectories: A particular precipitation event in Dronning Maud Land, Antarctica, *Ann. Glaciol.*, *39*, 293–299.

Helsen, M. M., R. S. W. van de Wal, M. R. van den Broeke, D. van As, H. A. J. Meijer, and C. H. Reijmer (2005), Oxygen isotope variability in snow from western Dronning Maud Land, Antarctica and its relation to temperature, *Tellus, Ser. B*, *57*, 423–435.

Hempel, L., F. Thyssen, N. Gundestrup, H. B. Clausen, and H. Miller (2000), A comparison of radio-echo sounding data and electrical conductivity of the GRIP ice core, *J. Glaciol.*, *46*(154), 369–374.

Hofstede, C. M., et al. (2004), Firn accumulation records for the past 1000 years on the basis of dielectric profiling of six cores from Dronning Maud Land, Antarctica, *J. Glaciol.*, *50*(169), 279–291.

Holmlund, P., et al. (2000), Spatial gradients in snow layering and ten metre temperatures at potential EPICA-DML drill sites, *Ann. Glaciol.*, *30*, 13–19.

Holtslag, A. A. M., and E. I. F. D. Bruijn (1988), Applied modelling of the nighttime surface energy balance over land, *J. Appl. Meteorol.*, *27*, 689–704.

Hori, A., et al. (1999), A detailed density profile of the Dome Fuji (Antarctica) shallow ice core by X-ray transmission method, *Ann. Glaciol.*, *29*, 211–214.

Isaksson, E., and W. Karlén (1994), Spatial and temporal patterns in snow accumulation, western Dronning Maud Land, Antarctica, *J. Glaciol.*, *40*(135), 399–409.

Isaksson, E., W. Karlén, N. Gundestrup, P. Mayewski, S. Whitlow, and M. Twickler (1996), A century of accumulation and temperature changes in Dronning Maud Land, Antarctica, *J. Geophys. Res.*, *101*(D3), 7085–7094.

Isaksson, E., M. R. van den Broeke, J.-G. Winther, L. Karlöf, J.-F. Pinglot, and N. Gundestrup (1999), Accumulation and proxy-temperature variability in Dronning Maud Land, Antarctica, determined from shallow firn cores, *Ann. Glaciol.*, *29*, 17–22.

Jacobel, R. W., and S. M. Hodge (1995), Radar internal layers from the Greenland summit, *Geophys. Res. Lett.*, *22*(5), 587–590.

Jacobel, R. W., B. C. Welch, E. J. Steig, and D. P. Schneider (2005), Glaciological and climatic significance of Hercules Dome, Antarctica: An optimal site for deep ice core drilling, *J. Geophys. Res.*, *110*, F01015, doi:10.1029/2004JF000188.

Jezek, K. C., and E. A. Roeloffs (1983), Measurements of radar wave speeds in polar glaciers using a down-hole radar target technique, *Cold Reg. Sci. Technol.*, *8*, 199–208.

Johnsen, S. J. (1977), Stable isotope homogenization of polar firn and ice, *IAHS Publ.*, *118*, 388–392.

Joughin, I., et al. (2005), Continued deceleration of Whillans Ice Stream, West Antarctica, *Geophys. Res. Lett.*, *32*, L22501, doi:10.1029/2005GL024319.

Jourdain, B., and M. Legrand (2001), Seasonal variations of atmospheric dimethylsulfide, dimethylsulfoxide, sulphur dioxide, methanesulfonate, and non-sea-salt sulphate aerosols at Dumont d'Urville (coastal Antarctica) (December 1998 to July 1999), *J. Geophys. Res.*, *106*(D13), 14,391–14,408.

Jouzel, J., L. Merlivat, M. Pourchet, and C. Lorius (1979), A continuous record of artificial tritium fallout at the South Pole (1954–1978), *Earth Planet. Sci. Lett.*, *45*(1), 188–200.

Jouzel, J., et al. (2007), Orbital and millennial Antarctic climate variability over the past 800,000 years, *Science*, *317*(5839), 793–796, doi:10.1126/science.1141038.

Kaczmarska, M., et al. (2004), Accumulation variability derived from an ice core from coastal Dronning Maud Land, Antarctica, *Ann. Glaciol.*, *39*, 339–345.

Kameda, T., H. Shoji, K. Kawada, O. Watanabe, and H. B. Clausen (1994), An empirical relation between overburden pressure and firn density, *Ann. Glaciol.*, *20*, 87–94.

Kameda, T., N. Azuma, T. Furukawa, Y. Ageta, and S. Takahashi (1997), Surface mass balance, sublimation and snow temperatures at Dome Fuji Station, Antarctica, in 1995, *Proc. NIPR Symp. Pol. Meteorol. Glaciol.*, *11*, 24–34.

Kameda, T., K. Fujita, O. Sugita, and G. Hashida (2007), Glaciological data collected by the 44th Japanese Antarctic Research Expedition during 2003–2004, *JARE Data Rep. Glaciol.*, *32*, 92 pp.

Kameda, T., H. Motoyama, S. Fujita, and S. Takahashi (2008), Temporal and spatial variability of surface mass balance at Dome Fuji, East Antarctica, by the stake method from 1995 to 2006, *J. Glaciol.*, *54*(84), 107–116.

Kamiyama, K., Y. Ageta, and Y. Fujii (1989), Atmospheric and depositional environments traced from unique chemical compositions of the snow over an inland high plateau, Antarctica, *J. Geophys. Res.*, *94*(D15), 18,515–18,519.

Kanagaratnam, P., S. P. Gogineni, N. Gundstrup, and L. Larsen (2001), High-resolution radar mapping of internal layers at the North Greenland Ice Core Project, *J. Geophys. Res.*, *106*(D24), 33,799–33,812.

Karlöf, L. (2004), Temporal and spatial variability of snow accumulation and redistribution, and its impact on the interpretation of ice cores, Ph.D. thesis, Fac. of Math. and Nat. Sci., Univ. of Oslo, Oslo.

Karlöf, L., et al. (2000), A 1500 years record of accumulation at Amundsenisen western Dronning Maud Land, Antarctica, derived from electrical and radioactive measurements on a 120 m ice core, *J. Geophys. Res.*, *105*(D10), 12,471–12,483.

Karlöf, L., T. A. Oigard, F. Godtliebsen, M. Kaczmarska, and H. Fischer (2005a), Statistical techniques to select detection thresholds for peak signals in ice-core data, *J. Glaciol.*, *51*(175), 655–662.

Karlöf, L., et al. (2005b), Accumulation variability over a small area in east Dronning Maud Land, Antarctica, as determined from shallow firn cores and snow pits: Some implications for ice-core records, *J. Glaciol.*, *51*(174), 343–352.

Karlöf, L., D. P. Winebrenner, and D. B. Percival (2006), How representative is a time series derived from a firn core? A study at a low-accumulation site on the Antarctic plateau, *J. Geophys. Res.*, *111*, F04001, doi:10.1029/2006JF000552.

Kaser, G. (1982), Measurement of evaporation from snow, *Meteorol. Atmos. Phys.*, *30*, 333–340.

Kaspari, S., P. A. Mayewski, D. A. Dixon, V. B. Spikes, S. B. Sneed, M. J. Handley, and G. S. Hamilton (2005), Climate variability in West Antarctica derived from annual accumulation rate records from ITASE firn/ice cores, *Ann. Glaciol.*, *39*, 585–594.

King, J. C., P. S. Anderson, M. C. Smith, and S. D. Mobbs (1996), The surface energy and mass balance at Halley, Antarctica, during winter, *J. Geophys. Res.*, *101*(D14), 19,119–19,128.

King, J. C., P. S. Anderson, and G. W. Mann (2001), The seasonal cycle of sublimation at Halley, Antarctica, *J. Glaciol.*, *47*(156), 1–8.

King, J. C., P. S. Anderson, D. G. Vaughan, G. W. Mann, S. D. Mobbs, and S. B. Vosper (2004), Wind-borne redistribution of snow across an Antarctic ice rise, *J. Geophys. Res.*, *109*, D11104, doi:10.1029/2003JD004361.

Klok, E. J., M. Noland, and M. R. van den Broeke (2005), Analysis of meteorological data and the surface energy balance of McCall Glacier, Alaska, USA, *J. Glaciol.*, *51*(174), 451–461.

Knüsel, S., D. E. Piguet, M. Schwikowski, and H. W. Gäggeler (2003), First results of trace element analysis in ice cores using Continuous Ice Melting (CIM) Inductively Coupled Plasma Sector Field Mass Spectrometry (ICP-SFMS), *J. Phys. IV Fr.*, *107*, doi:10.1051/jp4:20030399.

Kohler, J., J. C. Moore, and E. Isaksson (2003), Comparison of modelled and observed responses of a glacier snowpack to ground-penetrating radar, *Ann. Glaciol.*, *37*, 293–297.

Korth, W., and R. Dietrich (1996), *Ergebnisse geodätischer Arbeiten im Gebiet der Schirmacheroase/Antarctica 1988–1993*, *Publ. Ser. B Angew. Geod.*, vol. 301, Dtsch. Geod. Komm., Bayer. Akad. der Wiss., Munich, Germany.

Kovacs, A., A. J. Gow, and R. M. Morey (1995), The in-situ dielectric constant of polar firn revisited, *Cold Reg. Sci. Technol.*, *23*, 245–256.

Krinner, G., O. Magand, I. Simmonds, C. Genthon, and J.-L. Dufresne (2007), Simulated Antarctic precipitation and surface mass balance at the end of the 20th and 21st centuries, *Clim. Dyn.*, *28*, 215–230, doi:10.1007/s00382-006-0177-x.

Lambert, G., B. Ardouin, J. Sanak, C. Lorius, and M. Pourchet (1977), Accumulation of snow and radioactive debris in Antarctica: A possible refined radiochronology beyond reference levels, in *Symposium Isotopes et Impuretés dans les neiges et glaces, Colloque de Grenoble, IAHS Publ.*, *118*, 146–158.

Legrand, M., and R. J. Delmas (1984), The ionic balance of Antarctic snow: A 10-year detailed record, *Atmos. Environ.*, *18*, 1867–1874.

Legrand, M., and P. A. Mayewski (1997), Glaciochemistry of polar ice cores: A review, *Rev. Geophys.*, *35*, 219–243.

Li, J., and H. J. Zwally (2002), Modeled seasonal variations of firn density induced by steady-state surface air-temperature cycle, *Ann. Glaciol.*, *34*, 299–302.

Li, J., and H. J. Zwally (2004), Modeling the density variation in the shallow firn layer, *Ann. Glaciol.*, *38*, 309–313.

Li, L., and J. W. Pomeroy (1997), Estimates of threshold wind speeds for snow transport using meteorological data, *J. Appl. Meteorol.*, *36*, 205–213.

Lipenkov, V. Y., A. A. Ekaykin, N. I. Barkov, and M. Pourchet (1998), O svyazi plotnosti poverhnostnogo sloya snega v Antarktide so skorost'yu vetra (On the relationship of surface snow density in Antarctica and wind speed), *Mater. Glyatsiol. Issled.*, *85*, 148–158.

Looyenga, H. (1965), Dielectric constant of heterogeneous mixtures, *Physica*, *31*(3), 401–406.

Magand, O., M. Frezzotti, M. Pourchet, B. Stenni, L. Genoni, and M. Fily (2004), Climate variability along latitudinal and longitudinal transects in East Antarctica, *Ann. Glaciol.*, *39*, 351–358.

Magand, O., C. Genthon, M. Fily, G. Krinner, G. Picard, M. Frezzotti, and A. A. Ekaykin (2007), An up-to-date quality-controlled surface mass balance data set for the 90°–180°E Antarctica sector and 1950–2005 period, *J. Geophys. Res.*, *112*, D12106, doi:10.1029/2006JD007691.

Mann, G. W., P. S. Anderson, and S. D. Mobbs (2000), Profile measurements of blowing snow at Halley, Antarctica, *J. Geophys. Res.*, *105*(D19), 24,491–24,508.

Masson-Delmotte, V., et al. (2008), A review of Antarctic surface snow isotopic composition: Observations, atmospheric circulation and isotopic modelling, *J. Clim.*, in press.

Matsuoka, K., T. Furukawa, S. Fujita, H. Maeno, S. Uratsuka, R. Naruse, and O. Watanabe (2003), Crystal orientation fabrics within the Antarctic ice sheet revealed by a multipolarization plane and dual-frequency radar survey, *J. Geophys. Res.*, *108*(B10), 2499, doi:10.1029/2003JB002425.

Matsuoka, K., S. Uratsuka, S. Fujita, and F. Nishio (2004), Ice-flow induced scattering zone within the Antarctic ice sheet revealed by high-frequency airborne radar, *J. Glaciol.*, *50*(170), 382–388.

Mavrocordatos, C., E. Attema, M. Davidson, H. Lentz, and U. Nixdorf (2004), Development of ASIRAS (Airborne SAR/Interferometric Altimeter System), in *Geoscience and Remote Sensing Symposium IGARSS '04*, vol. 4, pp. 2465–2467, IEEE Int., New York, doi:10.1109/IGARSS.2004.1369792.

Mayewski, P. A., and I. D. Goodwin (1997), International Trans-Antarctic Scientific Expedition (ITASE), *PAGES Rep. 1997-1*, 48 pp., Past Global Changes Proj., Bern.

Mayewski, P. A., L. D. Meeker, S. Whitlow, M. S. Twickler, M. C. Morrison, R. B. Alley, P. Bloomfield, and K. Taylor (1993), The atmosphere during the Younger Dryas, *Science*, *261*(5118), 195–197, doi:10.1126/science.261.5118.195.

Mayewski, P. A., et al. (2005), The International Trans-Antarctic Scientific Expedition (ITASE): An overview, *Ann. Glaciol.*, *41*, 180–185.

McConnell, J. R., R. C. Bales, and D. R. Davis (1997), Recent intra-annual snow accumulation at South Pole: Implications for ice core interpretation, *J. Geophys. Res.*, *102*(D18), 21,947–21,954.

McMorrow, A. J., M. A. J. Curran, T. D. van Ommen, V. Morgan, I. Allison, and M. J. Pook (2001), Intercomparison of firn core and meteorological data, *Antarct. Sci.*, *13*(3), 329–337.

Meyerson, E. A., P. A. Mayewski, K. J. Kreutz, L. D. Meeker, S. I. Whitlow, and M. S. Twickler (2002), The polar expression of ENSO and sea-ice variability as recorded in a South Pole ice core, *Ann. Glaciol.*, *35*, 430–436.

Millar, D. H. H. (1981), Radio echo layering in polar ice sheets and past volcanic activity, *Nature*, *292*, 441–443.

Minikin, A., D. Wagenbach, W. Graf, and J. Kipfstuhl (1994), Spatial and seasonal variations of the snow chemistry at the central Filchner–Ronne Ice Shelf, Antarctica, *Ann. Glaciol.*, *20*, 283–290.

Monaghan, A. J., et al. (2006), Insignificant change in Antarctic snowfall since the International Geophysical Year, *Science*, *313*(5788), 827–831, doi:10.1126/science.1128243.

Moore, J. C. (1988), Dielectric variability of a 130 m Antarctic ice core: Implications for radar sounding, *Ann. Glaciol.*, *11*, 95–99.

Moore, J. C., and R. Mulvaney (1989), Dielectrical stratigraphy of ice: A new technique for determining total ionic concentrations in polar ice cores, *Geophys. Res. Lett.*, *16*(10), 1171–1179.

Moore, J. C., and J. G. Paren (1987), New technique for dielectric logging of Antarctic ice cores, *J. Physi. Colloq. C1)*, *48*(3), 155–160.

Moore, J. C., H. Narita, and N. Maeno (1991), A continuous 770-year record of volcanic activity from East Antarctica, *J. Geophys. Res.*, *96*(D9), 17,353–17,359.

Morey, R. M., and A. Kovacs (1985), Analysis of wide-angle reflection and refraction measurements, *CRREL Spec. Rep.*, *85-5*, 53–60.

Morgan, V. I., and T. H. Jacka (1981), Mass balance studies in East Antarctica, in *Sea Level, Ice, and Climatic Change*, edited by I. Allison, *IAHS Publ.*, *131*, 253–260.

Morgan, V. I., I. D. Goodwin, D. M. Etheridge, and C. W. Wookey (1991), Evidence from Antarctic ice cores for recent increases in snow accumulation, *Nature*, *354*, 58–60.

Morris, E. D., and J. D. Cooper (2003), Density measurements in ice boreholes using neutron scattering, *J. Glaciol.*, *49*(167), 599–604.

Mosley-Thompson, E., and L. G. Thompson (1982), Nine centuries of microparticle deposition at the South Pole, *Quat. Res.*, *17*, 1–13.

Mosley-Thompson, E., L. G. Thompson, J. F. Paskievitch, M. Pourchet, A. J. Gow, M. E. Davis, and J. Kleinman (1995), South Pole snow accumulation has increased in recent decades, *Ann. Glaciol.*, *21*, 131–138.

Mosley-Thompson, E., J. F. Paskievitch, A. J. Gow, and L. G. Thompson (1999), Late 20th century increase in South Pole snow accumulation, *J. Geophys. Res.*, *104*(D4), 3877–3886.

Mulvaney, R., H. Oerter, D. A. Peel, W. Graf, C. Arrowsmith, E. C. Pasteur, B. Knight, G. C. Littot, and W. D. Miners (2002), 1000 year ice-core records from Berkner Island, Antarctica, *Ann. Glaciol.*, *35*, 45–51.

Murray, T., G. W. Stuart, P. J. Miller, J. Woodward, A. M. Smith, P. R. Porter, and H. Jiskoot (2000), Glacier surge propagation by thermal evolution at the bed, *J. Geophys. Res.*, *105*(B6), 13,491–13,507.

Muszynski, I., and G. E. Birchfield (1985), The dependence of Antarctic accumulation rates on surface temperature and elevation, *Tellus, Ser. A*, *37*, 204–208.

Neftel, A. (1991), Use of snow and firn analysis to reconstruct past atmospheric composition, in *Seasonal Snowpacks*, *NATO ASI, Ser. G*, vol. 28, edited by T. D. Davies, M. Tranter, and H. Jones, pp. 385–415, Springer, Berlin.

Nemazi, M., G. Lambert, C. Lorius, and J. Labeyrie (1964), Mesure du taux d'accumulation de la neige au bord du continent Antarctique par la méthode du Plomb-210, *C. R. Hebd. Seances Acad. Sci.*, *259*(19), 3319–3322.

Nereson, N. A., C. F. Raymond, R. W. Jacobel, and E. D. Waddington (2000), The accumulation pattern across Siple Dome, West Antarctica, inferred from radar-detected internal layers, *J. Glaciol.*, *46*(156), 75–87.

Neumann, T. A., and E. D. Waddington (2004), Effects of firn ventilation on isotopic exchange, *J. Glaciol.*, *50*(169), 183–194.

Neumann, T. A., E. D. Waddington, E. J. Steig, and P. M. Grootes (2005), Non-climate influences on stable isotopes at Taylor Mouth, Antarctica, *J. Glaciol.*, *51*(173), 248–258.

Nishio, F., et al. (2002), Annual-layer determinations and 167 year records of past climate of H72 ice core in east Dronning Maud Land, Antarctica, *Ann. Glaciol.*, *35*, 471–479.

Noone, D., J. Turner, and R. Mulvaney (1999), Atmospheric signals and characteristics of accumulation in Dronning Maud Land, Antarctica, *J. Geophys. Res.*, *104*(D16), 19,191–19,211.

Oerlemans, J. (2003), Analysis of a 3 year meteorological record from the ablation zone of Morteratschgletscher, Switzerland: Energy and mass balance, *J. Glaciol.*, *46*(155), 571–579.

Oerter, H. (2005), Stable oxygen isotopes of snow pit DML25S02_03 (SS0203), *PANGAEA*, doi:10.1594/PANGAEA.264585.

Oerter, H., W. Graf, F. Wilhelms, A. Minikin, and H. Miller (1999), Accumulation studies on Amundsenisen, Dronning Maud Land, Antarctica, by means of Tritium, dielectric profiling and stable-isotope measurements: First results from the 1995–96 and 1996–97 field seasons, *Ann. Glaciol.*, *29*, 1–9.

Oerter, H., F. Wilhelms, F. Jung-Rothenhäusler, F. Göktas, H. Miller, W. Graf, and S. Sommer (2000), Accumulation rates in Dronning Maud Land as revealed by dielectrical-profiling measurements at shallow firn cores, *Ann. Glaciol.*, *30*, 27–34.

Oerter, H., W. Graf, H. Meyer, and F. Wilhelms (2004), The EPICA ice core Dronning Maud Land: First results from stable-isotope measurements, *Ann. Glaciol.*, *39*(39), 307–312.

Osterberg, E. C., M. J. Handley, S. B. Sneed, P. A. Mayewski, and K. J. Kreutz (2006), Continuous ice core melter system with discrete sampling for major ion, trace element and stable isotope analyses, *Environ. Sci. Technol.*, *40*, 3355–3361.

Palais, J. M., I. M. Whillans, and C. Bull (1982), Snow stratigraphic studies at Dome C, East Antarctica: An investigation of depositional and diagenetic processes, *Ann. Glaciol.*, *3*, 239–242.

Palais, J. M., M. S. Germani, and G. A. Zielinski (1992), Interhemispheric transport of volcanic ash from a 1259 A.D. volcanic eruption to the Greenland and Antarctic ice sheets, *Geophys. Res. Lett.*, *19*(8), 801–804.

Pälli, A., J. C. Kohler, E. Isaksson, J. C. Moore, J. F. Pinglot, V. A. Pohjola, and H. Samuelsson (2002), Spatial and temporal variability of snow accumulation using ground-penetrating radar and ice cores on a Svalbard glacier, *J. Glaciol.*, *48*(162), 417–424.

Palmer, A. S., T. D. van Ommen, M. A. J. Curran, V. Morgan, J. M. Souney, and P. A. Mayewski (2001), High-precision dating of volcanic events (A.D. 1301–1995) using ice cores from Law Dome, Antarctica, *J. Geophys. Res.*, *106*(D22), 28,089–28,095.

Parrenin, F., R. Hindmarsh, and F. Remy (2006), Analytical solutions for the effect of topography, accumulation rate and flow divergence on isochrone layer geometry, *J. Glaciol.*, *52*(177), 191–202.

Petit, J.-R., J. Jouzel, M. Pourchet, and L. Merlivat (1982), A detailed study of snow accumulation and stable isotope content in Dome C (Antarctica), *J. Geophys. Res.*, *87*(C6), 4301–4308.

Pettré, P., J. F. Pinglot, M. Pourchet, and L. Reynaud (1986), Accumulation in Terre Adélie, Antarctica: Effect of meteorological parameters, *J. Glaciol.*, *32*(112), 486–500.

Picciotto, E., and S. Wilgain (1963), Fission products in Antarctic snow, a reference level for measuring accumulation, *J. Geophys. Res.*, *68*(21), 5965–5972.

Picciotto, E., G. Crozaz, and W. D. Breuck (1964), Rate of accumulation of snow at South Pole as determined by radioactive measurements, *Nature*, *203*, 393–394.

Picciotto, E., G. Crozaz, and W. de Breuck (1971), Accumulation on the South Pole–Queen Maud Land Traverse, 1964–1968, in *Antarctic Snow and Ice Studies II*, *Antarct. Res. Ser.*, vol. 16, edited by A. Crary, pp. 257–315, AGU, Washington, D. C.

Pinglot, F., and M. Pourchet (1979), Low-level beta counting with an automatic sample changer, *Nucl. Instrum. Methods*, *166*(3), 483–490.

Pinglot, J. F., and M. Pourchet (1981), Gamma-ray bore-hole logging for determining radioactive fallout layers in snow, in *Methods of Low-Level Counting and Spectrometry*, pp. 161–172, Int. At. Energy Agency, Vienna.

Pinglot, J. F., and M. Pourchet (1994), Spectrométrie Gamma à trés bas niveau avec anti-compton NaI (T1) pour l'étude des glaciers et des sédiments, *J. Spectrom. Gamma X*, *93*, 291–296.

Pourchet, M., F. Pinglot, and C. Lorius (1983), Some meteorological applications of radioactive fallout measurements in Antarctic snows, *J. Geophys. Res.*, *88*(C10), 6013–6020.

Pourchet, M., et al. (1997), Distribution and fall-out of 137Cs and other radionuclides over Antarctica, *J. Glaciol.*, *43*(145), 435–445.

Pourchet, M., O. Magand, M. Frezzotti, A. A. Ekaykin, and J. G. Winter (2003), Radionuclides deposition over Antarctica, *J. Environ. Radioact.*, *68*, 137–158.

Qin, D. H., J. W. Ren, J. C. Kang, C. D. Xiao, Z. Q. Li, Y. S. Li, B. Sun, W. Z. Sun, and X. X. Wang (2000), Primary results of glaciological studies along an 1100 km transect from Zhongshan station to Dome A, East Antarctic ice sheet, *Ann. Glaciol.*, *31*, 198–204.

Ramillien, G., A. Lombard, A. Cazenave, E. R. Ivins, M. Llubes, F. Remy, and R. B. Ramilien (2006), Interannual variations of the mass balance of the Antarctica and Greenland ice sheets from GRACE, *Global Planet. Change*, *53*(3), 198–208, doi:10.1016/j.gloplacha.2006.06.003.

Rasmussen, S. O., K. K. Andersen, S. J. Johnsen, M. Bigler, and T. McCormack (2005), Deconvolution-based resolution enhancement of chemical ice core records obtained by continuous flow analysis, *J. Geophys. Res.*, *110*, D17304, doi:10.1029/2004JD005717.

Reijmer, C. H., and M. R. V. D. Broeke (2003), Temporal and spatial variability of the surface mass balance in Dronning Maud Land, Antarctica, as derived from automatic weather stations, *J. Glaciol.*, *49*(167), 512–520.

Reijmer, C. H., M. R. van den Broeke, and M. P. Scheele (2002), Air parcel trajectories to five deep drilling locations on Antarctica, based on the ERA-15 data set, *J. Clim.*, *15*, 1957–1968.

Reinhardt, H., M. Kriews, H. Miller, O. Schrems, C. Ludke, E. Hoffmann, and J. Skole (2001), Laser ablation inductively coupled plasma mass spectrometry: A new tool for trace element analysis in ice cores, *Fresenius J. Anal. Chem.*, *370*, 629–636.

Ren, J. W., Q. Dahe, and I. Allison (1999), Variations of snow accumulation and temperature over past decades in the Lambert Glacier basin, Antarctica, *Ann. Glaciol.*, *29*, 29–32.

Ren, J. W., I. Allison, C. D. Xiao, and D. H. Qin (2002), Mass balance of the Lambert Glacier basin, East Antarctica, *Sci. China Ser. D, Earth Sci.*, *45*(9), 842–850.

Richardson, C., and P. Holmlund (1999), Spatial variability at shallow snow-layer depths in central Dronning Maud Land, East Antarctica, *Ann. Glaciol.*, *29*, 10–16.

Richardson, C., E. Aarholt, S.-E. Hamran, P. Holmlund, and E. Isaksson (1997), Spatial distribution of snow in western Dronning Maud Land, East Antarctica, mapped by a ground-based snow radar, *J. Geophys. Res.*, *102*(B9), 20,343–20,353.

Richardson-Näslund, C. (2001), Spatial distribution of snow in Antarctica and other glacier studies using ground-penetrating radar, *Thesis Geogr. Emphasis Phys. Geogr.*, vol. 18, Dep. of Phys. Geogr. and Quat. Geol., Stockholm Univ., Stockholm.

Richardson-Näslund, C. (2004), Spatial characteristics of snow accumulation in Dronning Maud Land, Antarctica, *Global Planet. Change*, *42*, 31–43.

Robin, G. d. Q., S. Evans, and J. T. Bailey (1969), Interpretation of radio echo sounding in polar ice sheets, *Philos. Trans. R. Soc. London, Ser. A*, *146*, 437–505.

Röthlisberger, R., M. Bigler, M. Hutterli, S. Sommer, B. Stauffer, H. G. Junghans, and D. Wagenbach (2000), Technique for continuous high-resolution analysis of trace substances in firn and ice cores, *Environ. Sci. Technol.*, *34*, 338–342.

Rotschky, G., O. Eisen, F. Wilhelms, U. Nixdorf, and H. Oerter (2004), Spatial characteristics of accumulation patterns derived from combined data sets in Dronning Maud Land, Antarctica, *Ann. Glaciol.*, *39*, 265–270.

Rotschky, G., W. Rack, W. Dierking, and H. Oerter (2006), Retrieving snowpack properties and accumulation estimates from combination of SAR and scatterometer measurements, *IEEE Trans. Geos. Rem. Sens.*, *44*(4), 943–956, doi:10.1109/TGRS.2005.862524.

Rotschky, G., P. Holmlund, E. Isaksson, R. Mulvaney, H. Oerter, M. R. van den Broeke, and J.-G. Winther (2007), A new surface accumulation map for western Dronning Maud Land, Antarctica, from interpolation of point measurements, *J. Glaciol.*, *53*(182), 385–398, doi:10.3189/002214307783258459.

Saigne, C., and M. Legrand (1987), Measurements of methanesulphonic acid in Antarctic ice, *Nature*, *330*, 240–242, doi:10.1038/330240a0.

Satake, H., and K. Kawada (1997), The quantitative evaluation of sublimation and the estimation of original hydrogen and oxygen of a firn core at east Queen Maud Land, Antarctica, *Bull. Glacier Res.*, *15*, 93–97.

Schlosser, E., N. van Lipzig, and H. Oerter (2002), Temporal variability of accumulation at Neumayer station, Antarctica, from stake array measurements and a regional atmospheric model, *J. Glaciol.*, *48*(160), 87–94.

Schwander, J., A. Neftel, H. Oeschger, and B. Stauffer (1983), Measurement of direct current conductivity on ice samples for climatological applications, *J. Phys. Chem.*, *87*, 4157–4160.

Scott, J. B. T., D. Mair, P. Nienow, V. Parry, and E. Morris (2006), A ground-based radar backscatter investigation in the percolation zone of the Greenland ice sheet, *Remote Sens. Environ.*, *104*(4), 361–373.

Sigg, A., K. Fuhrer, M. Anklin, T. Staffelbach, and D. Zurmühle (1994), A continuous analysis technique for trace species in ice cores, *Environ. Sci. Technol.*, *28*(2), 204–209.

Sinisalo, A., A. Grinsted, J. C. Moore, E. Kärkäs, and R. Pettersson (2005), Snow-accumulation studies in Antarctica with ground-penetrating radar using 50, 100 and 800 MHz antenna frequencies, *Ann. Glaciol.*, *37*, 194–198.

Smeets, C. J. P. P., and M. R. van den Broeke (2008), Temporal and spatial variation of momentum roughness length in the ablation zone of the Greenland ice sheet, *Boundary Layer Meteorol.*, in press.

Smith, B. T., T. D. Van Ommen, and V. I. Morgan (2002), Distribution of oxygen isotope ratios and snow accumulation rates in Wilhelm II Land, East Antarctica, *Ann. Glaciol.*, *35*, 107–110.

Sommer, S., D. Wagenbach, R. Mulvaney, and H. Fischer (2000a), Glacio-chemical study spanning the past 2 kyr on three ice cores from Dronning Maud Land, Antarctica: 2. Seasonally resolved chemical records, *J. Geophys. Res.*, *105*(D24), 29,423–29,433.

Sommer, S., et al. (2000b), Glacio-chemical study covering the past 2 kyr on three ice cores from Dronning Maud Land, Antarctica: 1. Annually resolved accumulation rates, *J. Geophys. Res.*, *105*(D24), 29,411–29,421.

Spikes, V. B., G. S. Hamilton, S. A. Arcone, S. Kaspari, and P. A. Mayewski (2004), Variability in accumulation rates from GPR profiling on the West Antarctic plateau, *Ann. Glaciol.*, *39*, 238–244.

Stearns, C. R., and G. A. Weidner (1993), Sensible and latent heat flux estimates in Antarctica, in *Antarctic Meteorology and Climatology, Studies Based on Automatic Weather Stations*, *Antarct. Res. Ser.*, vol. 61, edited by D. H. Bromwich and C. R. Stearns, pp. 109–138, AGU, Washington, D. C.

Steffen, K., and J. Box (2001), Surface climatology of the Greenland ice sheet: Greenland Climate Network 1995–1999, *J. Geophys. Res.*, *106*(D24), 33,951–33,964.

Steig, E. J., et al. (2005), High-resolution ice cores from US ITASE (West Antarctica): Development and validation of chronologies and determination of precision and accuracy, *Ann. Glaciol.*, *41*, 77–84.

Stenberg, M., M. Hansson, P. Holmlund, and L. Karlöf (1999), Variability in snow layering and snow chemistry in the vicinity of two drill sites in western Dronning Maud Land, Antarctica, *Ann. Glaciol.*, *29*, 33–37.

Stenni, B., R. Caprioli, L. Cimino, C. Cremisini, O. Flora, R. Gragnani, A. Longinelli, V. Maggi, and S. Torcini (1999), 200 years of isotope and chemical records in a firn core from Hercules Néé, northern Victoria Land, Antarctica, *Ann. Glaciol.*, *29*, 106–112.

Stenni, B., F. Serra, M. Frezzotti, V. Maggi, R. Traversi, S. Becagli, and R. Udisti (2000), Snow accumulation rates in Northern Victoria Land (Antarctica) by firn core analysis, *J. Glaciol.*, *46*(155), 541–552.

Stenni, B., V. Masson-Delmotte, S. Johnsen, J. Jouzel, A. Longinelli, E. Monnin, R. Röthlisberger, and E. Selmo (2001), An oceanic cold reversal during the last deglaciation, *Science*, *293*(5537), 2074–2077, doi:10.1126/science.1059702.

Stenni, B., M. Proposito, R. Gragnani, O. Flora, J. Jouzel, S. Falourd, and M. Frezzotti (2002), Eight centuries of volcanic signal and climate change at Talos Dome (East Antarctica), *J. Geophys. Res.*, *107*(D9), 4076, doi:10.1029/2000JD000317.

Stenseng, L., R. Forsberg, K. Keller, S. M. Hvidegaard, and C. Leuschen (2005), Comparison of airborne laser scanning and D2P radar altimetry, *Geophys. Res. Abst.*, *7*, 06393.

Stroeven, A. P., and V. A. Pohjola (1991), Glaciological studies in Scharffenbergbotnen, in *The Expedition ANTARKTIS-VIII of RV "POLARSTERN" 1989/90*, *Report of Leg ANT-VIII/5, Ber. Polarforschung*, vol. 86, edited by H. Miller and H. Oerter, pp. 126–130, Alfred-Wegener-Inst. für Polar- und Meeresforsch., Bremerhaven, Germany.

Swedish Antarctic Research Programme (2003), Annual report, Stockholm.

Takahashi, S., and T. Kameda (2007), Snow density for measuring the surface mass balance using the stake method, *J. Glaciol.*, *53*(183), 677–680.

Takahashi, S., and O. Watanabe (1997), Snow accumulation in Antarctica: East Queen Maud Land, *Glaciol. Folio, sheet 3-1*, Natl. Inst. of Pol. Res., Tokyo.

Takahashi, S., Y. Ageta, Y. Fujii, and O. Watanabe (1994), Surface mass balance in east Dronning Maud Land, Antarctica, observed by Japanese Antarctic Research Expeditions, *Ann. Glaciol.*, *20*, 242–253.

Taylor, K. C., and R. B. Alley (2004), Two-dimensional electrical stratigraphy of the Siple Dome (Antarctica) ice core, *J. Glaciol.*, *50*(16), 231–235.

Taylor, K. C., et al. (2004), Dating the Siple Dome (Antarctica) ice core by manual and computer interpretation of annual layering, *J. Glaciol.*, *50*(170), 453–461.

Tiuri, M. T., A. H. Sihvola, E. G. Nyfors, and M. T. Hallikainen (1984), The complex dielectric constant of snow at microwave frequencies, *IEEE J. Oceanic Eng.*, *9*(5), 377–382.

Traufetter, F., H. Oerter, H. Fischer, R. Weller, and H. Miller (2004), Spatio-temporal variability in volcanic sulphate deposition over the past 2 kyr in snow pits and firn cores from Amundsenisen, Antarctica, *J. Glaciol.*, *50*(168), 137–146.

Traversi, R., S. Becagli, E. Castellano, A. Migliori, M. Severi, and R. Udisti (2002), High resolution fast ion chromatography (FIC) measurements of chloride, nitrate and sulphate along the EPICA Dome C ice core, *Ann. Glaciol.*, *35*, 291–298.

Udisti, R. (1996), Multiparametric approach for chemical dating of snow layers from Antarctica, *Int. J. Environ. Anal. Chem.*, *63*, 225–244.

Udisti, R., S. Becagli, E. Castellano, R. Mulvaney, J. Schwander, S. Torcini, and E. Wolff (2000), Holocene electrical and chemical measurements from the EPICA Dome C ice core, *Ann. Glaciol.*, *30*, 20–26.

Urbini, S., L. Vittuari, and S. Gandolfi (2001), GPR and GPS data integration: Examples of application in Antartica, *Ann. Geofis.*, *44*(4), 687–702.

Urbini, S., M. Frezzotti, S. Gandolfi, C. Vincent, C. Scarchilli, L. Vittuari, and M. Fily (2008), Historical behaviour of Dome C and Talos Dome (East Antarctica) as investigated by snow accumulation and ice velocity measurements, *Global Planet. Change*, *60*(3–4), 576–588, doi:10.1016/j.gloplacha.2007.08.002.

van de Berg, W. J., M. R. van den Broeke, C. H. Reijmer, and E. van Meijgaard (2006), Reassessment of the Antarctic surface mass balance using calibrated output of a regional atmospheric climate model, *J. Geophys. Res.*, *111*, D11104, doi:10.1029/2005JD006495.

van den Broeke, M. R., and N. P. M. van Lipzig (2003), Factors controlling the near-surface wind field in Antarctica, *Mon. Weather Rev.*, *131*, 733–743.

van den Broeke, M., C. Reijmer, and R. van de Wal (2004a), Surface radiation balance in Antarctica as measured with automatic weather stations, *J. Geophys. Res.*, *109*, D09103, doi:10.1029/2003JD004394.

van den Broeke, M. R., W. J. van de Berg, and E. van Meijgaard (2004b), A study of the surface mass balance in Dronning Maud Land, Antarctica, using automatic weather stations, *J. Glaciol.*, *50*(171), 565–582.

van den Broeke, M., W. J. van de Berg, and E. van Meijgaard (2006a), Snowfall in coastal West Antarctica much greater than previously assumed, *Geophys. Res. Lett.*, *33*, L02505, doi:10.1029/2005GL025239.

van den Broeke, M., W. J. van de Berg, E. van Meijgaard, and C. Reijmer (2006b), Identification of Antarctic ablation areas using a regional atmospheric climate model, *J. Geophys. Res.*, *111*, D18110, doi:10.1029/2006JD007127.

Van der Veen, C. J., and J. F. Bolzan (1999), Interannual variability in the net accumulation on the Greenland Ice Sheet: Observations and implications for the mass-balance measurements, *J. Glaciol.*, *34*(118), 355–357.

Van de Wal, R. S. W., W. Greuell, M. R. van den Broeke, C. Reijmer, and J. Oerlemans (2005), Mass balance observations and automatic weather station data along a transect near Kangerlussuaq, West Greenland, *Ann. Glaciol.*, *42*, 311–316.

van Lipzig, N. P. M., J. C. King, T. A. Lachlan-Cope, and M. R. van den Broeke (2004a), Precipitation, sublimation, and snow drift in the Antarctic Peninsula region from a regional atmospheric model, *J. Geophys. Res.*, *109*, D24106, doi:10.1029/2004JD004701.

van Lipzig, N. P. M., J. Turner, S. R. Colwell, and M. R. van den Broeke (2004b), The near-surface wind field over the Antarctic continent, *Int. J. Climatol.*, *24*(15), 1973–1982.

Vaughan, D. G. (2006), Recent trends in melting condition on the Antarctic Peninsula and their implications for ice-sheet mass balance and sea level, *Arctic Antarct. Alpine Res.*, *38*(1), 147–152.

Vaughan, D. G., J. L. Bamber, M. Giovinetto, and A. P. R. Cooper (1999a), Reassessment of net surface mass balance in Antarctica, *J. Clim.*, *12*, 933–946.

Vaughan, D. G., H. F. J. Corr, C. S. M. Doake, and E. D. Waddington (1999b), Distortion of isochronous layers in ice revealed by ground-penetrating radar, *Nature*, *398*, 323–326.

Vaughan, D. G., P. S. Anderson, J. C. King, G. W. Mann, S. D. Mobbs, and R. S. Ladkin (2004), Imaging of firn isochrones across an Antarctic ice rise and implications for patterns of snow accumulation rate, *J. Glaciol.*, *50*(170), 413–418.

Velicogna, I., and J. Wahr (2006), Measurements of time-variable gravity show mass loss in Antarctica, *Science*, *311*(5768), 1754, doi:10.1126/science.1120808.

Watanabe, O., et al. (1997), A preliminary study of ice core chronology at Dome Fuji Station, Antatactica, *Proc. NIPR Symp. Polar Meteorol. Glaciol.*, *11*, 9–13.

Weller, R., F. Traufetter, H. Fischer, H. Oerter, C. Piel, and H. Miller (2004), Postdepositional losses of methane sulfonate, nitrate, and chloride at the European Project for Ice Coring in Antarctica deep-drilling site in Dronning Maud Land, Antarctica, *J. Geophys. Res.*, *109*, D07301, doi:10.1029/2003JD004189.

Whillans, I. M., and J. F. Bolzan (1988), A method for computing shallow ice-core depths, *J. Glaciol.*, *34*(118), 355–357.

Whitlow, S., P. A. Mayewski, and J. E. Dibb (1992), A comparison of major chemical species input timing and accumulation at South Pole and Summit Greenland, *Atmos. Environ., Part A*, *26*(11), 2045–2054.

Wilgain, S., E. Picciotto, and W. D. Breuck (1965), Strontium 90 fallout in Antarctica, *J. Geophys. Res.*, *70*(24), 6023–6032.

Wilhelms, F. (1996), *Leitfähigkeits- und Dichtemessung an Eisbohrkernen* (Measuring the Conductivity and Density of Ice Cores), *Ber. Polarforsch.*, vol. 191, Alfred-Wegener-Inst. für Polar- und Meeresforsch., Bremerhaven, Germany.

Wilhelms, F. (2000), *Messung dielektrischer Eigenschaften polarer Eiskerne* (Measuring the Dielectric Properties of Polar Ice Cores), *Ber. Polarforsch.*, vol. 367, Alfred-Wegener-Inst. für Polar- und Meeresforsch., Bremerhaven, Germany.

Wilhelms, F. (2005), Explaining the dielectric properties of firn as a density-and-conductivity mixed permittivity (DECOMP), *Geophys. Res. Lett.*, *32*, L16501, doi:10.1029/2005GL022808.

Wilhelms, F., J. Kipfstuhl, H. Miller, K. Heinloth, and J. Firestone (1998), Precise dielectric profiling of ice cores: A new device with improved guarding and its theory, *J. Glaciol.*, *44*(146), 171–174.

Winebrenner, D. P., R. J. Arthern, and C. A. Shuman (2001), Mapping Greenland accumulation rates using observations of thermal emission at 4.5-cm wavelength, *J. Geophys. Res.*, *106*(D24), 33,919–33,934.

Wolff, E. B., J. C. Moore, H. B. Clausen, C. U. Hammer, J. Kipfstuhl, and K. Fuhrer (1995), Long-term changes in the acid and salt concentrations of the Greenland Ice Core Project ice core from electrical stratigraphy, *J. Geophys. Res.*, *100*(D8), 16,249–16,263.

Wolff, E. B., W. D. Miners, J. C. Moore, and J. G. Paren (1997), Factors controlling the electrical conductivity of ice from the polar reginos—A summary, *J. Phys. Chem. B*, *101*, 6090–6094.

Wolff, E. B., I. Basile, J.-R. Petit, and J. Schwander (1999), Comparison of Holocene electrical records from Dome C and Vostok, Antarctica, *Ann. Glaciol.*, *29*, 89–93.

Xiao, C. D., D. H. Qin, L. G. Bian, X. J. Zhou, I. Allison, and M. Yan (2005), A precise monitoring of snow surface height in the region of Lambert Glacier basin-Amery Ice Shelf, East Antarctica, *Sci. China, Ser. D, Earth Sci.*, *48*(1), 100–111.

Yilmaz, O. (1987), *Seismic Data Processing*, *Invest. Geophys.*, vol. 2, Soc. of Explor. Geophys., Tulsa, Okla.

Young, N. W., M. Pourchet, V. M. Kotlyakov, P. A. Korolev, and M. B. Dyugerov (1982), Accumulation distribution in the IAGP area, Antarctica: 90°E–150°E, *Ann. Glaciol.*, *3*, 333–338.

Zwally, H. J., and M. B. Giovinetto (1995), Accumulation in Antarctica and Greenland derived from passive-microwave data: A comparison with contoured compilations, *Ann. Glaciol.*, *21*, 123–130.

Zwally, H. J., M. B. Giovinetto, J. Li, H. G. Cornejo, M. A. Beckley, A. C. Brenner, J. L. Saba, and D. Yi (2005), Mass changes of the Greenland and Antarctic ice sheets and shelves and contributions to sea-level rise: 1992–2002, *J. Glaciol.*, *51*(175), 509–527, 19.

D. A. Dixon and S. Kaspari, Climate Change Institute, Department of Earth Sciences, University of Maine, 5790 Edward T. Bryand Global Sciences Center, Orono, ME 04469-5790, USA. (daniel_dixon@umit.maine.edu; susan.kaspari@maine.edu)

O. Eisen and H. Oerter, Stiftung Alfred-Wegener-Institut für Polar- und Meeresforschung, Posttach 120161, D-27515 Bremerhaven, Germany. (olaf.eisen@awi.de; hans.oerter@awi.de)

A. Ekaykin and V. Y. Lipenkov, Arctic and Antarctic Research Institute, 38 Bering Street, 199397 St. Petersburg, Russia. (ekaykin@aari.nw.ru; lipenkov@aari.nw.ru)

M. Frezzotti, ENEA Laboratory for climate observation, SP. Anguillarese, 301 I-00123 S.M. di Galeria (Roma), Roma, Italy. (frezzotti@casaccia.enea.it)

C. Genthon and O. Magand, LGGE, CNRS, Université Joseph-Fourier Grenoble, 54, Rue Molière, BP 96, Domaine Universitaire, F-38402 Saint-Martin d'H'eres, France. (genthon@lgge.obs.ujf-grenoble.fr; magand@lgge.obs.ujf-grenoble.fr)

P. Holmlund, Department of Physical Geography and Quaternary Geology, Stockholm University, SE-10691 Stockholm, Sweden. (per.holmlund@natgeo.su.se)

E. Isaksson, Norwegian Polar Institute, Polar Environmental Centre, N-9296 Tromsø, Norway. (elli@npolar.no)

T. Kameda and S. Takahashi, Snow and Ice Research Laboratory, Kitami Institute of Technology, 165 Koencho, Kitami, Hokkaido 090-8507, Japan. (kameda@mail.kitami-it.ac.jp; shuhei@mail.kitami-it.ac.jp)

L. Karlöf, Research and Development, SWIX SPORT AS, Servicebox, N-2626 Lillehammer, Norway. (l.karlof@swixsport.no)

M. R. van den Broeke, Institute for Marine and Atmospheric Research, Utrecht University, PO Box 80 005, NL-3508 TA Utrecht, Netherlands. (m.r.vandenbroeke@phys.uu.nl)

D. G. Vaughan, British Antarctic Survey, Natural Environment Research Council, High Cross, Madingley Road, Cambridge CB3 0ET, UK. (dgv@bas.ac.uk)

of certain natural heuristics. These include choosing colors that will result in the fewest local conflicts (mentioned on 11 surveys), as well as attempting to avoid conflicts with neighbors with high connectivity (mentioned on 39 surveys, and obviously applicable to only those two information views that revealed such neighboring information), presumably on the logic that highly connected vertices present the most constrained and difficult problems for subjects. Surveys and the experimental data also revealed a number of instances of signaling behavior by subjects, but here there was less consistency. Some subjects clearly alternated between two colors that were unused in their neighborhood in an attempt to inform neighbors of this fact. Others would alternate between colors in an attempt to call attention to conflicts. Although such signaling behaviors are apparent in the data, it is unclear whether they ever had their intended effects. Many subjects also reported introducing conflicts into their local neighborhood even when they had an available color, in an attempt to perturb the global state from a perceived stasis or local minimum. Even excluding perturbations introduced 2 s or less after the absence of any local conflicts (to account for reaction time), the 38 experiments together had 181 such incidents. This behavior might be viewed as a human analog of the deliberate injection of randomization or "thermal noise" into common optimization algorithms such as simulated annealing. Further work is needed to integrate these observations with statistical methods applied to the experimental data, in order to develop plausible stochastic models of individual behavior in the coloring problem. Ideally such models, when run in multiple independent copies, could predict which networks would be easy or difficult for human populations.

Although the results presented here are suggestive, they are limited in a variety of important ways. The human subject networks were small, a perhaps necessary consequence of the carefully controlled, simultaneous play experiments. It is tempting to contemplate Web-based studies (*25*) on a much larger scale, which will require addressing incentives, attrition, communication, and many other issues. The network topologies examined here were but a sampling of the rich space of possibilities and recent network formation models. Rather than imposing a chosen network structure on subjects, it would also be interesting to consider scenarios in which the subjects themselves participated in the network formation process, while still allowing some variability of structure. Future work should consider an even wider range of natural collective problems and activities. Candidates include problems of agreement or consensus rather than differentiation, and problems involving the formation of local teams or subgroups specifying certain properties (such as being fully connected or having at least one member of each of a fixed number of types or roles).

References and Notes

1. J. Travers, S. Milgram, *Sociometry* **32**, 425 (1969).
2. M. Gladwell, *The Tipping Point* (Little, Brown, Boston, 2000).
3. S. Milgram, *Psychol. Today* **61**, 60 (1967).
4. M. S. Granovetter, *AJS* **78**, 1360 (1973).
5. B. A. Huberman, L. A. Adamic, in *Complex Networks*, E. Ben-Naim, H. Frauenfelder, Z. Toroczkai, Eds. (Springer, Berlin, 2004), pp. 371–398.
6. O. Sporns, G. Tononi, G. M. Edelman, *Cereb. Cortex* **10**, 127 (2000).
7. A. Wagner, D. Fell, *Proc. R. Soc. London B. Biol. Sci.* **268**, 1803 (2001).
8. A. Broder *et al.*, in *Proceedings of the Ninth International World Wide Web Conference* (Elsevier, Amsterdam, 2000), pp. 309–320.
9. D. J. Watts, *Small Worlds: The Dynamics of Networks Between Order and Randomness* (Princeton Univ. Press, Princeton, NJ, 1999).
10. A.-L. Barabási, R. Albert, *Science* **286**, 509 (1999).
11. J. Kleinberg, *Nature* **406**, 845 (2000).
12. M. R. Garey, D. S. Johnson, *Computers and Intractability* (W. H. Freeman, New York, 1979).
13. J. A. Zoellner, C. L. Beall, *IEEE Trans. Electromagn. Compatibil.* **19**, 313 (1977).
14. J. Janssen, D. Krizanc, L. Narayanan, S. Shende, *J. Algorithms* **36**, 119 (2000).
15. R. M. Karp, in *Complexity of Computer Computations*, Proc. Sympos. IBM Thomas J. Watson Res. Center, Yorktown Heights, NY (Plenum, New York, 1972), pp. 85–103.
16. S. Khot, in *Proceedings of 42nd IEEE symposium on Foundations of Computer Science*, (2001).
17. U. Feige, J. Kilian, *J. Comput. Syst. Sci.* **57**, 187 (1998).
18. An earlier session of similarly controlled human subject experiments was conducted in September 2005 as a field test for the system. Although we do not report on these here because they used different network structures, they largely foreshadowed our main findings and influenced the design of the January 2006 experiments. The same was true of a graph-coloring exercise held in a University of Pennsylvania class in February 2005 in which communication between subjects was restricted to obey the network structure (but was otherwise unconstrained, and included open discussion and negotiation). Details are in the supporting material (*26*).
19. D. J. Watts, S. H. Strogatz, *Nature* **393**, 440 (1998).
20. For each network structure, trials were conducted under three information conditions. For each network, we also examined two different incentive or payment schemes for subjects. The variation across these two design variables yielded $3 \times 2 = 6$ trials of each network. Two networks were given an additional trial to examine potential learning effects, yielding a total of seven trials. Details in (*26*).
21. C. F. Camerer, *Behavioral Game Theory* (Princeton Univ. Press, Princeton, NJ, 2003).
22. One session of experiments used collective or global incentives, in which all 38 participants were each paid $5 for every experiment that resulted in a proper coloring within the 5 min allotted. The other session used individual or local incentives, in which a participant received $5 if an experiment ended (due either to proper coloring or the termination of 5 min) with their own color being different from all their network neighbors. There were no noteworthy differences between the two incentive schemes in any of the measures discussed.
23. There is a downward bias introduced in the average experiment durations because they were capped at 300 s. However, the distribution of unsolved experiments was such that allowing these experiments to continue to solution would only have strengthened the results reported here; see (*26*).
24. J. Kleinberg, in *Proceedings of the 32nd Annual ACM Symposium on Theory of Computing* (Association for Computing Machinery, New York, 2000), pp. 163–170.
25. P. Dodds, R. Muhamad, D. J. Watts, *Science* **301**, 827 (2003).
26. Materials and methods are available as supporting material on *Science* Online.

27. The authors thank D. Watts, C. Camerer, and T. Senator for their encouragement and for many helpful suggestions regarding this research. We are also grateful to H. Ni for his contributions to the early stages of the project. The work was supported by a grant from the Defense Advanced Research Projects Agency.

Supporting Online Material

www.sciencemag.org/cgi/content/full/313/5788/824/DC1
Materials and Methods
SOM Text

9 March 2006; accepted 15 June 2006
10.1126/science.1127207

Insignificant Change in Antarctic Snowfall Since the International Geophysical Year

Andrew J. Monaghan,[1]* David H. Bromwich,[1] Ryan L. Fogt,[1] Sheng-Hung Wang,[1] Paul A. Mayewski,[3] Daniel A. Dixon,[3] Alexey Ekaykin,[4] Massimo Frezzotti,[5] Ian Goodwin,[6] Elisabeth Isaksson,[7] Susan D. Kaspari,[3] Vin I. Morgan,[8] Hans Oerter,[9] Tas D. Van Ommen,[8] Cornelius J. Van der Veen,[2] Jiahong Wen[10]

Antarctic snowfall exhibits substantial variability over a range of time scales, with consequent impacts on global sea level and the mass balance of the ice sheets. To assess how snowfall has affected the thickness of the ice sheets in Antarctica and to provide an extended perspective, we derived a 50-year time series of snowfall accumulation over the continent by combining model simulations and observations primarily from ice cores. There has been no statistically significant change in snowfall since the 1950s, indicating that Antarctic precipitation is not mitigating global sea level rise as expected, despite recent winter warming of the overlying atmosphere.

Global sea level (GSL) has been increasing by 1.7 mm year^{-1} over the past century (*1*) and 2.8 mm year^{-1} over the past decade (*2*). One of the greatest uncertainties in predictions of GSL rise is the contribution of the Antarctic ice sheets (*3*). The Antarctic ice budget is balanced by the buildup of snowfall in the interior and wastage due to

melting and calving of ice along the coastal margins. Future scenarios from global climate models (GCMs) suggest that Antarctic snowfall should increase in a warming climate, mainly due to the greater moisture-holding capacity of warmer air (*4*), partially offsetting enhanced loss at the ice sheet peripheries. Perplexing temperature trends have been reported over Antarctica since continuous monitoring began with the International Geophysical Year (IGY) in 1957–1958, varying by the season, the region, and the time period analyzed (*5*, *6*). A recent study suggests a strong tropospheric warming signal has been manifested over Antarctica during winters since the early 1970s (*7*), the season during which much of the continent receives its maximum snowfall (*8*). Satellite-based ice velocity and altimetry measurements indicate that the West Antarctic Ice Sheet (WAIS) has been thinning over the past decade, with a contribution to GSL rise of 0.13 to 0.16 mm year^{-1} (*9*, *10*), consistent with widespread melting of ice sheet grounding lines (*11*). In light of these studies, it is essential to assess whether Antarctic snowfall has been increasing.

The latest studies using global and regional atmospheric models to evaluate changes in Antarctic snowfall indicate that no statistically significant increase has occurred since ~1980 over the entire grounded ice sheet, WAIS, or the East Antarctic Ice Sheet (EAIS) (*12*–*14*). A validation of the modeled-versus-observed changes (*12*) suggested that the recent model records are more reliable than the earlier global model records that inferred an upward trend in Antarctic snowfall since 1979 (*15*). The new studies also showed that interannual snowfall variability is considerable; yearly snowfall fluctuations of ±20 mm year^{-1} water equivalent (WEQ), i.e., ±0.69 mm year^{-1} GSL equivalent, are common (*12*) and might easily mask underlying trends over the short record. It is necessary to extend the snowfall record back to the IGY so that (i) trends can be assessed within a longer context, (ii) the snowfall record can be compared with the entire instrumental temperature record over Antarctica, and (iii) a 50-year benchmark for GCM evaluation is available.

[1]Polar Meteorology Group, Byrd Polar Research Center, [2]Department of Geological Sciences, Ohio State University, Columbus, OH 43210, USA. [3]Climate Change Institute, University of Maine, Orono, ME 04469, USA. [4]Arctic and Antarctic Research Center, St. Petersburg 199397, Russia. [5]National Agency for New Technologies, Energy, and the Environment, Rome 00060, Italy. [6]School of Environmental and Life Sciences, University of Newcastle, Callaghan, New South Wales 2308, Australia. [7]Norwegian Polar Institute, Tromso N-9296, Norway. [8]Department of the Environment and Heritage, Australian Antarctic Division and Antarctic Climate and Ecosystems Cooperative Research Centre, Private Bag 80, Hobart, Tasmania 7001, Australia. [9]Alfred Wegner Institute for Polar and Marine Research, Bremerhaven D-27515, Germany. [10]Department of Geography, Shanghai Normal University, Shanghai 200234, China.

*To whom correspondence should be addressed. E-mail: monaghan.11@osu.edu

The small volume of meteorological data over the Southern Ocean and Antarctica renders modeled snowfall amounts highly questionable before the modern satellite era (~1979) (*13*, *16*). The only other records of snowfall variability before 1979 are from ice cores, snow pits, and precipitation gauges. The spatial coverage of these data has been too sparse to accurately assess snowfall accumulation over the entire continent. However, in recent years scores of new ice core records have become available, due in large part to the International Transantarctic Scientific Expedition (ITASE), a multinational field program aimed at reconstructing the recent climate history of Antarctica through ice coring and related observations along an extensive network of traverses (*17*). In this study, we used these new records together with existing ice cores, snow pit and snow stake data, meteorological observations, and validated model fields to reconstruct Antarctic snowfall accumulation over the past 5 decades.

Each observational record is representative of an area surrounding it (a "zone"), the size of which depends on the atmospheric circulation, the interaction of wind with topography, and the time scale considered. Our method used meteorological model reanalysis fields to determine zones of snowfall coherence that correlate with the individual records at annual time scales. Assuming these zones adequately cover most of the continent given the available observational records, this information can be used to synthesize the observations into a continent-wide record of snowfall accumulation in a self-consistent manner. The model reanalysis data set we used is the European Centre for Medium-Range Weather Forecasts 40-Year Reanalysis (ERA-40) (*18*). We defined snowfall accumulation from ERA-40 precipitation fields that were adjusted to match long-term observed accumulation records (*19*). Precipitation dominates snowfall accumulation variability over Antarctica at model grid scales (*8*, *15*). ERA-40 precipitation was compared to independent observed accumulation records for overlap periods and shown to largely reproduce the interannual snowfall accumulation variability and

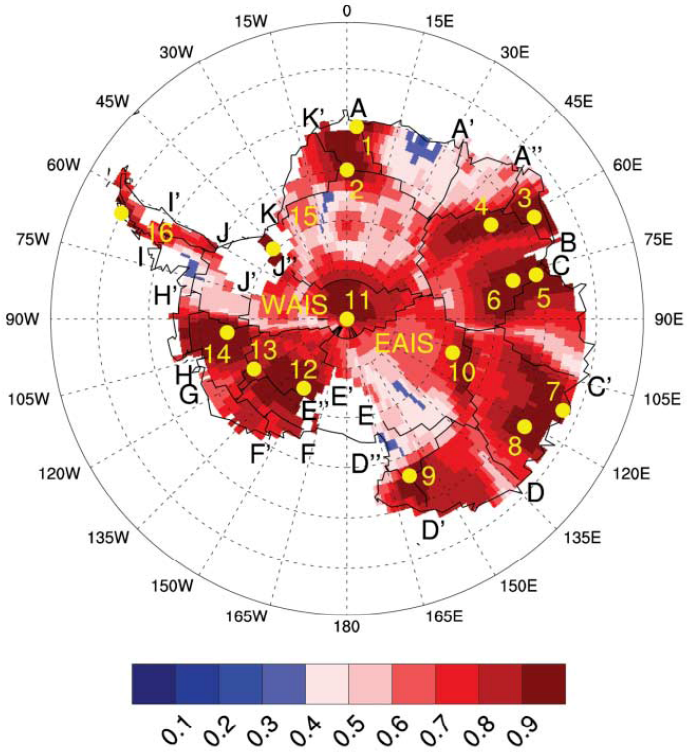

Fig. 1. The composite map of the maximum absolute value of the Pearson's correlation coefficient ($|r|$) resulting from correlating the ERA-40 1985–2004 percentage annual snowfall accumulation change (with respect to the 1985–1994 mean) for the grid box containing each of the 16 observation sites (yellow dots and numbers) with every other 1°-by-1° grid box over Antarctica (i.e., this map is a composite of 16 maps). Pink and red colors have correlations at $P < 0.01$. The black lines delineate ice drainage basins (*20*), which are identified alphabetically by the black letters where they intersect the grounding line. Detailed information about the observation sites is included in (*19*).

trends, justifying its use for this study (*19*). Figure 1 shows a composite map of the maximum correlation coefficient obtained by correlating the ERA-40 simulated percentage annual precipitation anomaly at the grid point closest to each core with every other grid point. Correlations greater than 0.5 ($P < 0.01$) occur over most of the grounded ice sheet, indicating that the zones of spatial coherence from the available observational records cover nearly the entire continent. We used this robust relationship to synthesize the observational data into a series of continent-wide snowfall accumulation maps for the period before 1985, when the precipitation variability simulated by ERA-40 is questionable (*12*). The result is a 5-decade time series of snowfall accumulation over the grounded ice sheet; the first 3 decades are inferred from observational records, and the final 2 decades from ERA-40. A detailed description of the methodology is given in (*19*).

The spatial distribution of the 50-year average annual snowfall accumulation (Fig. 2A) closely resembles the glaciological estimate of Vaughan *et al*. (*20*). The mean for the grounded ice sheet is 182 mm year^{-1} WEQ, larger than the value of 149 mm year^{-1} WEQ from the Vaughan map. A subsequent analysis (*21*) suggested that the Vaughan map underestimated coastal accumulation and that a more realistic estimate is 171 mm year^{-1} WEQ. Overall, our mean annual snowfall accumulation is at the high end of published estimates [119 to 197 mm year^{-1} WEQ (*13*, *22*)] but may be realistic in light of recent findings.

The percentage differences of annual snowfall accumulation for each decade with respect to the 50-year mean (Fig. 2A) are shown in Fig. 2, B to F. There are regions of both positive and negative change in all 5 decades, but no continental-scale changes of either sign dominate any period. The amplitude of the changes in Fig. 2, B to D, the decades reconstructed from ice cores, is slightly dampened compared with the final two decades (Fig. 2, E and F). This is partly due the reconstructed data having smaller interannual variability than the model data; however, this does not affect the sign of the changes and has little impact on the results at basin and continental scales (*19*).

There is no widespread signal of increased snowfall accumulation over the EAIS for 1995–2004 that would suggest a contribution to the recently reported thickening (*23*). The 1995–2004 changes are mostly negative over WAIS, where net ice sheet thinning is occurring (*9*, *10*). The statistical uncertainty associated with the change at each grid point (due to the decadal variability and methodology) is typically about 4 to 8%, enough to overwhelm the decadal changes in most places.

The time series of snowfall accumulation inferred from Fig. 2, B to F, and averaged over EAIS, WAIS, and the entire grounded ice sheet is shown in Fig. 3. All three regions are characterized by a steady upward trend from the beginning of the record through the early 1990s and then a downward trend thereafter that is most marked over WAIS (22 mm year^{-1} WEQ for the past decade compared with the prior decade). However, this change has low statistical significance ($P = 0.16$), indicating that decadal fluctuations of this magnitude (~7% of the 50-year mean) are probably common over WAIS. The upward trend over the ice sheets

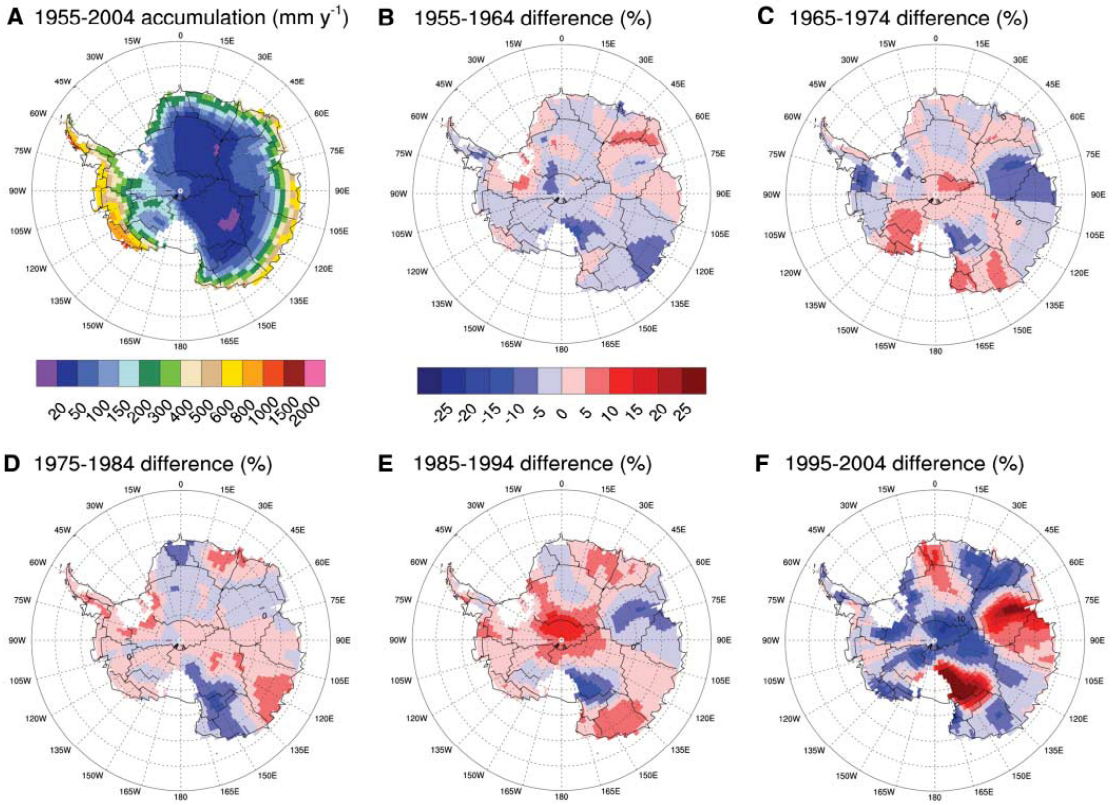

Fig. 2. (**A**) 50-year mean annual snowfall accumulation (mm year^{-1} WEQ). (**B** to **F**) Differences between mean annual snowfall accumulation for decade indicated and 50-year mean, expressed as a percentage of the 50-year mean. The scale shown in (B) applies to (B) to (F). The mean accumulation, trends, and uncertainty are quantified for each basin in (*19*).

before the most recent decade corroborates earlier studies that used regional records (*24*, *25*). Over EAIS, WAIS, and the grounded ice sheet, there are no statistically significant trends in snowfall accumulation over the past 5 decades, including recent years for which global mean temperatures have been warmest (*26*). We performed several experiments to test the sensitivity of the results in Fig. 3 by adjusting parameters within our methodology and by using other methods to reconstruct the accumulation, and the results were very robust (*19*).

Our findings are somewhat inconsistent with Davis *et al*. (*23*), who inferred from satellite altimetry data that an increase in snowfall accumulation was the primary cause of net thickening over EAIS for 1992–2003. One reason for the discrepancy may be that their radar data did not extend southward of 81.6°S, a region with strong downward trends in the past decade (Fig. 2F). Another factor may be their methodology. Zwally *et al*. (*10*) found a thickening over EAIS from satellite altimetry for a similar period that was a factor of 3 smaller than the value from the Davis study, arguing that their method more accurately accounts for firn compaction and interannual variability of the surface height. Lastly, because snowfall typically adjusts to climate change on much shorter time scales than the underlying glacial ice (*27*), a linear thickening trend as reported in the Davis study could be interpreted to mean that snowfall accumulation from 1992–2003 was stepwise higher than at some time in the past, when the accumulation rate and the ice sheet dynamical response were in equilibrium. In that case, the results of Davis *et al*. (*23*) may actually suggest that snowfall accumulation over EAIS has changed little in the past decade, consistent with our assessment. Despite our disagreement as to the causality, we do not dispute that altimetry indicates a clear thickening signal over EAIS (*10*, *23*) that mitigates sea level rise.

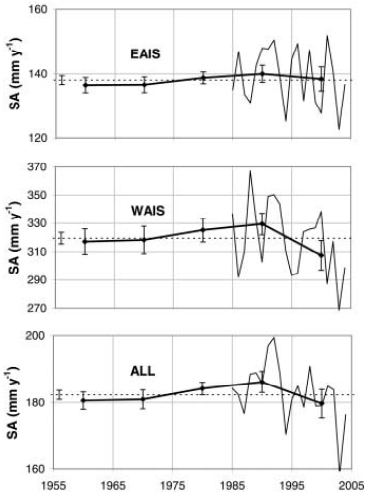

Fig. 3. Time series of decadal mean of annual snowfall accumulation (mm year^{-1} WEQ) for 1955–2004 for EAIS, WAIS, and the grounded ice sheet (ALL), calculated as described in the text. The annual accumulation is also shown for the past 2 decades, the period for which ERA-40 is used. The dotted line represents the 50-year mean. The basins that define EAIS, WAIS, and ALL are given in (*19*). Uncertainty bars are $\pm 1\sigma$ per our methodology (*19*). The uncertainty bar at the far left of each graph is for the 50-year mean.

The implications of our findings are categorized into two general ideas.

1) Interannual and interdecadal snowfall variability must be more seriously considered when assessing the rapid ice volume changes that are occurring over Antarctica. With regard to interannual variability, consider a recent estimate of Antarctic ice sheet mass loss that is the equivalent of 0.4 ± 0.2 mm year^{-1} GSL rise for 3 years (2002–2005) from satellite-derived time-variable gravity measurements (*28*). Antarctic-wide annual snowfall accumulation decreased by about 25 mm y^{-1} WEQ, or about 0.86 mm year^{-1} GSL rise, between calendar year 2002 and 2003 (Fig. 3), suggesting that the gravity fluctuations could be heavily influenced by interannual snowfall variations.

With regard to interdecadal variability, the ERA-40 snowfall accumulation is about 22 mm year^{-1} WEQ lower over WAIS for the past decade (1995–2004) compared with the previous decade (1985–1994) (Fig. 3), the GSL equivalent of 0.18 mm year^{-1}. This signal is of the same order as the 47 Gton (0.13 mm year^{-1} GSL equivalent) mass imbalance reported for WAIS (defined by a slightly different area) from satellite radar altimetry for roughly the past decade (*10*). In neither decade is the snowfall accumulation statistically significantly different from the 50-year WAIS mean, suggesting that such fluctuations are normal. The cause of the recent mass imbalance will remain unclear until a longer satellite record is available, but it may be partly related to accumulation variability.

2) Antarctic snowfall is not currently compensating for the oceanic-induced melting at the ice sheet periphery. If anything, our 50-year perspective suggests that Antarctic snowfall has slightly decreased over the past decade, while global mean temperatures have been warmer than at any time during the modern instrumental record (*26*). Radiosonde and ERA-40 temperature data indicate a uniform winter warming trend in the mid-troposphere over Antarctica since the early 1970s, but seasonally averaged ERA-40 precipitation data suggest that there has been no commensurate increase in winter snowfall since at least 1985 (*12*). These findings suggest that atmospheric circulation variability, rather than thermodynamic moisture increases, may dominate recent Antarctic snowfall variability.

Our technique of synthesizing observational records with model reanalysis has provided a coherent record of Antarctic-wide snowfall accumulation variability extending back before the modern satellite era. As more and improved (e.g., ground-penetrating radar) accumulation records become available, it will be possible to revisit this study with greater accuracy. A longer (1 to 2 centuries) reconstruction was not possible because of the limitations of the current data set but clearly is necessary to better understand the multidecadal Antarctic accumulation variability. Satellite-based techniques show great promise for precisely measuring Antarctic ice mass changes. It is critical to extend these records to distinguish thickening or thinning signals from snowfall variability.

Our results indicate that there is not a statistically significant global warming signal of increasing precipitation over Antarctica since the IGY, inferring that GSL rise has not been mitigated by recently increased Antarctic snowfall as expected. It may be necessary to revisit GCM assessments that show increased precipitation over Antarctica by the end of this century in conjunction with projected warming (*29*). Vigorous efforts are needed to better understand this remote but important part of the planet and its role in global climate and sea level rise.

References and Notes

1. J. A. Church, N. J. White, *Geophys. Res. Lett.* **33**, L01602 (2006).
2. E. Leuliette, R. Nerem, G. Mitchum, *Mar. Geod.* **27**, 79 (2004).
3. D. G. Vaughan, *Science* **308**, 1877 (2005).
4. P. Huybrechts, J. Gregory, I. Janssens, M. Wild, *Global Planet. Change* **42**, 83 (2004).
5. J. Turner *et al.*, *Int. J. Climatol.* **25**, 279 (2005).
6. J. C. Comiso, *J. Clim.* **13**, 1674 (2000).
7. J. Turner, T. A. Lachlan-Cope, S. Colwell, G. J. Marshall, W. M. Connolley, *Science* **311**, 1914 (2006).
8. D. H. Bromwich, *Rev. Geophys.* **26**, 149 (1988).
9. E. Rignot, R. H. Thomas, *Science* **297**, 1502 (2002).
10. H. J. Zwally *et al.*, *J. Glaciol.* **51**, 509 (2005).
11. E. Rignot, S. S. Jacobs, *Science* **296**, 2020 (2002).
12. A. J. Monaghan, D. H. Bromwich, S. H. Wang, *Philos. Trans. Royal Soc. A* **364**, 1683 (2006).
13. W. J. van de Berg, M. R. van den Broeke, C. H. Reijmer, E. van Meijgaard, *Ann. Glaciol.* **41**, 97 (2005).
14. M. R. van den Broeke, W. J. van de Berg, E. van Meijgaard, *Geophys. Res. Lett.* **33**, L02505 (2006).
15. D. H. Bromwich, Z. Guo, L.-S. Bai, Q.-S. Chen, *J. Clim.* **17**, 427 (2004).
16. D. H. Bromwich, R. L. Fogt, *J. Clim.* **17**, 4603 (2004).
17. P. A. Mayewski, I. Goodwin, "International Trans Antarctic Scientific Expedition (ITASE) '200 years of past antarctic climate and environmental change', science and implementation plan, 1996," *PAGES (Past Global Changes Project) Workshop Report Series 97-1* (1997).
18. S. M. Uppala *et al.*, *Q. J. R. Meteorol. Soc.* **131**, 2961 (2005).
19. Materials and methods are available as supporting material on *Science* Online.
20. D. G. Vaughan, J. L. Bamber, M. Giovinetto, J. Russell, A. P. R. Cooper, *J. Clim.* **12**, 933 (1999).
21. W. J. van de Berg, M. R. van den Broeke, C. H. Reijmer, E. van Meijgaard, *J. Geophys. Res.* **111**, D11104 (2006).
22. A. Ohmura, M. A. Wild, L. Bengtsson, *J. Clim.* **9**, 2124 (1996).
23. C. H. Davis, Y. Li, J. R. McConnell, M. M. Frey, E. Hanna, *Science* **308**, 1898 (2005); published online 19 May 2005 (10.1126/science.1110662).

24. V. I. Morgan, I. D. Goodwin, D. M. Etheridge, C. W. Wookey, *Nature* **354**, 58 (1991).
25. E. Mosley-Thompson *et al.*, *Ann. Glaciol.* **21**, 131 (1995).
26. Special issue on State of the Climate in 2004, *Bull. Am. Meteorol. Soc.* **86** (suppl.) (2005).
27. R. Thomas *et al.*, *Science* **306**, 255 (2004); published online 23 September 2004 (10.1126/science.1099650).
28. I. Velicogna, J. Wahr, *Science* **311**, 1754 (2006); published online 1 March 2006 (10.1126/science.1123785).
29. Intergovernmental Panel on Climate Change, *IPCC Third Assessment Report, Climate Change 2001: The Scientific Basis* (Cambridge Univ. Press, Cambridge, 2001).
30. This research was funded by the NSF Office of Polar Programs Glaciology Program, the Australian Government's Cooperative Research Centres Programme through the Antarctic Climate and Ecosystems Cooperative Research Center, the Italian National Antarctic Research Program (PNRA), and several other international scientific research programs. Sincere gratitude is owed to all of those who contributed to the planning, extraction, and analysis of the ice core, snow stake, and snow pit data. The ERA-40 data were obtained from the University Corporation for Atmospheric Research Data Support Section (www.dss.ucar.edu). This is contribution 1338 of the Byrd Polar Research Center.

Supporting Online Material
www.sciencemag.org/cgi/content/full/313/5788/827/DC1
Materials and Methods
References

13 April 2006; accepted 22 June 2006
10.1126/science.1128243

Divergent Induced Responses to an Invasive Predator in Marine Mussel Populations

Aaren S. Freeman* and James E. Byers

Invasive species may precipitate evolutionary change in invaded communities. In southern New England (USA) the invasive Asian shore crab, *Hemigrapsus sanguineus*, preys on mussels (*Mytlius edulis*), but the crab has not yet invaded northern New England. We show that southern New England mussels express inducible shell thickening when exposed to waterborne cues from *Hemigrapsus*, whereas naïve northern mussel populations do not respond. Yet, both populations thicken their shells in response to a long-established crab, *Carcinus maenas*. Our findings are consistent with the rapid evolution of an inducible morphological response to *Hemigrapsus* within 15 years of its introduction.

Anthropogenic introductions increasingly bring organisms into contact that have no shared evolutionary history, which results in novel interactions between non-native and native competitors, prey, and predators (*1*). These novel species combinations create potentially strong selection pressure that can drive evolutionary change of heritable traits (*1*–*3*). Although several studies have shown that invaders can evolve rapidly in a novel, invaded environment (*1*), examples of invader-driven rapid evolutionary change in native species are rarer (*1*, *3*, *4*). Rapid evolutionary change may particularly influence the ability of native prey to recognize and respond to novel invasive predators with inducible morphological defenses.

Inducible defenses are the expression of alternative forms (phenotypic plasticity) by organisms in response to cues from a predator or competitor. Some commonly noted inducible defenses include shape changes in barnacles, spines on bryozoans and cladocerans, thickened shells of mollusks, defensive chemicals in plants, and morphological and behavioral characters in anuran tadpoles (*5*, *6*). Although selection may act on inducible defenses (*5*), in terms of both the degree of plasticity (*7*) and the prey's capacity to recognize cues from predators (*8*, *9*), to date there have been no examples of an invasive species driving the rapid evolution and emergence of an inducible morphological response. To test for the evolution of predator recognition and expression of inducible morphological defenses in a marine mussel (*Mytilus edulis*), we juxtaposed the induced defenses of two mussel populations having different historical contact with two invasive crab predators.

The Asian shore crab, *Hemigrapsus sanguineus*, was first reported in North America in New Jersey in 1988 and currently ranges from North Carolina to the midcoast of Maine, U.S.A. (*10*, *11*). *M. edulis* is a large component of *H. sanguineus*' diet (*12*), but perhaps because this is a novel predator in the North Atlantic Ocean, nothing is known about inducible defenses in mussels to this crab. A longer term resident of New England, the green crab, *Carcinus maenas*, was introduced from Europe to the Mid-Atlantic United States in 1817 and currently ranges from New Jersey, U.S.A., to Prince Edward Island, Canada (*13*). *C. maenas* has had substantial impacts on native communities throughout its introduced range (*13*–*15*) and is known to induce defenses in *M. edulis* from several populations (*14*, *16*, *17*). Small mussels are vulnerable to both crab species (*12*), show high relative growth amenable to detecting induced defenses, and represent a crucial, prereproductive stage under strong selection.

Given the invasion history of these two crabs, *M. edulis* in northern New England (specifically northeastern Maine) has never experienced predation by *H. sanguineus*. Because the genus *Hemigrapsus* is not native to the Atlantic, neither have they been exposed to any *Hemigrapsus* congeners. However, they have experienced predation by *C. maenas* for more than 50 years. In contrast, mussels in southern New England have experienced predation by *C. maenas* and *H. sanguineus* for 100+ and ~15 years, respectively. To determine whether natural selection has altered the mussels' capacity to respond to these two crabs, we quantified the responses of mussels from these northern and southern populations to these two crab predators. If predator cues are species-specific, and if selection has altered the capacity of mussels to recognize and respond to these invasive predators, we expected that mussels from southern New England would respond to cues from both crabs, whereas northern mussels would respond to cues from *C. maenas* but not *H. sanguineus*.

To compare the inducible defenses of mussels from northern and southern New England in response to *C. maenas* and *H. sanguineus*, we collected mussels (13- to 20-mm shell length) from floating docks at six sites each in northern Maine and southern New England and brought them to Northeastern University's Marine Science Center at Nahant, MA (Fig. 1) (*18*). These mussels were then raised with nonlethal, waterborne cues from *C. maenas*, *H. sanguineus*, or no predator (control). Using the final measurements of each mussel's shell thickness index (STI), adjusted to its initial STI, we assessed the development of inducible defenses (*19*). After 3 months, mussels had grown, and mussels from northern and southern New England had thickened their shells differently in response to waterborne cues from the two invasive crab predators (i.e., there was a significant population by predator treatment interaction) (*20*). Mussels from southern sites thickened their shells in response to waterborne cues from *H. sanguineus* relative to controls ($P = 0.011$), and mussels appeared to thicken their shells in response to *C. maenas*, although the trend was not significant ($P = 0.145$) (Fig. 2). In contrast, although mussels from northern sites developed significantly thicker shells in response to cues from *C. maenas* ($P - 0.001$), they did not respond to cues from *H. sanguineus* ($P = 0.573$) (Fig. 2). In addition, there were clear population differences in the temperature-sensitive process of shell accretion, with mussels from northern populations thickening their shells more than mussels from southern populations (Fig. 2). These findings suggest that northern and southern mussel populations are

Zoology Department, Rudman Hall, University of New Hampshire, Durham, NH 03824, USA.
*To whom correspondence should be addressed. E-mail: afreeman@cisunix.unh.edu

GEOPHYSICAL RESEARCH LETTERS, VOL. 33, L16707, doi:10.1029/2006GL027057, 2006

Antarctic temperatures over the past two centuries from ice cores

David P. Schneider,[1] Eric J. Steig,[1] Tas D. van Ommen,[2] Daniel A. Dixon,[3] Paul A. Mayewski,[3] Julie M. Jones,[4] and Cecilia M. Bitz[5]

Received 30 May 2006; revised 26 June 2006; accepted 24 July 2006; published 30 August 2006.

[1] We present a reconstruction of Antarctic mean surface temperatures over the past two centuries based on water stable isotope records from high-resolution, precisely dated ice cores. Both instrumental and reconstructed temperatures indicate large interannual to decadal scale variability, with the dominant pattern being anti-phase anomalies between the main Antarctic continent and the Antarctic Peninsula region. Comparative analysis of the instrumental Southern Hemisphere (SH) mean temperature record and the reconstruction suggests that at longer timescales, temperatures over the Antarctic continent vary in phase with the SH mean. Our reconstruction suggests that Antarctic temperatures have increased by about 0.2°C since the late nineteenth century. The variability and the long-term trends are strongly modulated by the SH Annular Mode in the atmospheric circulation. **Citation:** Schneider, D. P., E. J. Steig, T. D. van Ommen, D. A. Dixon, P. A. Mayewski, J. M. Jones, and C. M. Bitz (2006), Antarctic temperatures over the past two centuries from ice cores, *Geophys. Res. Lett.*, *33*, L16707, doi:10.1029/2006GL027057.

1. Introduction

[2] Given the enormous amount of freshwater stored in the Antarctic ice sheet and the impact that temperature changes may have on the ice sheet mass balance, it is important to understand how and why Antarctic temperatures have changed. Several studies have presented summaries of Antarctic temperature change based on instrumental records [e.g., *Turner et al.*, 2005; *Jacka et al.*, 2004; *Vaughan et al.*, 2003]. The Antarctic Peninsula region has experienced some of the strongest surface warming on Earth during the past 50 years, while temperature trends across the continent differ in sign and magnitude among different time periods and seasons [*Turner et al.*, 2005]. Recent cooling across the continent in the summer and autumn has been linked to persistence of the positive index phase of the Southern Hemisphere Annular Mode (SAM) [*Thompson and Solomon*, 2002]. The recent trend in the SAM has been attributed to various combinations of stratospheric ozone depletion and rising atmospheric CO_2 concentrations [e.g., *Thompson and Solomon*, 2002; *Shindell and Schmidt*, 2004], implying anthropogenic influences on Antarctic climate. However, the temporal variability of Antarctic climate is not well known, as continuous meteorological observations in the Antarctic began only in the late 1950s. Quantitative reconstruction of Antarctic temperatures has been faced with several challenges. First, the short and sparse instrumental observations make it difficult to determine how well variations in temperatures at research stations represent regional temperature variations across the continent. Second, while stable isotope time series from Antarctic ice cores are well-known, reaching up to eight glacial cycles into the past [*EPICA Community Members*, 2004], such records have generally not been available at the high-resolution required for reconstructing the instrumental record. Finally, while statistical reconstruction approaches have been applied in regional to hemispheric-scale reconstructions [e.g., *Jones and Mann*, 2004], such approaches have not been applied to Antarctic data.

[3] New data and improved understanding of the mechanisms explaining Antarctic temperature and stable isotope variations enable the quantitative reconstruction of Antarctic temperatures for the first time. Targeted ice-coring projects, such as the International Trans-Antarctic Scientific Expedition (ITASE), which has the specific objective of collecting numerous high-resolution records, have greatly expanded the availability of proxy indicators of Antarctic climate [*Mayewski et al.*, 2006; *Steig et al.*, 2006]. The aim of this paper is to utilize these new data in a 200-year-long Antarctic temperature reconstruction (representing the main part of the continent) methodologically similar to temperature reconstructions covering other geographic regions.

2. Data

[4] For Antarctic surface temperature observations, we use the quality-controlled station records from the Antarctic READER project, which archives continuous monthly observations covering generally the late 1950s to present [*Turner et al.*, 2004]. Time series from eight stations on the coast and the continental interior are included in our analysis, while data from the Peninsula region are excluded due to their location with respect to the main climatic pattern that dominates the continent (see Methods, below).

[5] Subannually-resolved $\delta^{18}O$ and δD (hereafter denoted "δ") ice core records are compiled from Law Dome [*van Ommen et al.*, 2004], Siple Station [*Mosley-Thompson et al.*, 1990], Dronning Maud Land (DML) [*Graf et al.*, 2002], and two West Antarctic sites of the United States component of ITASE [*Steig et al.*, 2006] (Table 1). The Law Dome and DML records are stacks of several records

[1]Department of Earth and Space Sciences, University of Washington, Seattle, Washington, USA.
[2]Department of the Environment and Heritage, Australian Antarctic Division, Antarctic Climate and Ecosystems Cooperative Research Centre, Hobart, Tasmania, Australia.
[3]Climate Change Institute, University of Maine, Orono, Maine, USA.
[4]Institute for Coastal Research, GKSS Research Centre, Geesthacht, Germany.
[5]Department of Atmospheric Sciences, University of Washington, Seattle, Washington, USA.

0094-8276/06/2006GL027057$05.00

Table 1. Ice Core Site Characteristics

Core Name	Latitude	Longitude	Elevation, m	Time span	Isotope
Law Dome 2000 (stack)	66.78 S	112.82 E	1370	1800–1999	$\delta^{18}O$
Siple Station	75.92 S	84.1 W	1054	1800–1983	$\delta^{18}O$
Dronning Maud Land (several sites)[a]	~75 S	~0 E	~2900	1800–1997	$\delta^{18}O$
US ITASE 2000-1	79.38 S	111.23 W	1791	1800–1999	$\delta^{18}O$
US ITASE 2000-5	77.68 S	123.99 W	1828	1800–1999	δD

[a]DML cores (documented by *Graf et al.* [2002]) in the DML stack: DML18(FB9804); DML19(FB806); DML05(FB9807); DML20(FB9808); DML21(FB9810); DML22(FB9811); DML16(FB9813); DML14(FB9815); DML13(FB9816); DML12(FB9817); DML07(B31); DML05(B32); DML17(B33); DML03(FB9809).

from closely-spaced sites in the region. These records have been well-dated through counting of annual layers in ion-chemistry and δ concentrations, and by the identification of volcanic eruption marker horizons. All isotopic data were referenced to the VSMOW and SLAP (Standard Light Antarctic Precipitation) standards from the International Atomic Energy Agency.

[6] We also utilize gridded 2-m temperature (2-m T) data from a polar-adapted mesoscale climate model driven at the lateral boundaries by the ERA-40 Reanalysis over 1980–2001 [*Monaghan et al.*, 2006] to characterize the spatial variability of Antarctic temperatures.

3. Methods

[7] The gridded 2-m T data are too short in duration to use directly in the reconstruction, but they are used to assess the skill of the station network in representing the variance of Antarctic temperatures. The leading empirical orthogonal function (EOF) of annual mean 2-m T over the continent captures 46% of the variance (Figure 1a). This "cold-continent – warm Peninsula" pattern can be interpreted as the expression of the SAM, as illustrated by correlation of the station-based SAM index of *Marshall* [2003] with the 2-m T field (Figure 1b), or with satellite-derived temperatures [*Schneider et al.*, 2004]. The SAM is a roughly zonally symmetric seesaw in atmospheric mass between the Antarctic and the mid-latitudes, characterized by fluctuations in the strength of the westerly polar vortex [*Thompson and Wallace*, 2000]. Discussion of the physical mechanisms relating the SAM to temperature anomalies over the ice sheet is provided by *van den Broeke and van Lipzig* [2004].

[8] EOF analysis of annual station data spanning 1961–2003 indicates that the first EOF explains 43% of the total variance, with all stations having positive weights. These results are very similar to the gridded 2-m T data, indicating the robustness of the leading temperature pattern. The first PC is correlated at $r = 0.98$ with the simple average of the station temperature records. This average, which we call A8, is significantly correlated at $r = 0.76$ ($p < 0.01$) (degrees of freedom are reduced to account for autocorrelation for the significance of all correlations and trends discussed herein) with the mean of the 2-m T data over 1980–2001. In addition, the cold continent - warm Peninsula pattern is evident in the correlation of A8 with the 2-m T field (Figure 1c), showing that A8 provides a meaningful estimate of temperature variability on a continent-wide scale. While there is not a significant linear trend in A8, A8 depicts temperature increases in roughly the first half of the series and decreases in the second half (Figure 2), in agreement with other studies of recent Antarctic temperature trends [*Jacka et al.*, 2004; *Turner et al.*, 2005]. A8 is thus our target temperature index for reconstruction; it provides as long and homogeneous a record as is possible from existing Antarctic data.

[9] An advantage of isotopic records over many other climate proxy indicators is that the physics governing their variability is well understood. The relevant processes can be depicted in models ranging in completeness from simple Rayleigh models [e.g., *Dansgaard*, 1964] and intermediate complexity models [e.g., *Kavanaugh and Cuffey*, 2003], to full general circulation models (GCM) [e.g., *Werner and Heimann*, 2002; *Noone and Simmonds*, 2002]. In Antarctica, most isotope modeling studies have upheld the traditional interpretation of isotope anomalies as indicators of local temperature during precipitation, despite complexities in the processes that control isotope fractionation [*Jouzel et al.*, 1997; *Werner and Heimann*, 2002]. However, while

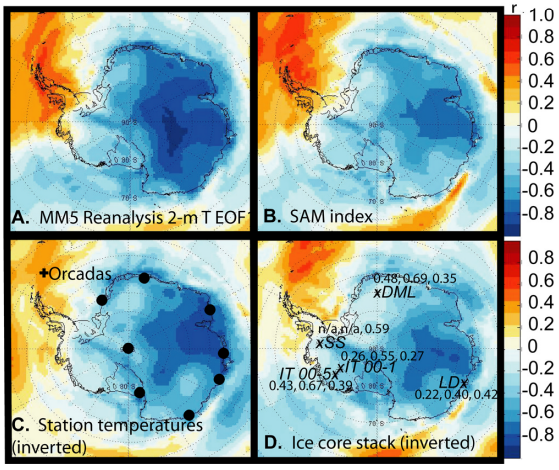

Figure 1. Correlation maps of several time series with 2-m T from the climate model simulation of *Monaghan et al.* [2006]. Negative correlations (blue) and positive correlations (red) imply negative and positive temperature anomalies, respectively: (a) The first principal component (PC) of 2-m T over the continent; (b) The SAM index; (c) The A8 composite temperature index (inverted) from the stations indicated by black dots; (d) The stacked ice core isotopic record (inverted), with core sites indicated by a black "x". At each site, the numbers indicate the correlation coefficient of the annual ice core data with the nearest grid-point 2-m T, PC1 of 2-m T, and A8, respectively.

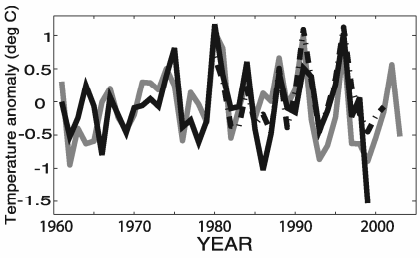

Figure 2. The gray line shows A8. Calibrated stacked ice core record (black line). Mean of 2-m T anomalies over the ice sheet (dashed line).

observed event-scale and seasonal correlations between δ and local temperature are very high [e.g., *Schneider et al.*, 2006; *van Ommen and Morgan*, 1997], interannual correlations, while positive, are generally low (e.g., see Figure 1d). A GCM study has suggested that the SAM leads to an observable, organized signature in stable isotopes, with a typical positive phase SAM anomaly ranging from −0.2 to −0.8 ‰ in $\delta^{18}O$ across the continent [*Noone and Simmonds*, 2002]. A number of mechanisms are involved; the primary contribution to the depletion of $\delta^{18}O$ is increased distillation along the path of moisture transport. The spatial pattern of isotope anomalies is analogous to and also physically linked with (via the local condensation temperature of precipitation [*Noone and Simmonds*, 2002; *Jouzel et al.*, 1997]) the SAM's expression in the temperature field. At three of our widely separated sites (DML, Law Dome, and ITASE 00-5), the covariance of the SAM index and $\delta^{18}O$ is significant, with a coefficient ranging from −0.30 to −0.90 ‰ per standard deviation of the SAM index, within the range of the model calculations. Thus, the positive phase SAM is associated both with lower temperatures and depleted stable isotopes on the scale of the continent.

[10] As opposed to the traditional use of local δ-temperature calibrations, our approach to temperature reconstruction is to combine multiple, annually-resolved ice core records into a single record, calibrated at the continental scale. This is supported on physical grounds both by the large-scale covariance of temperature and isotope anomalies and by the reduction of non-climate related noise when proxy records are combined. We first normalize the individual records with respect to their common 1800–1983 period of coverage. They are then combined through a weighted average on the basis of each record's detrended correlation with the A8 index (correlations indicated in Figure 1d.). This stack is significantly correlated with the A8 index at r = 0.63 ($p < 0.01$), and correlation with 2-m T shows that it corresponds to the cold continent - warm Peninsula pattern (Figure 1d), demonstrating that our stacked record captures the dominant pattern of Antarctic temperature variability. To calibrate the reconstruction, the ice core stack is adjusted to the variance and mean of the target A8 index over the 1961–1999 overlap interval. Despite local differences in the variance of temperatures, we find that A8 provides a good approximation of the variance of temperatures on the continental scale. The 2-m T data averaged over the ice sheet (excluding areas with negative weights in the first EOF), have a variance of 0.28°C, which is similar to the variance of A8 over 1961–1999 (Figure 2).

[11] In addition to the correlation coefficient, the reduction of error (RE) statistic provides a measure of reconstruction resolved variance [e.g., *Jones and Widmann*, 2003]. For the 1961–1999 calibration interval, the RE is 0.26, which indicates skill relative to climatology. Given the paucity of instrumental data, we do not have the luxury of a period of data to withhold for cross-verification. However, if we consider the two halves of the calibration interval as independent calibration/verification periods, we find that the calibration statistics and verification RE scores are quite similar (Table 2), supporting confidence in the reconstruction. The 2σ (i.e. 95%) confidence intervals of the reconstruction are estimated as twice the root-mean-square error of the calibration period correlation times the standard deviation of A8.

[12] We note potential sources of uncertainty, including possible changes in accumulation rates that could alter the relation of stable isotopes to annual mean temperature, and changes in sea surface temperatures (at the moisture source). With regard to accumulation rates, we note that a recent study of accumulation trends finds them to be highly spatially and seasonally variable, largely canceling out over the ice sheet in the annual mean [*Monaghan et al.*, 2006]. Seasonal accumulation trends could nonetheless alter the seasonal representativeness of the reconstruction. However, over the calibration period, the ice core stack is better correlated with the annual mean temperature than with any particular seasonal mean temperature, and the low-frequency behavior of the stacked record is consistent with that of A8. With regard to source conditions, available deuterium excess measurements (a proxy for moisture source conditions) show no evidence of long term trends.

4. Results and Discussion

[13] Our reconstruction (Figure 3a) depicts significant interannual to decadal scale variability, which may be traceable to the SAM. Prior to the late 1950s, there is only indirect evidence for the strength of the SAM. The only long instrumental polar data are from Orcadas station, situated to the northeast of the Peninsula, where the positive phase of the SAM results in higher than normal temperatures (r (SAM index, Orcadas temperature) = 0.33 ($p < 0.05$) see also Figure 1c.). The anti-phase temperature anomaly relationship between the Peninsula region and the continent can be represented by the significant correlation of (detrended) A8 and Orcadas temperature over 1961–2002 ($r = -0.47$, $p < 0.01$). The correlation of our temperature reconstruction with Orcadas temperature is nearly as high as the instrumental correlation ($r = -0.44$,

Table 2. Reconstruction Statistics for Different Calibration Periods

Period	*r* (A8, ice)[a]	Reduction of Error
1961–1999	0.63 $p < 0.01$	0.26 calibration
1961–1980	0.62 $p < 0.01$	0.24 verification
1981–1999	0.63 $p < 0.01$	0.25 verification

[a]Ice refers to the stacked ice core record.

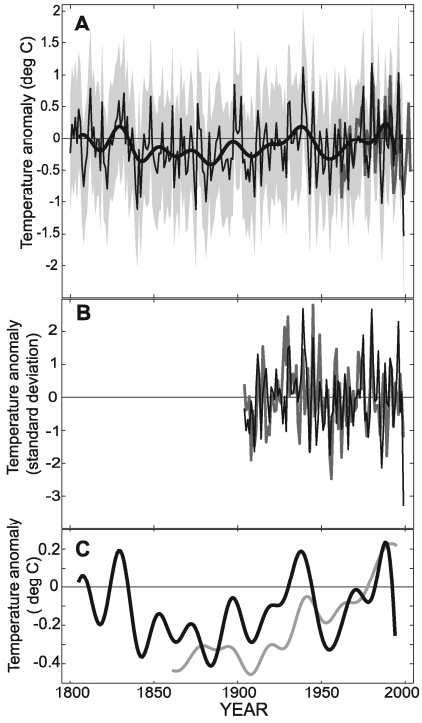

Figure 3. Antarctic temperature reconstruction: (a) Full annual resolution reconstruction (black line) with ±2σ uncertainty shaded in gray and multi-decadal smoothed version (heavy line). Instrumental calibration record, A8 (gray line); (b) Reconstruction (black line) compared with Orcadas temperature (gray line, inverted) after the linear trends have been removed; (c) Reconstruction (black line) compared with SH mean instrumental record (gray line) after a multi-decadal (0.05 cycles/yr cut-off) low-pass filter has been applied. In all plots, the zero line represents the 1961–1990 climatological mean.

$p < 0.01$ over 1904–1999), even in the pre-calibration period ($r = -0.44$, $p < 0.01$ over 1904–1960) (Figure 3b). This result is consistent with the observed cold continent - warm Peninsula pattern being a dominant feature of Antarctic climate variability. On a monthly timescale, analysis of gridded data indicates that about 17% of the spatial-temporal variance of temperature anomalies over the continent is explained by the SAM [*Schneider et al.*, 2004], and our results suggest that on interannual to decadal timescales, a similar amount of variance is explained by the SAM over at least the last century. Large variability associated with the SAM at these timescales has also been inferred from independent reconstructions of the SAM index using station sea-level pressure [*Jones and Widmann*, 2004, 2003].

[14] In addition to the significant high frequency variability, our reconstruction shows an extended period of cooler than present conditions from the mid-19th to early 20th-century. Existing evidence suggests that there was not an extended positive phase SAM over this time period that could explain the lower temperatures [*Jones and Widmann*, 2003]. From our reconstruction, we estimate that Antarctic temperatures over the 1961–1999 calibration period were about 0.2°C higher than in the period 1861–1899. Other evidence for long-term warming includes ice borehole temperature inversions at Siple Dome [*Engelhardt*, 2004] in West Antarctica and Law Dome [*Dahl-Jensen et al.*, 1999] in East Antarctica. At Law Dome, the minimum (~1850) to maximum (1990) temperature difference was quantified as 0.7°C, which agrees with the difference of 0.6°C that is evident in a smoothed version of our reconstruction between the low in the 1800s to the maximum around 1990 (Figure 3c). Some lower resolution isotopic records, at Siple Dome [*Mayewski et al.*, 2004] and Dronning Maud Land [*Isaksson et al.*, 1996], also suggest 20th-century warming.

[15] It is notable that the reconstructed Antarctic temperature record is in phase with the SH mean instrumental temperature record [*Folland et al.*, 2001], especially over the two well-known global warming periods, from ~1910 to ~1945 and from the 1970s to present (Figure 3c). This phasing can be explored with cross-spectral analyses of the Antarctic versus the SH mean and the Orcadas records. Although no significant spectral peaks are present in comparison with a simple red noise continuum, the phasing and coherency relationships are informative (Figure 4). The cold continent-warm Peninsula pattern is evident in the anti-phasing of the Orcadas record and the reconstruction in the broad band from about three to 10 years. The phasing with the SH mean becomes significantly coherent at the longest periods resolved, about 20 years.

[16] Since the SAM had a strong positive trend from the mid-1970s to the 1990s [*Marshall*, 2003], we separate temperature trends before and after 1975. From 1856 to 1975, trends (°C per 100 yr) in the SH mean (0.32 ± .10, $p < 0.01$) and Antarctic record (0.22 ± .26, $p < 0.10$) are similar, while they are markedly different from 1975–1999 (1.40 ± .59, $p < 0.01$ and −2.2 ± 3.8, not significant,

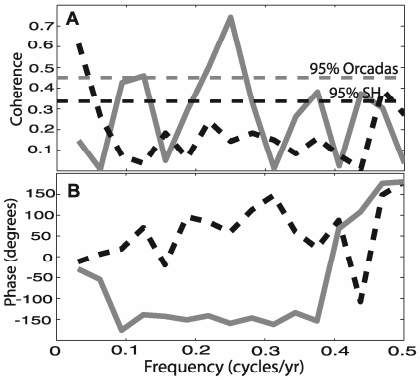

Figure 4. (a) Coherency and (b) phase estimates of the Antarctic temperature reconstruction versus the SH mean temperature (black dashed line) and the Orcadas temperature (gray solid line). Annual data were used, and cross-spectra were estimated with a Hanning Window width of 32 years using a fast Fourier transform. 95% confidence levels are indicated. Results are independent of linear trends in the records.

respectively). As discussed above, the reconstruction provides evidence for long-term Antarctic warming, and the linear trend for the full period of overlap with the SH mean (1856–1999) is an increase of 0.18 ±. 21°C per 100 yr ($p < 0.10$), which has greater mean and statistical significance (0.23 ± .21°C per 100 yr, $p < 0.05$) if the end date, 1999, is excluded because it is an outlier in comparison with the instrumental record. Thus, recent Antarctic cooling is superimposed on longer-term warming. These results support attribution of the cooling trend to the trend in the SAM [*Thompson and Solomon*, 2002], however, strong variability precludes unambiguous attribution of the SAM trend to anthropogenic forcing, such as ozone depletion.

5. Conclusions

[17] Our reconstruction based on high resolution stable isotope time series emphasizes that the short Antarctic instrumental records provide very limited context for assessing Antarctic temperature change, as there is large internannual to decadal scale variability, attributable in part to the SAM. In the longer-term context, our reconstruction, combined with other evidence, suggests that the Antarctic continent has experienced modest warming over the last 150 years. Similar phasing as the SH mean temperature record suggests that this warming may be linked to global changes and suggests that Antarctica will warm in parallel with the SH, in general accordance with model-based predictions [e.g., *Shindell and Schmidt*, 2004].

[18] **Acknowledgments.** The authors thank G. Marshall for providing the SAM index data, E. Mosley-Thompson for Siple Station ice core data, and H. Oerter for DML ice core data. READER data are from http://www.antarctica.ac.uk/met/READER, Polar MM5 output is from http://polarmet.mps.ohio-state.edu/PolarMet/ant_hindcast.html, and SH mean temperature data are from http://www.cru.uea.ac.uk/cru/data/temperature/. Primary support for this work, to D.P.S., E.J.S., D.A.D., and P.A.M. is from the U.S. National Science Foundation, Office of Polar Programs (grants 0229416 and 0196105). D.P.S. acknowledges additional support from the Scientific Committee on Antarctic Research. T.v O. acknowledges support from the Australian Government's Cooperative Research Centre Program. The authors thank anonymous reviewers for their constructive comments.

References

Dahl-Jensen, D., V. Morgan, and A. Elcheikh (1999), Monte Carlo inverse modeling of the Law Dome (Antarctica) temperature profile, *Ann. Glaciol.*, *29*, 145–150.

Dansgaard, W. (1964), Stable isotopes in precipitation, *Tellus*, *16*, 436–468.

Engelhardt, H. (2004), Ice temperature and high geothermal heat flux at Siple Dome, West Antarctica, from borehole measurements, *J. Glaciol.*, *50*, 251–256.

EPICA Community Members (2004), Eight glacial cycles from an Antarctic ice core, *Nature*, *429*, 623–626.

Folland, C. K., et al. (2001), Global temperature change and its uncertainties since 1861, *Geophys. Res. Lett.*, *28*, 2621–2624.

Graf, W., et al. (2002), Stable isotope records from Dronning Maud Land, Antarctica, *Ann. Glaciol.*, *35*, 195–201.

Isaksson, E., W. Karlén, N. Gundestrup, P. Mayewski, S. Whitlow, and M. Twickler (1996), A century of accumulation and temperature changes in Dronning Maud Land, Antarctica, *J. Geophys. Res.*, *101*, 7085–7094.

Jacka, T. H., W. F. Budd, and A. Holder (2004), A further assessment of surface temperature changes at stations in the Antarctic and Southern Ocean, 1949–2002, *Ann. Glaciol.*, *39*, 331–338.

Jones, J. M., and M. Widmann (2003), Instrument and tree ring based estimates of the Antarctic Oscillation, *J. Clim.*, *16*, 3511–3524.

Jones, J. M., and M. Widmann (2004), Early peak in Antarctic Oscillation index, *Nature*, *432*, 290–291.

Jones, P. D., and M. E. Mann (2004), Climate over past millennia, *Rev. Geophys.*, *42*, RG2002, doi:10.1029/2003RG000143.

Jouzel, J., et al. (1997), Validity of the temperature reconstruction from water isotopes in ice cores, *J. Geophys. Res.*, *102*(C12), 26,471–26,488, doi:10.1029/97JC01283.

Kavanaugh, J. L., and K. M. Cuffey (2003), Space and time variation of $\delta^{18}O$ and δD in Antarctic snow revisited, *Global Biogeochem. Cycles*, *17*(1), 1017, doi:10.1029/2002GB001910.

Marshall, G. J. (2003), Trends in the Southern Annular Mode from observations and reanalysis, *J. Clim.*, *16*, 4134–4143.

Mayewski, P. A., et al. (2004), A 700-year record of Southern Hemisphere extratropical climate variability, *Ann. Glaciol.*, *39*, 127–132.

Mayewski, P. A., et al. (2006), The International Trans-Antarctic Scientific Expedition (ITASE): An overview, *Ann. Glaciol.*, *41*, 180–185.

Monaghan, A. J., D. H. Bromwich, and S.-H. Wang (2006), Recent trends in Antarctic snow accumulation from Polar MM5, *Philos. Trans. R. Soc. London, Ser. A*, *364*, 1683–1708.

Mosley-Thompson, E., L. G. Thompson, P. M. Grootes, and N. Gunderstrup (1990), Little Ice Age (Neoglacial) paleoenvironmental conditions at Siple Station, Antarctica, *Ann. Glaciol.*, *14*, 199–204.

Noone, D. C., and I. Simmonds (2002), Annular variations in moisture transport mechanisms and the abundance of $\delta^{18}O$ in Antarctic Snow, *J. Geophys. Res.*, *107*(D24), 4742, doi:10.1029/2002JD002262.

Schneider, D. P., E. J. Steig, and J. C. Comiso (2004), Recent climate variability in Antarctica from satellite-derived temperature data, *J. Clim.*, *17*, 1569–1583.

Schneider, D. P., E. J. Steig, and T. van Ommen (2006), High-resolution ice core stable isotopic records from Antarctica: Towards interannual climate reconstruction, *Ann. Glaciol.*, *41*, 63–70.

Shindell, D. T., and G. A. Schmidt (2004), Southern Hemisphere climate response to ozone changes and greenhouse gas increases, *Geophys. Res. Lett.*, *31*, L18209, doi:10.1029/2004GL020724.

Steig, E. J., et al. (2006), High-resolution ice cores from US-ITASE (West Antarctica): Development and validation of chronologies and determination of precision and accuracy, *Ann. Glaciol.*, *41*, 77–84.

Thompson, D. W. J., and S. Solomon (2002), Interpretation of recent Southern Hemisphere climate change, *Science*, *296*, 895–899.

Thompson, D. W. J., and J. M. Wallace (2000), Annular modes in extratropical circulation, part 1: Month-to-month variability, *J. Clim.*, *13*, 1000–1016.

Turner, J., et al. (2004), The SCAR READER Project: Toward a high-quality database of mean Antarctic meteorological observations, *J. Clim.*, *17*, 2890–2898.

Turner, J., et al. (2005), Antarctic climate change during the last 50 years, *Int. J. Climatol.*, *25*, 279–294.

van den Broeke, M. R., and N. P. M. van Lipzig (2004), Changes in Antarctic temperature, wind, and precipitation in response to the Antarctic Oscillation, *Ann. Glaciol.*, *39*, 119–126.

van Ommen, T. D., and V. Morgan (1997), Calibrating the ice core paleothermometer using seasonality, *J. Geophys. Res.*, *102*(D8), 9351–9357.

van Ommen, T. D., V. Morgan, and M. A. J. Curran (2004), Deglacial and Holocene changes in accumulation at Law Dome, *Ann. Glaciol.*, *39*, 359–365.

Vaughan, D. G., et al. (2003), Recent rapid regional climate warming on the Antarctic Peninsula, *Clim. Change*, *60*, 243–274.

Werner, M., and M. Heimann (2002), Modelling the interannual variability of water isotopes in Greenland and Antarctica, *J. Geophys. Res.*, *107*(D1), 4001, doi:10.1029/2001JD900253.

C. M. Bitz, Department of Atmospheric Sciences, University of Washington, Box 351640, Seattle, WA 98195, USA.

D. A. Dixon and P. A. Mayewski, Climate Change Institute, University of Maine, 303 Edward T. Bryand Global Sciences Center, Orono, ME 04469-5790, USA.

J. M. Jones, Institute for Coastal Research, GKSS Research Centre, Max-Planck-Strasse 1, D-21502 Geesthacht, Germany.

D. P. Schneider and E. J. Steig, Department of Earth and Space Sciences, University of Washington, Box 351310, Seattle, WA 98195, USA. (schneidd@u.washington.edu)

T. D. van Ommen, Department of the Environment and Heritage, Australian Antarctic Division, Antarctic Climate and Ecosystems CRC, Private Bag 80, Hobart, Tas 7001, Australia.

Solar forcing of the polar atmosphere

Paul Andrew MAYEWSKI,[1] Kirk A. MAASCH,[1] Yuping YAN,[1,2] Shichang KANG,[1,3] Eric A. MEYERSON,[1] Sharon B. SNEED,[1] Susan D. KASPARI,[1] Daniel A. DIXON,[1] Erich C. OSTERBERG,[1] Vin I. MORGAN,[4] Tas VAN OMMEN,[4] Mark A.J. CURRAN[4]

[1]*Climate Change Institute, and Department of Earth Sciences, University of Maine, 303 Bryand Global Sciences Center, Orono, ME 04469-5790, USA*
E-mail: paul.mayewski@maine.edu
[2]*China Meteorological Administration, 46 Zhongguancun South Avenue, Beijing 100081, China*
[3]*Institute of Tibetan Plateau Research, Chinese Academy of Sciences, Beijing 100085, China*
[4]*Department of the Environment and Heritage, Australian Antarctic Division, and Antarctic Climate and Ecosystems CRC, Hobart, Tasmania 7001, Australia*

ABSTRACT. We present highly resolved, annually dated, calibrated proxies for atmospheric circulation from several Antarctic ice cores (ITASE (International Trans-Antarctic Scientific Expedition), Siple Dome, Law Dome) that reveal decadal-scale associations with a South Pole ice-core ^{10}Be proxy for solar variability over the last 600 years and annual-scale associations with solar variability since AD 1720. We show that increased (decreased) solar irradiance is associated with increased (decreased) zonal wind strength near the edge of the Antarctic polar vortex. The association is particularly strong in the Indian and Pacific Oceans and as such may contribute to understanding climate forcing that controls drought in Australia and other Southern Hemisphere climate events. We also include evidence suggestive of solar forcing of atmospheric circulation near the edge of the Arctic polar vortex based on ice-core records from Mount Logan, Yukon Territory, Canada, and both central and south Greenland as enticement for future investigations. Our identification of solar forcing of the polar atmosphere and its impact on lower latitudes offers a mechanism for better understanding modern climate variability and potentially the initiation of abrupt climate-change events that operate on decadal and faster scales.

INTRODUCTION

Although the sun is the driver of Earth's climate, demonstrating a direct connection between solar variability and climate change has proved difficult. One of the problems is that while solar particle emissions and shortwave radiation change by large amounts in a solar cycle, total irradiance only varies by ~0.1% (Wilson and Hudson, 1988) and accurate measurements have only been available in the satellite era. Some associations, however, have been observed between historical records of solar activity and climate change (Lean and others, 1995; Hansen and others, 1998) and also between variability in cosmogenic proxies for solar variability (Stuiver and Braziunas, 1989; Beer, 2000) and millennial-scale variability in paleoclimate records from moraine sequences, Greenland ice cores and North Atlantic marine sediments (Denton and Karlén, 1973; O'Brien and others, 1995; Mayewski and others, 1997; Bond and others, 2001). In addition, a major feature of atmospheric circulation, the polar vortex, has been linked to interactions between Northern Hemisphere tropospheric temperature and wind, North Atlantic storm tracks and solar sunspot cycles (Brown and John, 1979; Nastrom and Belmont, 1980; Tinsley, 1988; Van Loon and Labitzke, 1988; Labitzke and Van Loon, 1989; Venne and Dartt, 1990; Burnett, 1993).

In our examination of the potential link between climate and solar variability, we utilize high-resolution, annually dated, glaciochemical series from ice cores at several sites across West Antarctica (ITASE (International Trans-Antarctic Scientific Expedition) 00-1 and 01-2; Siple Dome (Kreutz and others, 1997)) and East Antarctica (Law Dome (Palmer and others, 2001a; Souney and others, 2002)) (Fig. 1) and examples from several older Northern Hemisphere ice cores introduced later in this study.

The Antarctic ice-core series are converted to proxies for atmospheric circulation using calibration techniques and correlations previously described (e.g. Kreutz and others, 2000; Meeker and Mayewski, 2002; Souney and others, 2002) that invoke climate data available from the US National Centers for Environmental Prediction/US National Center for Atmospheric Research (NCEP/NCAR) re-analysis (Kalnay and others, 1996) and other climate indices. Correlations are robust over the full interval of NCEP/NCAR re-analysis data. We focus our study on the period since AD 1400 to avoid proxy calibration complications related to changes in climate boundary conditions that may have occurred prior to the AD 1350–1400 transition from the Medieval Warm Period to the Little Ice Age.

Dust from Australia, Africa and South America and sea salt from the Southern Ocean are the primary sources for Ca^{2+} in West Antarctic ice cores. Changes in Ca^{2+} in the Siple Dome and ITASE 00-1 ice cores (Fig. 1) are correlated with changes in the September–November (SON) surface mean zonal wind surrounding Antarctica, most notably the region close to 40–50° S in the Indian and Pacific Oceans (Fig. 1). SON timing is consistent with the seasonal maximum in Ca^{2+} in Antarctic ice cores (Whitlow and others, 1992; Yan and others, 2005). Siple Dome and ITASE 00-1 Ca^{2+} annually averaged series are positively correlated ($r = 0.38$, $P < 0.01$ and $r = 0.44$, $P < 0.01$, respectively; 3 year smoothed series: $r = 0.56$, $P < 0.01$ and $r = 0.75$,

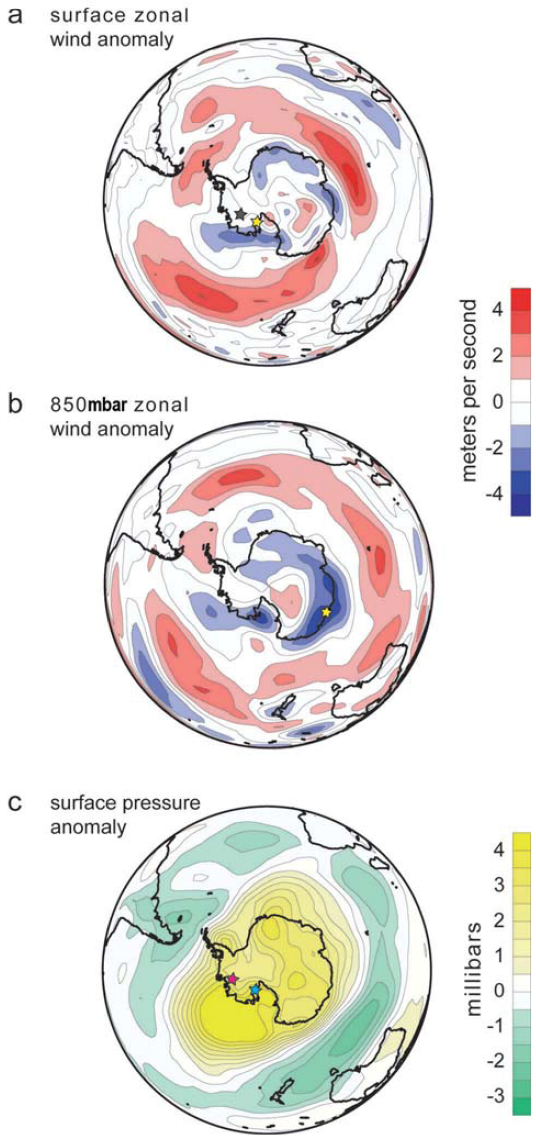

Fig. 1. Ice-core proxies for atmospheric circulation plotted using maps from the NCEP/NCAR re-analysis (US National Oceanic and Atmospheric Administration–Cooperative Institute for Research in Environmental Sciences (NOAA–CIRES) Climate Diagnostics Center, http://www.cdc.noaa.gov/) based on the period AD 1948–2002. (a) Map of SON zonal wind anomalies ($m\,s^{-1}$) composited from years where Ca^{2+} (ITASE 00-1 ice core) exceeds the mean by +1 standard deviation ($+1\sigma$) minus years where Ca^{2+} falls below -1σ. Positive (negative) anomalies correspond to increased (decreased) Ca^{2+}. Yellow star (eastern) is location of ITASE 00-1, and yellow star (western) of Siple Dome. (b) Map of JJA 850 mbar zonal wind anomalies composited similarly from NO_3^- (in the Law Dome ice core) except that the sense is low ($<-1\sigma$) years minus high ($>+1\sigma$). Thus positive (negative) anomalies correspond to decreased (increased) NO_3^-. Yellow star is location of Law Dome. (c) Map of SON surface pressure anomalies composited from Na^+ (in the ITASE 01-2 ice core), in the sense high ($+1\sigma$) minus low (-1σ) years. Positive (negative) anomalies correspond to an increase (decrease) in Na^+. A major negative anomaly defines the general region of the Amundsen Sea low. Red star is location of ITASE 01-2, and yellow star of Siple Dome.

$P<0.01$, respectively) with the SON surface circumpolar mean zonal wind over the period of NCEP/NCAR re-analysis coverage (AD 1948–2002) (Yan and others, 2005). Anomalies as high as $4\,m\,s^{-1}$ (Fig. 1) exist in regions where mean (AD 1948–2002) SON winds are $8–12\,m\,s^{-1}$. From this correlation we demonstrate that stronger (weaker) westerly winds are conducive to more (less) transport of crustal and marine source Ca^{2+} to both ice-core sites. Correlation between Ca^{2+} series and higher levels of zonal wind in the atmosphere (500 mbar, not shown) reveals a similar westerly wind influence.

Nitrate ion (NO_3^-) input to Antarctica is dominated by transport from long-range sources through the upper troposphere and stratosphere (Legrand and Kirchner, 1990), and, other than sites where significant re-emission to the atmosphere occurs (very low accumulation rate), concentrations range from high to low between inland and coastal Antarctica (Mulvaney and Wolff, 1994). As such, increased levels of NO_3^- at near-coastal sites such as Law Dome suggest increased transport of inland source air toward the coast. Recent results from an ice core 600 km east of Law Dome reveal correlations between the June–August (JJA; the period of maximum NO_3^- input (Whitlow and others, 1992)) surface pressure gradient from East Antarctica to the sub-Antarctic and NO_3^- in this core ($r = -0.52$, $P<0.005$, AD 1948–90) and strong surface wind drainage (Goodwin and others, 2003). We find a similar relationship using changes in Law Dome NO_3^- and JJA 850 mbar zonal wind. Anomalies in JJA 850 mbar zonal wind up to $4\,m\,s^{-1}$ over the general region of Law Dome (Fig. 1) are found where the mean (AD 1948–2002) JJA 850 mbar flow is $3–7\,m\,s^{-1}$. Furthermore, as Law Dome NO_3^- decreases (increases) there is an increase (decrease) in zonal wind transport over the ocean near 40–50° S of up to $3\,m\,s^{-1}$ where mean (AD 1948–2002) JJA winds are $5–16\,m\,s^{-1}$ (Fig. 1).

Previous work indicates that higher (lower) Na^+ concentrations in the Siple Dome ice core are coincident with higher (lower) levels of SON cyclone intensity in one of the major quasi-stationary lows in the circumpolar trough, the Amundsen Sea low (ASL) (Kreutz and others, 2000). SON timing is consistent with the seasonal maximum in Na^+ in Antarctic ice cores (Whitlow and others, 1992; Kreutz and others, 2000; Steig and others, 2005). The same association is demonstrated for ITASE 01-2 ice core (Fig. 1). Annual values of Na^+ in the Siple Dome ice core are correlated ($r = -0.32$, $P<0.001$ (annual series) and $r = -0.51$, $P<0.001$ (3 year smoothed series)) with SON surface pressure changes over much of the South Pacific for the period AD 1900–95 (Kreutz and others, 2000). For the period AD 1948–2002, negative anomalies close to 7 mbar in the region of the ASL are associated with increased levels of Siple Dome Na^+ (Fig. 1).

In summary, the ice-core records chosen for our study allow tracing of three different transport pathways. Sea-salt Na^+ (equivalent to total Na^+) and some of the Ca^{2+} associated with sea salt are mainly representative of medium- to low-range circulation, inside the polar vortex. Crustal Ca^{2+} (most of the Ca^{2+} identified in the EOF analysis reported below) is representative of zonal atmospheric circulation near the edge of the polar vortex, because its sources are mainly located at 40–50° S. Nitrate is affected by long-range tropospheric and stratospheric transport with more poorly understood pathways.

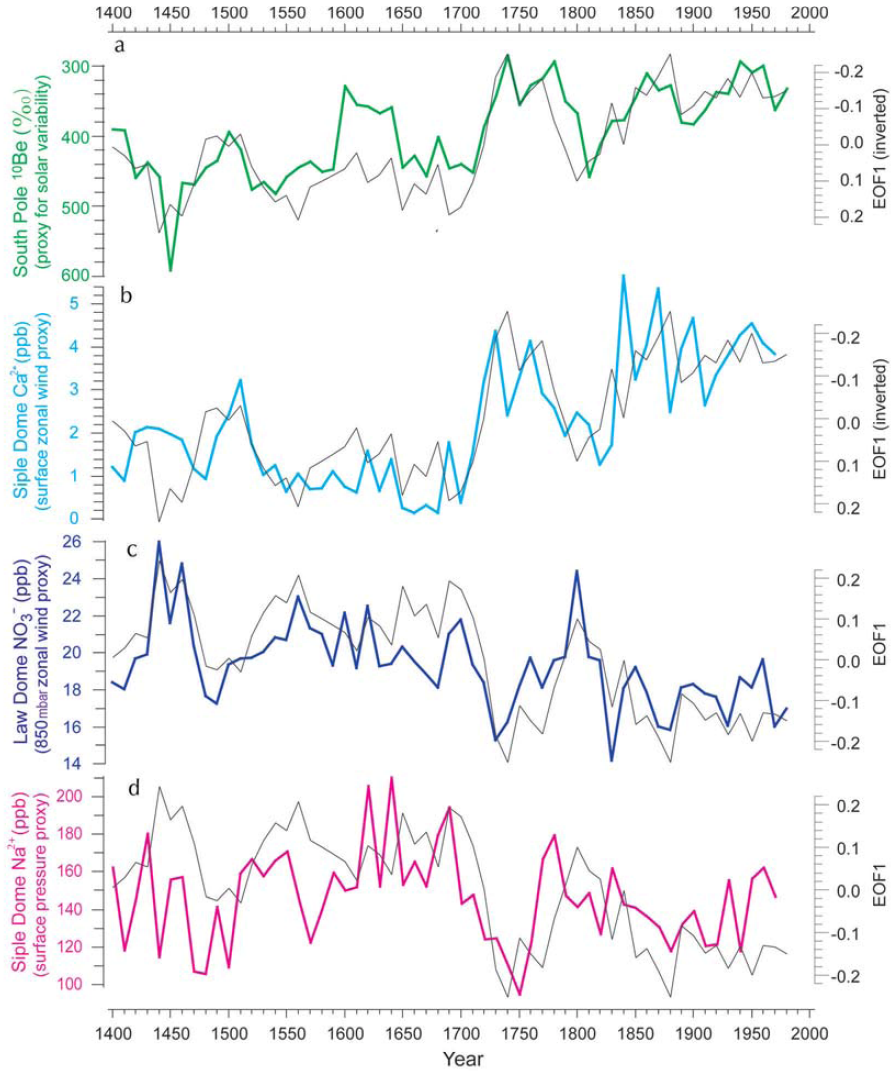

Fig. 2. Jointly associated variance represented by EOF1 (black light line, normalized units) between proxies for solar variability and atmospheric circulation (thick lines) using 10 year resampled data. Proxies are: (a) South Pole ^{10}Be (‰) proxy for solar variability; (b) Siple Dome Ca^{2+} (parts per billion (ppb)) proxy for SON surface zonal wind; (c) Law Dome NO_3^- (ppb) proxy for JJA 850 mbar zonal wind; and (d) Siple Dome Na^+ (ppb) proxy for SON surface pressure. Proxy for solar variability is plotted as the inverse of the ^{10}Be series (Bard and others, 2000). EOF1 is oriented in all plots to aid in visually examining the statistical fit.

DECADAL- AND LONGER-SCALE ASSOCIATIONS BETWEEN SOLAR VARIABILITY AND ATMOSPHERIC CIRCULATION

To investigate the association between solar variability and the ice-core proxies for atmospheric circulation used in this study, we compare the latter to a record of ice-core ^{10}Be. The most proximal record for our study comes from a South Pole ice core (Raisbeck and others, 1990). The cosmogenic nuclide data from this study are reported in Bard and others (2000) as changes per mil vs present value and also reported as reconstructed solar irradiance ($W m^{-2}$) by scaling to various estimates of reductions in solar irradiance during the Maunder Minimum compared to present values (e.g. Zhang and others, 1994; Solanki and Fligge, 1998). Since the South Pole ^{10}Be time series ranges in resolution from 2 to 22 years (mean 7.8; <12% of samples >10 year resolution) over the 600 years focused upon in this study, we resample all series to a common 10 year resolution.

Statistical associations between South Pole ^{10}Be and ice-core proxies for zonal wind (Siple Dome Ca^{2+} and Law Dome NO_3^-) and surface pressure (Siple Dome Na^+) are investigated using multidimensional (empirical orthogonal function (EOF)) analysis (Fig. 2) and linear correlations. EOF analysis reveals shared variance between ^{10}Be and the atmospheric proxies. EOF1 contains the greatest shared variance such that 62% of the ^{10}Be is inversely associated with 60% of the Siple Dome Ca^{2+} and directly associated with 61% of Law Dome NO_3^- and 30% of Siple Dome Na^+. On EOF2, 58% of the Siple Dome Na^+ variance is inversely

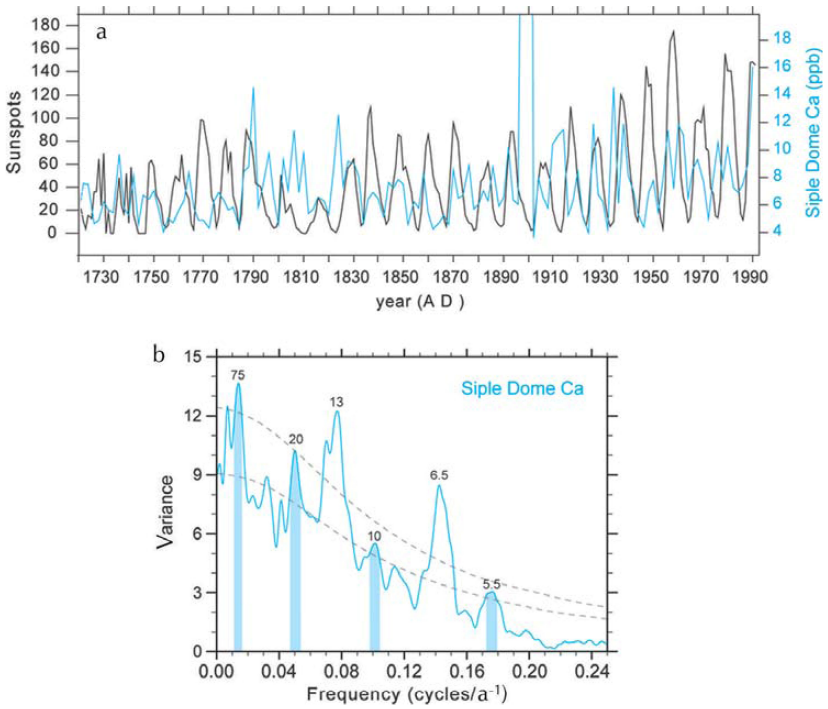

Fig. 3. (a) Annual values of the Siple Dome Ca^{2+} proxy for surface zonal wind compared to annual values of the solar cycle (sunspot number, ftp.ngdc.noaa.gov) for the period 1720–1990. (b) Multi-taper method (Mann and Lees, 1996): three 2σ prolate tapers smoothing of Siple Dome Ca^{2+}. Dashed lines refer to 95% (lower) and 99% (upper) significance estimated using a robust red-noise method (Mann and Lees, 1996), and numbers above peaks refer to mean period (years). Periodicities close to previously suggested solar cycles are shaded.

associated with 18% of the ^{10}Be variance. Remaining EOFs do not reveal significant (>10%) variance association between ^{10}Be and the atmospheric proxies. Straight linear correlations between ^{10}Be and Siple Dome Ca^{2+}, Law Dome NO_3^- and Siple Dome Na^+ are, respectively, $r = -0.55$, $r = 0.61$ and $r = 0.39$ for $P > 0.01$ (maximum at 0 lag).

Figure 2 demonstrates the close decadal-scale correspondence between the ^{10}Be ice-core proxy for solar variability and ice-core proxies for polar atmospheric circulation. Shared variance between all of the series is represented by EOF1 in this figure. When solar irradiance increases (decreases), Siple Dome Ca^{2+} concentrations increase (decrease). From Figure 1 increased Ca^{2+} is characterized by intensification of zonal winds over, in particular, the Indian and Pacific Oceans. When solar irradiance increases (decreases), Law Dome NO_3^- concentrations decrease (increase). From Figure 1 low NO_3^- is characterized by an increase in zonal wind strength.

Referring to Figure 1, when the 39% of the variance in Siple Dome Na^+ associated with ^{10}Be through EOF1 increases (decreases), solar irradiance (inverse of ^{10}Be) decreases (increases). EOF2 captures 58% of the joint variance in the inversely associated Siple Dome Na^+ and ^{10}Be series. Clearly there is a strong but complicated association between solar irradiance and the Siple Dome Na^+ proxy for the ASL that may be more precisely constrained by investigating the position of the ASL over time through the examination of more ice-core records.

ASSOCIATIONS BETWEEN THE SOLAR CYCLE AND SOUTHERN HEMISPHERE ATMOSPHERIC CIRCULATION

To further investigate the association between solar irradiance and proxies for zonal wind we compare annual values of these proxies with annual values of the solar cycle for the common period of high-resolution overlap (AD 1720–1990). Although there is a weak identified association between Law Dome NO_3^- and solar flares (Palmer and others, 2001b), there is no significant correlation between NO_3^- and sunspot number. However, visual inspection of Siple Dome Ca^{2+} series compared to the sunspot record reveals similar behaviour and since AD 1825 very nearly in-phase structure (Fig. 3). Differences in phasing between Ca^{2+} and the sunspot record may be a consequence of dating errors in the older portion of the ice-core record and/or non-linearities in the association between Ca^{2+} and surface zonal wind produced by changes in boundary conditions, such as sea-ice extent, not constrained by this study. The largest departure in relative magnitude between Ca^{2+} and the sunspot record is during the period AD 1896–1901, close to the nominal end of the Little Ice Age. The only other major Ca^{2+} concentration anomaly of the last 1200 years occurs near the onset of the Little Ice Age (Kreutz and others, 1997). These Ca^{2+} concentration anomalies (five and ten times, respectively, the mean of the last 1200 years) appear to signal major periods of climate reorganization.

Statistically based associations between solar variability and the Siple Dome Ca^{2+} proxy for surface zonal wind

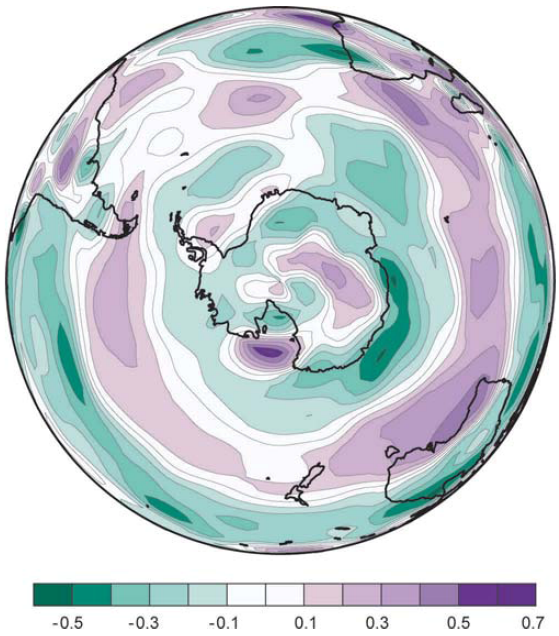

Fig. 4. Association between solar flux and SON surface zonal wind for the period 1975–2002 using an image created on the NCEP/NCAR re-analysis (NOAA–CIRES Climate Diagnostics Center, http://www.cdc.noaa.gov/). Values of $r > 0.345$, $P = 0.990$.

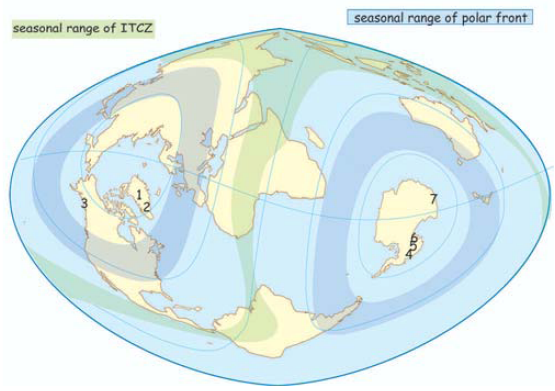

Fig. 5. Eckert–Greifendorff global projection displaying the location of ice-core sites utilized in this study as well as the position of the seasonal range of the northern and southern polar fronts and the Inter-Tropical Convergence Zone (ITCZ) for general perspective. 1. GISP2; 2. 20D; 3. Mount Logan; 4. ITASE 01-2; 5. ITASE 00-1; 6. Siple Dome; and 7. Law Dome.

(Fig. 3) reveal significant similarities. Periodicities at 5.5, 10, 20 and 75 years coincide with the 10–11 year Schwabe sunspot cycle, harmonics of the Schwabe cycle (5.5 years and the 22 year Hale double sunspot cycle), and are close to the 80–90 year Gleissberg cycle. Highly prominent peaks in the surface zonal wind proxy at 6.5 and 13 years demonstrate that the solar–atmospheric circulation association suggested in this study is only part of a more complex series of controls on Southern Hemisphere atmospheric circulation related perhaps to changes in sea-ice extent and natural oscillations in the ocean–atmosphere system. Alternately dating errors of ±1–2 years in the older (>50 years) sections of the Siple Dome Ca^{2+} record may introduce sufficient artefacts in timing to make periodicities of 5.5–6.5 years and 10–13 years not differentiable from the half Schwabe and full Schwabe cycles, respectively.

A MECHANISM FOR SOLAR FORCING OF ATMOSPHERIC CIRCULATION

While we cannot definitively demonstrate the mechanism by which changes in solar irradiance affect the changes in atmospheric circulation over the Antarctic and Southern Ocean observed in our records, we note that our findings are consistent with other studies, notably, model results and observational data. These suggest that increased solar ultraviolet radiation leads to increased production of stratospheric ozone, resulting in increased (decreased) temperatures in the lower stratosphere (troposphere) (Randel and Cobb, 1994; Chandra and others, 1996; McCormack and Hood, 1996), and consequently an increase in the thermal gradient from high to low latitudes attended by an increase in lower-tropospheric zonal wind speeds over the Northern Hemisphere (Shindell and others, 1999). We note that the association between solar variability and zonal wind speed developed using the NCEP/NCAR re-analysis over the Southern Hemisphere (Fig. 4) is consistent with the solar–zonal-wind relationship utilized in this study. It should be noted that recent anthropogenically induced depletion of ozone over Antarctica would subdue the solar–zonal-wind relationship during maxima in the solar cycle. As a consequence, results in Figure 4 may underestimate the natural solar–zonal-wind relationship.

ARCTIC EXAMPLES OF THE ASSOCIATION BETWEEN SOLAR VARIABILITY AND ATMOSPHERIC CIRCULATION

Northern Hemisphere ice-core records also reveal decadal-scale associations with solar variability over the Holocene (O'Brien and others, 1995; Mayewski and others, 1997) and Schwabe cycle periodicities (Mayewski and others, 1993a). To investigate the association between Northern Hemisphere climate and solar variability further, we examine three ice-core records that provide proxies for atmospheric circulation spanning the North Pacific to Eurasia. The Greenland Ice Sheet Project 2 (GISP2) K^{+} record from central Greenland provides a proxy for the behaviour of the Siberian high (Meeker and Mayewski, 2002). The 20D Ca^{2+} record from south Greenland (Mayewski and others, 1993b) is not calibrated with an atmospheric circulation feature but offers evidence of dust transport off adjacent continents through most probably the activity of westerly atmospheric flow. The Mount Logan Ca^{2+} record from Yukon Territory, Canada, (Mayewski and others, 1993b) reveals statistically significant correlations with the behaviour of the Kara Sea low (E.C. Osterberg and others, unpublished information).

We utilize these records in a preliminary examination only because all are relatively old and the sample resolution and dating for each is generally poorer than the Antarctic records discussed here. Some of these records will be reinvestigated using newly collected ice cores from sites close to the older records, so we present the following

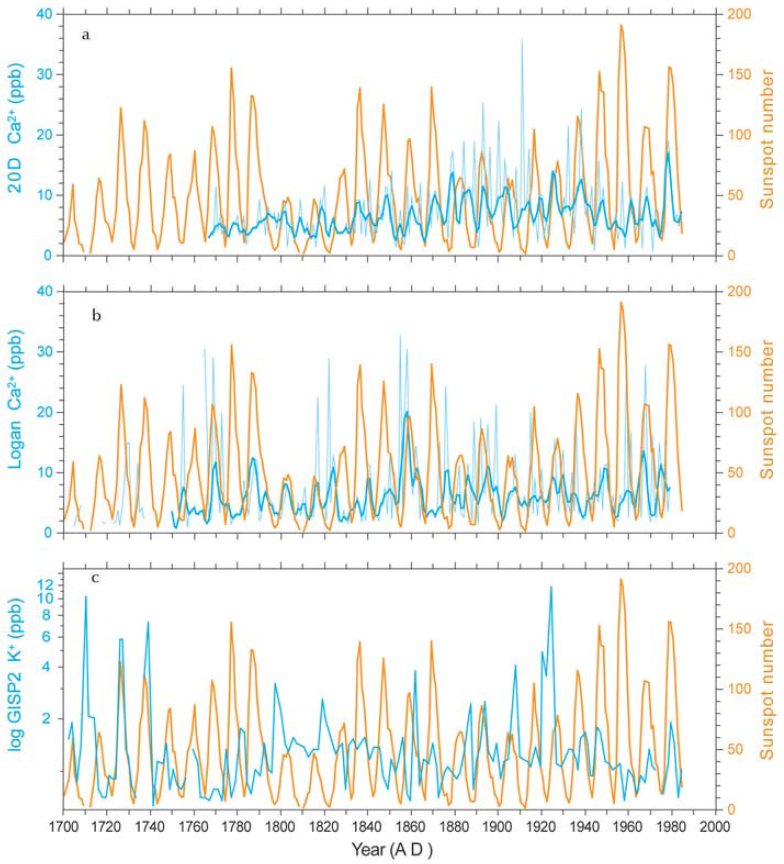

Fig. 6. Sunspot number (ftp.ngdc.noaa.gov) (red) compared to: (a) 20D Ca^{2+} annual values (light blue) and robust spline (dark blue); (b) Mount Logan Ca^{2+} annual values (light blue) and robust spline (dark blue); and (c) GISP2 K^{+} raw data values (dark blue).

primarily to stimulate future investigations. The three ice-core records we use in conjunction with the Antarctic data already presented offer a bipolar perspective (Fig. 5) of solar forcing of the polar atmosphere.

In Figure 6 we compare the annually dated portions of these Northern Hemisphere ice-core records with the sunspot record. Since these comparisons are based on older records we will present only a visual examination in this study. Robust splined annual values of 20D Ca^{2+} are positively coincident with solar cycles from AD 1983 to 1924, 1896 to 1833 and 1782 to 1764 and more poorly coincident during intervening periods. Positively correlated periods suggest intensified westerly transport during the positive phase of the solar cycle. Robust-splined annual values of Mount Logan Ca^{2+} are positively coincident with the solar cycle over the periods from AD 1970 to 1892, 1870 to 1840 and 1820 to 1770 and less clearly related during intervening periods. Positively correlated periods reveal intensification of the Kara Sea low coincident with the positive phase of the solar cycle. Raw values of GISP2 K^{+} coincide positively with solar cycles over the periods AD 1984 to 1936, 1920 to 1890 and 1774 to 1723 and are inverse to the solar cycle throughout much of the intervening portion of the record. Periods with a positive correlation indicate intensification of the Siberian high coincident with the positive phase of the solar cycle.

The positive periods of correlation for these ice-core series and the solar cycle are generally consistent with the timing of periods of greater sunspot activity. In general, the Siberian high, Kara Sea low and westerly flow appear to be intensified (lessened) during the positive (negative) phase of sunspot cycles and most consistently during the positive phase of more active sunspot cycles. Further investigation into the timing and mechanism of the solar–climate association in the Northern Hemisphere must wait for ice cores covering more recent portions of the record.

CONCLUSIONS AND IMPLICATIONS

In this paper we demonstrate that, on multi-decadal to annual timescales, increases in solar irradiance lead to intensification of zonal winds near the edge of the polar vortex over much of the Southern Ocean and Antarctica and perhaps to intensification of atmospheric circulation throughout portions of the mid–upper latitudes of the Northern Hemisphere. Despite the assertion of a solar–climate association in both hemispheres, comparison between solar-irradiance-induced changes in atmospheric circulation in the Northern and Southern Hemispheres may not be straightforward due to differences in geography between the hemispheres.

The identification of a solar–climate link and of a possible mechanism for this link will help to elucidate controls on the global climate system and should enhance predictability. However, recent changes in Southern Hemisphere tropospheric circulation, such as anthropogenically driven photochemical ozone depletion in the lower stratosphere over Antarctica (Thompson and Solomon, 2002), and other anthropogenically induced changes in climate will no doubt provide challenges to the natural order imposed by the sun–climate association. Decoding the natural climate system, however, is essential to the prediction of global climate change.

There is significant societal relevance in understanding and eventually predicting the behaviour of climate. For example, Southern Hemisphere circumpolar winds influence atmospheric circulation over the Indian and Pacific Oceans and through this association may change the hydrologic balance over currently drought-ridden portions of Australia.

The solar-irradiance–atmospheric-circulation association suggested here vies for a key role in the control of Holocene, and perhaps older, abrupt climate-change events. The association displays fast onset/decay, broad geographic impact and is consistent with observed and modelled mechanisms for solar–climate forcing. Whether change in solar irradiance can provide sufficient forcing to be the sole trigger for abrupt climate change, or whether it is just sufficient to offset the critical balance of natural oscillations in the climate system, remains to be demonstrated.

ACKNOWLEDGEMENTS

The authors appreciate the support provided by the 109th Air National Guard, Ice Core Drilling Services, Raytheon Polar Services and many colleagues in the field. The research was funded by the US National Science Foundation (OPP 0096299, 0096305, 0240878) and the Australian Government's Cooperative Research Centres Programme.

REFERENCES

Bard, E., G. Raisbeck, F. Yiou and J. Jouzel. 2000. Solar irradiance during the last 1200 years based on cosmogenic nuclides. *Tellus,* **52**(3), 985–992.

Beer, J. 2000. Polar ice as an archive for solar cycles and the terrestrial climate. *In* Wilson, A., *ed. The Solar Cycle and Terrestrial Climate: Proceedings of the First Solar and Space Weather Euroconference, Santa Cruz de Tenerife, September 25–30.* Noordwijk, European Space Agency, 671–676.

Bond, G. *and 9 others.* 2001. Persistent solar influence on North Atlantic climate during the Holocene. *Science,* **294**(5549), 2130–2136.

Brown, G.M. and J.I. John. 1979. Solar cycle influences in tropospheric circulation. *J. Atmos. Terr. Phys.,* **41**, 43–52.

Burnett, A.W. 1993. Size variations and long-wave circulation within the January Northern Hemisphere circumpolar vortex 1946–89. *J. Climate,* **6**, 1914–1920.

Chandra, S. *and 6 others.* 1996. Ozone variability in the upper stratosphere during the declining phase of Solar Cycle 22. *J. Geophys. Res.,* **23**, 2935–2938.

Denton, G.H. and W. Karlén. 1973. Holocene climatic variations: their pattern and possible causes. *Quat. Res.,* **3**(2), 155–205.

Goodwin, I., H. De Angelis, M. Pook and N.W. Young. 2003. Snow accumulation variability in Wilkes Land, East Antarctica and the relationship to atmospheric ridging in the 130°–170° E region since 1930. *J. Geophys. Res.,* **108**(D21), 4673. (10.1029/2002JD002995.)

Hansen, J., A. Lacis, R. Ruedy, M. Sato and H. Wilson. 1998. Climate forcings in the industrial era. *Proc. Nat. Acad. Sci. USA,* **95**, 12,753–12,758.

Kalnay, E. *and 21 others.* 1996. The NCEP/NCAR 40-year reanalysis project. *Bull. Am. Meteorol. Soc.,* **77**(3), 437–471.

Kreutz, K.J. and P.A. Mayewski. 1999. Survey of Antarctic surface snow glaciochemistry. *Antarct. Sci.,* **11**(1), 105–118.

Kreutz, K.J., P.A. Mayewski, L.D. Meeker, M.S. Twickler, S.I. Whitlow and I.I. Pittalwala. 1997. Bipolar changes in atmospheric circulation during the Little Ice Age. *Science,* **277**(5330), 1294–1296.

Kreutz, K.J., P.A. Mayewski, I.I. Pittalwala, L.D. Meeker, M.S. Twickler and S.I. Whitlow. 2000. Sea level pressure variability in the Amundsen Sea region inferred from a West Antarctic glaciochemical record. *J. Geophys. Res.,* **105**(D3), 4047–4059.

Labitzke, K. and H. van Loon. 1989. Associations between the 11-year solar cycle, the QBO and the atmosphere. Part III: aspects of association. *J. Climate,* **2**(6), 554–565.

Lean, J., J. Beer and R. Bradley. 1995. Reconstruction of solar irradiance since 1610: implications for climate change. *Geophys. Res. Lett.,* **22**(23), 3195–3198.

Legrand, M.R. and S. Kirchner. 1990. Origins and variations of nitrate in south polar precipitation. *J. Geophys. Res.,* **95**(D4), 3493–3507.

Legrand, M. and P. Mayewski. 1997. Glaciochemistry of polar ice cores: a review. *Rev. Geophys.,* **35**(3), 219–243.

Mann, M.E. and J.M. Lees. 1996. Robust estimation of background noise and signal detection in climatic time series. *Climate Change,* **33**, 409–445.

Mayewski, P.A. *and 8 others.* 1993a. Greenland ice core 'signal' characteristics: an expanded view of climate change. *J. Geophys. Res.,* **98**(D7), 12,839–12,847.

Mayewski, P.A. *and 7 others.* 1993b. Ice-core sulfate from three Northern Hemisphere sites: source and temperature forcing implications. *Atmos. Environ.,* **27A**(17–18), 2915–2919.

Mayewski, P.A. *and 6 others.* 1997. Major features and forcing of high-latitude Northern Hemisphere atmospheric circulation using a 110,000-year-long glaciochemical series. *J. Geophys. Res.,* **102**(C12), 26,345–26,366

McCormack, J.P. and L.L. Hood. 1996. Apparent solar cycle variation in upper stratospheric ozone and temperature: latitude and seasonal variations. *J. Geophys. Res.,* **101**(D15), 20,933–20,944.

Meeker, L.D. and P.A. Mayewski. 2002. A 1400-year long record of atmospheric circulation over the North Atlantic and Asia. *The Holocene,* **12**(3), 257–266.

Mulvaney, R. and E.W. Wolff. 1994. Spatial variability of the major chemistry of the Antarctic ice sheet. *Ann. Glaciol.,* **20**, 440–447.

Nastrom, G.D. and A.D. Belmont. 1980. Evidence for a solar cycle signal in tropospheric winds. *J. Geophys. Res.,* **85**, 443–452.

O'Brien, S.R., P.A. Mayewski, L.D. Meeker, D.A. Meese, M.S. Twickler and S.I. Whitlow. 1995. Complexity of Holocene climate as reconstructed from a Greenland ice core. *Science,* **270**(5244), 1962–1964.

Palmer, A.S., T.D. van Ommen, M.A.J. Curran, V.I. Morgan, J.M. Souney and P.A. Mayewski. 2001a. High precision dating of volcanic events (AD 1301–1995) using ice cores from Law Dome, Antarctica. *J. Geophys. Res.,* **106**(D22), 28,089–28,096.

Palmer, A.S., T.D. van Ommen, M.A.J. Curran and V. Morgan. 2001b. Ice-core evidence for a small solar-source of atmospheric nitrate. *Geophys. Res. Lett.,* **28**(10), 1953–1956.

Raisbeck, G.M., F. Yiou, J. Jouzel and J.R. Petit. 1990. ^{10}Be and ^{2}H in polar ice cores as a probe of the solar variability's influence on climate. *Philos. Trans. R. Soc. London A,* **330**(1615), 463–470.

Randel, W.J. and J.B. Cobb. 1994. Coherent variations of monthly mean total ozone and lower stratospheric temperature. *J. Geophys. Res.,* **99**, 5433–5447.

Shindell, D., D. Rind, N.K. Balachandran, J. Lean and P. Lonergan. 1999. Solar cycle variability, ozone, and climate. *Science,* **284**(5412), 305–308.

Solanki, S.K. and M. Fligge. 1998. Solar irradiance since 1874 revisited. *Geophys. Res. Lett.,* **25**, 341–344.

Souney, J.M., P. Mayewski, I. Goodwin, V.I. Morgan and T. van Ommen. 2002. A late Holocene climate record from Law Dome, East Antarctica. *J. Geophys. Res.,* **107**(D22), 4608–4617.

Steig, E.J. *and 16 others.* 2005. High-resolution ice cores from US ITASE (West Antarctica): development and validation of chronologies and determination of precision and accuracy. *Ann. Glaciol.,* **41** (see paper in this volume).

Stuiver, M. and T.F. Braziunas. 1989. Atmospheric ^{14}C and century-scale oscillations. *Nature,* **338**, 405–408.

Thompson, D.W.J. and S. Solomon. 2002. Interpretation of recent Southern Hemisphere climate change. *Science,* **296**(5569), 895–899.

Tinsley, B.A. 1988. The solar cycle and the QBO influences on the latitude of storm tracks in the North Atlantic. *Geophys. Res. Lett.,* **15**(5), 409–412.

Van Loon, H. and K. Labitzke. 1988. Association between the 11-year solar cycle, the QBO and the atmosphere. Part II: Surface and 700 mb in the Northern Hemisphere in winter. *J. Climate,* **1**, 905–920.

Venne, D.E. and D.G. Dartt. 1990. An examination of possible solar cycle–QBO effects in the Northern Hemisphere troposphere. *J. Climate,* **3**, 272–281.

Whitlow, S., P.A. Mayewski and J.E. Dibb. 1992. A comparison of major chemical species seasonal concentration and accumulation at the South Pole and Summit, Greenland. *Atmos. Environ.,* **26A**(11), 2045–2054.

Wilson, R.C. and H.S. Hudson. 1998. The Sun's luminosity over a complete solar cycle. *Nature,* **332**, 810–812.

Yan, Y., P.A. Mayewski, S. Kang and E. Meyerson. 2005. An ice core proxy for Antarctic circumpolar zonal wind intensity. *Ann. Glaciol.,* **41** (see paper in this volume).

Zhang, Q., W.H. Soon, S.L. Baliunas, G.W. Lockwood, B.A. Skiff and R.R. Radick. 1994. A method of determining possible brightness variations of the sun in past centuries from observations of solar-type stars. *J. Astroph.,* **427**, L111–L114.

Appendix B

ELEMENT NAMES AND SYMBOLS

Element Symbol	Element Name
Al	Aluminium
As	Arsenic
Ba	Barium
Bi	Bismuth
Ca	Calcium
Cd	Cadmium
Ce	Cerium
Co	Cobalt
Cr	Chromium
Cs	Cesium
Fe	Iron
K	Potassium
La	Lanthanum
Li	Lithium
Mg	Magnesium
Mn	Manganese
Na	Sodium
Pb	Lead
Pr	Praseodymium
S	Sulfur
Sr	Strontium
Ti	Titanium
U	Uranium
V	Vanadium

Major Ion Symbol	Major-Ion Name
Ca^{2+}	Calcium
Cl^{-}	Chloride
K^{+}	Potassium
Mg^{2+}	Magnesium
MS^{-}	Methylsulfonate
Na^{+}	Sodium
NO_3^{-}	Nitrate
SO_4^{2-}	Sulfate

Table B.1. List of element symbols and their corresponding names. Also listed are the major ion symbols with their corresponding names.

BIOGRAPHY OF THE AUTHOR

Daniel A. Dixon was born on June 18th 1974, and raised in London, England. He graduated from Drayton Manor High School in Hanwell, London. He received his B.Sc. in Geology and Oceanography from the School of Ocean and Earth Science at the University of Southampton. His undergraduate thesis was based on a Training Through Research (TTR) cruise in the Atlantic Ocean. The UNESCO-IOC Floating University ran the TTR cruise, and along the way the Southwest Iberian continental margin and mud volcanoes in the Gulf of Cadiz were studied. Throughout the cruise many new seafloor features were imaged in high resolution using sidescan sonar; they were also "ground-truthed" using a 4m-long gravity corer and a 2-ton hydraulic grab.

Since arriving in Maine in October 2000, Dan has been involved in the U.S. ITASE traverses in Antarctica. He has spent five field seasons there from 2001-2008 and helped to drill many hundreds of meters of ice core during that time. Dan has also been involved in ice core drilling expeditions in the Cordillera Darwin and Southern Patagonian Ice Cap, the Southern Alps of New Zealand, and the Central Chilean Andes.

Dan received his Master of Science degree in Quaternary and Climate Studies from The University of Maine in August, 2004. Since that time he has been pursuing his Ph.D. Dan is a candidate for the Doctor of Philosophy degree in Earth Sciences from The University of Maine in May, 2011.